PNL-7220
UC-202

18L

The University of Minnesota Aquifer Thermal Energy Storage (ATES) Field Test Facility-System Description, Aquifer Characterization, and Results of Short-Term Test Cycles

June 1991

Prepared for the U.S. Department of Energy
Contract DE-AC06-76RLO 1830

Pacific Northwest Laboratory
Operated for the U.S. Department of Energy
by Battelle Memorial Institute

Battelle

PNL-7220

DISCLAIMER

PACIFIC NORTHWEST LABORATORY
operated by
BATTELLE MEMORIAL INSTITUTE
for the
UNITED STATES DEPARTMENT OF ENERGY
under Contract DE-AC06-76RLO 1830

Printed in the United States of America

Available to DOE and DOE contractors from the Office of Scientific and Technical Information, P.O. Box 62, Oak Ridge, TN 37831; prices available from (615) 576-8401. FTS 626-8401.

Available to the public from the National Technical Information Service, U.S. Department of Commerce, 5285 Port Royal Rd., Springfield, VA 22161.

PNL-7220
UC-202

THE UNIVERSITY OF MINNESOTA AQUIFER THERMAL ENERGY STORAGE (ATES) FIELD TEST FACILITY - SYSTEM DESCRIPTION, AQUIFER CHARACTERIZATION, AND RESULTS OF SHORT-TERM TEST CYCLES

M. Walton, Principal Investigator

M. C. Hoyer
S. J. Eisenreich
N. L. Holm
T. R. Holm
R. Kanivetsky
M. A. Jirsa
H. C. Lee
J. L. Lauer
R. T. Miller
J. L. Norton
H. Runke

Minnesota Geological Survey
University of Minnesota
St. Paul, Minnesota

June 1991

Prepared by
Minnesota Geological Survey
University of Minnesota
for Pacific Northwest Laboratory
under Contract DE-AC06-76RLO 1830
with the U.S. Department of Energy
Subcontract 007601-A-0

Pacific Northwest Laboratory
Richland, Washington 99352

FOREWORD

Seasonal thermal energy storage (STES) involves storing thermal energy, such as winter chill, summer heat, and industrial waste heat, for future use in heating and cooling buildings or for industrial processes. Widespread development and implementation of STES would significantly reduce the need to generate primary energy in the United States. Data indicate that STES is technically suitable for providing 5 to 10% of the nation's energy, with major contributions in the commercial and industrial sectors and in district heating and cooling applications.

Aquifer thermal energy storage (ATES) is predicted to be the most cost-effective technology for seasonal storage of low-grade thermal energy. Approximately 60% of the United States is underlain by aquifers that are potentially suitable for underground energy storage. ATES has the potential to substantially reduce energy consumption and electrical demand. However, the geohydrologic environment that the system will use is a major element in system design and operation, and this environment must be characterized for development of efficient energy recovery.

Under sponsorship of the U.S. Department of Energy (DOE), The Pacific Northwest Laboratory (PNL) manages DOE's STES Program and directs numerical modeling, laboratory studies, and field testing of ATES at several sites. PNL is operated by Battelle Memorial Institute for the Department of Energy under contract DE-AC06-76RLO-1830.

This report describes aquifer characterization and the results of the initial short-term heat injection/recovery cycles at the St. Paul (Minnesota) field test facility (FTF). The St. Paul FTF, operated by the University of Minnesota, is the principal U.S facility for research on relatively high-temperature ATES. The primary objectives of investigations at the St. Paul

FTF are to: 1) evaluate the technical issues associated with design and operation of a high-temperature (>100°C) ATES system and 2) obtain data on fundamental geotechnical processes to validate laboratory and bench-scale geochemical testing and geohydrothermal modeling.

Landis D. Kannberg, Ph.D.
Manager, Seasonal Thermal Energy Storage Program

PREFACE

This report presents the results obtained during the first phase of the University of Minnesota Aquifer Thermal Energy Storage (ATES) Project. The various sections of this report were authored by the investigators listed below by section. Unless otherwise indicated, the individuals were at the University of Minnesota when the work was performed.

Executive Summary	M. Hoyer, M. Walton
1.0 Introduction	M. Hoyer, M. Walton
2.0 Field Test Facility	M. Hoyer, M. Walton
3.0 Geology and Hydrogeology	M. Jirsa, M. Hoyer
4.0 Water-Level Analysis and Hydraulic Parameters	R. Kanivetsky
5.0 Hydrogeologic Test and Thermal Test Program	M. Hoyer
6.0 Water Chemistry	T.R. Holm, S.J. Eisenreich, H.C. Lee, N.L. Holm
7.0 Bacteriological Analysis of Waters	J.L. Lauer
8.0 Environmental and Institutional Considerations	M. Hoyer, M. Walton
9.0 Conclusions	M. Walton, M. Hoyer
Appendix A	J.L. Norton (Orr-Schelen-Mayeron)
Appendix B	H. Runke (ERG, Inc.)
Appendix C	M. Hoyer, M. Jirsa
Appendix D	T.R. Holm, N.L. Holm

Work on the aquifer modeling for this project was done by J. Guswa and R.T. Miller of the United States Geological Survey. The modeling for this phase of the project is to be documented in a series of U.S. Geological Survey Professional Papers authored by R.T. Miller. Many data discussions are incomplete without reference to the data to be included in the U.S. Geological Survey publications.

Current addresses and affiliations for primary authors are given below.

M. Hoyer	Underground Space Center University of Minnesota 500 Pillsbury Drive S.E. Minneapolis, MN 55455
M. Walton M. Jirsa R. Kanivetsky	Minnesota Geological Survey 2642 University Avenue St. Paul, MN 55114
S. Eisenreich	Department of Civil and Mineral Engineering University of Minnesota 500 Pillsbury Drive S.E. Minneapolis, MN 55455
T. Holm	Illinois State Water Survey 2204 Griffith Drive Champaign, IL 61820

ABSTRACT

Phase I of the Aquifer Thermal Energy Storage (ATES) Project at the University of Minnesota was to test the feasibility, and model, the ATES concept at temperatures above 100°C using a confined aquifer for the storage and recovery of hot water. Phase I included design, construction, and operation of a 5-MW thermal input/output field test facility (FTF) for four short-term ATES cycles (8 days each of heat injection, storage, and heat recovery). Phase I was conducted from May 1980 to December 1983.

This report describes the FTF, the Franconia-Ironton-Galesville (FIG) aquifer used for the test, and the four short-term ATES cycles. Heat recovery; operational experience; and thermal, chemical, hydrologic, and geologic effects are all included.

The FTF consists of monitoring wells and the source and storage well doublet completed in the FIG aquifer with heat exchangers and a fixed-bed precipitator between the wells of the doublet.

The FIG aquifer is highly layered and areally anisotropic. The upper Franconia and Ironton-Galesville parts of the aquifer, those parts screened, have hydraulic conductivities of ~0.6 and ~1.0 m/d, respectively.

Ambient temperature testing preceded any heated water injection. The initial attempt at heated water injection resulted in clogging the storage well screen with calcium carbonate scale. Following acid remediation of the well, a precipitator, consisting of a packed bed of high-purity calcite, was designed and added to the FTF to protect the storage well.

Four ATES short-term cycles were successfully conducted following the addition of the precipitator. Stored water temperatures averaged 89.4, 97.4, 106.1, and 114.8°C for the respective cycles. Recovered water temperatures averaged 59.2, 55.2, 81.1, and 89.1°C for the respective cycles. Energy recovery factors for the cycles using source water temperature as a base were 0.59, 0.46, 0.62, and 0.58, respectively. Mechanical problems with the storage well pump caused Cycle 2 to have a storage period of 90 days, which lowered the energy recovery for that cycle.

Primary ions in the ambient ground water are calcium and magnesium bicarbonate. Ambient temperature FIG ground water is saturated with respect to calcium/magnesium bicarbonate. Heating the ground water caused most of the dissolved calcium to precipitate out as calcium carbonate in the heat exchanger and precipitator. Silica, calcium, and magnesium were significantly higher in recovered water than in injected water, suggesting dissolution of some constituents of the aquifer during the cycles. Further work on the ground water chemistry is required to understand water-rock interactions.

EXECUTIVE SUMMARY

The objectives of phase I of the Aquifer Thermal Energy Storage (ATES) Project at the University of Minnesota were to test and model the ATES concept at temperatures above 100°C using a confined aquifer for the storage and recovery of hot water. The phase I test program included design, construction and operation of a 5-MW thermal input/output test facility to perform a series of 24-day ATES test cycles (short-term test cycles) entailing 8 days of heat injection, 8 days of storage and 8 days of heat recovery. The purposes of these test cycles were to investigate the thermal and hydraulic responses of a confined aquifer to the introduction of heated water both with field experiments and computer modeling; to demonstrate the feasibility of ATES at temperatures above 100°C in a confined aquifer; to characterize the Franconia-Ironton-Galesville (FIG) aquifer; and to determine the aquifer parameters most important in predicting thermal recovery characteristics of the aquifer. The FIG aquifer was chosen because it is little used in the vicinity of the University site, has a very low hydraulic gradient and is well-confined by overlying and underlying confining beds.

A goal of the program was to test the feasibility of storing and recovering water at relatively high temperatures. An early objective was to acquire as quickly as possible the engineering parameters needed to design an application of ATES to the University of Minnesota heating plant with a maximum power input/output of 20-MW thermal. Program changes eliminated this phase of the project.

Phase I of the ATES field test program at the University of Minnesota ended December 7, 1983 with the completion of the fourth and final short-term test cycle performed under contract to Pacific Northwest Laboratory's[(a)] Underground Energy Storage Program. Project management, engineering design and construction of the facility were under the direction of the Physical Plant Engineering and Construction Division of the University of Minnesota, Warren

---

(a) Operated for the U.S. Department of Energy by Battelle Memorial Institute under contract DE-AC06-76RLO 1830.

Soderberg, Director. Test operations were managed by the Minnesota Geological Survey with the U.S. Geological Survey as a subcontractor for instrumentation and hydraulic modeling.

The ATES field test facility comprises a well-doublet of pumping/injecting wells located 255 m apart, a surrounding array of monitoring wells, and piping connecting the wells with heat exchangers and a heat source. The pumping/injecting wells are completed in the FIG aquifer; the monitoring wells are completed in the FIG aquifer, as well as adjacent aquifers and confining beds. The system is designed to inject water heated to 150°C for storage and to return water to the source well following storage and heat extraction at a temperature of 84°C. The heat source is 150 psi (1034 kPa) saturated steam from the University's St. Paul campus heating plant. Design flow is 18.9 L/sec; design delta T is 66°C; resulting power input/output rate is 5-MW thermal.

Funding for the project was awarded in May 1980; a permit for the short-term test cycles was granted in July 1980; and well drilling and construction started in September 1980. System design, construction, instrumentation, system debugging, well development, and hydraulic testing were completed in May 1982, about 1 year behind schedule. Major delays were due to: difficulties with drilling and well construction in the friable and broken sandstone and dolomite aquifers which overlie the FIG aquifer; late delivery and repeated failures of the pressure transducers, which required modification for deep immersion in the monitor wells; and clogging of the injection well from air entrainment and bubble formation. Hydraulic testing procedures ended with a successful 8-day injection of ground water at ambient temperature (11°C).

The first injection test attempt with hot water (85°C) was started in May 1982 and was terminated after about 50 hours when it became evident that severe clogging from the precipitation of calcium carbonate was occurring in the well. Calcium and magnesium bicarbonate are the primary dissolved solids in the water and are at saturation. Total dissolved solids content is approximately 235 mg/L. Components other than carbonates increase in solubility with increasing temperature; carbonates decrease. An immediate attempt to backflush the well was aborted when the pump's lineshaft bearings, which were synthetic rubber, failed in the hot water. Delays ensued while a means of

handling the carbonate precipitation problem was developed, the lineshaft bearings were replaced, and the storage well was restored by acid treatment and pumping.

It was clear that without a method for preventing calcium carbonate ($CaCO_3$) precipitation in the heat storage well a test of the ATES concept would not be possible. The variance granted to allow the ATES testing stipulated that no chemical additives be used to treat the water. A calcium carbonate precipitator/filter was developed, tested and placed in the system between the heat exchanger and the storage well. The heated water, supersaturated with respect to $CaCO_3$, passed through a set of columns filled with sized, crushed, high purity limestone to allow nucleation and precipitation of $CaCO_3$. Supersaturation reduction prevented well-clogging and allowed the short-term test program to proceed.

Following the installation and testing of the filter the first short-term cycle was conducted in November-December 1982 (Table 1). A second filter array was installed before the second test cycle to allow longer running time before maintenance was required. The second short-term cycle (May-August 1983) had a 90-day storage period because of a second failure of the pump's lineshaft bearings to perform in hot water. A redesigned lineshaft and lineshaft bearings of bronze and bronze-graphite were installed and performed satisfactorily through the recovery phase of Cycle 2 and all of Cycles 3 and 4. Cycles 3 and 4 were conducted from September to December 1983 (Table 1).

The temperature of the water injected into storage was warmer in each successive cycle because the source water was warmer during each cycle (Table 1). The injected (stored) water temperature was not constant during any short-term cycle. Temperatures decreased as scale accumulated in the condenser. A rapid decline in temperature began each period of injection as the condenser accumulated calcium carbonate scale. The controls of the temperature were the capacity of the system and the scale accumulation in the condenser. Mean injected water temperatures by cycle, were 89.4, 97.4, 106.1, and 114.8°C, respectively.

The temperature of water recovered from storage during the four cycles increased to a peak for several hours, then decreased with continued pumping

TABLE 1. Summary of ATES Short-Term Test Cycles Conducted at the University of Minnesota Field Test Facility

	Short-Term Cycle			
	1	2	3	4
Duration, days				
Injection, pumping	5.2	8	7.7	7.7
Injection, total	17	10	10.4	12
Storage	13	90	9.7	10.1
Recovery, pumping	5.2	8	7.7	7.7
Recovery, total	5.2	8	8	7.7
Temperature, °C				
Source water	11.0	20.5	36.1	52.6
Injected water	89.4	97.4	106.1	114.8
Recovered water	59.2	55.2	81.1	89.1
Flow rate, L/sec				
Injection	18.4	17.6	18.3	17.9
Recovery	18.1	17.8	17.3	17.8
Volume, 10^4 m^3				
Injection	0.83	1.22	1.22	1.19
Recovery	0.81	1.23	1.18	1.19
Energy, GWh				
Added	0.770	1.084	0.989	0.867
Recovered	0.453	0.495	0.617	0.503
Energy recovery factor				
(using source water temperature)	0.59	0.46	0.62	0.58
(using ambient water temperature)	0.59	0.52	0.71	0.75

(cumulative flow, time). The duration of storage affected the peak and average temperature of the water withdrawn. Mean recovered water temperatures, by cycle, were 59.2, 55.2, 81.1, and 89.1°C, respectively. Recovered energy was from 46% (Cycle 2) to more than 60% (Cycle 3) (Table 1).

Calcium carbonate precipitation resulting from heating the ambient ground water was the critical water chemistry problem. The precipitator and condenser prevented scale from developing in the storage well. Trends of the water chemistry during recovery were similar to those predicted by modeling. Recovered water had a higher total dissolved solid content than injected water. Dissolved silica, calcium, magnesium, and bicarbonate were near saturation at all recovered water temperatures. Water chemistry in the immediate vicinity of the storage well did change during the ATES cycles. Water chemistry is critically important for successful implementation of ATES.

Hydraulic parameters were determined by pumping tests. Examination and testing of core from the FIG and confining beds, together with packer testing conducted in the core holes revealed the FIG to be vertically inhomogeneous. The FIG aquifer is divided into four hydrologic zones. The Ironton-Galesville part of the aquifer is the most permeable part of the aquifer, with hydraulic conductivity from 0.3 to 1.2 m/d. The lower Franconia part of the aquifer has a low hydraulic conductivity (<0.03 m/d); the upper Franconia part of the aquifer has a hydraulic conductivity of 0.6 m/d. Preliminary work suggested the above values. Calculated values from field testing are approximately twice the above values. The upper Franconia (UF) and Ironton-Galesville (IG) transport almost all the water in the aquifer; thus the pumping/injecting wells were completed with only those intervals screened. Analysis of pumping test results indicate that the FIG is also laterally anisotropic. The direction of highest permeability is aligned NW-SE in the Ironton-Galesville section and NE-SW in the Franconia section. Water levels monitored before and during the test cycles indicate that the FIG is hydrologically well-separated from the overlying and underlying aquifers. Aquifer modeling before injection testing, for both ambient and high-temperature conditions, closely approximated the aquifer response results from the test cycles.

The Minnesota Pollution Control Agency (MPCA), the Minnesota Department of Health (MDH), and the Minnesota Department of Natural Resources (DNR) have environmental regulatory requirements that required a significant amount of attention during the project. Well construction, water use, and reinjection of the ground water all require permits or variances. Regulations in the State of Minnesota are among the strictest in the country, and regulatory

procedures were a source of significant delay. Plans, procedures, and periodic reports were supplied routinely to the agencies for review. Meetings with staff members were held during the planning and design stages of the facility, prior to beginning any heated-water test cycles, and after the second and fourth cycles. Deviations from schedule due to delays required two extensions of permits and variances. Delays caused by mechanical failure and the remedial actions planned and taken were communicated to and discussed with the concerned agencies.

Primary conclusions of these tests are:

1. It is feasible to store superheated water in a confined aquifer and recover a significant amount of the stored heat.
2. Mechanical and chemical problems can be resolved.
3. An aquifer system can be reasonably characterized with relatively complete standard methods of study.
4. Modeling of hydraulic and thermal effects can reasonably approximate the actual results of heated-water injection and recovery if provided with appropriate parameters.

ACKNOWLEDGMENTS

The support and leadership of Mr. Warren E. Soderberg, former Director of the Physical Plant and Project Co-Manager have been essential to the initiation and completion of this phase of the project. Mr. James O'Gara, Principal Plant Engineer of the Physical Plant, managed the project during the design and construction stages, allowing the testing to be started.

Mr. Ray Jackson and Mr. Stanley Borys of the Physical Plant engineering staff provided insights, advice, and aided in the maintenance of the system through the many problems encountered. Mr. Stephen A. Richards, Physical Plant Fiscal Manager, handled accounting and reporting requirements for the project. Mr. James Norton and others from Orr-Schelen-Mayeron and Associates, Inc. were instrumental in the design of the ATES system.

Professor Perry Blackshear, Department of Mechanical Engineering, was instrumental in the development of the precipitator added to the system which allowed the short-term test cycles to be completed.

Many individuals from the St. Paul Office of the U.S. Geological Survey, Water Resources Division, and from the Minnesota Geological Survey were called upon to staff the site during the test cycles. Many skilled workers from the Physical Plant staff at the St. Paul campus provided services essential to the operations of the ATES field test facility.

The support, advice, and encouragement of John Raymond and Landis Kannberg at Pacific Northwest Laboratory were significant contributions. The work was supported by the U.S. Department of Energy as part of the Underground Energy Storage Program administered by Pacific Northwest Laboratory.

Linda McDonald and Jeanne Perrin from the Minnesota Geological Survey prepared the text for reproduction.

CONTENTS

FIGURES

TABLES

THE UNIVERSITY OF MINNESOTA AQUIFER THERMAL ENERGY STORAGE (ATES) FIELD TEST FACILITY - SYSTEM DESCRIPTION, AQUIFER CHARACTERIZATION, AND RESULTS OF SHORT-TERM TEST CYCLES

1.0 INTRODUCTION

The University of Minnesota was awarded a contract in May 1980 to design, construct and operate an aquifer thermal energy storage (ATES) test facility for a series of short-term test cycles. The project is administered by Pacific Northwest Laboratory (PNL)[(a)]. The purpose of these tests was to evaluate the feasibility of storing high temperature (150°C) water in the Franconia-Ironton-Galesville (FIG) confined aquifer and later recovering the heated water for space heating. The facility has a nominal 5-MW thermal input/output capacity and uses a deep confined aquifer below the St. Paul campus of the University. The test facility is designed for operation at temperatures up to 150°C (302°F), flow rates up to 18.9 L/sec (300 gpm), and a delta T (temperature change) of 66°C (119°F). The original purpose was to acquire the basic hydrogeological, hydrogeochemical and hydrogeothermal data to determine design parameters for a 20-MW ATES demonstration system to be incorporated into the University of Minnesota heating/cooling system. As a result of program changes, the purpose of this first phase changed to acquiring the above data in the short-term field tests and testing of the ATES concept in a deep confined aquifer. This has included monitoring the system, describing the aquifer, modeling the aquifer and its responses, and monitoring and modeling the water chemistry.

The University of Minnesota Physical Plant Operations supervised design and construction of the facility, and provided operations maintenance. The Minnesota Geological Survey (MGS) provided site geologists during well drilling, supervised coring and core studies, coordinated site operations, collated the field data, and coordinated the technical studies. Water chemistry studies

---

(a) Operated for the U.S. Department of Energy by Battelle Memorial Institute under Contract DE-AC06-76RLO 1830.

and modeling were done at the Environmental Engineering Laboratory of the Department of Civil and Mineral Engineering at the University. The U.S. Geological Survey Water Resources Division, St. Paul, was responsible for subsurface data acquisition and aquifer modeling.

With the granting of a variance by the Minnesota Pollution Control Agency in July 1980 to allow injection of waters for the short-term ATES cycles, and appropriate permits from the Minnesota Department of Health and Minnesota Department of Natural Resources, the final designs of the test facility and monitor array were prepared. Construction began in September 1980 with the drilling of core holes at the heat-storage and water-supply sites. Construction of monitor wells, pumping wells and connecting piping, heat exchangers, and electrical connections continued, with many delays, until December 1981. Delay due to the late delivery and repeated failure of pressure transducers to perform in the monitor wells did not allow injection testing to begin until May 1982.

Packer testing of several intervals was conducted in the core holes, the recovered core was examined and water chemistry and water-rock interaction were studied. These results provided the framework for locating the well screens in the pumping wells, and also the preliminary model parameters. Pump tests and isothermal (ambient) testing of the aquifer, water-rock experiments, and preliminary water chemistry modeling were completed by May 1982. Non-isothermal (heated water) testing began in May 1982.

Problems due to precipitation of calcium carbonate ($CaCO_3$) from the heated aquifer water stopped the initial heated water injection after about 50 hours. Attempts to pump the storage well failed as a result of failure of the lineshaft bearings in the storage well. A significant delay followed in rehabilitating the well. During this delay a study of solutions to the precipitation problem without the use of water treatment chemicals resulted in the designing of a precipitator to protect the heat-storage well.

Following acid treatment of the well, replacement of the pump's lineshaft bearings and installation of a precipitating filter to prevent clogging of the well screen, a successful first test cycle was conducted in November and

December 1982. Following the granting of an extension to the permit for injection, the second test cycle was begun in May 1983.

Upon a second failure of the lineshaft bearings, a new lineshaft assembly was installed in the pumping wells. The resulting delay caused the storage interval during the second test cycle to be 90 days. Heat recovery from the second cycle, and the remaining third and fourth test cycles, was completed with no problems from the mechanical systems in the wells. Problems with the condenser tubes due to scale buildup and acid-etching did cause some delays. These problems are due to the frequent need for acid-cleaning the accumulated $CaCO_3$ from the pipes of the condenser.

The field test facility is described in Section 2 and Appendix A. Many of the problems encountered and solutions to them are presented as well. The geological and hydrogeological setting, description of the rocks of the FIG aquifer and its confining beds as revealed by examination, testing and geophysical logging are presented in Section 3. Hydraulic parameters as determined by field methods and analysis of the water levels in the various monitored intervals are presented in Section 4. Description of the testing conducted, flow rates and temperature data obtained from the thermal test cycles are presented in Section 5. Section 6 presents details of the water-chemistry sampling, analysis and modeling. Included is a discussion of the efficiency of the precipitator installed to protect the heat-storage well. Section 7 presents the results of the sampling for bacteriological analysis of waters and a discussion of implications. Section 8 outlines the environmental and institutional considerations and concerns that were expressed at the onset of the project. Section 9 presents a review of conclusions reached during these studies. Appendices include tabular analytical data, site descriptions and materials related to various sections within the report.

Results of aquifer modeling of the site and of the short-term cycles and the data from underground monitoring are included in a series of U.S. Geological Survey publications authored by R.T. Miller (1985, 1989).

2.0 FIELD TEST FACILITY

The field test facility (FTF) is located on the St. Paul campus of the University of Minnesota. For the short-term test cycles the facility consisted of: 1) two pumping/injection (source and storage) wells completed in the FIG aquifer; 2) eight monitoring wells completed in the FIG aquifer, its confining beds, and the Jordan and Mt. Simon aquifers; 3) connecting piping, heat exchangers and a precipitator/filter between the source and storage wells; and 4) piping to supply steam to the heat exchangers (Figures 2.1, 2.2, and 2.3). Appendix A presents design and construction information about the facility.

2.1 SOURCE AND STORAGE WELLS

The source well (B), and the storage well (A), are separated by 255 m (835 ft). They are each completed with two screened intervals in the FIG aquifer. The wells are both constructed the same way. The only differences are due to the differences in well head elevation. The head of well A is at an altitude of 287 m (941 ft) above mean sea level (msl). The head of well B is 278 m (912 ft) above msl. The upper 13.7 m (45 ft) section of 25-slot stainless-steel screen is opposite the upper portion of the Franconia formation in the interval between 104 m (341 ft) msl and 90 m (296 ft) msl. The lower 22.9 m (70 ft) section of screen is opposite the entire thickness of the Ironton and Galesville sandstones and small thicknesses of the lowermost Franconia and uppermost Eau Claire formations (Figures 2.3, 2.4). The construction of the wells in the screened interval is shown diagrammatically in Figure 2.4.

The wells are constructed to accommodate thermal expansion in the screened interval and restrain it in the grouted interval. Originally the pumps in the wells were set in both wells at an elevation of 133 m (436 ft); when the wells were modified (Section 5.2), both were installed at the same depth. The turbine pumps in each well are set at a depth of 154 m (505 ft), corresponding to an altitude of 133 m (436 ft) msl in well A and 124 m (406 ft) in well B.

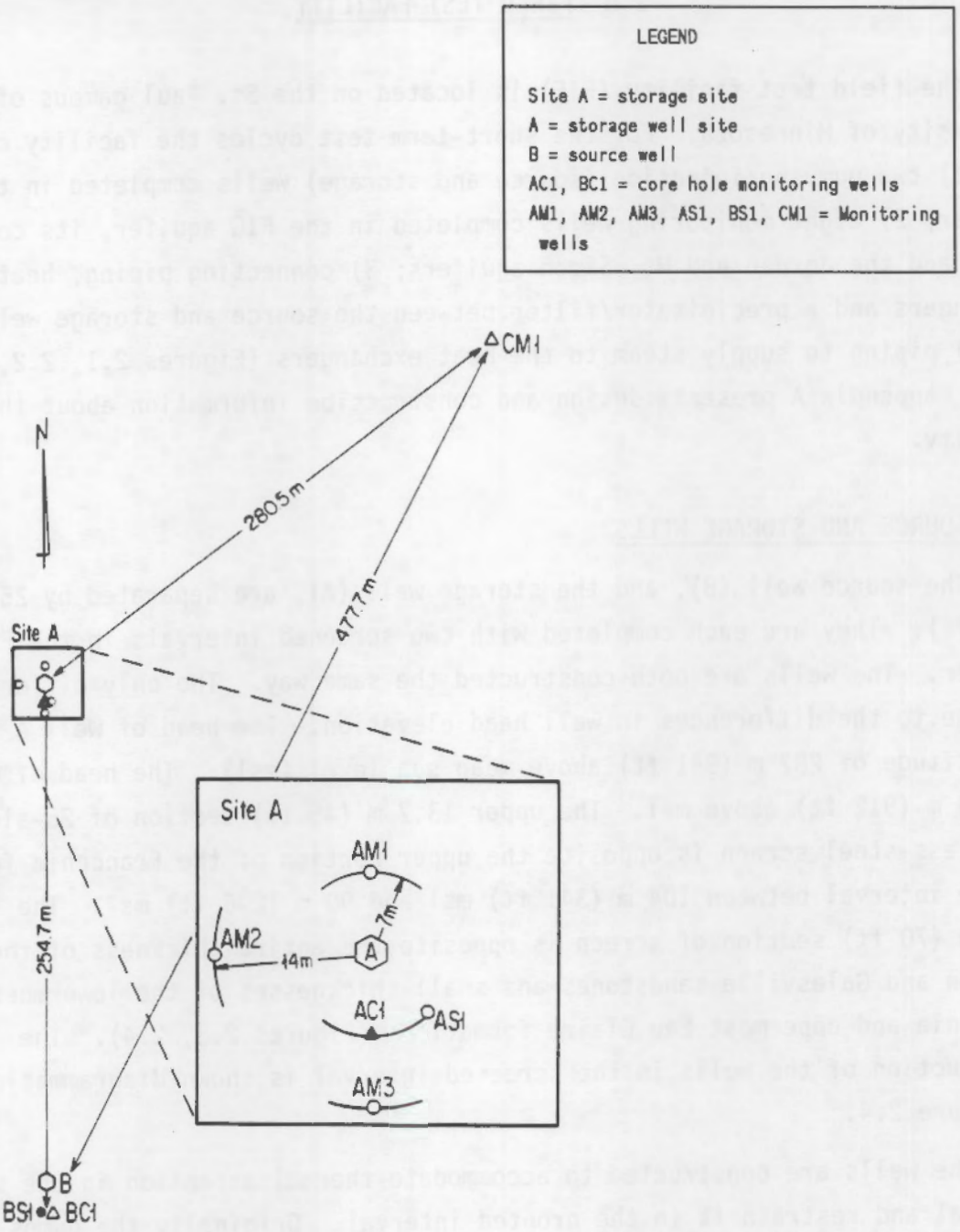

FIGURE 2.1. Well Plan of University of Minnesota St. Paul Field Test Facility

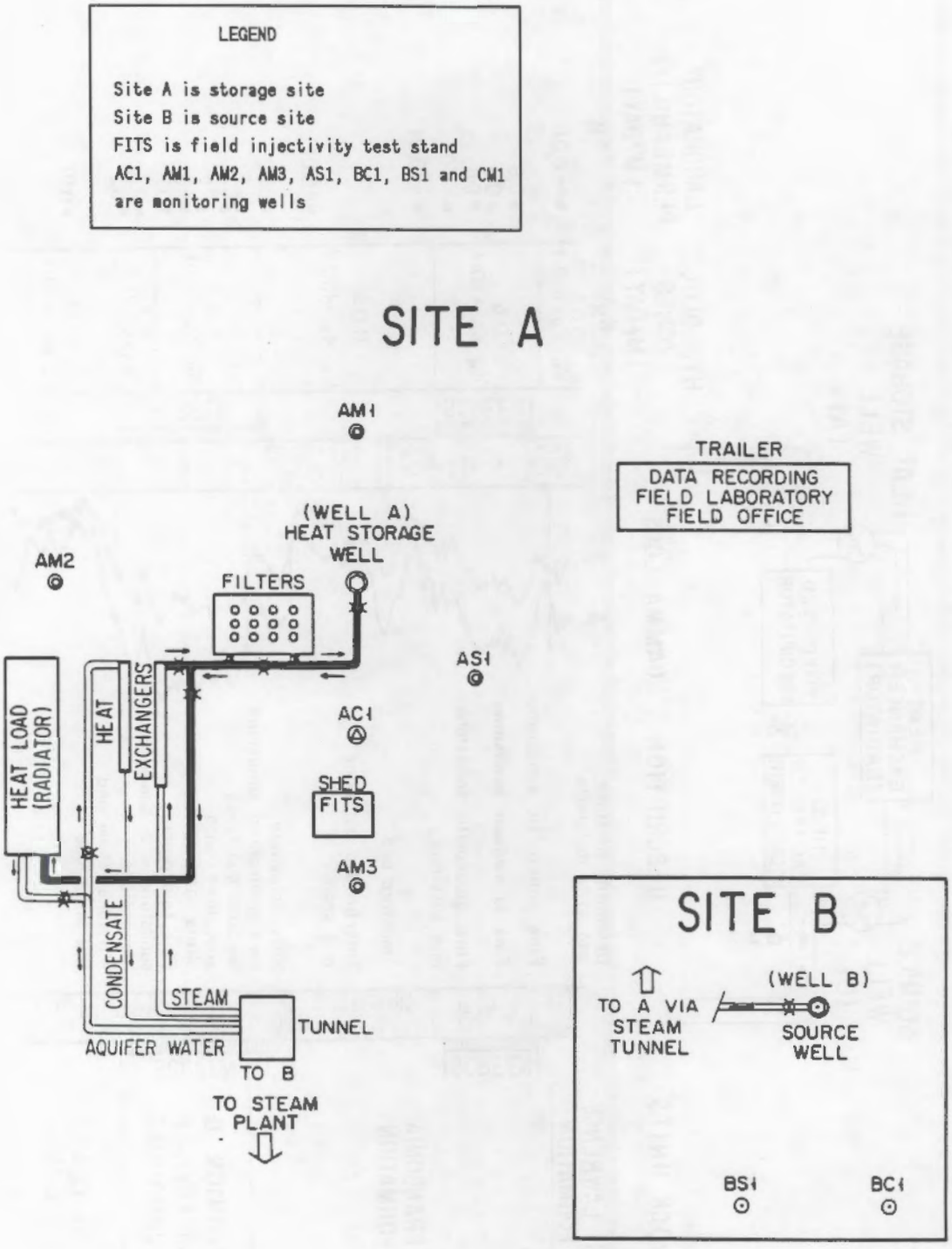

FIGURE 2.2. Sites A and B at the University of Minnesota St. Paul Field Test Facility, Short-Term Cycles

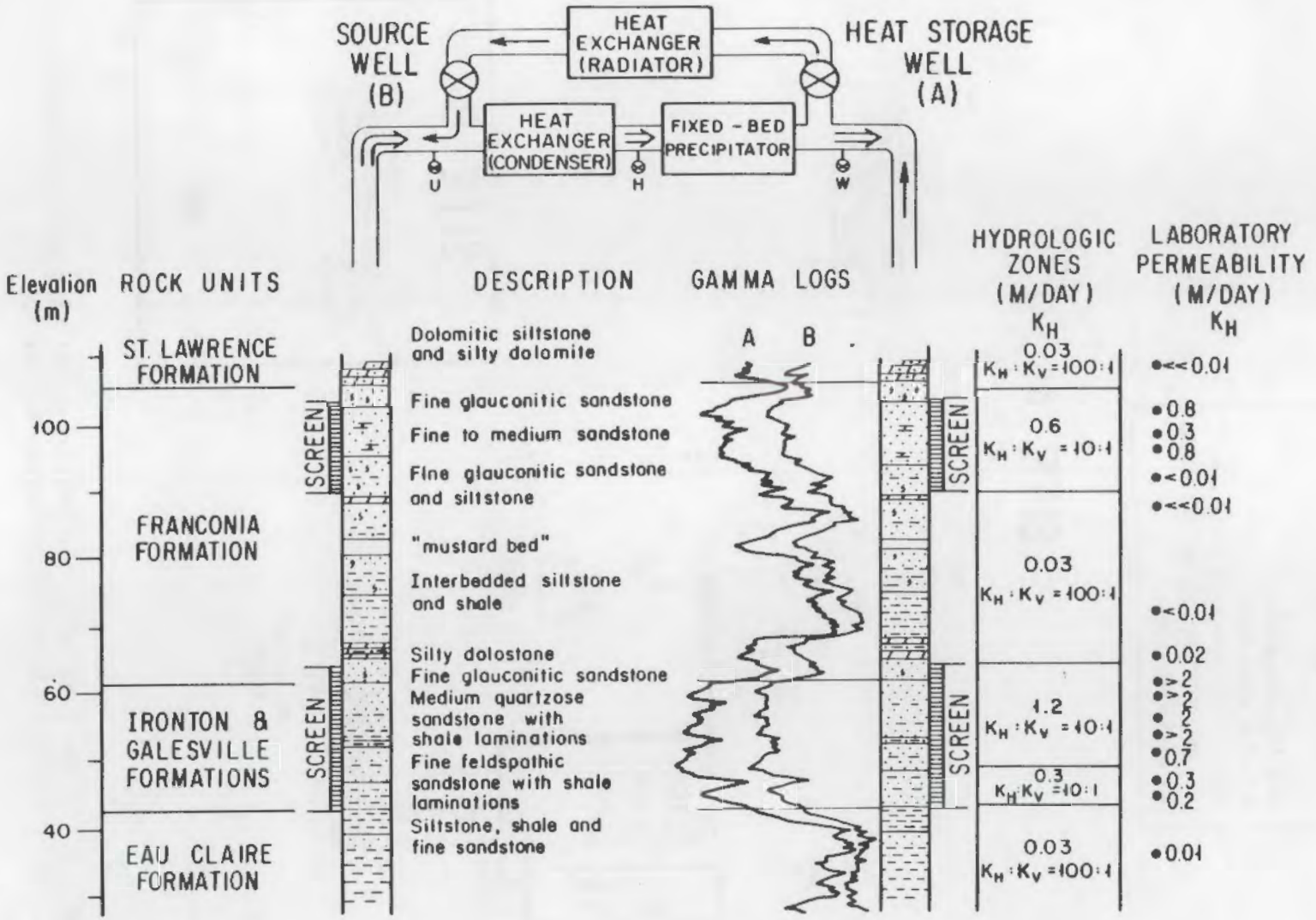

FIGURE 2.3. Stratigraphy and Hydrogeologic Units at the St. Paul ATES Field Test Facility and Flow Path for the Short-Term Cycles

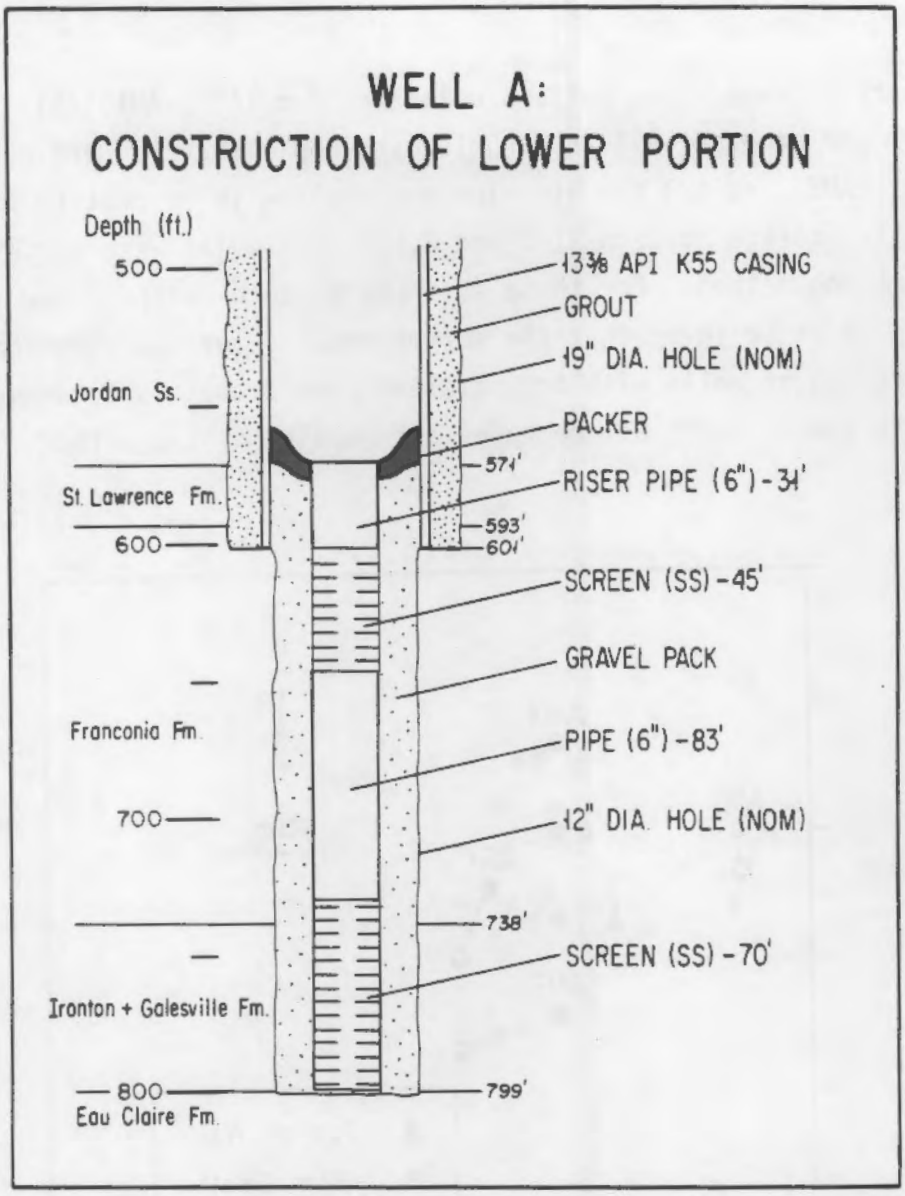

FIGURE 2.4. Diagram of Lower Portion of Well A

2.2 MONITORING WELLS

Eight monitoring wells provide instrumentation for the full stratigraphic interval affected by the system. Parameters measured at monitoring wells are temperature, pressure (water level), and composition of the ground water. Five wells are located at the storage site (site A), two at the source site (site B), and one at site C, located 280.5 m (920 ft) northeast of the storage well to detect any unexpected far-field effects of heat storage (Figure 2.1).

At the storage site, wells are located 7 m (AC1, AM1, AS1) and 14 m (AM2, AM3) from the storage well. Downhole gyroscopic surveys were conducted in wells AM1, AM2, and AM3 to determine positions with respect to the storage well at the storage horizons (Figure 2.5). All wells were surveyed as drilled by a plumb bob method. For those surveyed by both methods, the results were similar. It is believed that the survey results for the plumb bob method suffice for those wells with insufficient pipe diameters to survey with the gyroscopic tool. Table 2.1 compares the results of the methods.

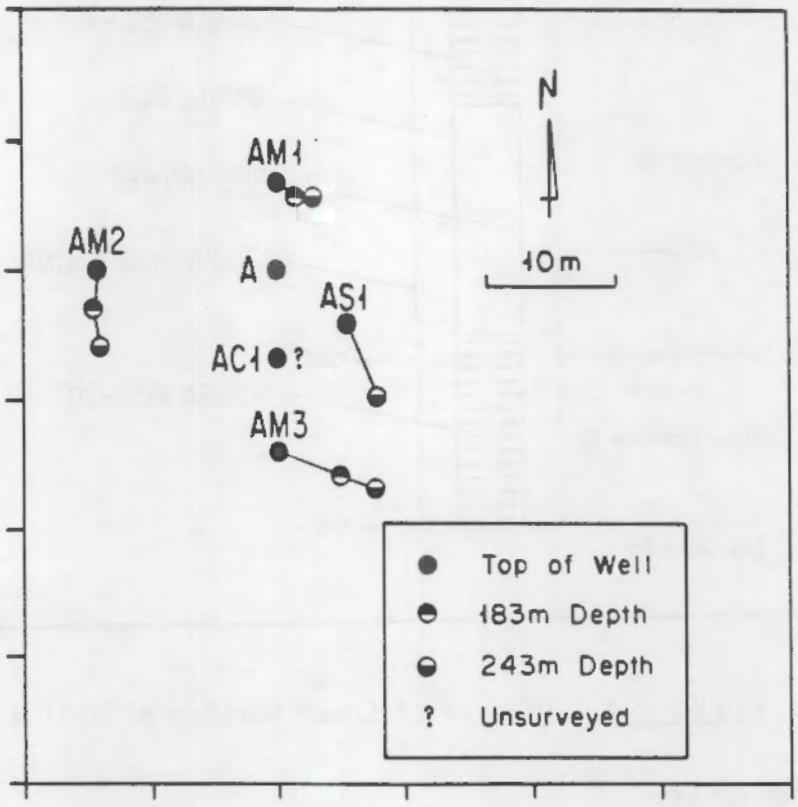

FIGURE 2.5. Plan View of Downhole Gyroscopic Surveys of Wells AM1, AM2, and AM3

TABLE 2.1. Comparison Between Downhole Surveyed Positions of Monitoring Wells at 243 m Depth

Well	Driller's Survey		Gyroscopic Survey		
	Displacement, m	Azimuth, °	Displacement, m	Azimuth, °	Difference, m
AM1	- [a]	-	2.51	99°01'	--
AM2	6.49	173°25'	5.99	178°28'	0.74
AM3	8.38	112°22'	8.27	110°39'	0.27
AS1	6.24	157°20'	- [b]	-	--

(a) instrument failed
(b) unable to survey; pipe too small for tool

All wells at the storage site, have multiple-pair thermocouple strings for monitoring temperatures in the FIG aquifer and the immediately over- and underlying formations (Figure 2.6), with the exception of AC1 which was not used for monitoring because of problems in completion (see Section 4). These thermocouple strings are in closed-end pipes except in AM1, which was constructed with an external thermocouple string attached to the pipe extending to the Eau Claire formation.

At the source site the monitoring wells are 10 m from the source well. These wells have not been gyroscopically surveyed. The location of the bottom of well BS1 is known to be immediately adjacent to well B because during the drilling of well B, well BS1 was intersected at a depth of about 206 m (675 ft). Eight different horizons are monitored at the site, from the Jordan to the Mt. Simon aquifers. Each monitored interval has a 0.9 m (3 ft) screen installed at the depths indicated in Figure 2.4. The Mt. Simon and Jordan pipes are to provide samples for water analyses as well as observing pressure (water level) and temperature. The remaining pipes are for monitoring pressure (water level) and temperature.

Water samples were collected from the Jordan, Mt. Simon, and FIG aquifers at site A before and after all the tests conducted. The 0.03-m (1.25-in.) pipes in monitor wells AM1, AM2, AS1, BC1, BS1, and CM1 are the sampling and

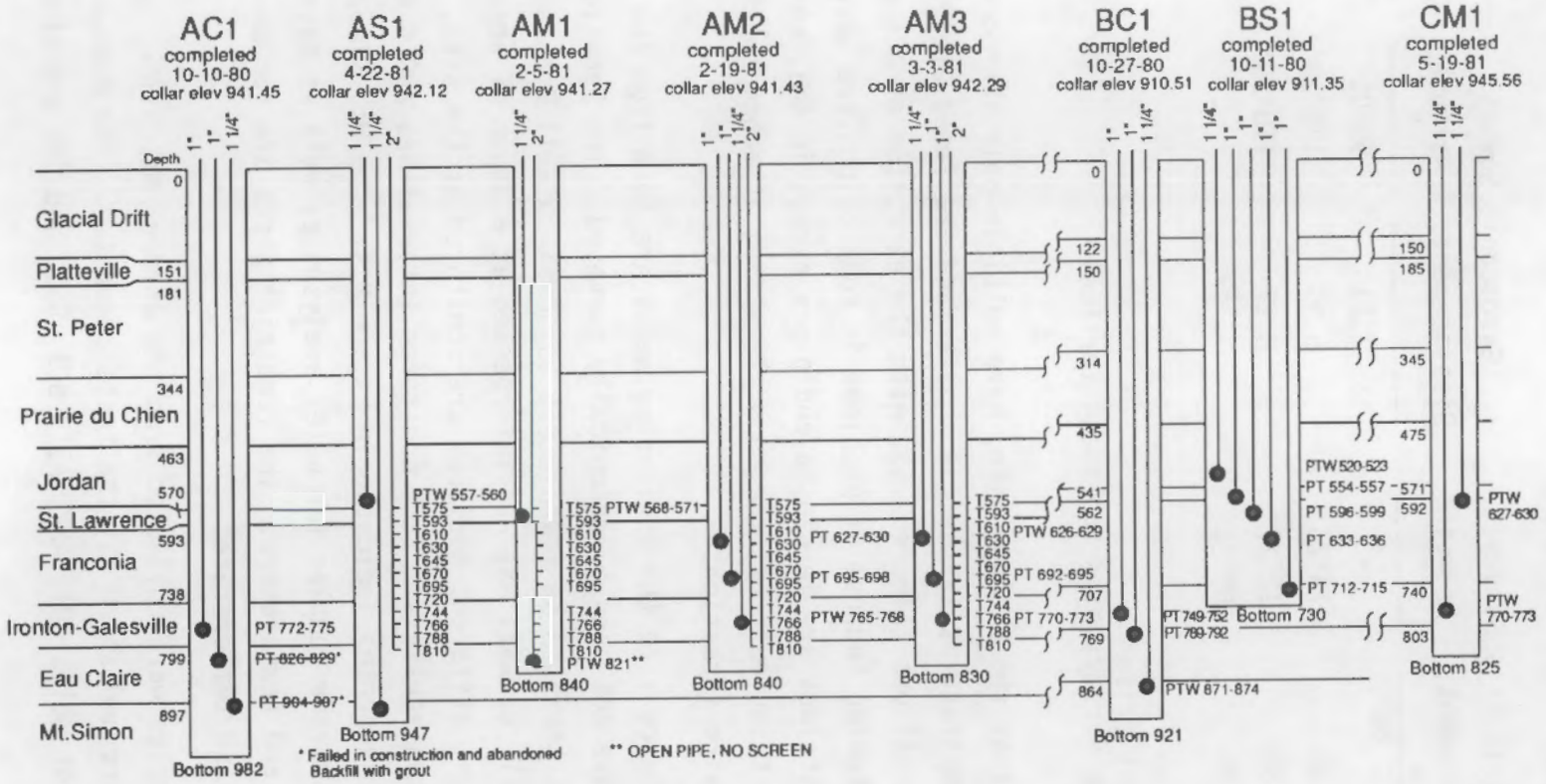

FIGURE 2.6. Monitor Well Instrumentation

water level measuring (piezometer) pipes. The sampling pipe installed in AM3 was plugged, apparently with grout during construction, and the pipe in the upper Franconia in well CM1 was accidently plugged with a pump while attempting to sample water (see Section 6).

2.3 CONNECTIVE PIPING, HEAT EXCHANGERS, AND PRECIPITATOR

The physical arrangement of the facilities at the site is presented in Figure 2.2. Flow path of the aquifer water during the cycles is presented in Figure 2.3. A description follows.

2.3.1 Piping and Heat Exchangers

Piping connecting sites A and B, and from the campus steam plant to site B, is routed through a pre-existing steam and utilities tunnel which passes under sites A and B. A provision for sending water from the wells to waste, via the existing storm sewer, was added so that the system may be flushed before beginning injection or recovery, and so that pumping tests can be conducted and, if necessary, pumping out heated water at the conclusion of the project can be done. Six-inch lines are used for steam and connective piping. The condensate return line is 2-in., and lines to waste are 4-in.

The aquifer water is heated in a tube-and-shell subcooler and tube-and-shell condenser connected in series. The aquifer water is on the tube side, and the 150 psia steam and condensate are on the shell side. Both exchangers are two-pass on the tube side and single-pass on the shell side. Temperature of the aquifer water is regulated during injection by a self-operated valve controlled by a temperature bulb in the aquifer water line downstream of the condenser.

A fan-cooled water-to-air heat exchanger (radiator) is the simulated heating load for experimental cycles. Temperature of the water leaving the radiator controls the operation of the radiator fans when operated in an automatic mode. During short-term Cycles 1 and 2, the radiator fans were not turned on because the water recovered was all cooler than 85°C, the planned maximum temperature for well B. During Cycles 3 and 4, the fans were operated when the recovered water was above 85°C.

2.3.2 Precipitator

The precipitator/filter was added to the system when it became clear during the initial hot-water injection attempt (Sections 5 and 6) that severe scaling in the storage well would take place unless a method to prevent scaling in the well was found. Permit restrictions specifically stated that no water treatment chemicals could be added. This restriction eliminated from consideration standard water treatments (for example, ion-exchange softening) without a major change in the permit. To complete the short-term cycles, a precipitator/filter assembly consisting of a column filled with sized, high-purity limestone ($CaCO_3$) was designed, tested, and installed. The purpose of the precipitator/filter was to speed the precipitation of the $CaCO_3$ from hot water and filter any crystallites produced so that the degree of supersaturation of the injected water was low enough so that precipitation was not a problem. Sections 5 and 6 describe the precipitators and their operation. For the short-term cycles this solution was acceptable. For a continuing operation, an automated method of switching or recycling media and cleaning the heat exchanger would be necessary. Alternatively, another method of preventing scaling would be satisfactory. Sections 5 and 6 outline the operations of the filters.

3.0 GEOLOGY AND HYDROGEOLOGY

3.1 GEOLOGIC SETTING

The ATES FTF lies near the center of the Twin Cities Basin. This basinal feature overlies the northern portion of a Paleozoic depositional lowland called the Hollandale Embayment, which extends from the Ancestral Forest City Basin in Iowa into southeastern Minnesota and western Wisconsin (Austin 1969; Mossler 1972). The Twin Cities Basin is delineated by closure of structural contours on Paleozoic formations (Figure 3.1). Near its center, the basin is estimated to contain 1,525 m (5,000 ft) of sedimentary rocks (Mossler 1972). The lower 1,200 (4,000 ft) consist of Middle Proterozoic clastic rocks and the upper 1,000 ft (305 m) contain Paleozoic sandstone, siltstone, shale, and dolomite. Because of the basinal structure, the oldest rocks of the sequence subcrop and crop out near the periphery of the basin and successively younger strata occur toward the center.

The bedrock in most of the area is overlain by Quaternary, glacially derived sediments consisting of till, outwash, and lake sediments. The bedrock surface is dissected by a system of valleys; most are now filled with Quaternary sediments. Quaternary materials typically are less than 52 m (170 ft) but locally as thick as 183 m (600 ft). Bedrock outcrops occur predominantly adjacent to the Mississippi, Minnesota, and St. Croix rivers and their tributaries. Much of what is known about the rocks in the central part of the basin is from drilling records and samples from thousands of water wells and test borings. The major bedrock formations of the Twin Cities Basin are described in Figure 3.2.

3.2 HYDROGEOLOGY

The Twin Cities Basin is a hydrogeologic artesian basin that contains four major bedrock aquifers and variable water-yielding Quaternary sediments. The Quaternary materials are only locally utilized, although there typically is a perched water table, particularly at the bedrock-drift contact. The four major bedrock aquifers are described below, and some generalized hydrologic parameters are given in Tables 3.1 and 3.2. Specific hydrologic data and

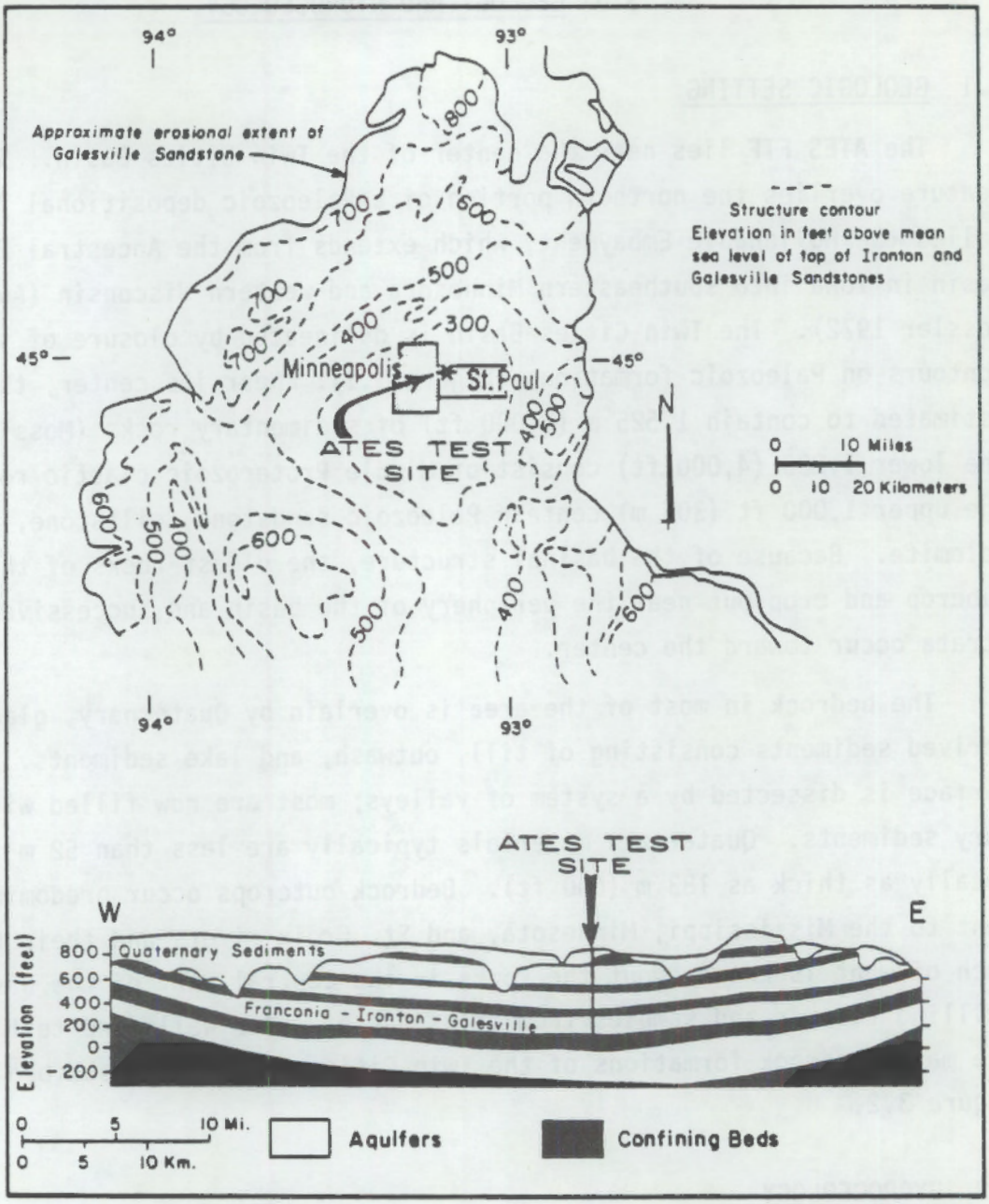

FIGURE 3.1. Structural Contour Map of the Top of the Ironton and Galesville Sandstones Showing the Structure of the Twin Cities Basin (modified from Mossler, 1983), and Generalized Geologic Section Through the ATES Test Site

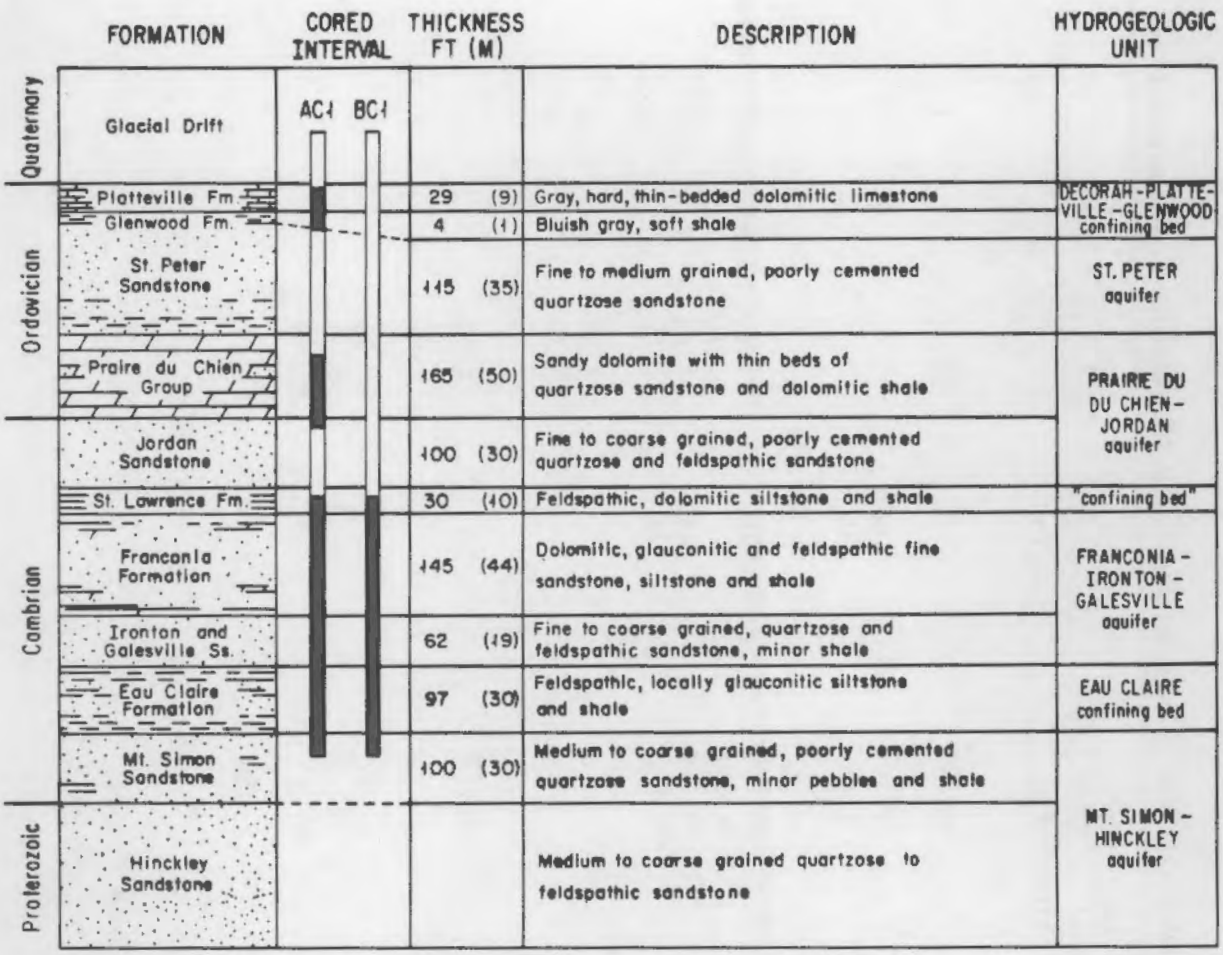

FIGURE 3.2. Generalized Stratigraphic Section at the ATES Test Site. Thicknesses are from Core Hole AC1

TABLE 3.1. Laboratory Permeability and Effective Porosity of Samples from Core BC1

Rock Unit	Depth (ft)	Permeability (millidarcies) Horizontal	Permeability (millidarcies) Vertical	Horizontal/ Vertical Ratio	Effective Porosity, %	Hydrologic Zone
St. Lawrence formation	560.5	0.323	<0.001	>300	16.40	1
Franconia formation	579	933.0	<0.1	>1000	23.80	2
	588	340.5	3.79	90	30.38	2
	596	974.6	736.6	1.3	30.42	2
	606	3.52	2.65	1.3	27.10	2
	620.5	2.05	<0.1	>20	25.98	3
	641.2	0.006	<0.001	>6	30.18	3
	673.6	4.79	0.016	300	34.12	3
	697	17.87	<0.1	180	23.56	3
Ironton sandstone	710	6039[a]	-	-	24.84	4
	717.7	-	-	-	18.35	4
Ironton-Galesville sandstone	729	2353	41.67	56	24.18	4
	739.2	5661[b]	-	-	25.77	4
Galesville sandstone	746	845.0	25.97	33	23.99	
	760	390.4	345.87	31.1	25.78	4
	766.4	283.1	205.9	1.4	28.68	5
Eau Claire formation	797	14.44	2.058	7	31.57	6

(a) Friable sample; determined on repacked sample.
(b) Unable to determine; sample flowed out of holder.

TABLE 3.2. Summary of Hydrogeologic Parameters in the Major Bedrock Aquifers in the Twin Cities (metric conversions in parentheses) (summarized from Madsen and Norvitch 1979; (Kanivetsky and Walton 1979)

Aquifer	SWL(a) in feet (meters)	Transmissivity gpd/ft (m^2/day)	Storage Coefficient	Hydraulic Conductivity gpd/ft^2 (m/day)	Porosity %
St. Peter	760 (232)	18,000 - 25,000 (223 - 310)	9.0×10^{-5} to 9.85×10^{-3}	115-138 (4.7-5.5)	28-30
Prairie du Chien-Jordan	775 (236)	100,000 (1,240)	5×10^{-5} to 3×10^{-4}	400 (16)	30
Franconia	772 (235)				
Ironton	761 (232)	> 30,000 (370)	> 1×10^{-6} to 1×10^{-4}	> 15 (0.6)	> variable (see Table 3.3)
Galesville	759 (231)				
Mt. Simon-Hinckley	680 (207)	30,000 (370)	1×10^{-6} to 1×10^{-2}	175 (7)	no data

(a) Static water level above MSL at Site A

test results of the bedrock aquifers and confining beds are given in sections of this report and Miller (1984).

3.2.1 St. Peter Aquifer

The St. Peter sandstone has been used extensively in the Twin Cities Basin for tunnel and sewer construction, and less commonly for underground buildings, but its use for water supply is relatively minor. At the ATES site, the St. Peter is capped by the Platteville-Glenwood confining bed. Its entire 50 m (163 ft) thick section is saturated and has a small artesian head of about 1.5 m (5 ft). Water table conditions exist southwest of the site. Shale beds in the basal St. Peter separate it from the underlying Prairie du Chien-Jordan aquifer.

3.2.2 Prairie du Chien-Jordan Aquifer

The Prairie du Chien Group and the Jordan sandstone comprise the aquifer most commonly used for ground water in the Twin Cities Basin. The aquifer is under artesian conditions with a static water level approximately 3 to 5 m (10 to 15 ft) above that of the St. Peter aquifer (Table 3.2). The type of porosity is dependent on rock type: dolomite of the Prairie du Chien group has secondary vug and fracture porosity; the Jordan sandstone has primary intergranular porosity.

3.2.3 Franconia-Ironton-Galesville (FIG) Aquifer

The FIG aquifer is not used extensively for water resources except near the periphery of the Twin Cities Basin. The aquifer is heterogeneous and is divided into five distinct geohydrologic zones (Figure 2.3), three within the Franconia formation, and two in the Ironton and Galesville sandstones. The heterogeneity of the aquifer is further indicated by variable static water levels (Table 3.2).

3.2.4 Mt. Simon-Hinckley Aquifer

This aquifer is used particularly for municipal and industrial water supplies where high yields are essential. The Mt. Simon-Hinckley aquifer is separated from the FIG aquifer by the Eau Claire formation. The ATES drill hole AC1 penetrated 26 m (85 ft) of the Mt. Simon sandstone and did not intersect the contact with the underlying Hinckley sandstone.

3.3 SITE GEOLOGY

The cores from holes AC1 and BC1, and the cuttings and downhole geophysical data from all holes were used to characterize the geology of the ATES site. These data indicate that the top surface of bedrock has gentle relief with elevations at sites A, B, and C (Figure 2.1) of 241 m (790 ft), 240 m (788 ft), and 248 m (812 ft) above msl, respectively. The thicknesses of unconsolidated sediments overlying bedrock are 46 m (151 ft), 37 m (122 ft), and 41 m (133 ft) at sites A, B, and C, respectively.

Particular attention is given in this geologic description to the units of the FIG aquifer (Franconia formation and Ironton and Galesville sandstones) and the confining beds that overlie (St. Lawrence formation) and underlie (Eau Claire formation) the aquifer. The degree of correlation of these units between sites A and B is shown in Figures 2.3, 3.2, 3.3, and C.1. Cores from both AC1 and BC1 were described in detail; however, because the units are correlative, a detailed lithologic log is illustrated only for core AC1 (Figure C.2). The modal compositions of samples from AC1 are given in Table 3.3 and plotted for classification in Figure 3.4. Photographs of some typical bedding and lithologic characteristics are shown in Figure 3.5.

3.3.1 St. Lawrence Formation

Dolomitic siltstone and intraclastic conglomerate composed of flat dolomite pebbles make up more than 85% of the St. Lawrence formation. The minor rock types are laminated mudstone and silty and sandy dolomite. The formation is laminated to thinly bedded, although in some parts bedding is obscure due to the presence of burrows. The basal contact is marked by a moderately abrupt increase in the abundance of glauconitic sandstone. The major mineralogic components are dolomite and K-feldspar; quartz and glauconite typically are minor. The samples are classified on Figure 3.4 as highly feldspathic arenites; however this classification scheme ignores dolomite content. A more appropriate term might be highly feldspathic, dolomitic arenites. Vugs occur in several beds, but particularly in the conglomeratic parts where dolomitic intraclasts and matrix were partially removed by dissolution (Figure 3.5a). In general, porosity is moderately low (Tables 3.1 and 3.3) and is a combination of intergranular, intercrystalline and secondary types. Note on

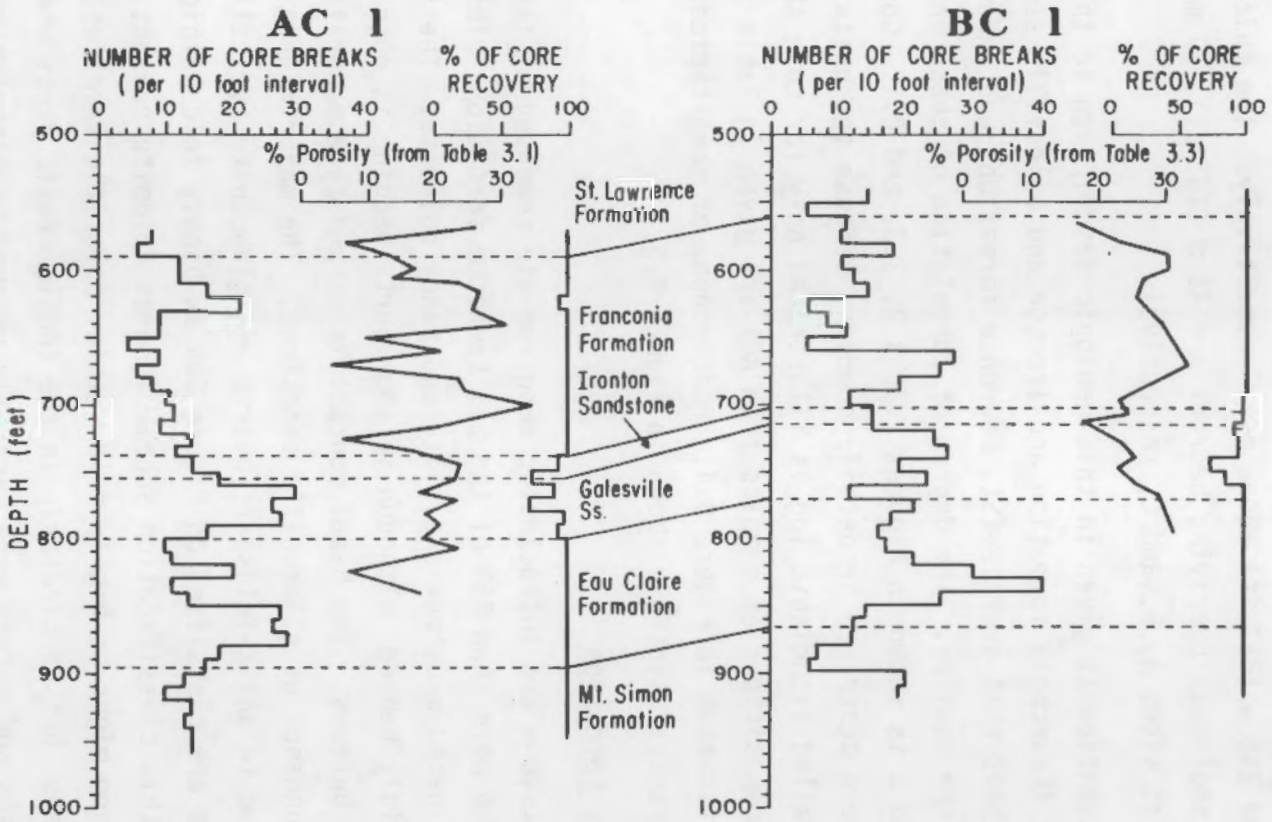

FIGURE 3.3. Number of Core Breaks per 10-ft Interval, Percentage of Core Recovery, and Porosity of Selected Parts of Cores AC1 and BC1

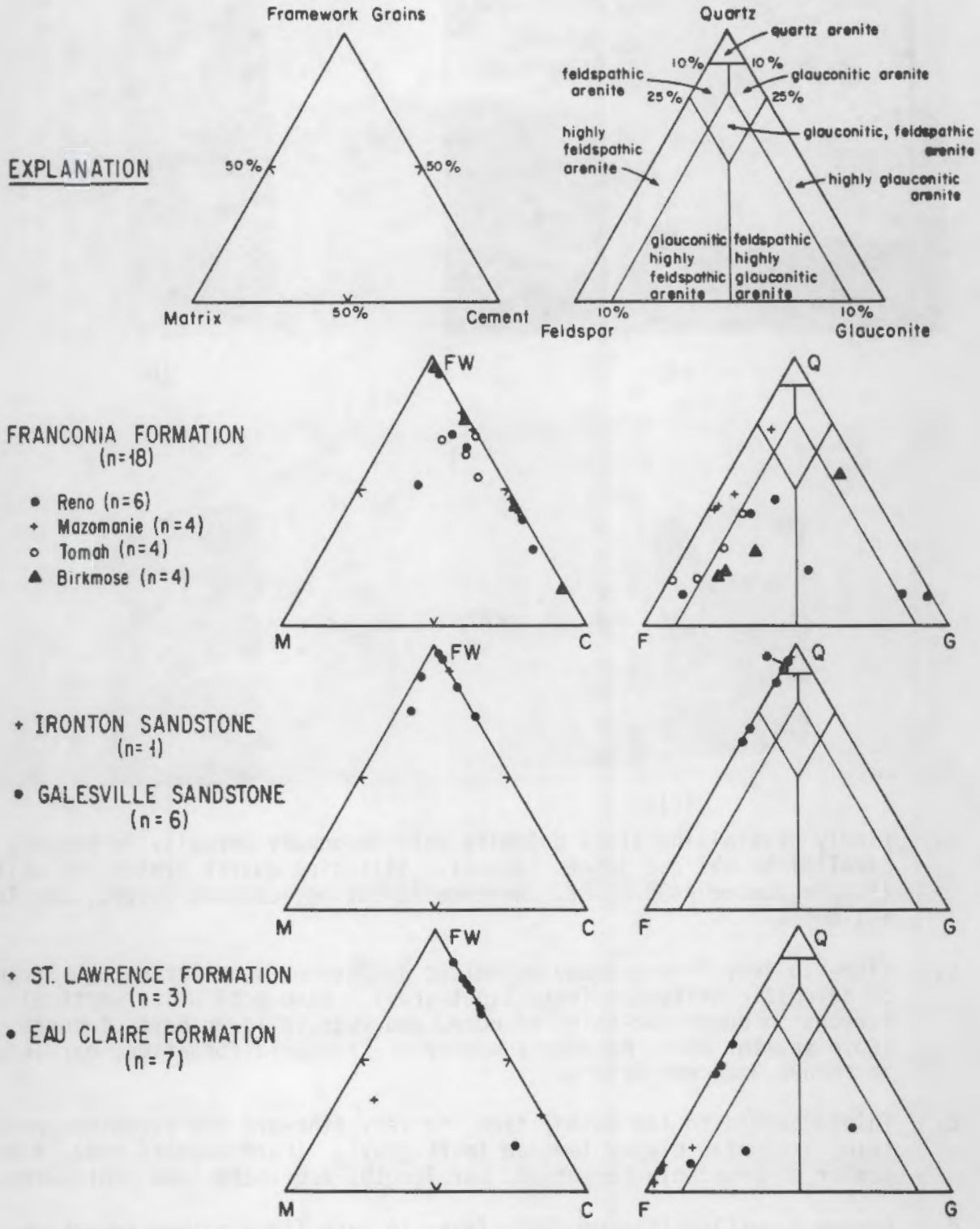

FIGURE 3.4. Classification of Arenites Based on Modes of Selected Samples of Core AC1. Classification system of Odom (1975); n equals number of samples

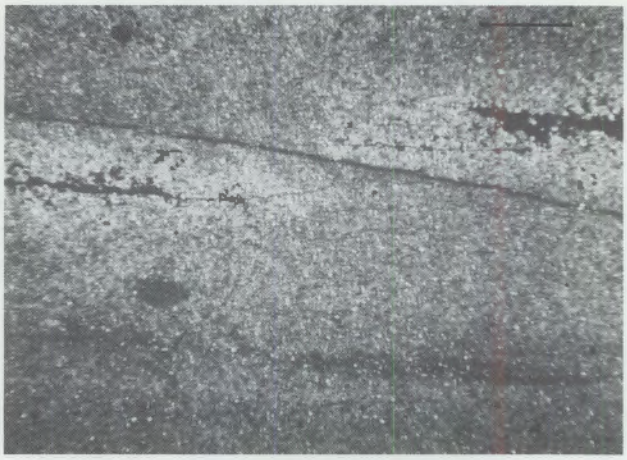

(a)

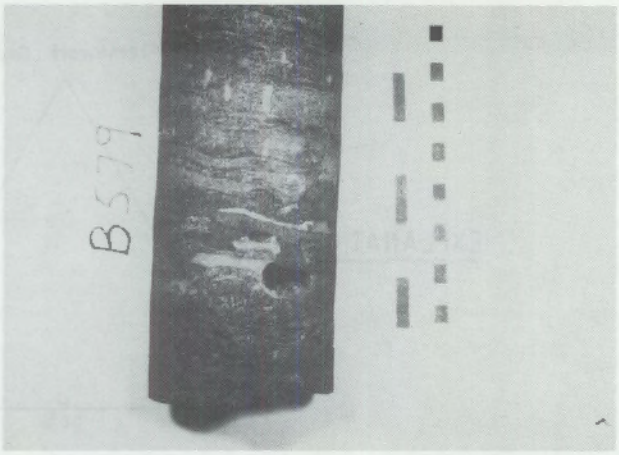

(b)

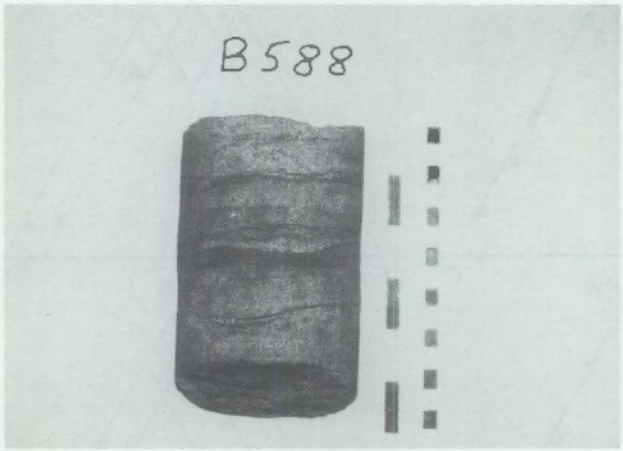

(c)

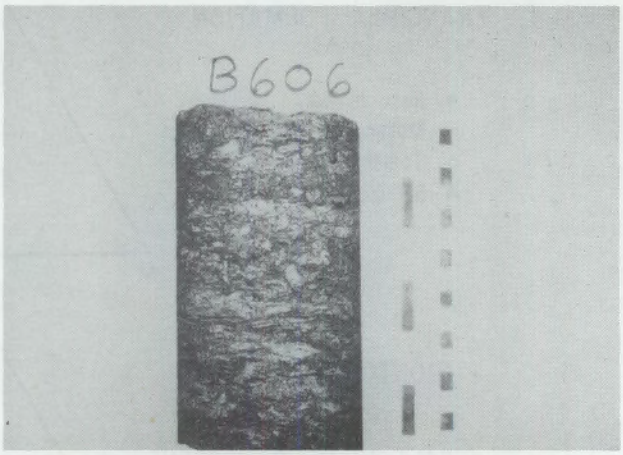

(d)

a. Finely crystalline silty dolomite with secondary porosity in bedding parallel to oblique joints (black). Silt-size quartz grains are white. (Sample number A580.8, St. Lawrence formation, crossed polars, bar length = 1 mm)

b. Fine- to very fine-grained dolomitic sandstone, with irregular intraclasts of dolomitic siltstone (very light gray). Also note white vertical burrows in upper one-third of core, and vugs in lower part of core. (Core segment B579, Mazomanie member of Franconia formation, bar lengths in inches and centimeters)

c. Thinly bedded to laminated, fine- to very fine-grained sandstone with thin, irregular clayey laminae (dark gray). (Core segment B588, Mazomanie member of Franconia formation, bar lengths are inches and centimeters.)

d. Burrow - mottled (bioturbated) fine- to very fine-grained sandstone. (Core segment B606, Reno member of Franconia formation, bar lengths are inches and centimeters)

FIGURE 3.5. Photographs of Typical Rock Types and Bedding Features

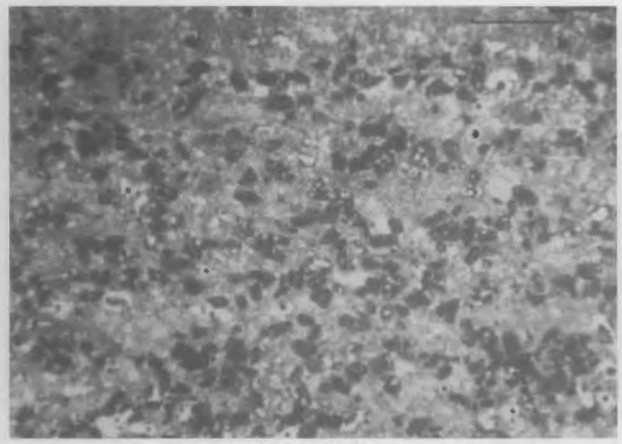

(e)

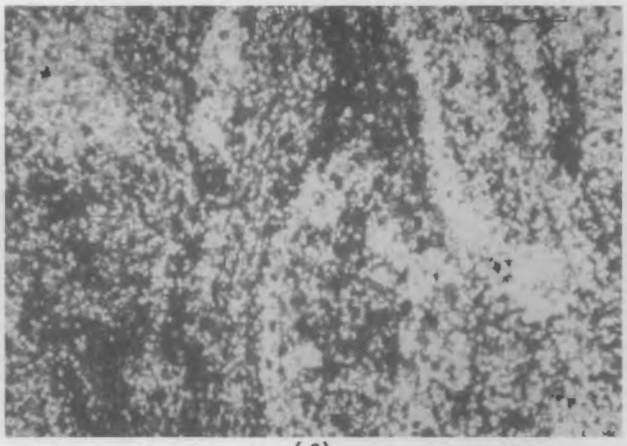

(f)

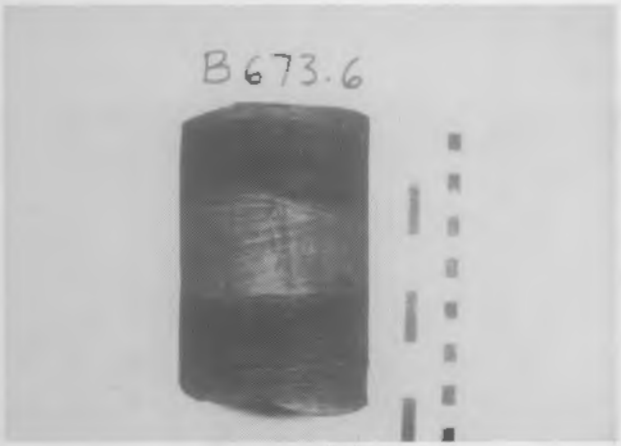

(g)

(h)

e. Dolomitic, glauconitic fine-grained sandstone. Glauconite is dark gray, interstitial dolomite is light gray, sand grains of quartz and K-feldspar are white. (Sample number A649.4, Reno member of the Franconia formation, one polar, bar length = 1 mm)

f. Burrow-mottled fine-grained sandstone. White grains are quartz and K-feldspar. Interstitial dark-colored material is clayey matrix. (Sample number A661.9, Reno member of the Franconia formation, one polar, bar length = 1 mm)

g. Core segment of thinly bedded and cross-bedded, very fine-grained sandstone (light gray) and laminated shale (dark gray). (Segment B673.6, Tomah member of Franconia formation, bar lengths in inches and centimeters)

h. Fine-grained quartz-feldspar-glauconite sandstone (very light gray and white) with irregular interbeds of silty shale (dark gray) and pyrite-rich, dolomitic shale (black-dark gray). (Sample number A691.4, Tomah member of Franconia formation, one polar, bar length = 1 mm)

FIGURE 3.5. Photographs of Typical Rock Types and Bedding Features (contd)

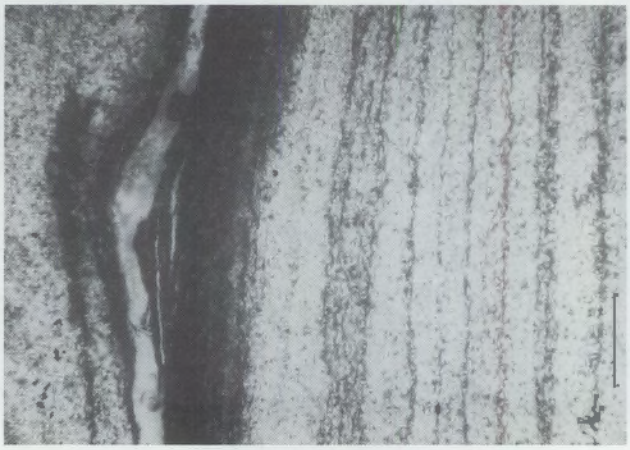

(i)

(j)

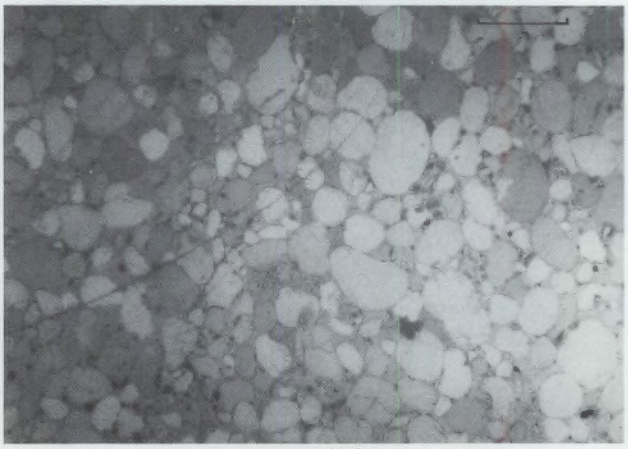

(k)

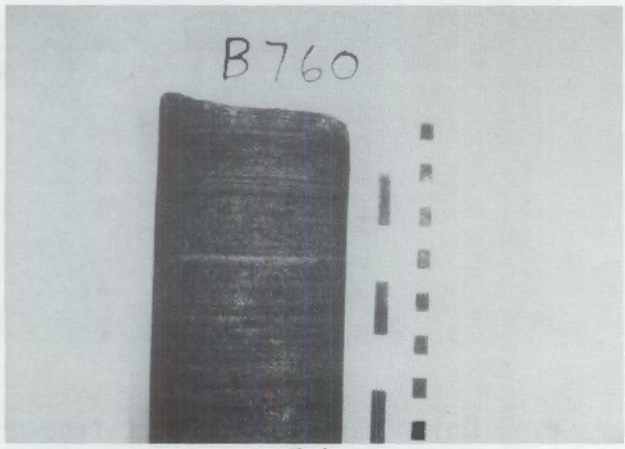

(l)

i. Laminated very fine-grained sandstone (white) and shale (dark). (Sample number B678.8, Tomah member of Franconia formation, one polar, bar length = 1 mm)

j. Glauconitic, fine-grained sandstone. Glauconite is dark gray, white round grains are quartz and feldspar. Note that most porosity is occluded by tightly packed glauconite grains. (Sample number A734.8, Birkmose member of Franconia formation, one polar, bar length = 1 mm)

k. Medium- to coarse-grained quartz sandstone. Note intergranular porosity (stippled-appearing, gray). (Sample number A741.5, Ironton sandstone, one polar, bar length = 1 mm)

l. Thinly bedded sandstone. (Segment B760, Galesville sandstone, bar lengths are inches and centimeters)

FIGURE 3.5. Photographs of Typical Rock Types and Bedding Features (contd)

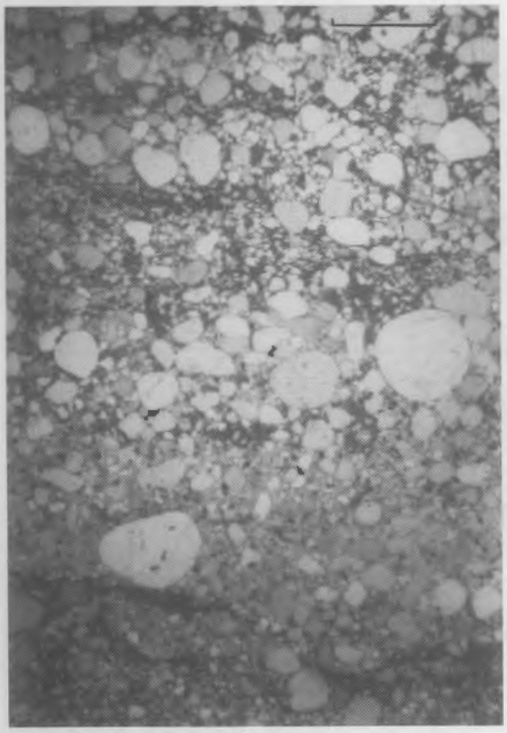

(m)

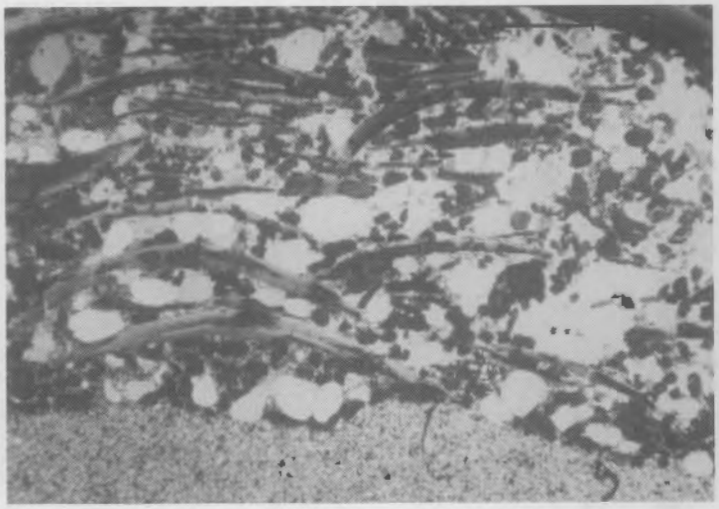

(n)

m. Poorly sorted, fine- to coarse-grained quartzose sandstone with interstitial clayey matrix (dark gray). (Sample number A762.8, Galesville sandstone, one polar, bar length = 1 mm)

n. Upper part contains dark, elongate, arcuate fossils, white, fine- to coarse-grained quartz and medium-grained glauconite (very dark gray); below is quartz- and feldspar-rich siltstone. (Sample number A833.4, Eau Claire formation, one polar, bar length = 1 mm)

FIGURE 3.5. Photographs of Typical Rock Types and Bedding Features (contd)

TABLE 3.3. Modal Mineralogy and Porosity of Selected Samples from Core AC1

Number[a]	Rock Unit[b]	Rock Type[c]	80% Grain Size[d] (mm)	Framework Grains[e]									
				Qtz	KFg	Dolr	Glau	Musc	Opq	RkF	HvyM	Fos	Other
A574.2	SL	Sln	0.01-0.05	5.6	41.1	21.5	-	1.2	0.7	-	0.2	-	-
A580.8	SL	Sln-Sh	0.01-0.03	1.3	28.3	-	-	T	4.7	-	-	-	-
A590.7	SL	Dol,Sln	0.02-0.08	6.7	18.7	T	2.8	-	0.2	-	-	-	-
A596.5	Fr(R)	Ss	0.05-0.2	4.3	19.3	-	32.1	-	0.5	-	0.5	T	-
A607.6	Fr(M)	Ss	0.1-0.25	2.0	6.1	T	2.7	T	1.0	-	-	0.2	-
A610.4	Fr(M)	Ss	0.1-0.25	9.4	17.4	T	1.1	T	T	0.2	T	0.2	-
A616.5	Fr(M)	Ss	0.1-0.2	3.0	34.1	-	1.4	T	0.4	T	T	T	-
A627.3	Fr(M)	Ss	0.1-0.2	9.0	27.0	T	2.3	T	0.5	0.3	0.5	-	-
A638.0	Fr(R)	Ss	0.08-0.15	9.0	15.2	T	16.6	0.2	0.5	0.2	T	0.2	
A649.4(L1)	Fr(R)	Dol	0.05-0.15	4.4	3.6	T	30.0	-	0.3	-	-	-	-
	Fr(R)	Sln	0.01-0.08	3.5	19.4	-	2.5	1.4	0.4	-	-	-	-
A661.9	Fr(R)	Sh,Ss	0.08-0.12	24.8	14.4	0.8	9.2	1.3	0.7	T	0.4	0.6	-
A673.8	Fr(R)	Ss	0.1-0.5	9.7	0.5	-	55.5	0.2	28.3	-	-	1.2	-
A681.7	Fr(T)	Ss	0.05-0.15	31.7	2.28	-	10.4	1.4	0.9	-	0.7	T	1.7
A701.9	Fr(T)	Sln	0.02-0.05	12.0	37.5	-	1.1	4.0	0.4	-	T	0.2	-
	Fr(T)	Ss, Sln	0.05-0.1	16.0	40.7	T	8.4	2.2	1.9	0.2	0.3	0.5	-
A725(L1,2)	Fr(B)	Dol	0.1-0.25	3.9	5.4	-	3.5	-	0.6	-	-	-	
(L3)	Fr(B)	Ss-Sln	0.05-0.15	15.9	40.2	-	14.1	0.7	2.5	-	1.8	0.7	-
(Total)	Fr(B)		0.05-0.25	9.5	21.7	-	8.5	0.3	1.5	-	0.9	0.3	-
A734.8	Fr(B)	Ss	Bi	52.0	6.7	-	33.7	0.2	1.5	-	0.2	3.9	-
A741.5	In	Ss	0.05-0.8	86.7	2.0	-	-	-	1.0	T	0.7	-	-
A752.8	Gv	Ss,Sh	Bi	83.7	1.9	-	-	0.2	0.3	0.9	T	-	-
A762.8	Gv	Ss,Sh	0.01-0.15	65.9	7.8	-	-	0.6	0.2	0.2	0.2	-	-
A771.5	Gv	Ss	Bi	88.9	4.8	-	-	-	0.7	0.2	T	0.2	0.2
A781.9	Gv	Ss	0.2-0.4	90.2	2.1	-	-	-	0.4	0.4	T	0.6	-
A787.8	Gv	Ss	0.05-0.15	49.1	25.6	-	0.1	0.7	1.6	0.3	0.1	0.4	-
A797.3	Gv	Ss	0.05-0.18	65.5	15.1	-	T	0.3	0.8	0.2	0.3	0.5	-
A801.8	EC	Ss	0.05-0.15	53.4	19.6	-	T	0.2	1.9	0.5	0.3	0.7	-
A807.9	EC	Ss,Sh	0.03-0.1	45.5	31.8	T	T	0.5	1.0	T	0.3	1.5	-
A824.7	EC	Dol,Sh	0.01-0.08	8.5	6.3	T	T	0.5	0.6	-	T	2.3	-
A833.4(L1)	EC	Sln	Bi*	7.6	43.9	-	5.5	3.8	0.4	-	-	8.4	-
(L2)	EC	Ss	Bi*	16.3	10.3	-	37.2	0.5	0.3	-	0.3	22.5	-
(L3)	EC	Sln	0.03-0.05	8.2	54.3	-	0.4	4.3	0.8	-	0.4	0.4	-
(Total)	EL			11.0	32.2	-	18.0	2.5	0.5	-	0.2	12.3	-

(a) Different rock types within sample indicated by (L1), (L2), Total = total slide.
(b) SL = St. Lawrence formation, Fr = Franconia formation, Fr(R) = Reno member, Fr(M) = Mazomanie member, Fr(T) = Tomah member, Fr(B) = Birkmose member, In = Ironton sandstone, Gv = Galesville sandstone, EC = Eau Claire formation.
(c) Ss = sandstone, Sln = siltstone, Sh = shale, Dol = dolomite.
(d) Approximate size in millimeters of 80% of the grains. Bi = bimodal, see comments.
(e) Qtz = quartz, KFg = K-feldspar, Dolr = dolomite as replacements of other grains, Glau = glauconite, Musc = muscovite, Opq = opaque minerals, RkF = rock fragments (mostly chert and other quartzose clasts), HvyM = heavy minerals other than opaques, Fos = fossils, Other = other grains: 681.7 and 690.9 = biotite, 771.5 = plagioclase, T = trace amounts.
(f) Dolc = dolomite cement, KFo = K-feldspar overgrowths and cement; Other cements: ** = pyrite, * = quartz overgrowths. T = trace amounts.
(g) Porosity not included in modal analyses.
(h) X = X-rayed sample.

TABLE 3.3. (cont)

Number[a]	Rock Unit[b]	Rock Type[c]	80% Grain Size[d] (mm)	Cement[f] Matrix Clay	Dolc	KFo	Other	Porosity[g] %	Comments[h]
A574.2	SL	Sln	0.01-0.05	T	15.9	13.8	-	26	X
A580.8	SL	Sln-Sh	0.01-0.03	53.1	12.6	-	-	7	X
A590.7	SL	Dol,Sln	0.02-0.08	-	62.4	9.2	-	13	X
A596.5	Fr(R)	Ss	0.05-0.2	4.1	22.0	7.2	-	17	
A607.6	Fr(M)	Ss	0.1-0.25	0.2	54.4	3.4	-	14	
A610.4	Fr(M)	Ss	0.1-0.25	-	43.1	8.6	-	24	X
A618.5	Fr(M)	Ss	0.1-0.2	-	-	21.1	-	27	
A627.3	Fr(M)	Ss	0.1-0.2	-	11.6	19.4	-	28	
A638.0	Fr(R)	Ss	0.08-0.15	6.6	9.3	12.2	-	31	
A649.4(L1)	Fr(R)	Dol	0.05-0.15	-	61.7	-	-	7	
	Fr(R)	Sln	0.01-0.08	1.4	64.4	7.0	-	18	
A661.9	Fr(R)	Sh,Ss	0.08-0.12	27.7	8.3	11.8	-	21	
A673.8	Fr(R)	Ss	0.1-0.5	-	4.6	-	-	5	X
A681.7	Fr(T)	Ss	0.05-0.15	11.5	3.4	15.5	-	24	
A701.9	Fr(T)	Sln	0.02-0.05	6.7	10.5	27.6	-	35	X
	Fr(T)	Ss,Sln	0.05-0.1	-	2.4	27.4	-	21	
A725(L1,2)	Fr(B)	Dol	0.1-0.25	-	84.7	1.9	-	2	
(L3)	Fr(B)	Ss-Sln	0.05-0.15	-	3.3	26.7	-	18	
(Total)	Fr(B)		0.05-0.25	-	46.6	10.7	-	6	
A734.8	Fr(B)	Ss	Bi	1.4	-	0.4	-	17	0.03-0.05 0.1-0.35
A741.5	In	Ss	0.05-0.8	-	-	2.6	**6.6	24	X
A752.8	Gv	Ss,Sh	Bi	11.4	-	0.7	*0.9	23	0.6-1.5 0.1-0.3
A762.8	Gv	Ss,Sh	0.01-0.15	19.8	-	4.1	**1.2	18	
A771.5	Gv	Ss	Bi	-	-	3.7	*1.5	24	0.4-0.9
A781.9	Gv	Ss	0.2-0.4	0.6	-	1.3	**4.5	19	
A787.6	Gv	Ss	0.05-0.15	0.1	T	19.4	**2.5	21	X
A797.3	Gv	Ss	0.05-0.18	1.1	-	16.2	-	28	
A801.8	EC	Ss	0.05-0.15	T	1.5	26.9	**1.0	19	
A807.9	EC	Ss,Sh	0.03-0.1	T	0.2	19.1	-	24	
A824.7	EC	Dol,Sh	0.01-0.08	13.3	65.5	3.0	-	7	
A833.4(L1)	EC	Sln	Bi*	0.8	22.8	6.8	**T	15	
(L2)	EC	Ss	Bi*	-	11.6	1.0	**T	28	
(L3)	EC	Sln	0.03-0.05	-	1.6	29.7	**T	5	
(Total)	EL			0.2	11.7	10.9	**T	18	

(a) Different rock types within sample indicated by (L1), (L2), Total = total slide.
(b) SL = St. Lawrence formation, Fr = Franconia formation, Fr(R) = Reno member, Fr(M) = Mazomanie member, Fr(T) = Tomah member, Fr(B) = Birkmose member, In = Ironton sandstone, Gv = Galesville sandstone, EC = Eau Claire formation.
(c) Ss = sandstone, Sln = siltstone, Sh = shale, Dol = dolomite.
(d) Approximate size in millimeters of 80% of the grains. Bi = bimodal, see comments.
(e) Qtz = quartz, KFg = K-feldspar, Dolr = dolomite as replacements of other grains, Glau = glauconite, Musc = muscovite, Opq = opaque minerals, RkF = rock fragments (mostly chert and other quartzose clasts), HvyM = heavy minerals other than opaques, Fos = fossils, Other = other grains: 681.7 and 690.9 = biotite, 771.5 = plagioclase, T = trace amounts.
(f) Dolc = dolomite cement, KFo = K-feldspar overgrowths and cement; Other cements: ** = pyrite, * = quartz overgrowths. T = trace amounts.
(g) Porosity not included in modal analyses.
(h) X = X-rayed sample.

Table 3.1 that the percentages of porosity are consistently larger than those determined by point counting and listed on Table 3.3. This relationship is true not only for the St. Lawrence but for all formations, and is probably due in part to the difficulty of determining the abundance of very small intergranular and intercrystalline pores by petrographic methods.

3.3.2 Franconia Formation

The Franconia formation is divided into four members (Figures 3.4 and C.1): 1) glauconitic, feldspathic, fine-grained sandstone and siltstone (Reno and Birkmose members); 2) dolomitic, feldspathic, fine-grained sandstone (Mazomanie member); 3) alternating, thin beds of micaceous, feldspathic siltstone and shale (Tomah member); and 4) sandy or silty dolomite and dolomitic, intraclastic conglomerate (Birkmose and Reno members). Significant amounts of the authigenic minerals dolomite and K-feldspar are present. In general, the formation contains moderate to very abundant amounts of glauconite.

The Reno member in the upper Franconia formation contains glauconitic, fine- and very fine-grained sandstone in beds as thick as 1.5 ft (0.5 m). Typical beds are burrowed at the top and grade downward to laminated at the base. Beds of intraclastic conglomerate with intraclasts of very fine sandstone are common.

The Mazomanie member contains abundant quartz, dolomite and feldspar, but minor glauconite. Although burrow-mottled beds similar to those in the Reno occur; horizontal, cross and wavy bedding types are most common (Figures 3.5b,c).

The portion of the Reno member that underlies the Mazomanie is similar to that above it, but also contains a 0.6 m (2 ft) thick massive glauconitic dolomite bed (Figure 3.5d,e). The base of the Reno member contains a 1.5 m (5 ft) thick unit informally termed the "mustard bed" because of its light olive-brown color (5G5/6)[(a)] and earthy texture and aroma. This unit contains a very large percentage of glauconite which is partially altered to limonite and goethite. The mustard bed is characterized by a distinctive low on gamma-ray logs, both within and adjacent to the ATES site.

(a) Munsell color designation.

The Tomah member is an interbedded sequence of fine- to very fine grained, silty sandstone beds and siltstone or shale beds (Figures 3.5g,h,i). Most shale beds are less than 0.2 cm thick, and the thickness of sandstone-shale pairs of beds is typically less than 1.5 cm. The core in this interval is friable, and breaks are common along sandstone-shale bedding planes (Figure 3.3).

The top of the Birkmose member is marked by the appearance of glauconitic, silty dolomite, dolomitic siltstone and intraclastic conglomerate. Below this is a sequence of burrow-mottled to laminated, fine- to very fine-grained glauconitic sandstone with minor shale beds (Figure 3.5j), which extend to the base of the member. Some beds near the base of the Franconia formation contain medium- and coarse-grained, fossiliferous sandstone similar to the Ironton sandstone. These beds grade upward into the fine sandstone and shale, and downward into a highly burrow-mottled, glauconitic, fine sandstone. The lower contact of the Franconia is placed at the base of the lowest glauconitic beds.

The types and percentages of porosity are dependent on rock type (see Tables 3.1 and 3.3). The glauconitic, feldspathic, fine-grained sandstone and siltstone have a moderately large percentage of intergranular porosity. The dolomitic, feldspathic, fine-grained sandstone has intergranular and secondary (vug) porosity. This rock type makes up much of the relatively permeable portion of the Franconia formation (Mazomanie member). Cementation in these beds is variable and both friable and well-indurated beds occur. Porosity is to joints (fractures) and vugs in units composed of alternating feldspathic siltstone and shale beds. The majority of joints are nearly vertical and vugs typically are less than 0.5 cm in diameter. The rocks which contain abundant dolomite exhibit a large range of secondary porosities, depending on the amount of dissolution of dolomite cement.

3.3.3 Ironton and Galesville Sandstones

The Ironton and Galesville sandstones consist of medium-, coarse-, and fine-grained quartzose sandstone, fine-grained feldspathic sandstone, and minor thin shale (Figure 3.4). The Ironton sandstone is about 3 m (10 ft) thick and consists of coarse- to medium-grained quartzose sandstone (Figure 3.5k)

with large-scale cross bedding and many fossiliferous intervals. The two formations could not be differentiated on gamma logs, but the contact is placed at the change from predominantly coarse-grained sandstone above, to mostly medium- and fine-grained sandstone below. The upper 5.7 m (18.6 ft) of the Galesville contain medium and minor coarse-grained, fossiliferous quartzose sandstone with bedding features similar to those in the overlying Ironton. Discontinuous beds of fine-grained sandstone and thin beds of shale make up a small percentage of this unit. Below this is a 0.8 m (2.7 ft) thick interval of poorly sorted, fine-grained, feldspathic sandstone with minor shale beds (Figure 3.5l). This is underlain by 6.3 m (20.7 ft) of friable, medium- and fine-grained quartzose sandstone (Figure 3.5m). The basal 3 m (10 ft) of the Galesville contains fine- to very fine-grained sandstone and minor shale. The basal contact is gradational with the underlying Eau Claire formation. A significant percentage of both sandstones is friable and core recovery was relatively low (see Figure 3.3). The porosity is intergranular, and both porosity and permeability values are moderately large (Table 3.1).

3.3.4 Eau Claire Formation

The Eau Claire formation consists of thinly bedded to laminated alternations of the following fine-grained rock types: (1) silty feldspathic sandstone, (2) feldspathic siltstones, (3) silty mudstone, (4) shale, and (5) minor silty dolomite. The variability of rock types is reflected in the modal mineralogy data (Table 3.3) and in Figure 3.5n. Glauconite is abundant in some beds. Fossil fragments are moderately abundant and some beds contain more than 50% of inarticulate brachiopod shell fragments. The upper contact of the formation is marked by an increase in the abundance of shale and silt. The basal contact is placed at the appearance of coarse-grained quartzose sandstone of the Mt. Simon formation. Porosity in the Eau Claire is dominantly intergranular and extremely variable due to the diversity of rock types and local occlusion of porosity by secondary dolomite and K-feldspar.

3.4 PETROLOGY

Detailed petrographic descriptions were done only for AC1; however, thin sections of core BC1 were used for comparison. Samples for petrologic study

were taken at intervals selected to document the compositional variability in the major rock units of the FIG aquifer and its confining beds. The thin sections of cores AC1 were point-counted (500 points per section) for estimation of modal mineralogy and 300 additional points were counted to approximate porosity. The results are shown on Table 3.3. Most thin sections were stained with cobaltinitrate to aid identification of K-feldspar. Many of the sections were X-rayed to confirm mineralogic identification.

In general, the rock samples contain variable amounts of quartz, K-feldspar, dolomite, and glauconite, with only minor amounts of other minerals. Figure 3.6 shows photomicrographs of some characteristic petrographic features. The following petrologic description and Table 3.3 are arranged into categories of framework grains, matrix, and cement minerals.

3.4.1 Framework Grains

The common detrital grains are quartz, K-feldspar, and glauconite. Intraclasts are abundant in some units and typically consist of elongate, rounded clasts of dolomitic mudstone (micrite) or very fine-grained sandstone. Because total sample compositions (modes) are more significant to this study than the sedimentologic aspects, intraclasts do not appear on Table 3.3 as a separate category, and instead, the components of intraclasts are included in the modal mineralogy.

3.4.1.1 Quartz

Quartz is ubiquitous in all stratigraphic units but is most abundant (>75%) in the Ironton and Galesville sandstones. Detrital quartz grains vary from angular to rounded; the majority, however, are moderately well rounded, clear, unit (single crystal) grains. Several unit grains are surrounded by abraded quartz overgrowths, indicating derivation from previously lithified sandstone. Polycrystalline grains occur mainly in coarse-grained sandstone. These characteristics indicate that the quartz-rich rocks are moderately mature to mature.

3.4.1.2 Feldspar

Microcline with distinctive grid twinning is the most common detrital feldspar (Figure 3.6a), and orthoclase is present in minor amounts. These

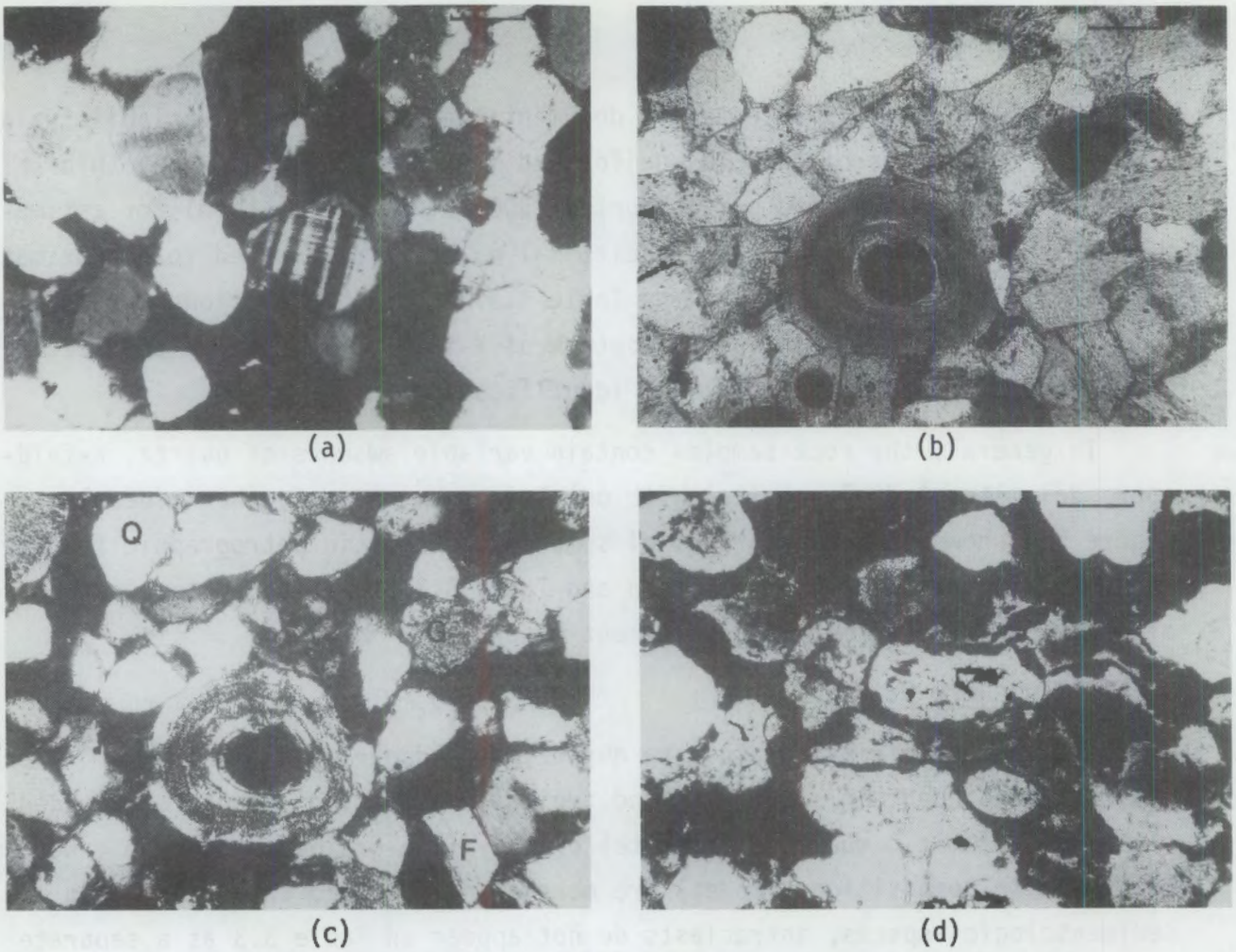

a. Subround, twinned microcline grain (center) with untwinned K-feldspar overgrowth. Other grains and overgrowths can be seen. Porosity is only partially occluded by K-feldspar, and pores are dark colored. (Sample number B578.5; Mazomanie member of Franconia formation, crossed polars, bar length = 0.1 mm)

b. Glauconite grain (center) showing concentric bands of the typical aggregate and oriented (lighter shade) textures surrounding magnetite core. Other grains are quartz (white), feldspar (light gray), glauconite (dark), and dolomite (subhedral, gray). (Sample number A638.0; Reno member of Franconia formation, plane light, bar length = 0.1 mm)

c. Same field as b, but with crossed polars. Oriented texture is white. Other grains are glauconite (G), quartz (Q) and K-feldspar (F)

d. Altered, compaction-deformed glauconite grains (stippled in appearance). Limonite alteration (black) defines original grain boundaries and partially to completely replaces glauconite. White grains are quartz, locally with thin, incomplete rims of dolomite. (Sample number A673.8; "mustard bed" of Reno member of Franconia formation, plane light, bar length = 0.1 mm)

FIGURE 3.6. Photomicrographs of Typical Petrographic Features

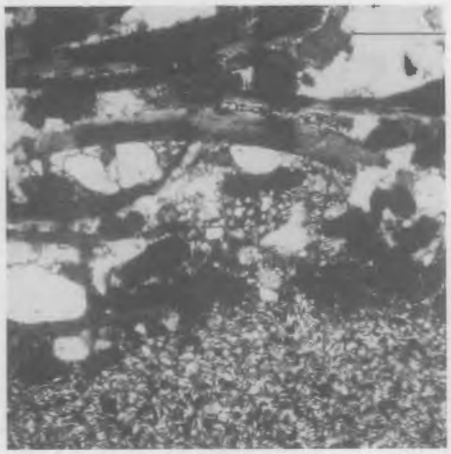

(e)

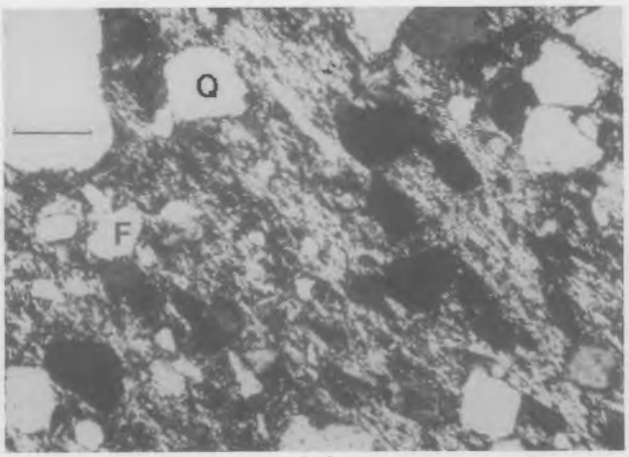

(f)

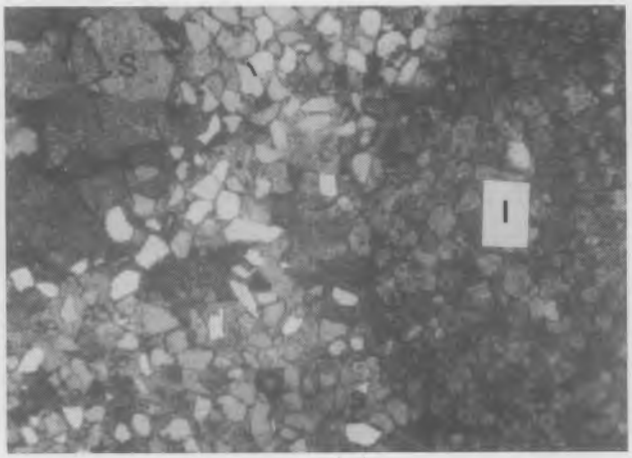

(g)

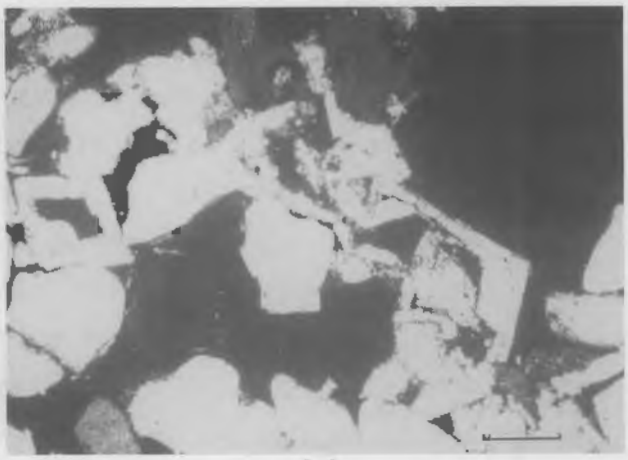

(h)

e. Rock type below is very fine-grained sandstone composed of K-feldspar, quartz and glauconite (most of small dark grains). Rock type above is bimodal with medium- and coarse-grained quartz (white), glauconite (dark gray-black and round), brachiopod shell fragments (dark gray, elongate) and interstitial fine grains of quartz and K-feldspar. Dolomite cement (white, light gray) occurs in upper rock type. (Sample number A833.4; Eau Claire formation, plane light, bar length = 0.5 mm)

f. Clay matrix (bright white and dark gray) surrounding grains of K-feldspar (F) and quartz (Q). (Sample number A596.5; Reno member of Franconia formation, crossed polars, bar length = 0.1 mm)

g. Intraclast (I) of finely crystalline dolomite with magnetite-rich rim, sparry dolomite crystals (S) separated by voids and fine-grained quartzose sandstone, cemented and partially replaced by dolomite (light gray). (Sample number A607.6; Mazomanie member of Franconia formation, plane light, bar length = 0.5 mm)

h. Rhombic dolomite crystals (white) with euhedral voids in cores (black). The cores probably were occupied by calcite which has been dissolved after dolomitization. Broken remnants of dolomite rhombs indicate that some compaction occurred subsequent to dissolution--possibly due to collapse into void spaces. (Sample number B578.5, Mazomanie member of Franconia formation, crossed polars, bar length = 0.1 mm)

FIGURE 3.6. Photomicrographs of Typical Petrographic Features (cont)

K-feldspar grains typically are angular to subrounded, and fine-grained. The abundance of feldspar is related to grain size of the sample and the relationship is consistent with that observed by Odom (1975), in which samples with a grain size range of 0.03 mm to 0.1 mm contain 25% to 65% K-feldspar, those in the 0.1 mm to 0.15 mm range contain 10% to 25%, and those coarser than 0.15 mm typically contain less than 10% K-feldspar.

Plagioclase as weathered (sericitized) rounded grains with relict albite twinning is very rare.

3.4.1.3 Glauconite

Glauconite constitutes as much as 60% of some samples from the Franconia formation, is rare to moderately abundant in the St. Lawrence and Eau Claire formations, but typically is absent from other units. Glauconite grains are rounded to subangular, and variable in size, form, and internal structure. The three major external habits are: 1) rounded grains with distinct grain boundaries, 2) irregular grains with indistinct boundaries, and 3) vermicular or micaceous grains. The two dominant internal structural types are those which are aggregates of very fine-grained, dark-green crystallites, and those with a more coarsely crystalline oriented or fibroradiating texture. The oriented glauconite occurs as partial to complete rims surrounding aggregate-textured cores, and as apparently dislodged fragments of those rims which are themselves grains. The vermicular and micaceous grains are tabular to acicular and contain oriented glauconite. Glauconite with oriented texture has higher birefringence and typically is pleochroic from green to clear. Some grains contain concentrically banded alternations of oriented and aggregate texture, often with opaque minerals (presumably magnetite) associated with the aggregate bands (Figures 3.6b,c). Euhedral magnetite crystals also occur in both grain cores and grain rims.

Several characteristics of the grains indicate the nature of glauconite during deposition and diagenesis. The grains commonly are slightly coarser than other detrital grains with which they occur, implying that glauconite was less dense than quartz and K-feldspar grains. Several samples contain compaction-deformed grains. In one sample (A673.8), nearly all porosity is occluded by irregular masses of deformed glauconite grains (Figure 3.6d). This implies

that glauconite was moderately soft during deposition and compaction. The presence of fragments of oriented rims, however, indicates that these more coarsely crystalline portions were sufficiently brittle to be broken off glauconite grains and incorporated into the sediment. Thus it is suggested that glauconite rims crystallized prior to deposition, whereas the aggregate cores remained moderately plastic until after compaction. An alternate explanation is that the apparent plasticity of the aggregate-textured glauconite is related to the nature of crystal contacts; i.e., crystals of the aggregate texture may have been poorly bonded and allowed slippage along irregular crystal faces during compaction, whereas in the oriented texture bonding of crystal contacts was tighter and resulted in the more brittle structure.

Microprobe data (Odom 1976) indicate that chemical differences exist between oriented and aggregate-texture glauconite. The oriented glauconite typically contains less FeO than aggregate-texture glauconite. However, no corresponding data from these rocks were collected to substantiate the differences.

3.4.1.4 Mica

The dominant mica present is muscovite which occurs typically as subangular flakes smaller than 1 mm in the clayey and very fine-grained parts of all formations. Muscovite flakes are locally bent around other detrital grains, indicating that they are detrital. Trace amounts of detrital, brown biotite also are present (as in sample A690.9). A green, pleochroic mica occurs in a few samples and appears to be an altered form of glauconite.

3.4.1.5 Rock Fragments

With the exception of intraclasts (not shown on Table 3.3), rock fragments typically are rare, and are most common in coarse- and very coarse-grained sandstone. The most abundant fragments are rounded grains of chert and chert with iron oxides, possibly derived from iron-formation. A few fragments are composed of elongate, sutured-boundary, undulose quartz with small intergrown mica. These presumably were derived from metamorphic rocks.

3.4.1.6 Opaque Minerals

Opaque minerals of the following types were noted:

- small, detrital, subrounded grains, typically of magnetite but also of hematite and ilmenite
- very fine, "dusty" inclusions of magnetite in other grains, such as glauconite, feldspar, clay, fossil fragments, and dolomite
- euhedral, variably sized, interstitial crystals of magnetite
- pyrite, in the form of small euhedral crystals, very large poikilotopic crystals and crystal aggregates.

Pyrite is included in the column on cement in Table 3.3 and is described below.

3.4.1.7 Non-Opaque Detrital Heavy Minerals

These typically occur as subangular to rounded grains that are smaller than the average size of the sediment in which they occur. Tourmaline and zircon are the most common heavy minerals; rutile, garnet, and sphene are uncommon to rare. It is interesting to note that heavy minerals are more abundant and more diverse in form and mineralogy in the very fine sand and silt-size units in all formations.

3.4.1.8 Fossil Shell Fragments

Fragments of fossils, which appear to be inarticulate brachiopods, are elongate, 0.05 mm to 1 cm long, arcuate, and abraded (Figure 3.6e). Most are internally banded mixtures of the light-brown isotropic phosphate mineral collophane (microcrystalline apatite) and magnetite. The X-ray diffractograms verified the presence of apatite in fossiliferous samples analyzed.

3.4.2 Matrix

A clayey matrix occurs as patchy, interstitial material in the St. Lawrence, Franconia and Eau Claire formations. Macroscopically this matrix is light green and light greenish gray to light brown. The matrix is extremely variable in composition and typically contains moderately birefringent microcrystalline aggregates of scales and plates of clear to light-brown clay (Figure 3.6f). The exact composition of the clay is unknown, but X-ray

diffractograms indicate that illite is present in all samples and a montmorillonite component is present in some samples. In addition to clay, the matrix material typically contains several of the following: detrital muscovite, silt-size detrital grains of quartz and K-feldspar, iron oxides, dolomite rhombs and irregular patches, and sericite-altered feldspar. Where it was possible to distinguish individual matrix minerals during point counts, these were included in the appropriate mode category of Table 3.3.

3.4.3 Cement

The dominant cement minerals are dolomite and K-feldspar, though quartz, iron oxides, and pyrite occur in minor amounts in some units. Note that no distinction is made in the modal data (Table 3.3) between dolomite which filled a void (i.e., true cement) versus that which crystallized from a fine-grained, carbonaceous sediment because it is very difficult in most cases to distinguish between the two.

3.4.3.1 Dolomite

Dolomite occurs as a cement, as replacement mineral, and as individual crystals in a clay matrix. It is most abundant in the St. Lawrence, Franconia, and Eau Claire formations. Dolomite cement varies from coarse-grained sparite with interlocking euhedral crystals to irregular interstitial patches of subhedral crystals (Figure 3.6g). Another common form is finely crystalline, intergrown dolomite (micrite) which makes up intraclasts and discontinuous laminae and which presumably crystallized from a carbonaceous mud. Poikilotopic dolomite cement, which encloses several detrital grains in one large crystal, also occurs.

Several carbonate-rich samples were X-rayed to determine if calcite is present. No calcite peaks were observed on diffractograms. Microscopic inspection indicated that very small, anhedral carbonate inclusions in some dolomite crystals may be calcite; however grain sizes are too small to accurately determine their optical properties. Some dolomite crystals have open rhombic cores from which calcite may have been dissolved (Figure 3.6h). Additional data, such as those from microprobe analyses, might identify minor amounts of calcite or other carbonate minerals such as ankerite and siderite.

3.4.3.2 K-Feldspar

A K-feldspar cement is present in all formations, but it is most abundant in finer-grained units which contain significant amounts of detrital K-feldspar grains. It occurs as overgrowths on K-feldspar grains which impinge and locally interlock to form cement (Figure 3.6a). The overgrowths typically are euhedral, except where impingement occurs against adjacent crystals or grains. Most overgrowths appear to be composed of adularia, which is optically complex, never twinned and has slightly lower refractive indices than microcline. The presence of adularia could not be positively verified by X-ray data because the diffractogram pattern of adularia is essentially the same as that for orthoclase, which exists as detrital grains. In some samples, the overgrowths are large enough to occlude nearly all porosity. Another form of K-feldspar cement observed in small amounts in a few samples is a very fine crystalline mosaic.

3.4.3.3 Quartz

Overgrowths of quartz in optical continuity with the quartz-grain hosts form a weak-bonding cement in some samples of the Ironton and Galesville sandstones.

3.4.3.4 Iron Oxides

Iron oxides, presumably goethite and limonite, are weak cementing minerals occurring on grain boundaries of glauconite in some samples (e.g., Figure 3.6d).

3.4.3.5 Pyrite

Aggregates of small, cubic pyrite crystals and larger, pyrite-cemented, discontinuous stratabound lenses occur in some samples of the Ironton and Galesville sandstones.

3.4.4 Diagenesis

Diagenesis refers to all of the physical and chemical processes that change a sediment into a sedimentary rock. It is assumed that most conditions under which diagenesis occurred (pressure, temperature, water chemistry) were quite similar for all formations described. Therefore, original composition

and porosity are the crucial variables which controlled mineralogy during and after diagenesis. The diagenetic changes represented in these samples are compaction, deformation, crystallization (including cementation), and alteration. Evidence of these diagenetic processes and the minerals involved are listed below:

1. Compaction
   - reduction of pore space by packing
   - deformation of aggregate-texture glauconite grains
   - crushed dolomite rhombs with open (dissolved) cores (indicating minor compaction-deformation subsequent to dolomitization)

2. Crystallization
   - aggregate texture glauconite
   - microcrystalline clay minerals in matrix
   - dolomite rhombs in matrix and between detrital grains
   - quartz overgrowths
   - K-feldspar overgrowths and minor finely crystalline cement
   - euhedral magnetite and pyrite crystals, the latter forming cement locally

3. Replacement and alteration
   - partial to complete replacement of calcite by dolomite (see below)
   - partial replacement of K-feldspar grains and overgrowth by dolomite
   - partial replacement of glauconite and fossil fragments by dolomite
   - partial replacement of glauconite by K-feldspar and minor magnetite
   - partial to complete alteration of glauconite to limonite

Dolomite typically is thought to be a replacement of a precursor carbonate--mainly calcite (Zenger, Dunham, and Ethington 1980). However, only minor evidence of that replacement exists in samples of these rocks, such as the local presence of dolomite rhombs with cloudy, inclusion-rich cores and clear rims. This characteristic has been interpreted by Sibley (1982) to indicate the replacement of calcite by dolomite, producing the inclusion-rich core, followed by enlargement of the dolomite crystal, producing the clear rim.

Much of the dolomite appears to be true cement, i.e., it was introduced during one or more periods of dolomitization and precipitated into interparticle space. The timing relationship between this and the probable replacements of calcite by dolomite is unknown.

A summary of the apparent sequence of crystallization and replacement is shown in Figure 3.7.

3.5 SUMMARY

The St. Paul FTF is located in an ideal location. It is near the center of the Twin Cities Artesian Basin where the regional ground-water flow rate is very low. The FIG aquifer is well-separated from the overlying and underlying aquifers.

The Franconia formation, Ironton sandstone, and Galesville sandstone make up the FIG aquifer. The upper Franconia formation (Mazomanie member) and the combined Ironton and Galesville sandstones are the water-yielding parts of the FIG aquifer. The glauconitic Reno and Birkmose members, and the highly-feldspathic Tomah member of the Franconia formation are confining beds that separate the two water-yielding units.

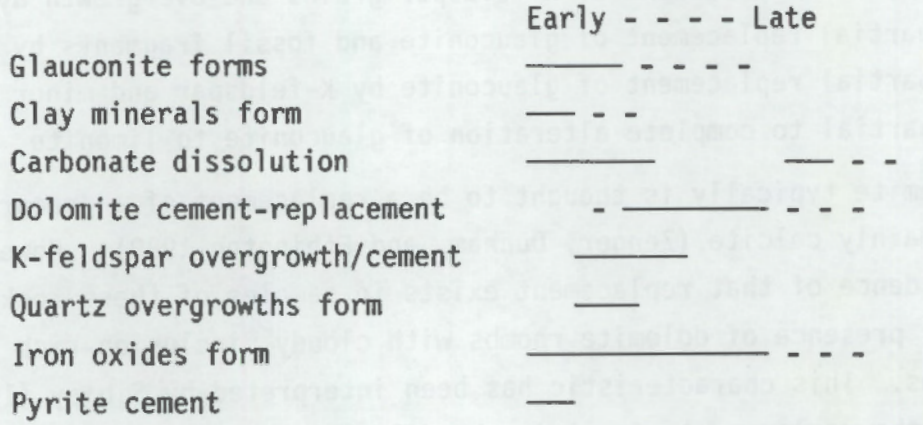

FIGURE 3.7. Paragenetic Sequence of Secondary Minerals Based on Thin-Sections of Core AC1

The Mazomanie member is primarily a fine- to medium-grained feldspathic sandstone with a significant amount of dolomite and a small amount of glauconite. Few barriers to vertical flow are present. The Ironton and Galesville sandstones are friable quartzose sandstone and less friable feldspathic sandstone with many thin shale/clay stringers. The many shale/clay stringers are barriers to vertical flow.

Petrographic examination reveals that extensive diagenetic changes have taken place in these rocks since deposition. The secondary minerals and fabrics indicate a history of water-rock interaction through geologic time. Examination of the FIG aquifer rock samples following ATES test cycles will be very informative of actual water-rock interaction in a short time period at relatively high temperatures.

4.0 WATER LEVEL ANALYSES AND HYDRAULIC PARAMETERS

Determining an aquifer's potential as an effective thermal energy storage medium requires thorough knowledge of the hydraulic properties of aquifers and their confining beds. Baseline data on water-level fluctuations are needed to estimate any potential impact of aquifer thermal storage in the FIG aquifer, as well as for aquifers and confining beds below and above it. In the Twin Cities metropolitan area, the Prairie du Chien-Jordan (upper aquifer) and the Mt. Simon-Hinckley (lower aquifer) are used extensively for municipal, industrial and commercial water supply, so any significant heat flow from the FIG aquifer into these aquifers would be detrimental to the water supply. Ground-water levels from an array of monitoring wells at the University of Minnesota ATES site have been measured regularly since wells were constructed. Characterizing the water-level data before heat injection is initiated allows the establishment of baseline data on water levels for each aquifer and confining bed and for a comparison with the water levels during and after pumping tests and heat injection.

4.1 WATER-LEVEL MEASUREMENTS AND ANALYSIS

4.1.1 Observation Wells and Instrumentation

The position and spacing of the heat storage and water supply wells and the observation well network are shown in Figure 4.1. In each monitoring well a cluster of 1 in., 1-1/4 in. and 2 in. pipes has been installed. The pipes were terminated in screens at various intervals to provide instrument stations at selected points within the aquifers and overlying and underlying beds. The screened interval is backfilled with pea gravel, and the remainder of the hole is backfilled with grout or fine sand, as required. Thermocouples and pressure transducers can be lowered down the pipe to the screened section and withdrawn, if necessary, for replacement or servicing. The monitoring well instrumentation is shown diagrammatically in Figure 4.2. Before pressure transducers were installed, water levels were measured manually. Initial measurements began on October 14, 1980, when the first array of observation

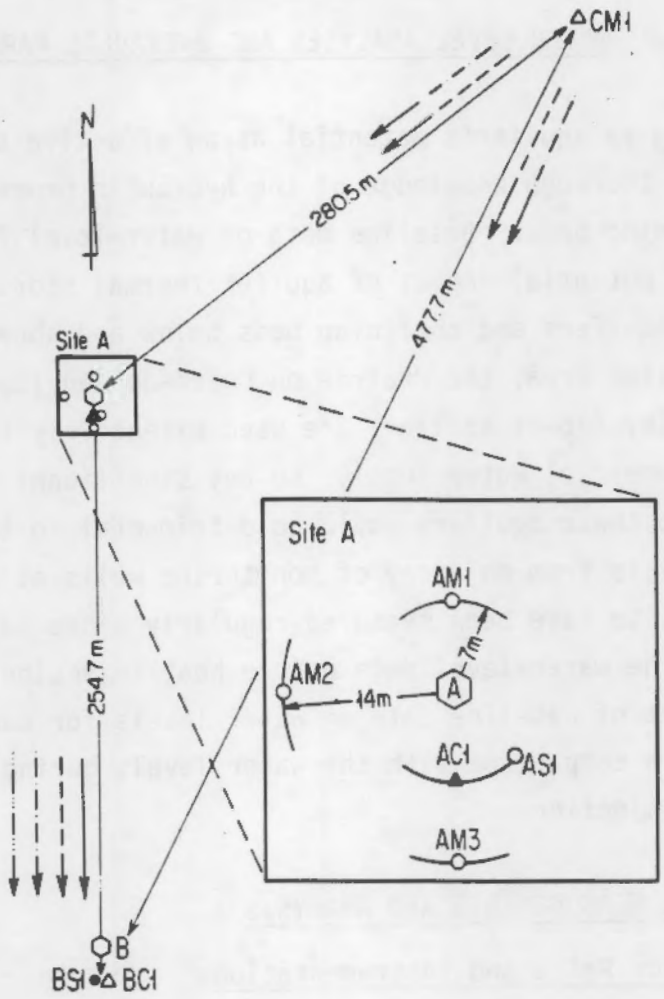

FIGURE 4.1. ATES Wells and General Directions of Ground-Water Movement at ATES Field Test Facility

wells at sites A and B had been completed. Table 4.1 shows geologic formations that are being monitored, along with information on measurement periods and instrumentation.

Methods used to measure water levels in the wells include 1) chalked steel tape, 2) electric tape, 3) strip-chart recorder and 4) pressure transducers. The first two methods monitor a periodic record, the latter two monitor a

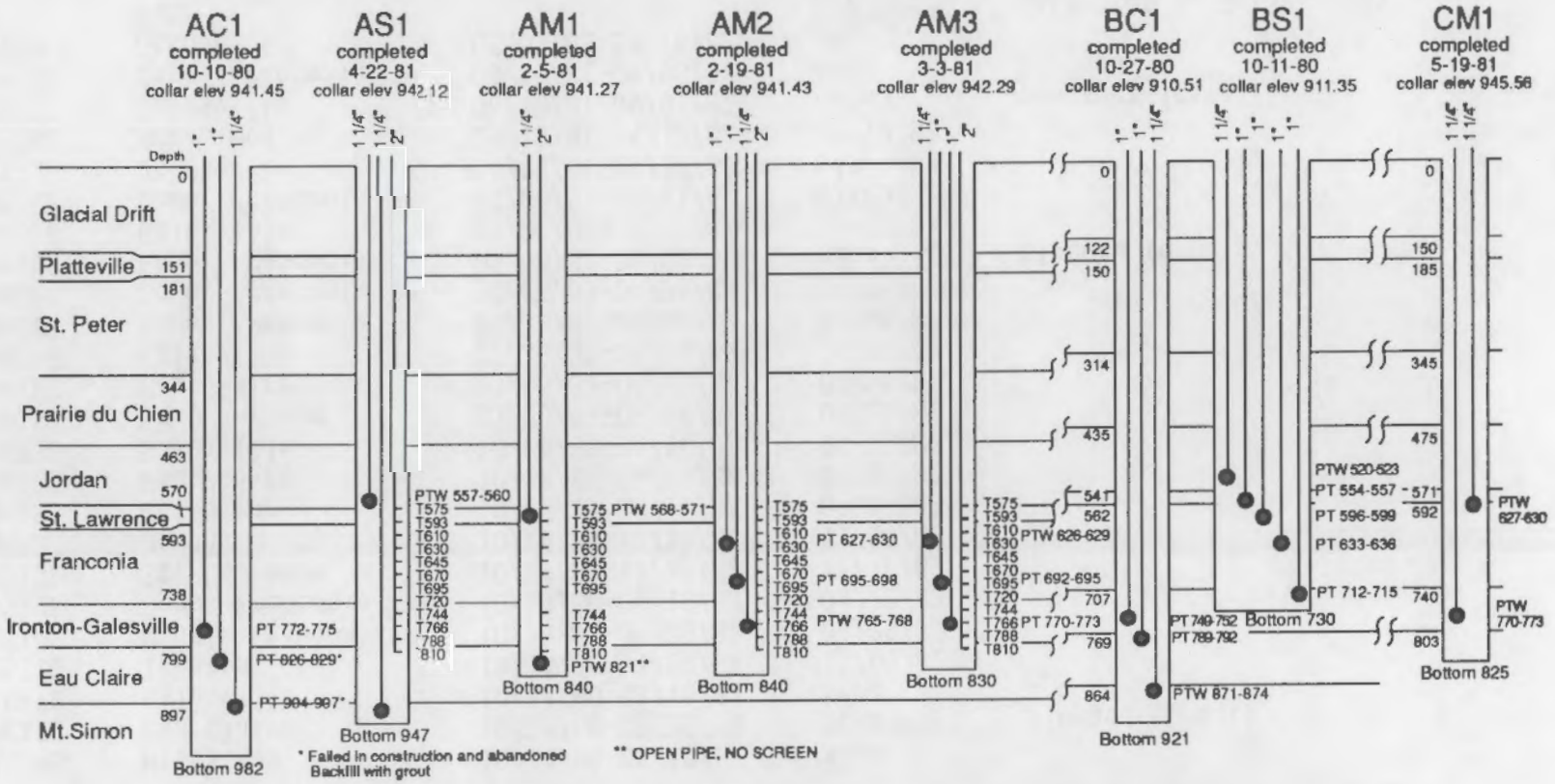

FIGURE 4.2. Monitor Well Instrumentation for Short-Term Cycles

TABLE 4.1. Pre-Cycle Monitoring Information for Observation Wells

Well	Unit	Measurement Period	Pressure Transducers Installed	Remarks
AC1MS	Mt. Simon	10/14/80-05/15/82	none	
AC1EC	Eau Claire	10/14/80-02/25/81	none	plugged (grout)
AC1IG	Galesville	10/14/80-03/15/82	none	
BS1IG	Ironton	10/14/80-11/09/82	11/09/82	
BS1MF	Middle Franconia	10/14/80-04/28/82	04/28/82	
BS1UF	Upper Franconia	10/14/80-04/16/82	04/22/82	
BS1SL	St. Lawrence	10/14/80-11/10/82	11/10/82	
BS1J	Jordan	10/14/80-11/10/82	11/10/82	
BC1MS	Mt. Simon	10/28/80-02/19/82	03/03/82	
BC1EC	Eau Claire	10/28/80-04/19/82	04/19/82	
BC1IG	Galesville	10/28/80-04/16/82	04/16/82	
AM1SL	St. Lawrence	03/05/81-04/16/82	04/16/82	
AM1EC	Eau Claire	03/05/81-04/16/82	04/16/82	
AM2IG	Galesville	02/26/81-04/06/82	04/06/82	
AM2UF	Upper Franconia	02/26/81-04/06/82	04/06/82	
AM2LF	Lower Franconia	02/26/81-04/06/82	04/06/82	
AM3UF	Upper Franconia	03/06/81-08/02/82	none	plugged (grout)
AM3IG	Galesville	03/06/81-12/31/81	01/06/82	
AM3LF	Lower Franconia	03/06/81-03/11/82	03/20/82	
AS1J	Jordan	05/13/81-04/16/82	04/27/82	
AS1MS	Mt. Simon	05/13/81-04/12/82	04/12/82	
CM1IG	Galesville	06/10/81-09/01/82	none	recorder install
CM1UF	Upper Franconia	06/10/81-09/08/82	none	plugged
STP3	Jordan	06/03/81-11/16/82	none	
A	FIG		04/28/82	data from J. Oelin, USGS
B	FIG		05/04/82	

continuous record. The strip-chart recorder gives an ink-drawn hydrograph of fluctuating water levels. The strip-chart recorder is installed in piezometer tube CM1IG. Pressure transducers are installed in wells listed in Table 4.1. Transducers are lowered into each pipe to a calculated depth at which the transducer will remain submerged in water at maximum drawdown during any pumping. Pressure transducers are calibrated at the site as they are installed by continuous lowering of each transducer down a piezometer tube to the static water level. The depth increment in feet (0.3048 m) below water level is converted to pounds per square inch (psi) of pressure by the relationship: 1.0 ft of water = 0.43351 psi (1.0 m of water = 9.8 kPa). Pressure transducers at sites A and B are connected to the data logger. The data logger samples incoming signals from each instrument at the sampling interval chosen for monitoring and modeling the procedure underway. Data are transmitted directly to computer tape and, for a backup and a check on values, to a paper tape output. The logger operates automatically or with an operator standby control.

4.1.2 Water Levels and Factors Affecting Their Fluctuation

Water-level fluctuations may reflect natural phenomena or man-made stress. In the Twin Cities area, ground water is extensively used for municipal, industrial and commercial water supply. Large withdrawals of water amounting to 80% the total ground-water use in 1979 (Horn 1983) were from the Prairie du Chien-Jordan aquifer. From the Franconia-Ironton-Galesville aquifer withdrawal is about 7% and from the Mt.Simon-Hinckley-Fond du Lac aquifer, about 10%. As a result of ground-water regional withdrawal, water levels in the Prairie du Chien-Jordan and the Mt. Simon-Hinckley-Fond du Lac aquifers have been declining since 1890 (Steinhilber and Young 1979). However, water levels in the Prairie du Chien-Jordan aquifer show no regional decline since 1958 (Norvitch, Ross and Brietkrietz 1973; Horn 1983). Thus, it is assumed that the Prairie du Chien-Jordan aquifer, at its present level of development, is near equilibrium condition. Regional water levels in the Mt. Simon-Hinckley-Fond du Lac aquifer rose about 3 to 6 m (10 to 20 ft) since 1958, probably due to redistribution of ground-water withdrawal in the central part of the Twin Cities artesian basin. Data are lacking on the regional ground-water fluctuation of the Franconia-Ironton-Galesville aquifer because of limited use of the aquifer.

In addition to the regional picture, local withdrawal of ground water greatly affects the ground-water level fluctuations.

Water levels decline in all aquifers during the summer, generally between April and August, due to increased water use, followed by recovery in the fall and winter to near pre-summer levels (Figures 4.3, 4.5a-e, 4.7). Water levels measured in the St. Lawrence confining beds (Figure 4.4) fluctuate as if they were located in the upper Franconia unit. Step-drawdown pumping tests at sites A and B in 1981 revealed that the St. Lawrence piezometers are insufficiently separated from the upper Franconia unit by grout. Water levels of the Eau Claire confining bed (Figure 4.6) do not show any particular trend. Table 4.2 summarizes ambient water-level changes observed before any thermal testing occurred.

In addition to seasonal water-level fluctuations, a clear weekly cycle can be seen in wells of the Jordan aquifer. Water levels are 0.9 to 1.2 m (3 to 4 ft) higher on Mondays than on the preceding Fridays, because withdrawal decreases during weekends from two St. Paul campus wells. A water-level measurement summary is given in Table 4.3.

It must be remembered that the responses shown on the water level plots after hot water injection (Figures 4.4, 4.5a-e, 4.6, 4.7) have been affected by the thermal affects upon the FIG aquifer and contained water. The densities of the water and rock decrease, and the viscosity of the water decreases. Recorded water levels will be raised by the less dense warm water.

4.2 EVALUATION OF HYDRAULIC PARAMETERS OF AQUIFERS

4.2.1 Ground-Water Movement and Hydraulic Gradients

Analysis of data shows that ground-water movement can be determined from water-level measurements in wells that are reasonably far apart. Therefore the difference in water levels between sites A and B, A and C, and B and C is used in determining direction of flow. Data from monitoring wells at sites A and B do not give reliable information because the accuracy of measurements and even minor water-level fluctuations due to changes in barometric pressure become important factors.

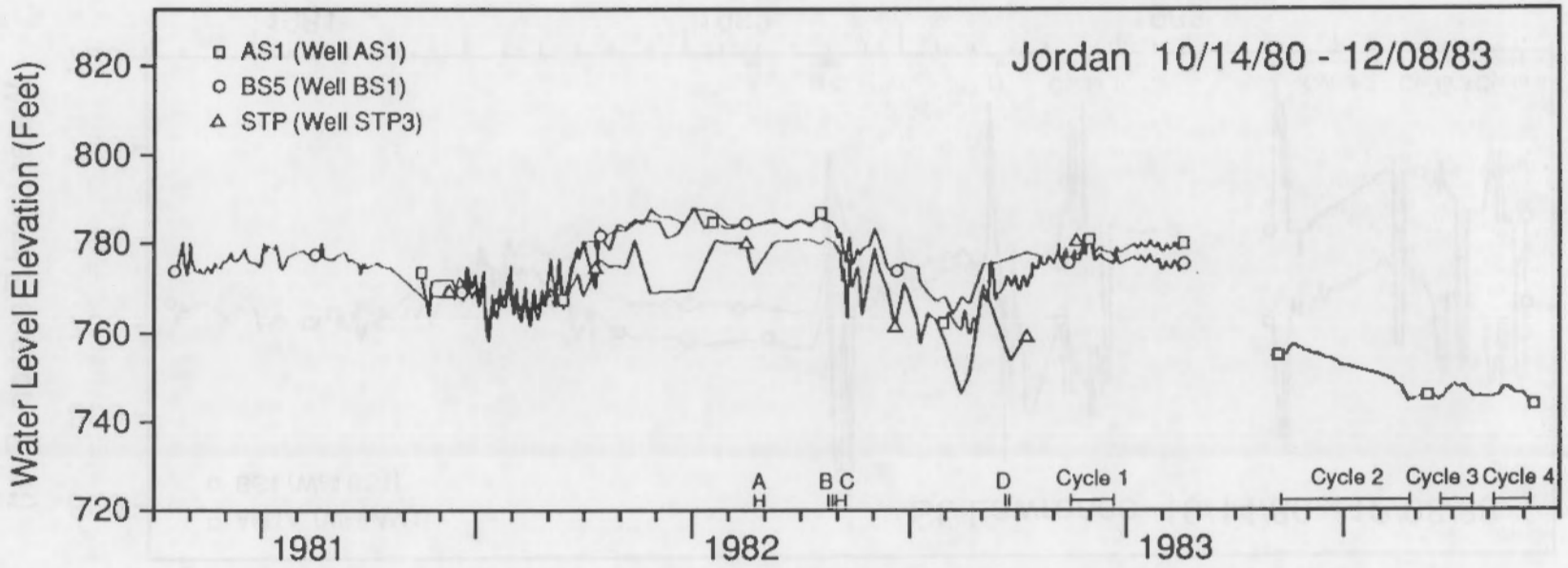

FIGURE 4.3. Water Levels in Jordan Aquifer, 10/80 to 12/83

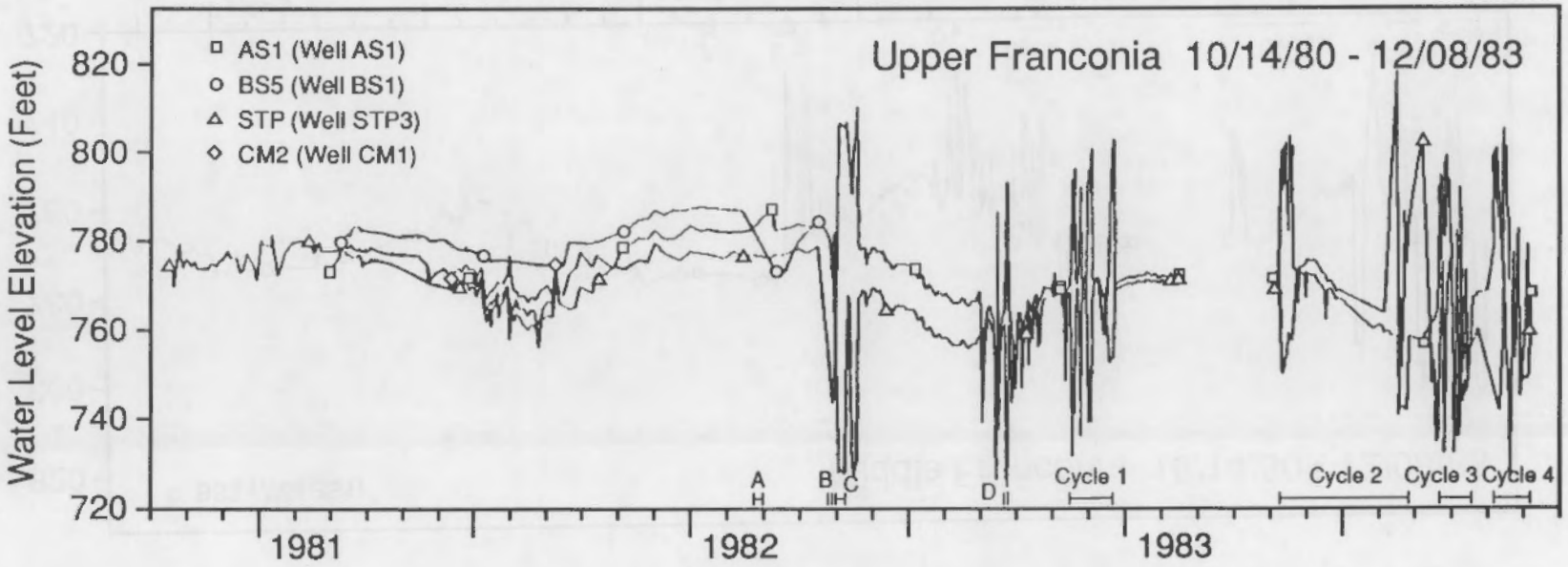

FIGURE 4.5a. Water Levels in Franconia-Ironton-Galesville Aquifer, 10/80 to 12/83--Upper Franconia

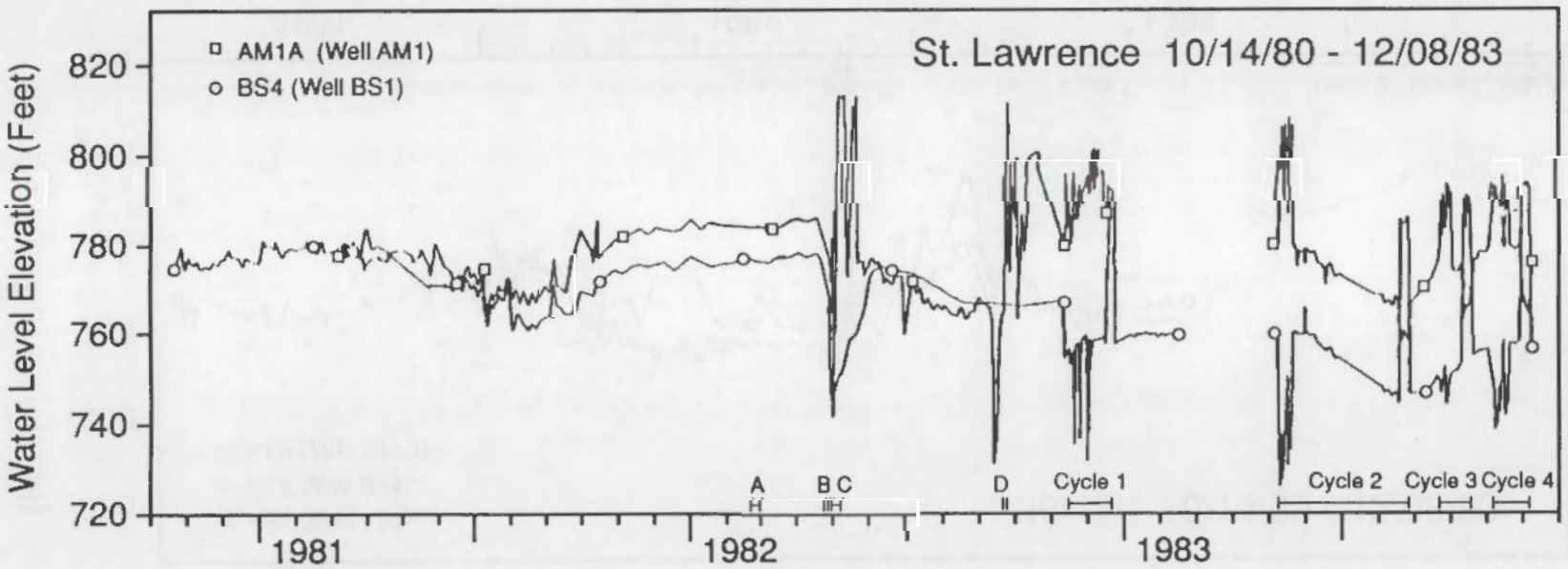

FIGURE 4.4. Water Levels in St. Lawrence Confining Bed, 10/80 to 12/83

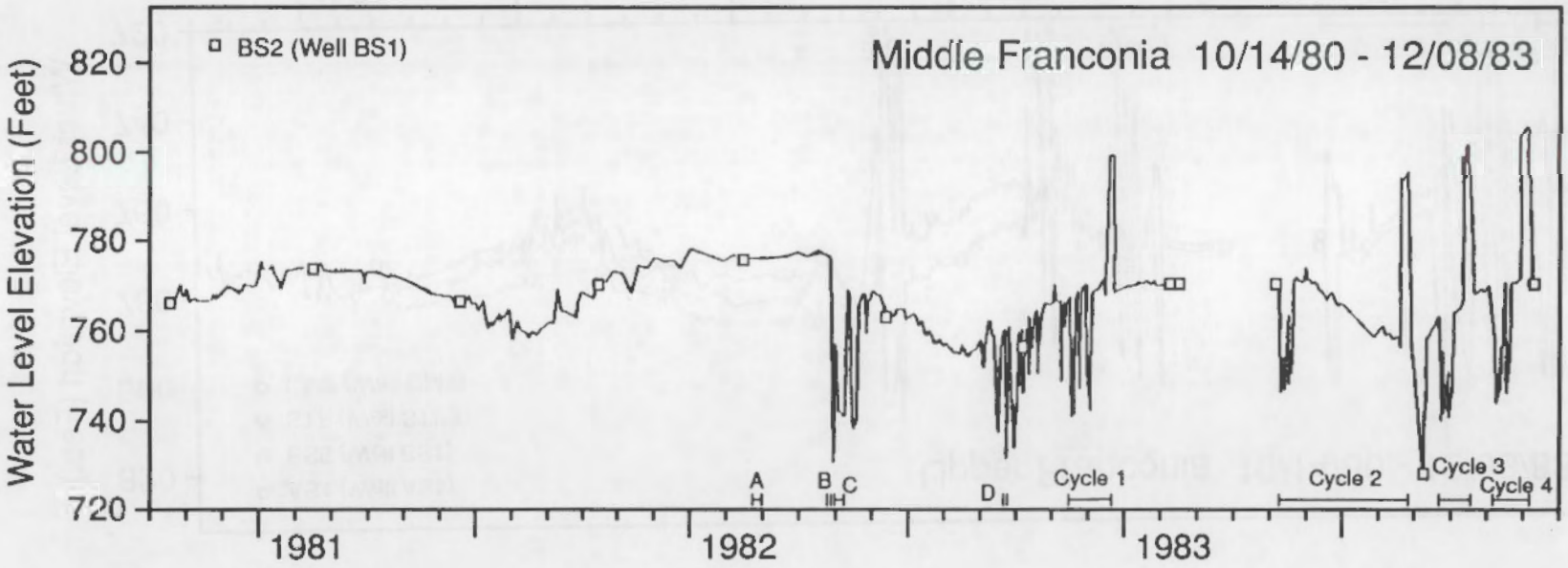

FIGURE 4.5b. Water Levels in Franconia-Ironton-Galesville Aquifer, 10/80 to 12/83--Middle Franconia

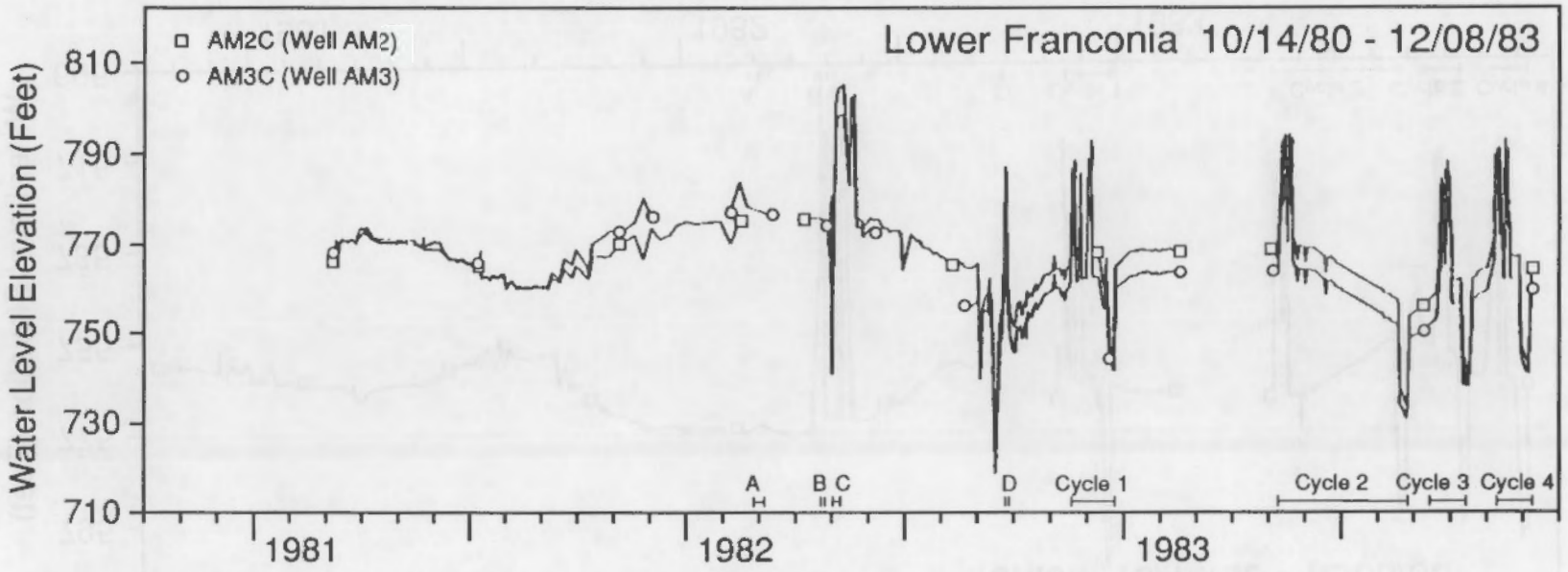

FIGURE 4.5c. Water Levels in Franconia-Ironton-Galesville Aquifer, 10/80 to 12/83--
Lower Franconia

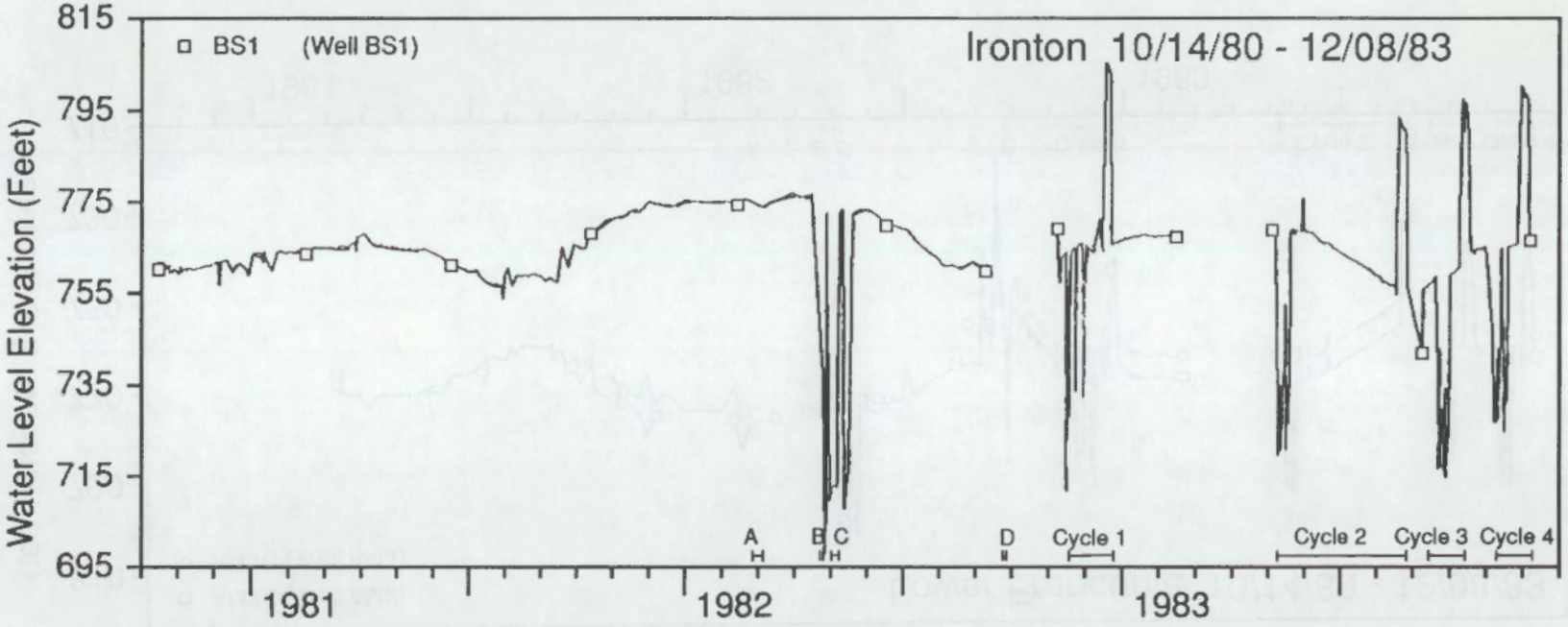

FIGURE 4.5d. Water Levels in Franconia-Ironton-Galesville Aquifer, 10/80 to 12/83--Ironton

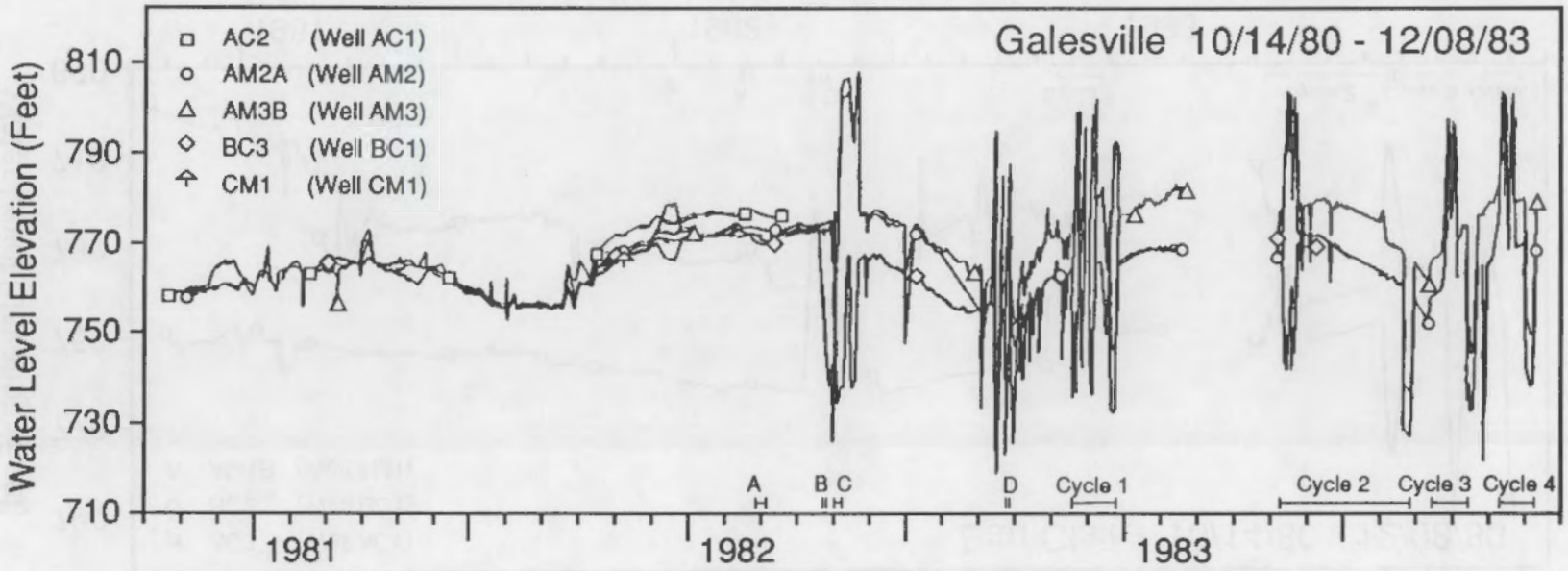

FIGURE 4.5e. Water Levels in Franconia-Ironton-Galesville Aquifer, 10/80 to 12/83--Galesville

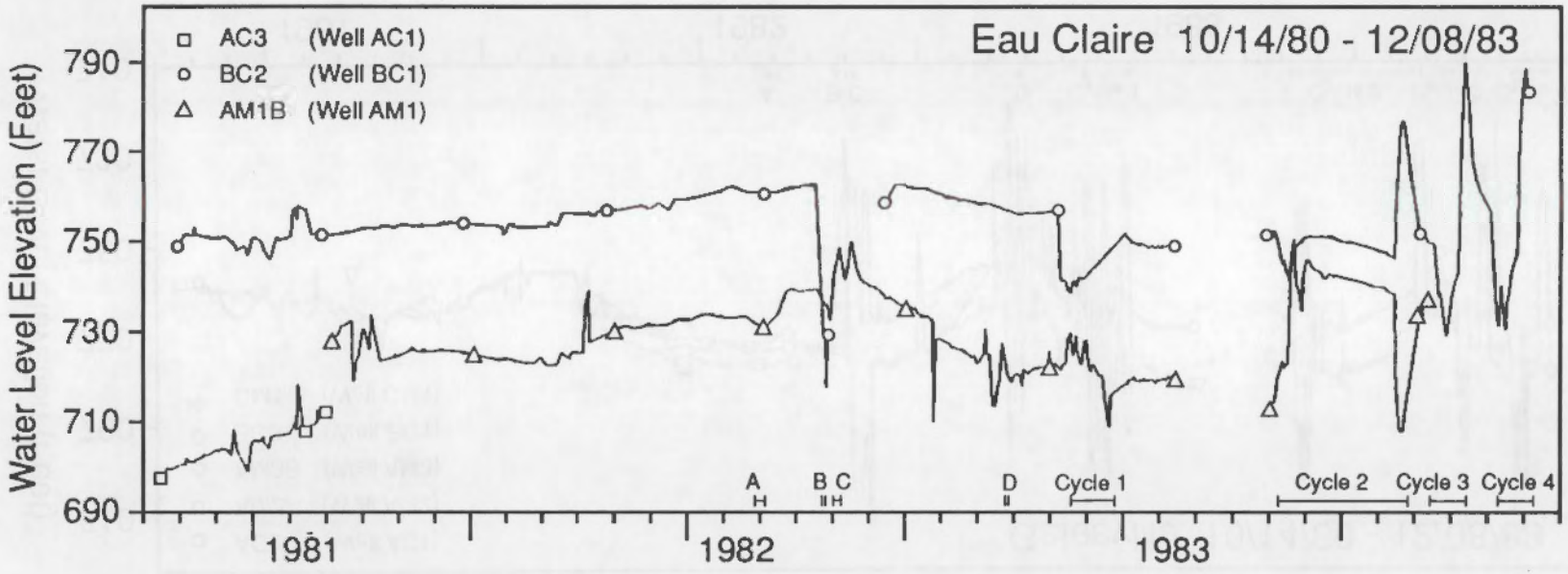

FIGURE 4.6. Water Levels in Eau Claire Confining Bed, 10/80 to 12/83

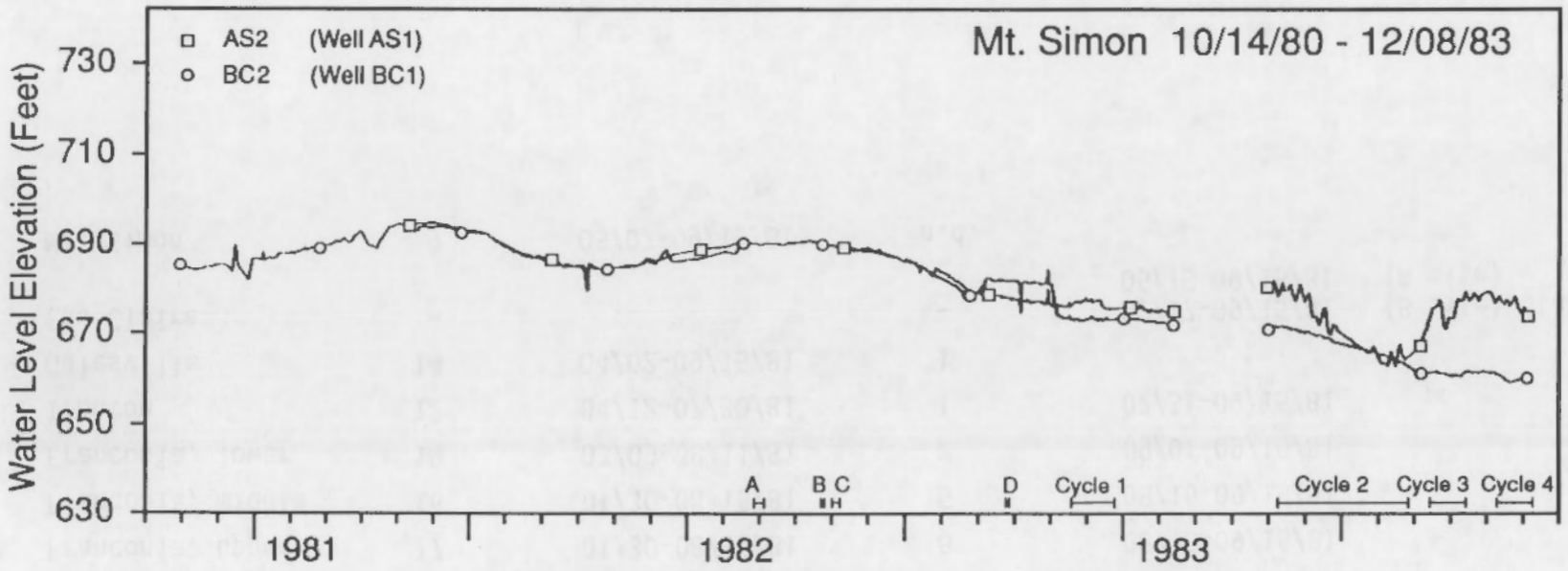

FIGURE 4.7. Water Levels in Mt. Simon Aquifer, 10/80 to 12/83

TABLE 4.2. Seasonal Water-Level Changes, October 13, 1980, to September 15, 1981

Unit	Decline (-) in ft[(a)]	Period	Rise (+) in ft[(a)]	Period	Remarks
Jordan	13	04/19-08/15/81	4	08/16-09/15/81	
St. Lawrence	16	03/09-08/15/81	10	08/16-09/15/81	Acts as upper Franconia
Franconia, upper	17	01/30-08/15/81	6	08/16-09/15/81	
Franconia, middle	16	01/30-08/15/81	5	08/16-09/15/81	
Franconia, lower	10	03/09-08/11/81	2	09/01-09/15/81	
Ironton	12	04/12-07/30/81	1	07/31-09/15/81	
Galesville	14	04/02-09/15/81	1		
Eau Claire	-		-	02/17-09/15/81 05/15-09/15/81	(B site) Stable (A site)
Mt. Simon	9	05/07-09/15/81	n.d.		

(a) m = ft x 0.3048

TABLE 4.3. Summary of Measured Water-Levels from October 14, 1980, to September 15, 1981

Unit	Well	Average, ft[(a)]		Highest, ft[(a)]		Lowest, ft[(a)]	
		Depth	Elevation	Depth	Elevation	Depth	Elevation
Mt. Simon	AC1MS	234.04	707.41	226.69	714.76	244.33	697.12
Galesville	AC1IG	181.66	759.79	172.33	769.12	187.58	753.87
Eau Claire	AC1EC	236.81	704.64	223.07	718.38	242.92	698.53
Mt. Simon	BC1MS	222.80	687.71	217.47	693.04	230.00	680.51
Eau Claire	BC1EC	158.65	751.86	153.29	757.22	165.00	745.51
Galesville	BC1IG	151.41	759.10	142.93	767.58	158.78	751.73
Ironton	BS1IG	152.31	759.04	145.68	765.67	159.97	751.38
Franconia (middle)	BS1MF	144.57	766.78	137.54	773.81	154.43	756.92
Franconia (upper)	BS1UF	141.66	769.69	133.00	778.35	153.98	757.37
St. Lawrence	BS1SL	141.29	770.06	133.78	777.57	154.05	757.30
Jordan	BS1J	140.06	771.29	132.40	778.95	153.87	757.48
St. Lawrence	AM1SL	170.70	770.57	161.15	780.12	179.66	761.61
Eau Claire	AM1EC	215.85	725.42	207.81	733.46	222.27	719.00
Galesville	AM2IG	182.04	759.39	172.92	768.50	187.26	754.17
Franconia (upper)	AM2UF	172.74	768.69	165.28	776.15	187.78	753.65
Franconia (lower)	AM2LF	176.56	764.87	169.68	771.75	182.83	758.60
Franconia (upper)	AM3UF	166.91	775.38	162.00	780.29	170.78	771.51
Galesville	AM3IG	182.71	759.58	171.03	771.26	188.30	753.99
Franconia (lower)	AM3LF	176.76	765.53	169.42	772.87	183.71	758.58
Jordan	AS1J	173.67	767.78	166.61	774.84	181.41	760.04
Mt. Simon	AS1MS	252.19	689.35	248.89	692.56	257.30	684.15
Galesville	CM1IG	188.56	757.00	184.00	761.56	191.06	754.50
Franconia (upper)	CM1UF	177.33	768.23	171.66	773.90	182.02	763.54
Jordan	STP3J	137.77	766.92	131.76	772.93	145.64	759.05

(a) m = ft x 0.3048

Histogram analysis has been used in determining hydraulic gradients of aquifers. The differences of water levels in the same unit have been statistically grouped into classes, and the frequency of each class has been determined. Classes in which the frequency of distribution is insignificant may have artificial factors such as pumping measurement errors. Classes with the highest frequency of distribution are used in determining hydraulic gradient for different units of aquifers.

General direction of ground-water flow in all units is from north to south, as shown in Figure 4.1, and is in good agreement with the regional direction toward the Mississippi River. Table 4.4 summarizes hydraulic gradients obtained by histogram analysis. Average hydraulic gradients at the site are:

Jordan = 2.7×10^{-3}
Upper Franconia = 2.6×10^{-3}
Galesville = 0.7×10^{-3}
Mt. Simon = 0.4×10^{-3}

TABLE 4.4. Hydraulic Gradients of Units at ATES Site

Unit	Wells Used	Distance, ft	Average Hydraulic Gradient, 10^{-3}	Ranges of Observed Hydraulic Gradients, 10^{-3}
Jordan	AS1J-BS1J	854.0	3.4	2.3 to 4.2
	AS1J-STP3	899.5	1.2	0.0 to 2.2
	BS1J-STP3	546.8	3.4	1.8 to 5.5
Upper Franconia	AM2UF-BS1UF	867.6	2.4	1.1 to 4.6
	AM2UF-CM1UF	957.0	2.6	2.0 to 4.2
	BS1UF-CM1UF	1599.4	2.9	1.9 to 4.4
Ironton-Galesville	AC1IG-BC1IG	843.9	0.93	0.0 to 2.4
	AC1IG-CM1IG	934.9	0.58	0.0 to 1.0
	AM2IG-BC1IG	868.6	0.71	0.0 to 1.1
	AM2IG-CM1IG	957.0	0.57	0.26 to 0.78
	AM3IG-BC1IG	820.9	0.62	0.0 to 1.2
	AM3IG-CM1IG	949.7	0.72	1.0 to 0.52
	BC1IG-CM1IG	1590.0	0.79	1.2 to 0.62
Mt. Simon	AS1MS-BC1MS	853.5	0.4	0.0 to 1.2

Approximate vertical hydraulic gradients observed are:

between the Jordan and the upper Franconia = 7.6×10^{-2} (site B)
between the Galesville and the Mt. Simon = 7.5×10^{-1} (site B)
= 8.0×10^{-1} (site A)

4.2.2 Transmissivity and Permeability

The method of determining transmissivity of the Franconia-Ironton-Galesville aquifer is based on first response from the stress center (pumping or injection) to the observation point.

From the basic formula of ground-water flow under confined conditions it can be seen that the drawdown (recovery) is a function of distance and the velocity of drawdown or pressure at any point can be determined as the first derivative:

$\frac{\Delta s}{\Delta t}$ or $\frac{\Delta p}{\Delta t}$ has a maximum at a time

$$\frac{\partial s}{\partial t^2} = \frac{Q\, e^{-\frac{r^2}{4Dt}}}{4\pi T t^2}\left(\frac{r^2}{4Dt} - 1\right) = 0$$

from which: $\frac{r^2}{4Dt_o} = 1$ and $D = \frac{r^2}{4t_o}$ (Kovalevsky 1968, p. 135) (4.1)

where Q = rate of pumping (injection), m^3/day
D = hydraulic diffusivity, m^2/day
t = period of pumping (injection), days
t_o = time of first response to pumping (injection), days
s = drawdown (p-pressure) in observation well, m
r = distance between pumping (injection) well and observation point, m
T = transmissivity, as defined in Equation (4.2).

Knowing hydraulic diffusivity, the transmissivity can be determined from the modified nonequilibrium Theis equation:

$$T = \frac{Q \ln \frac{2.25\ Dt}{r^2}}{4\pi s} \qquad (4.2)$$

where all the symbols are the same as in Equation (4.1).

Numerous pumping and injection tests using the Franconia-Ironton-Galesville aquifer have been performed at sites A and B and responses have been mostly recorded at site C. Table 4.5 summarizes these data.

Some variations in calculated parameters are due to the uncertainty in accuracy of the measurements and drawdown. Pumping rates have been measured periodically and no cumulative data exist. Response time and drawdown data are transferred from the chart and are subject to some individual interpretation. Nevertheless, average parameters give satisfactory results on hydraulic characteristics.

Average transmissivity from Table 4.5 gives the value of 103 m^2/day (1108 ft^2/day). Pumping test data at sites A and B have been analyzed by R. Miller of the U.S. Geological Survey by the graphical method and the minimization technique (Walton 1981). Miller (1984) analyzed pumping test data for transmissivity and anisotropy. He calculated an average maximum transmissivity of 1090 ft^2/day (101 m^2/day) and an average minimum transmissivity of 480 ft^2/day (45 m^2/day) for the Ironton-Galesville part of the aquifer. It must be noted that in Miller's calculations, anisotropy within the upper Franconia part of the aquifer also was taken into account for the model grid (Miller and Voss 1986). Values are in close agreement with the value 1108 ft^2/day calculated using the first response method.

The packer test conducted during 1980 core hole studies and the pumping tests show that the major permeable zones of the aquifer are the upper

TABLE 4.5. Pumping Test Data and Calculated Parameters from FIG Aquifer

Date and Wells Used	Pumping Rate, Q, m^3/day (gpm)	Pumping Time, t, minutes (day)	Distance Between Pumping Well and Observation Well, m (ft)	Response Time at Observation Well t_o, After Pumping Start Stop min.	Stop days (10^{-3})	Drawdown at Observation Well, m (ft)	Calculated Parameters Diffusivity, D m^2/day	Transmissivity m^2/day	Transmissivity ft^2/day
10/08/81	2146	475	264.7	3.97	2.7	5.36	6.5 x 10^6	135	1453
A, BC1IG	(394)	(0.33)	(868.4)	n.d.		(17.59)			
02/26-03/02/82	1851	6410	280.54	5.37	3.7	6.71	5.3 x 10^6	143	1585
A, BC1IG	(340)	(4.45)	(920.4)	n.d.		(22.01)			
11/16/82	2725	19.25	280.54	5.0	3.5	1.22	5.6 x 10^6	134	1442
A, CM1IG	(500)	(0.0133)	(920.4)	6.25	4.3	(4.0)	4.5 x 10^6	96	1033
09/26/82	1716	273	477.7	6.5	4.5	4.0	1.3 x 10^7	109	1173
B, CM1IG	(315)	(0.19)	(1567.2)	7.0	4.9	(13.1)	1.2 x 10^7	106	1141
09/27/82	1635	624	477.7	10.4	7.2	5.27	7.9 x 10^6	87	936
B, CM1IG	(300)	(0.43)	(1567.2)	9.5	6.6	(17.3)	8.6 x 10^6	89	958
09/28/82	1608	468	477.7	8.25	5.7	4.66	1.0 x 10^7	95	1022
B, CM1IG	(295)	(0.325)	(1567.2)	8.5	5.9	(15.3)	9.7 x 10^6	94	1011
09/29/82	1580	834	477.7	10.0	6.9	5.21	8.3 x 10^6	92	990
B, CM1IG	(290)	(0.56)	(1567.2)	6.5	4.5	(17.1)	1.3 x 10^7	102	1098
09/30/82	1608	505	477.7	6.0	4.2	4.42	1.36 x 10^7	111	1194
B, CM1IG	(295)	(0.35)	(1567.2)	6.0	4.2	(14.5)	1.36 x 10^7	111	1194
10/14/82	1662	467	477.7	9.3	6.4	5.42	8.9 x 10^6	81	872
B, CM1IG	(305)	(0.32)	(1567.2)	11.5	8.0	(17.5)	7.1 x 10^6	76	818
10/15/82	1662	122	477.7	11.0	7.6	2.04	7.5 x 10^6	118	1270
B, CM1IG	(305)	(0.084)	(1567.2)	10.0	6.9	(6.7)	8.3 x 10^6	125	1345
10/19/82	1690	377	477.7	9.8	6.8	4.66	8.4 x 10^6	89	958
B, CM1IG	(310)	(0.26)	(1567.2)	8.0	5.5	(15.3)	1.0 x 10^7	94	1011
10/21/82	1662	174	477.7	9.5	6.6	2.88	8.6 x 10^6	107	1151
B, CM1IG	(305)	(0.12)	(1567.2)	n.d.		(9.45)			
11/08/82	1618	448	447.7	12.5	8.7	4.57	6.6 x 10^6	85	915
B, CM1IG	(297)	(0.31)	(1567.2)	10.0	6.9	(15.0)	8.3 x 10^6	91	979

Franconia and Ironton-Galesville (738 to 799 ft). Miller[(a)] estimated the average transmissivity of the upper Franconia to be 365 ft^2/day and the Ironton-Galesville 690 ft^2/day, which yielded a total transmissivity of 1055 ft^2/day. Assuming that the same ratio exists for transmissivity determined by the response method the transmissivity of the upper Franconia equals 383 ft^2/day and the Ironton-Galesville equals 725 ft^2/day.

The hydraulic conductivities of the upper Franconia and Ironton-Galesville parts of the FIG aquifer using the response method values are:

Upper Franconia = 2.6 m/day (8.5 ft/day)
Ironton-Galesville = 3.62 m/day (11.9 ft/day)

Average hydraulic conductivity for the Franconia-Ironton-Galesville aquifer is:

FIG (average) = 1.64 m/day (5.4 ft/day)

4.2.3 Storage Coefficient

Storage coefficient of a saturated confined aquifer is defined as the volume of water an aquifer releases from or takes into storage per unit surface area of the aquifer per unit change in head. The storage coefficient (S) is:

$$S = \frac{T}{D} \text{ (dimensionless)} \qquad (4.3)$$

where T = transmissivity in m^2/day
D = diffusivity in m^2/day.

Using data from Table 4.5, the storage coefficients for each pumping test are between 2.7×10^{-5} and 7.8×10^{-6} with an average of 1.2×10^{-5}. Estimates from an average diffusivity of 8.9×10^6 m^2/day and average transmissivity of 103 m^2/day (1108 ft^2/day) give approximately the same value of average storage coefficient of 1.16×10^{-5}.

(a) written communication, 1982.

4.2.4 Discharge and Actual Velocities

From the data on hydraulic gradients, hydraulic conductivities and porosities of material constituting the aquifer discharge and actual velocities of ground water were determined.

Petrological analysis (Section 3) showed that the porosities of the permeable parts of the Franconia are 0.14 to 0.18 and of the Ironton-Galesville are 0.18 to 0.27.

Assuming an average porosity of 0.16, transmissivity of 35.6 m^2/day (383 ft^2/day), hydraulic conductivity of 2.6 m/day (8.5 ft/day) and hydraulic gradient of 2.6×10^{-3}, the discharge velocity and actual velocities of the upper Franconia are 6.7×10^{-3} m/day (2.2×10^{-2} ft/day) and 4.3×10^{-2} m/day (0.14 ft/day), respectively.

Assuming an average porosity of 0.22, a hydraulic conductivity of 3.62 m/day (11.9 ft/day) and a hydraulic gradient of 7×10^{-4}, the discharge and actual velocities of the Ironton-Galesville are 2.6×10^{-3} m/day (8.4×10^{-3} ft/day) and 1.2×10^{-2} m/day (0.04 ft/day), respectively.

4.3 EVALUATION OF LEAKAGE AND PERMEABILITY OF CONFINING BEDS

Five methods of estimating the vertical leakage and permeability of the confining beds were tried. The data were collected during ambient temperature observations and pumping tests.

4.3.1 Terzaghi's Solution

Freeze and Cherry (1979) recommended the Terzaghi solution to determine permeability of a confining bed.

The basic formula is as follows:

$$C_v = \frac{k_o}{\rho \alpha g} \qquad (4.4)$$

where C_v = coefficient of consolidation or confining bed parameter, m sec^2/kg
k_o = hydraulic conductivity of confining bed, m/day

ρ = density of water, kg/m^3

g = gravitational acceleration, m/sec^2

α = coefficient of compressibility of aquifer, 10^{-9} m sec^2/kg

K. Terzaghi further defined dimensionless time factor T_f as:

$$T_f = \frac{C_v\, t}{(m_o)^2} \qquad (4.5)$$

where t is time of pumping test in days and m_o is thickness of a confining bed.

Freeze and Cherry (1979, p. 333) show a graphical presentation of Terzaghi's solution $h(z,T_f)$. It allows the prediction of the hydraulic head at any elevation z at any time t.

Hydraulic conductivity of the St. Lawrence confining bed has been determined using the following data (July 30-31, 1982, no pumping occurred through FIG aquifer):

h_o = 237.27 m (778.44 ft) initial hydraulic head in AM1SL

h = 0.14 m (0.46 ft) step-drawdown in Jordan (AS1)

t = 0.33 day (observation time for h_t)

m_o = 6.4 m (21.0 ft) (thickness of the St. Lawrence confining bed)

g = 9.8 m/sec^2 (gravitational acceleration)

α = 10^{-9} m sec^2/kg (coefficient of compressibility; Freeze and Cherry 1979, p. 55)

h_t = 232.22 m (761.88 ft) hydraulic head in AM1SL at t = 0.16 day

z = 19.03 ft (5.8 m) elevation of piezometer in St. Lawrence confining bed above the base of the confining bed

From Figure 8.7 of Freeze and Cherry (1979, p. 333):

$$T_f = 0.02$$

$$C_v = [T_f\,(m_o)^2]/t = 2.48 \text{ m}^2/\text{day}$$

and $k_o = C_{vg}\alpha\rho = 2.4 \times 10^{-5}$ m/day.

4.3.2 Neuman-Witherspoon Method

Neuman and Witherspoon (1972) propose using the ratio of the drawdown that was measured in the confining bed to that measured in the aquifer at the same time and the same radial distance from the pumping well in order to estimate hydraulic properties of confining beds.

Pumping test data - 09/24/81, well B

s' = 0.076 m (0.25 ft), drawdown in St. Lawrence (AM1) confining bed

s = 2.13 m (6.99 ft), drawdown in Upper Franconia (AM2)

t = 0.32 day elapsed time corresponding to drawdown in aquifers and confining bed

r = 254.7 m (835.6 ft), distance between wells AM1 and B

m_o = 6.4 m (21 ft), thickness of confining bed.

Dimensionless time at any given radial distance from the pumping well can be determined as follows:

$$t_D = Tt/Sr^2 \qquad (4.6)$$

where T = FIG = 107 m^2/day, transmissivity of aquifer

t = 0.32 day, elapsed time

$S = 1.3 \times 10^{-5}$, storage coefficient of the Franconia-Ironton-Galesville aquifer

resulting in $t_D = 41$.

The ratio $\frac{s'}{s} = 3.6 \times 10^{-2}$

From Neuman and Witherspoon (1972) graph (p. 1289) one finds that these values of s'/s and t_D correspond to $t_D' = 0.14$.

Specific storage value of the confining bed could be calculated by using the formula

$$S_s' = \alpha \gamma_w/(1 + e) \qquad (4.7)$$

where $\alpha = 10^{-9}$ m sec^2/kg, coefficient of the compressibility of confining bed

$\gamma_w = 1.0$ kg/(m^2 sec^2), specific weight of water

$e = 0.25$, void ratio

resulting in S_s' of 7.8×10^{-6} m^{-1}.

Then hydraulic conductivity of the confining bed could be estimated from the equation:

$$k_o = t_D' \, S_s' m_o^2/t = 1.4 \times 10^{-4} \text{ m/day} \qquad (4.8)$$

4.3.3 Thermal Profile Method

Thermal profile measurements were taken at site B in well BC1MS to the Eau Claire formation. Temperature decreased from 13.8°C (56.8°F) at the surface to 10.0°C (50°F) at a depth of 109 m (358 ft), and then increased gradually to 11.7°C (53.1°F) at a depth of 242 m (793 ft) (Figure 4.8). The changes at a depth of 109 m (358 ft) are presumably caused by continuous withdrawal of water from the Prairie du Chien-Jordan aquifer (man-made conditions). The increase in temperature to a depth of 242 m (793 ft) is caused by the heat flow in relatively undisturbed conditions.

Determination of rates of vertical ground-water movement using the thermal profile data have been recommended by Bredehoeft and Papadopolus (1965). The basic formulas are:

$$\frac{T_z - T_o}{T_L - T_o} = f(\beta, \frac{z}{L}) \qquad (4.9)$$

and

$$\beta = (V_z \, C_o \, \rho_o L)/K \qquad (4.10)$$

where T_z = temperature measurement at any depth, °C

T_o = uppermost temperature measurement of the confining bed, °C

T_L = lowermost temperature measurement of the confining bed, °C

L = length of vertical section over which measurement extends, cm (vertical distance between T_o and T_L)

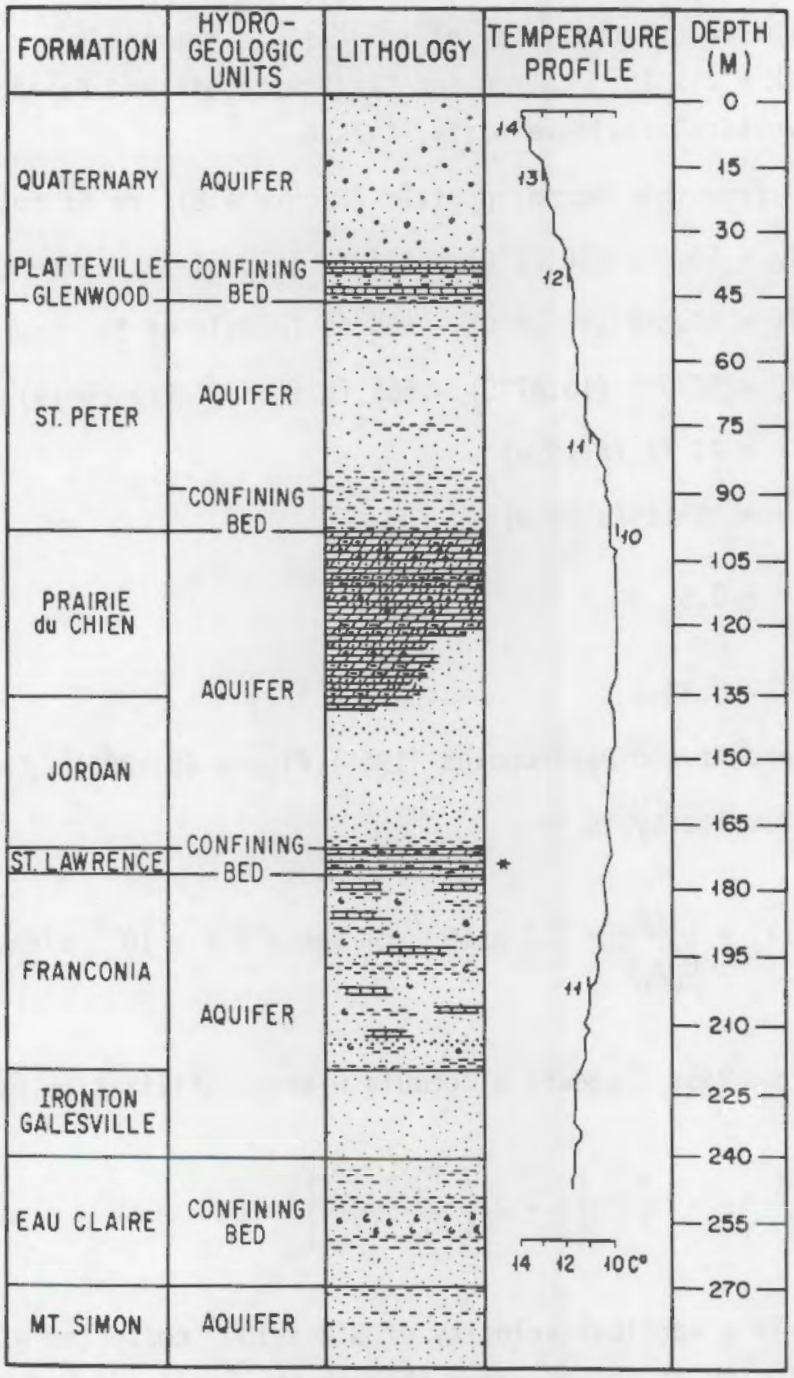

FIGURE 4.8. Thermal Profile of Well BC1, 11/82

C_o = specific heat of fluid (water C_o = 1.0)

ρ_o = density of fluid (water = 1.0), g/cm^3

K = thermal conductivity of solid-fluid complex
(K = 2 x 10^{-3} cal/cm sec °C (Bredehoeft and Papadopolus 1965)

V_z = vertical fluid velocity, cm/sec.

Data obtained from the thermal profile (Figure 4.8) are as follows:

T_o = 50.4°F (10.22°C) - 545 ft (top of St. Lawrence)

T_z = 50.6°F (10.34°C) - 555 ft (middle of St. Lawrence)

T_L = 50.9°F (10.47°C) - 565 ft (top of Franconia)

L = 20 ft (6.10 m)

z = 10 ft (3.05 m)

$\frac{z}{L}$ = 0.5

$f(\beta, \frac{z}{L})$ = 0.48

From the Bredehoeft and Papadopolus (1965) figure (p. 326), β = 0.1.

Vertical fluid velocity is

$$V_z = \frac{K\beta}{C_o \rho_o L} = 3.3 \times 10^{-7} \text{ cm/sec} = 2.8 \times 10^{-4} \text{ m/day} \qquad (4.11)$$

Frolov (1976, p. 236) suggests a formula without utilization of a graph:

$$V_z = \frac{2K}{z} \left[1 - 2\left(\frac{T_z - T_o}{T_L - T_o}\right)\right] \qquad (4.12)$$

which results in a vertical velocity of 5.2 x 10^{-7} cm/sec or 4.5 x 10^{-4} m/day. Calculated velocity of ground water through the confining bed using both equations is in good agreement.

Water-level information in the Jordan and upper Franconia is used to evaluate vertical hydraulic gradient. The most reliable hydraulic gradients

could be approximated during the period of no pumping from these units. Data on November 24, 1981, were used when Δh was 3.33 m (10.94 ft) and m_o was 6.40 m (21 ft), resulting in $\Delta h/m_o$ of 0.52. Hydraulic conductivity (k_o) of the confining bed using Equation 4.11 is then 5.4×10^{-4} m/day.

4.3.4 Hydrochemical Method

The hydrochemical method is similar to the thermal profile method. Instead of water temperature changes, this method uses changes in chemical concentration of elements that have no significant lithologic sources (Cl and F) or natural isotopes.

The basic equations that describe diffusion-convection mass transfer through the confining bed are (Plougina 1979):

$$C = \frac{\exp(\bar{V} \times \bar{z}) - 1}{\exp \bar{V} - 1} \qquad (4.13)$$

where $$C = \frac{C_z - C_1}{C_2 - C_1}$$

$$\bar{V} = \frac{m_o V_z}{D_f}$$

$$\bar{z} = \frac{z}{m_o}$$

C_z, C_2, C_1 = concentration of elements in the confining bed, upper and lower aquifers respectively, ppm

m_o = thickness of the confining bed, m

z = distance between the top of the confining bed and the observation point within the confining bed, m

O_f = diffusion coefficient of porous media ($D = 10^{-4}$ to 10^{-6} m^2/day)

V_z = vertical velocity of flow through the confining bed, m/day

The diffusion coefficient for fluoride has been estimated using the formula:

$$D_f = \frac{RT}{F^2} \times \frac{\lambda_1}{|Z_1|} \quad \text{(Weast and Astle 1979, p. F.62)} \qquad (4.14)$$

where R = gas constant = 8.314 j $mole^{-1}$ $°K^{-1}$

T = temperature in °K

F = Faraday's constant = 9.65 x 10^{-4} coulombs $mole^{-1}$

λ_1 = equivalent conductance (coul•$cm^2 sec^{-1} volt^{-1} mole^{-1}$) = approx. 40

Z_1 = ionic charge = 1.0

resulting in a value for D_f of 1.0 x 10^{-5} cm^2/sec or 1.0 x 10^{-4} m^2/day.

Data on the concentration of chloride and fluoride were used from wells AS1J, AM1SL, AM2IG, and AC1MS (Tables D.13 and D.14). Chemical analyses of water samples collected from monitoring wells indicate a wide range of chloride concentration, probably caused by contamination during the well completion and grouting. Therefore, data on chloride concentration have not been used to estimate permeability of the confining bed. Fluoride concentration exhibits a relatively linear vertical distribution.

Existing data on fluoride content in the Jordan (AS1) (6.8 μM, or 1.29 x 10^{-7} ppm) on 8/31/82, the St. Lawrence (AM1) (14.0 μM, or 2.66 x 10^{-7} ppm), and the Franconia-Ironton-Galesville (well A) (13.7 μM, or 2.6 x 10^{-7} ppm) on 4/27/82 to 5/5/82 could not produce satisfactory results, conceivably due to unreliable concentration of fluoride in well AM1. Preliminary calculations show that concentration of fluoride in the St. Lawrence should be lower than indicated in Section 6 and Appendix D (14 μM, or 2.66 x 10^{-7} ppm). Additional sampling from well AM1 (11/2/83) showed that concentrations of F in St. Lawrence (12.5 μM, or 2.37 x 10^{-7} ppm) and FIG aquifer (13.7 μM, or 2.6 x 10^{-7} ppm) are very close. Results of fluoride sampling confirm data from step-drawdown pumping that the St. Lawrence well (AM1SL) is connected to the upper Franconia.

4.3.5 Hydrodynamic Method

Gussein-Zade (1961) gives a solution for two aquifers separated by a confining bed:

$$H_{U_x} = C_1 + C_2 x + C_3 \cosh \lambda x + C_4 \sinh \lambda x \quad (4.15)$$

$$H_{L_x} = C_1 + C_2 x - (b_1/b_2)\, C_3 (\cosh \lambda x + C_4 \sinh \lambda x) \quad (4.16)$$

$$C_1 = (H_L'' + H_U'')(b_1/b_2)/[1 + (b_1/b_2)] \quad (4.17)$$

$$C_3 = (H_U'' - H_L'')/[1 + (b_1/b_2)] \quad (4.18)$$

$$C_2 = \frac{[(b_1/b_2)(H_U' - C_1 - C_3 \cosh \lambda x)] + H_L' - C_1 + C_3(b_1/b_2) \cosh \lambda L}{L[1 + (b_1/b_2)]} \quad (4.19)$$

$$C_4 = (H_L - H_U) - C_3[1 + (b_1/b_2) \cosh \lambda L]/[1 + (b_1/b_2) \cosh \lambda L] \quad (4.20)$$

where $b_1 = k_o/(T_L\, m_o)$

$b_2 = k_o/(T_U\, m_o)$

$\lambda = (b_1 + b_2)^{1/2}$

$k_o = (\lambda^2\, m_o)/[(1/T_L) + (1/T_U)]$

C_1, C_2, C_3, C_4 = constants

H_U'' and H_U' = hydrostatic pressure of the upper aquifer (Jordan) at two points, upgradient and downgradient, respectively, m

H_L'' and H_L' = hydrostatic pressure of the lower aquifer (Franconia-Ironton-Galesville) at two points, upgradient and downgradient, respectively, m

H_{U_x} = hydrostatic pressure at the arbitrary point of the upper aquifer (Jordan), m

H_{L_x} = hydrostatic pressure at the arbitrary point of the lower aquifer (FIG), m

T_U = transmissivity of the upper aquifer (Jordan), m^2/day

T_L = transmissivity of the lower aquifer (Franconia-Ironton-Galesville), m^2/day

k_o = hydraulic conductivity of the confining bed (St. Lawrence), m/day

x = distance to the arbitrary point, m

L = total length of cross-section between upgradient and downgradient, m.

Substituting data from the ATES site:

H_U' = 237.18 m (BS1J, Nov. 24, 1981)

H_L' = 233.84 m (BS1UF, Nov. 24, 1981)

H_U'' = 237.44 m (AS1) Nov. 24, 1981)

H_L'' = 236.66 m (AM3UF, Nov. 24, 1981)

T_U = 700 m^2/day (well STP3)

T_L = 107 m^2/day (well A and B)

L = 254.7 m

x = 100 m

H_{U_x} = 237.3 m

H_{L_x} = 234.9 m

m_o = 6.4 m

Resulting in:

C_1 = 234.27 m

C_3 = 2.90 m

$C_2 = (2.8 - 0.43 \cosh 100\,\lambda + 0.43 \cosh 2.547\,\lambda)/293.6$

$C_4 = (0.84 - 3.35 \cosh 254.7\,\lambda)/(1.15 \cosh 254.7\,\lambda)$

Solving Equations (4.15) and (4.16) with respect to λ by trial and error, constants C_2 and C_4 are determined:

$$237.3 = 234.27 + 100\ C_2 + 2.9 \cosh 100\ \lambda + C_4 \sinh 100\ \lambda$$

$$234.9 = 234.27 + 100\ C_2 - 0.15(2.9 \cosh 100\ \lambda + C_4 \sinh 100\ \lambda)$$

Thus, λ equals 1.2×10^{-3} and hydraulic conductivity (k_o) of the St. Lawrence confining bed is 8×10^{-4} m/day (2.6×10^{-3} ft/day).

4.4 SUMMARY

Analysis of the water level data indicates that ground-water movement in the Franconia-Ironton-Galesville aquifer is relatively slow. Discharge and actual velocities are 2.6×10^{-3} m/day and 0.01 m/day (8.4×10^{-3} ft/day and 0.04 ft/day), respectively.

The transmissivity, determined by the response method, is 37 m^2/day (383 ft^2/day) for the upper Franconia and 70 m^2/day (725 ft^2/day) for the Ironton-Galesville. The total transmissivity of the Franconia-Ironton-Galesville aquifer is about 103 m^2/day (1108 ft^2/day). Hydraulic conductivity values of the upper Franconia and Ironton-Galesville aquifer are 2.6 m/day and 3.6 m/day (8.51 ft/day and 11.89 ft/day), respectively. Average hydraulic conductivity for the full thickness of the aquifer is 1.64 m/day (5.38 ft/day).

Storage coefficient values range between 2.7×10^{-5} and 7.8×10^{-6}, averaging 1.16×10^{-5}.

The permeability of the confining bed over the FIG aquifer, St. Lawrence formation, using various methods is within the range 2.4×10^{-5} to 8×10^{-4} m/day (7.8×10^{-4} to 2.6×10^{-3} ft/day), indicating that the Franconia-Ironton-Galesville aquifer is relatively well separated hydrologically from the overlying Prairie du Chien-Jordan aquifer.

5.0 HYDROGEOLOGIC TEST PROGRAM

The hydrogeologic test program can be divided into unheated-water (isothermal, ambient temperature) testing and heated-water (non-isothermal) testing. Table 5.1 outlines all the significant on-site hydrogeologic testing. Sections 4, 6, 7, and 8, as well as this one, present data and results from these tests.

5.1 AMBIENT TEMPERATURE TESTING

5.1.1 Pumping Tests

The very first pumping tests were conducted in the two core holes (AC1 and BC1) with inflatable packers used to isolate the intervals to be tested. Each isolated interval was pumped, the flow measured, and the pressure differences recorded for the adjacent interval. These tests were conducted by the U.S. Geological Survey to identify the various hydrologic units of the aquifers for the modeling, to determine the probable capability of the aquifer to provide a satisfactory yield, assist in design parameters for the pumping wells, and assist in selection of horizons to be used for pressure transducers in monitoring wells. Hydrologic zones identified are shown on Figures 2.3 and 2.6.

The next opportunity for a pumping test was when the pumping wells were being completed. At this time for both wells A and B a temporary pump was installed immediately after the well-screens had been emplaced for development pumping. The testing consisted of step-drawdown tests at wells A and B (Table 5.1). Miller (1984, 1985) summarizes these results; they are also discussed in Section 4.

Following the completion of the connecting piping and the addition of a 4-inch line running to the storm sewer at site A, the system pumps were turned on for the first time in December 1981. In February 1982 a 4.5 day constant-rate pump test was conducted on well A (Miller 1984, 1985).

TABLE 5.1. Summary of Hydrogeologic Tests at the University of Minnesota ATES Field Test Facility

Date, yr/mo/day	Duration	Type of Test
800927	-	Packer test, AC1 (7 intervals)
801025/801026	-	Packer test, BC1 (18 intervals)
811008	11.1 hour	Step-drawdown test, well B (220, 380, 735 gpm)
8109	9.7 hour	Step-drawdown test, well A (267, 480, 584, 1000 gpm)
820224/820302	4.5 days	Constant rate pump test, well A
820427/820428	1 day	Constant rate pump test, well B
820429/820430		Ambient-temperature water injection test (original configuration)[a]
820430/820501		Well rehabilitation (step-drawdown test and pumpout) (well A)
820502/820509	8 days	Ambient-temperature water injection (revised configuration)[b]
820515/820519		Initial heated-water injection test cycle attempt
820519/820629		Pumpout attempts - pump failures
820902/820903		Well rehabilitation (acid-treatment and step drawdown test, well A)
820909/820916		Pumpout of heated water
820922/820924	2 days	Ambient-temperature water injection test
820926/821110		Testing precipitator/filters
821116/821222		SHORT-TERM CYCLE 1
	(5.2 in 17.0 days)[c]	Heat storage
	(13.0 days)	Storage period
	(5.2 days)	Heat recovery (59%)
830509/830826		SHORT-TERM CYCLE 2
	(8.0 in 10.4 days)[c]	Heat storage
	(90 days)[d]	Storage period
	(8.0 days)	Heat recovery (45%)
830921/831019		SHORT-TERM CYCLE 3
	(7.7 in 10.4 days)[c]	Heat storage
	(9.7 days)	Storage period
	(7.7 days)	Heat recovery (62%)
831107/831207		SHORT-TERM CYCLE 4
	(7.7 in 12.0 days)[c]	Heat storage
	(10.1 days)	Storage period
	(7.7 days)	Heat recovery (59%)

(a) Water introduced to heat storage well through annular space between column pipe and casing.
(b) Water introduced to heat storage well through column pipe; configuration for all subsequent water injections.
(c) Actual duration of heated-water injection and days from beginning to completion.
(d) Long storage period due to pump failure. Pump design revised and new design installed prior to heat recovery. Pumping attempts failed on 3 separate days in May and June. Replaced well A assembly in August before Heat Recovery, Cycle 2; replaced well B assembly in September following Cycle 2.

5.1.2 Ambient Temperature Injections

Two ambient temperature injection tests were conducted following the arrival and installation of enough pressure transducers to allow performance of an injection test. For the first, the plan was to introduce water to well A at a moderate rate 6.3 L/sec (100 gpm) for 1 day, then increase the rate to 18.9 L/sec (300 gpm) if all was satisfactory. For this test, the annular space between the column pipe and the casing of well A was used for injection, following the designed plan. Unfortunately, this did not allow the maintenance of a continuous water column from the surface to the water level in the well. The water cascaded down the annular space and incorporated a significant amount of air. While the injection rate was only one-third of the pumping rate it was not possible to detect the effect. However, shortly after beginning the 300 gpm injection rate it became obvious that the system was clogging as a result of air-entrainment (Figure 5.1). Injection was stopped and rehabilitation pumping started immediately. The water recovered initially was "effervescent." Because the dissolved oxygen (DO) level of the source water is at levels considerably less than 1 ppm, DO levels in the water pumped out were measured to assess when enough pumping had been done to eliminate the clogging. Initial DO levels in water pumped out were greater than 12 ppm. After 20 hours of pumping at increasing rates, the DO levels returned to less than 1 ppm.

For all subsequent injections the water was routed inside the column pipe of the receiving well. This use of the column pipe as a drop pipe allows the pressure to be maintained on the system, preventing air entrainment. At elevated temperatures this prevents flashing to steam. This modification eliminated the air-entrainment problem.

A second measure taken to maintain pressure was to conduct all subsequent injection at or near the design rate of 300 gpm. Following a successful 8-day injection of ambient-temperature water (Figure 5.1) final preparations for heated-water injection were made.

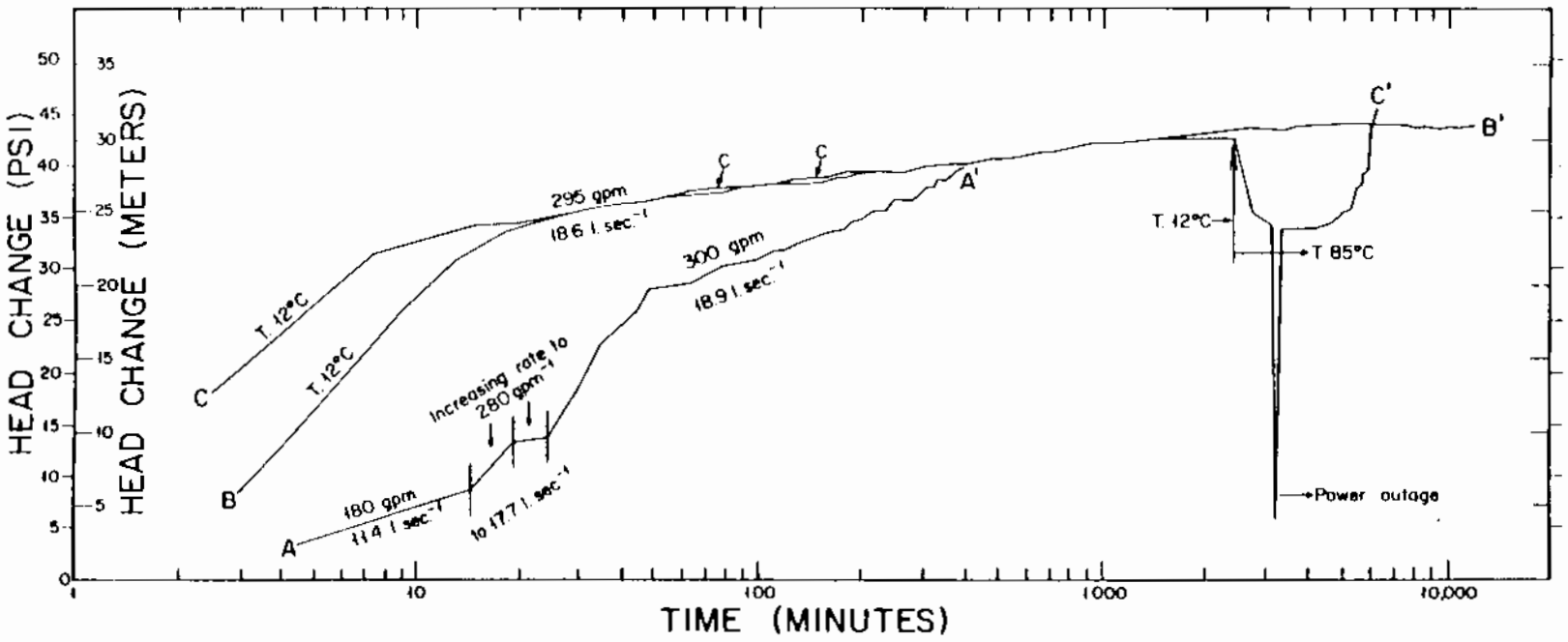

LEGEND

A-A' - ambient temperature (12°C) water introduced through annular space (A-A' begins 24 hours after start of injection).

B-B' - ambient temperature (12°C) water intorudced through column pipe.

C-C' - ambient temperature (12°C) water followed by 82° to 85° water introduced through column pipe.

FIGURE 5.1. Head Changes in Well A as a Function of Time During Injection. The sudden drop in pressure when the heated water injection began is the result of the abrupt decrease in kinematic viscosity.

5.2 HEATED-WATER TESTING: PROBLEMS AND SOLUTIONS

The non-isothermal testing was originally planned as four 24-day test cycles (short-term cycles). Each cycle was to consist of 8 days of heated-water injection, 8 days of storage in the aquifer, and 8 days of heated-water recovery pumping. Two major problems affected the actual test cycle schedules. The first significant problem, precipitation of $CaCO_3$ in the heated water, caused significant deviation from this original plan. The second problem, failure of the pump's lineshaft bearings to allow hot-water pumping, also affected the original plan.

The subsection below deals with the different steps in the heated-water testing, problems encountered, and remedial actions.

5.2.1 Initial Heated-Water Injection

Plans for the initial heated-water cycle called for ambient temperature water to be injected for 2 days to allow a direct comparison with the previous injection tests. On May 17, 1982, the water being injected was heated to 85°C (185°F). Approximately 45 minutes were required to stabilize the water temperature. Pressure in the injection well immediately dropped by 48 kPa (7 psi) as a result of the hot, much less viscous water being injected.

Injection continued (interrupted only by a brief power outage) for 50 hours when it became apparent that clogging was taking place in well A (Figure 5.1). The constant and increasing rate of head buildup in well A and the relative head changes in the Ironton-Galesville and upper Franconia portions of the aquifer suggested that 1) the Ironton-Galesville well screen was clogging, and 2) the clogging rate was increasing. Pressure differential across the condenser also increased as the injection proceeded. All of the above suggested that a significant amount of calcium carbonate was precipitating as the water was heated.

Temperature recorded in the Ironton-Galesville portion of the aquifer in well AS1 began to rise 17 hours after the heated-water injection began. No temperature change was recorded at other horizons.

Following the shutdown, attempts were made to pump out the heated water stored at well A to rehabilitate the well. Pumpout was impossible because the pump failed to operate once the water temperature reached 77° to 79°C (170° to 175°F). The pump was pulled to determine the cause of failure. Investigation revealed that the bearings supplied were not of the EPDM material called for by the pump manufacturer. Delay followed while replacement bearings were sought.

During the delay a downhole television log of well A revealed significant well-screen clogging. Inspection of the column pipe removed from the well revealed a scale buildup of about 1 mm; inspection of the exit side of the condenser revealed scale 2 mm thick. Methods to solve the problem of scale buildup were investigated during the delay caused by the bearing failure.

Water softening by ion-exchange was seriously considered. However, this would have required modification of the specific injection permit issued by the Minnesota Pollution Control Agency (MPCA) and the Minnesota Department of Health (MDH). The permit had a specific statement prohibiting the use of water treatment chemicals. A precipitator consisting of a fixed-bed reactor filled with high-calcium limestone was developed. The fixed-bed reactor (precipitator) consists of three parallel pairs of 1.8-m long, 0.36-m diameter pipes, which are filled with 0.94 m^3 of sized high-calcium limestone (Table 5.2). At a flow rate of 18.9 L/sec, residence time in the precipitator is about 15 sec. This reduces the degree of calcium carbonate supersaturation to levels that prevent extensive scale buildup in the well screen and pump assembly. It does not prevent the scaling of the condenser. Plans for both a model-scale and full-scale unit were made. These were built, installed, and testing began by late September 1982.

Well rehabilitation by acid treatment (223 kg of sulfamic acid) was done immediately before replacing the pump in well A. Immediately after replacing the pump, pumpout of the acid was initiated. Water was pumped to waste for 3 hours (Table 5.3). The pH of the initial water pumped was already 5.5, and by the end of the pumping it was to 7.0.

TABLE 5.2. Media for Precipitating Filters (Fixed-Bed Reactors)

Typical Sieve Analysis Cumulative Through (U.S. Screen):	Materials	
Grade	"Cage-Cal" FD6-20	"Shellmaker" FD3-12
3 mesh (1/4 in.) (6.35 mm)	-	100%
4 mesh (3/16 in.) (4.76 mm)	-	85%
6 mesh (1/8 in.) (3.175 mm)	100%	50%
12 mesh (1/16 in.) (1.588 mm)	60%	3%
16 mesh (3/64 in.) (1.191 mm)	25%	1%
20 mesh (1/32 in.) (0.794 mm)	5%	-
40 mesh (1/64 in.) (0.397 mm)	1%	-
Bulk density, lb/ft^3	100 lb/ft^3	110 lb/ft^3
Amount of each used:	18%	82%

Typical Chemical Analysis:

Calcium carbonate ($CaCO_3$)	98.3%
[Calcium (Ca)	39.3%]
Magnesium carbonate ($MgCO_3$)	0.5%
Silica and silicates (SiO_2)	0.3%
Aluminum and iron oxides (R_2O_3)	0.16%
Moisture (H_2O).	less than 0.10%

Source: Calcium Carbonate Company (Division of J.M. Huber Corporation) Ft. Dodge, Iowa plant. Mined from Gilmore City formation (Mississippian age) at underground quarry, Ft. Dodge, Iowa.

TABLE 5.3. Pumpout of Well A Following Acid Treatment

Time, hrs since start	Temperature, °C	pH	Flow Rate, gpm
0.1	14.4	5.5	413
1.1	16.9	>6	406
2.2	20.0	>6<6.5	408
2.6 (adjust flow)			
2.7	21.1	7.0	299
2.9 (pump off)			

A step-drawdown test was conducted the following day to assess the degree of rehabilitation accomplished with the acid treatment (Table 5.4). Analysis suggests that well A was more efficient following rehabilitation than during the initial step-drawdown test (Miller 1985).

Well A was pumped for 25 hours at ~325 gpm and for 54 hours at ~390 gpm to return the FIG aquifer around well A to nearly ambient temperature conditions. Peak water temperature was 30°C (86°F); final temperature was 21°C (70°F).

Following the pumpout, another ambient-temperature injection test using well A was conducted for 59 hours. The response of the aquifer was satisfactory (within 4 psi of the initial injection test) (Miller 1985).

The period following this injection was spent testing the effectiveness of the precipitator with different materials and sizes of material. Locally available outwash sand and gravel and crushed dolomitic limestone, as well as crushed high-purity limestone were tried. The final material selected, crushed, high-purity limestone, is listed in Table 5.2.

TABLE 5.4. Step-Drawdown Test of Well A Following Acid Treatment

Date	Time	pH	Temperature, °C	Flow, gpm	Remarks
820902	2100				Pump on
	2120	7.0	20.0	315	
	2230	7.0	21.1	315	
	2300	7.2	23.3	364	Switch rate
820903	0030	7.2	25.0	361	
	0100	7.2	25.5	405	Switch rate
	0330	7.2	28.1	405	00 <<1 ppm
	0400				Pump off

5.3 SHORT-TERM CYCLES

Following testing of the precipitators, Short-Term Cycle 1 was conducted from November 16 to December 22, 1982. The precipitator medium allowed about 1 day's operation before needing replacement because of head losses due to accumulation of precipitate (aragonite) in the precipitator. Each time the precipitator was changed the condenser was cleaned with hydrochloric acid to remove scale buildup.

Because of problems encountered with condenser tube leaks after the fourth cleaning and the approaching expiration of the injection permit, only about 5 days of injection were used for this cycle. The test went quite successfully. Changing of media and acid-cleaning of heat exchanger are quite labor-intensive. To accomplish this in about 8 hours requires the effort of three or four pipefitters, a crane operator and assistant, and a laborer. Not all are needed for the entire operation; however, they must be available at the appropriate times to complete a change in one shift. During this first test cycle, one-shift turn around was not accomplished. But for subsequent test cycles, no problems came up; it was nearly routine to complete the operation in a single shift.

The heat-injection (storage) phase is an intermittent injection with the use of the precipitators. Injection continues until new media or cleaning of heat exchanger is necessary, injection stops until the system is prepared and injection continues thereafter. This type of operation provides many more opportunities to observe the startup and shutdown behavior of the system and aquifer than an uninterrupted injection. These are extra opportunities to examine thermal and hydraulic behavior during the test cycles, and some interesting and perhaps important observations resulted.

During Cycle 1, a pressure transducer was placed in well A and operated satisfactorily. Unfortunately the transducer failed before Cycle 2 began.

Between Cycles 1 and 2, a second precipitator unit was installed so that a longer continuous run could be achieved before needing to stop for a media

change. Also, the tubes in the condenser were all replaced with stainless steel tubes. In addition to the leaking tubes that had been plugged, the original tubes had many cracks and weak spots.

During Cycle 2, mechanical problems with the heat-storage well included a broken lineshaft and failure of the EPDM bearings. As outlined in Section 2, these problems resulted in a long storage period (90 days) and the replacement of all lineshaft and lineshaft bearings in both the heat storage and water supply wells. A modified enclosed lineshaft with provision for product lubrication of bronze and graphite-bronze bearings was installed in well A prior to heated-water withdrawal. This design was installed in well B following the recovery period. The pumps have operated nearly perfectly following these modifications.

Prior to Cycle 3, pressure testing revealed numerous leaks in the tubes of the condenser. The condenser was re-tubed again with carbon steel tubes. The numerous pinhole leaks discovered in the tubes apparently resulted from insufficient flushing and neutralization of the acid used to clean the tubes after the last injection period in June (during Cycle 2).

Test Cycle 3 was conducted from September 21 to October 19, 1983. The operations went smoothly throughout the cycle. Cycle 4, ending on December 7, 1983 went just about as smoothly. However, several condenser tubes became plugged during the third injection period, and the system did not operate as well following this.

5.3.1 Cycle 1

The first complete short-term test cycle of the University of Minnesota ATES facility was conducted from November 16 to December 22, 1982. Table 5.5 summarizes the results of Cycle 1. Ambient temperature source water at 11°C (53°F) was heated to a mean temperature of 90°C (194°F), a mean delta T of 79°C, and injected at a mean flow rate of 18.4 L/sec (292 gpm) for 125.7 hours between November 16 and December 3. Five injection periods, each about 1 day long, were followed by 1 or more days of maintenance work on the aboveground systems and replacement of the reactor media (Figure 5.2). A total of 8.3 x 10^3 m^3 of heated water was injected.

TABLE 5.5. Cycle 1 - Summary

	Heat Storage (Injection)	Storage	Heat Recovery
Duration, days	5.2/17.0	13	5.2
Water temperatures, °C			
Mean source or return	11	-	59.0
Mean inject or recover	89.4	-	59.2
Highest inject or recover	104.4	-	76.7
Minimum inject or recover	82.0	-	39.4
Mean delta T	79	-	-
Mean flow rate, L/sec	18.4	-	18.1
Pumped volume, 10^3 m^3	8.28	-	8.09
Energy input/output rate, MW	6.2	-	3.7

	Energy balance, 10^9 Btu
Source steam	3.00
Returned condensate	0.08
Consumed steam	2.92
Source ground water[(a)]	-
Added to ground water	2.62
Energy to pump water	0.055
Recovered in ground water	1.56
Not recovered in ground water	1.05
Energy recovery factor (aquifer)	59%
System energy recovery factor[(b)]	51%

(a) Ambient temperature ground water assigned 0.
(b) Based upon source steam; does not include conversion of coal to steam.

Heat withdrawal began after a 13-day storage phase. The water withdrawn from storage reached a peak temperature of 76.7°C (170°F) after 12 hours of pumping. Water temperature decreased linearly with flow from this peak to 39°C (103°F) at the end of the 5 days (125.4 hours) of heat withdrawal (Figure 5.2). Mean temperature of water withdrawn was 59°C (140°F). A total of 8.1 x 10^3 m^3 of heated water was withdrawn from the storage well and returned to the supply well.

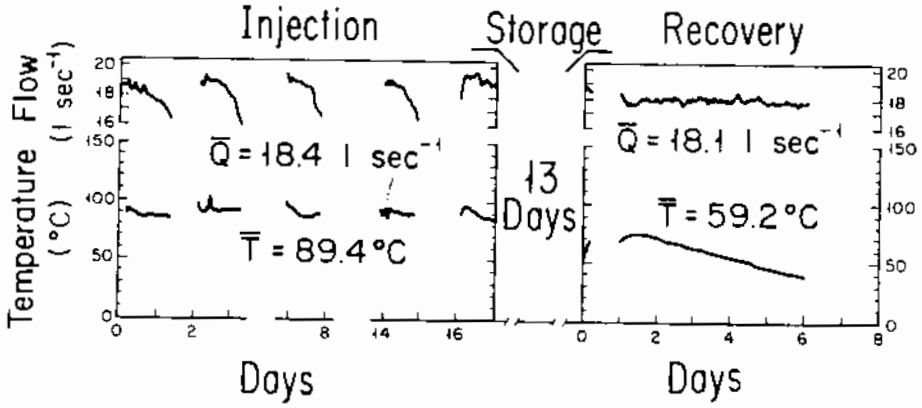

FIGURE 5.2. Flow Rates and Temperatures of Heated Water Injected and Recovered, Plotted Against Time - Cycle 1

Heat recovery from the aquifer during this first cycle was 0.59 based upon energy balance. This result is very close to that predicted by the computer-modeled cycle (0.60 versus 0.59). Energy balance summary for the system is given in Table 5.5.

The five injections of heated water provided the opportunity to compare the responses of the different portions of the aquifer for each injection. Pressure buildup in well A appeared to stabilize at levels 27 to 34 psi above the starting pressure. There is an indication in monitoring wells that the Ironton-Galesville portion had less head buildup in successive injections; there is no evidence of clogging. The temperature increases at Ironton-Galesville horizons have a greater effect on the pressure response than any relative change in pressure response. The upper Franconia showed only a small increase in temperature in any of the observation wells.

Temperatures in well AS1, nominally 7 m from the injection well, reached 80°C (176°F) at the most permeable horizon of the Franconia-Ironton-Galesville aquifer by the conclusion of heat injection (Figure 5.3). Following heat withdrawal, the peak temperature in well AS1 was 26°C (79°F).

Water withdrawn following storage showed chemical changes that closely followed predictive models (see Section 6 dealing with water analyses and chemical modeling). Dissolved silica decreased as the temperature decreased.

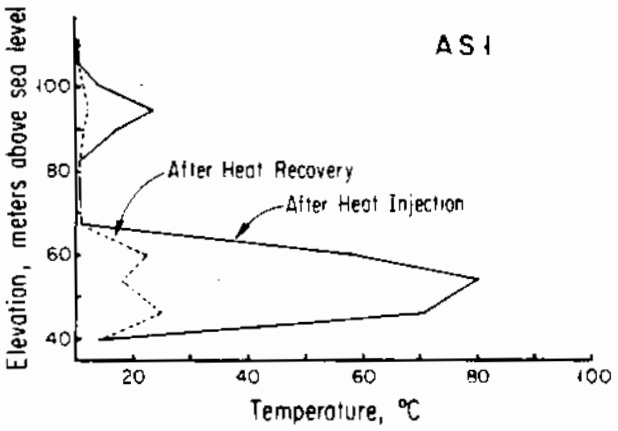

FIGURE 5.3. Temperatures Recorded in Well AS1 After Heat Injection and Recovery Phases - Cycle 1

Total calcium, hardness and sulfate increased as the temperature decreased. Chloride showed an initial increase, then a rapid decrease toward background levels. Total dissolved solids were about 210 mg/L as compared to 180 mg/L during injection.

This test was made possible by the operation of the precipitating filters installed to decrease the degree of $CaCO_3$ supersaturation in the heated aquifer water. During Cycle 1, the reactors behaved consistently. Typical heated water during Cycle 1 entered the fixed-bed precipitator with a supersaturation index (S.I. = log $[(Ca^{++})(CO_3^{-})/K]$) to aragonite of 0.88. Water injected into the well had a typical S.I. of 0.58 (see Table 6.7). Performance was consistent during the test. Total hardness was reduced from about 2.1 mM to 1.7 mM, which means that the units prevented about 162 kg (357 lb) of calcium carbonate from clogging the well. The injected water remained supersaturated, but by a much lower factor.

5.3.2 Cycle 2

Cycle 2 began May 9 and ended August 26, 1983 (Table 5.6, Figure 5.4). Five heated-water injections, totaling 192 hours (8 days) of injection, were conducted. Summary data for the injection phase show a mean injection rate of 17.7 L/sec (280.3 gpm), a mean temperature for the entire injection phase of

TABLE 5.6. Cycle 2 - Summary

	Heat Storage (Injection)	Storage	Heat Recovery
Duration, days	8.0/10.3	90	8.0
Water temperatures, °C			
Mean source or return	20.5	-	54.4
Mean inject or recover	97.4	-	55.2
Highest inject or recover	125.0	-	68.9
Minimum inject or recover	90.6	-	39.4
Mean delta T	76.9		-
Mean flow rate, L/sec	17.6	-	17.8
Pumped volume, 10^3 m^3	12.2	-	12.3
Energy input/output rate, MW	5.63	-	2.58

	Energy Balance, 10^9 Btu
Source steam	4.26
Returned condensate	0.21
Consumed steam	4.05
Source ground water[(a)]	0.43
Added to ground water	3.70
Energy to pump water	0.070
Recovered in ground water	1.69
Not Recovered in ground water	2.01
Energy recovery factor (aquifer)	46%
System energy recovery factor[(b)]	39%

(a) Ambient temperature ground water assigned 0.
(b) Based upon source steam; does not include conversion of coal to steam.

97.4°C (207°F), a mean delta T of 77°C (138°F), an energy flow rate of 5.6 MW, and a pumped volume of 12.2 x 10^3 m^3. The target temperature of 125°C was briefly attained twice during the cycle.

As a result of the addition of the second bank of precipitators, the heated-water injection continued for about 40 hours of operation before scheduled maintenance was required. The pressure transducer that had been

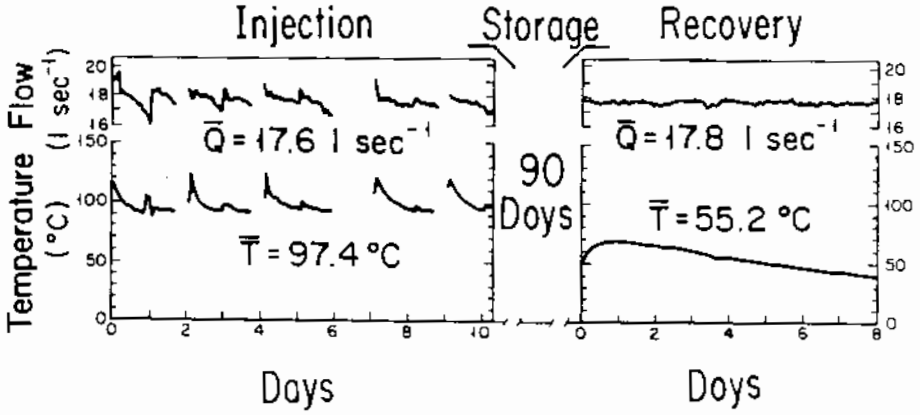

FIGURE 5.4. Flow Rates and Temperatures of Heated Water Injected and Recovered, Plotted Against Time - Cycle 2

installed in well A for Cycle 1 failed and a pressure gauge was installed at the well head to monitor the vapor pressure in the annular space of the well.

Total hardness of the injected heated water in Cycle 2 was about 1.7 mM. Performance of the reactors from initial data does not appear to have been as consistent as in Cycle 1; however some temperature corrections need to be applied to some of the data. Supersaturation index of injected water typically had a value of 0.22. As in the previous test, the precipitator removed approximately 31 kg (68 lb) per day of calcium carbonate from the heated water. Total dissolved solids averaged 188 mg/L in the injected water.

Highest temperature in well AS1 reached 94°C (201°F) after the last injection of heated water (Figure 5.5). Failure of the pumpshaft bearings in the storage well forced a long delay in the heat recovery phase of the test cycle. The temperature fell to 84°C (183°F) by August 9.

The heat recovery phase began 89 days, 17 hours, 10 minutes after storage began. Water recovered reached a peak temperature of 69°C (156°F) about 12 hours after startup (Figure 5.4). After several hours at the peak temperature, the temperature of the water withdrawn declined at a rate of about 0.1°C/hr (0.3°F/hr) to 39°C (103°F) at the end of 192 hours (8 days) of withdrawal.

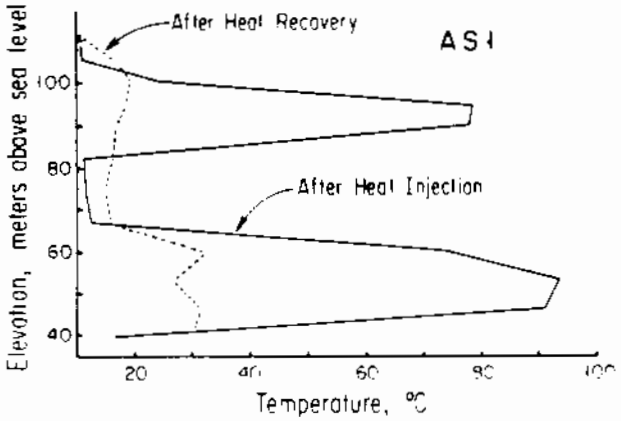

FIGURE 5.5. Temperatures Recorded in Well AS1 After Heat Injection and Recovery Phases - Cycle 2

Review of the data gives a mean temperature of 55.2°C (131°F). Net energy recovery factor for this cycle is 0.46.

During the heated-water injection phase there were four scheduled shutdowns for replacement of media in the precipitating filters and for removal of scale from the condenser (main heat exchanger). Changing the media and cleaning the condenser were accomplished in about 7 hours each. The total duration of the four shutdowns was about 52 hours. Each fill of the precipitating filters and cleaned condenser allowed about 40 hours of operation.

5.3.3 Cycle 3

Cycle 3 was conducted from September 21 to October 19, 1983 (Table 5.7, Figure 5.6). For most of the heated-water injection the temperature was maintained at above 100°C. The mean temperature of the water stored was 106.1°C (223°F). Flow was maintained at a rate of 18.3 L/sec (290 gpm) for 185 hours, storing 12.2 x 10^3 m^3 of hot water. Source water temperature for this cycle was 36°C (97°F), for a mean delta T of 70°C.

Temperatures recorded in well AS1 reached 102°C following the injection phase (Figure 5.7). At the end of the storage period the highest temperature was 103°C.

TABLE 5.7. Cycle 3 - Summary

	Heat Storage (Injection)	Storage	Heat Recovery
Duration, days	7.7/10.4	9.7	7.7/8
Water temperatures, °C			
Mean source or return	36.1	-	81.1
Mean inject or recover	106.1	-	76.6
Highest inject or recover	137.8	-	97.2
Minimum inject or recover	96.7	-	56.7
Mean delta T	70.0	-	-
Mean flow rate, L/sec	18.3	-	17.3
Pumped volume, 10^3 m^3	12.2	-	11.8
Energy input/output rate, MW	5.36	-	3.34

	Energy Balance, 10^9 Btu
Source steam	4.16
Returned condensate	0.27
Consumed steam	3.89
Source ground water[(a)]	1.18
Added to ground water	3.38
Energy to pump water	0.066
Recovered in ground water	2.115
Not recovered in ground water	2.45
Energy recovery factor (aquifer)	62%
System energy recovery factor[(b)]	50%

(a) Ambient temperature ground water assigned 0.
(b) Based upon source steam; does not include conversion of coal to steam.

Heat recovery followed the same pattern as in Cycle 1, peak temperature (106°C) was reached after about 12 hours of pumping (Figure 5.6). Net energy recovery factor for this cycle is 0.62, the highest attained during these short tests.

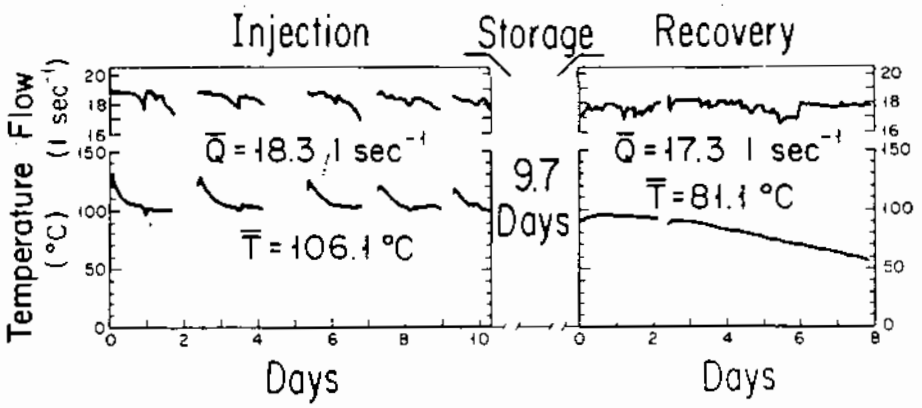

FIGURE 5.6. Flow Rates and Temperatures of Heated Water Injected and Recovered, Plotted Against Time - Cycle 3

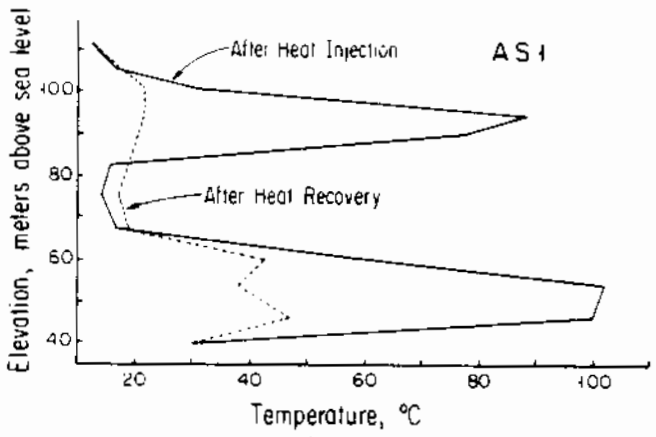

FIGURE 5.7. Temperatures Recorded in Well AS1 After Heat Injection and Recovery Phases - Cycle 3

5.3.4 Cycle 4

Cycle 4 was conducted from November 7 to December 7, 1983. Five heated-water injections totaling 184.5 hours were conducted (Table 5.8, Figure 5.8). Summary data for the heat-injection phase show a mean flow rate of 17.9 L/sec (284 gpm) at a mean temperature of 114.8°C (239°F). Peak temperature reached was 145.6°C (294°F). Source water temperature averaged 52.6°C (127°F).

Temperatures at well AS1 reached a high of 113°C (235°F) (Figure 5.9) at the conclusion of injection. The upper Franconia portion of the aquifer reached a temperature of 94°C (201°F) immediately following the last

TABLE 5.8. Cycle 4 - Summary

	Heat Storage (Injection)	Storage	Heat Recovery
Duration, days	7.7/12	10.1	7.7
Water temperatures, °C			
Mean source or return	52.6	-	75.7
Mean inject or recover	114.8	-	89.1
Highest inject or recover	145.6	-	106.1
Minimum inject or recover	106.1	-	63.9
Mean delta T	62.2	-	-
Mean flow rate, L/sec	17.9	-	17.8
Pumped volume, 10^3 m^3	11.9	-	11.9
Energy input/output rate, MW	4.69	-	2.72

	Energy Balance, 10^9 Btu
Source steam	3.70
Returned condensate	0.41
Consumed steam	3.39
Source ground water[(a)]	1.91
Added to ground water	2.96
Energy to pump water	0.070
Recovered in ground water	1.74
Not recovered in ground water	3.13
Energy recovery factor (aquifer)	59%
System energy recovery factor[(b)]	46%

(a) Ambient temperature ground water assigned 0.
(b) Based upon source steam; does not include conversion of coal to steam.

heated-water injection; the temperature at that level dropped by 15°C in 24 hours. This same type of behavior, rapid change in temperature (+ or -) upon the cessation of injection, occurred consistently at given levels.

Heat recovery for Cycle 4 began November 30, 1983 and continued for 185 hours. Mean temperature of water recovered was 89.1°C (192°F). Volume of water recovered was 11.9 x 10^3 m^3. The net energy recovery factor for the cycle was 0.58.

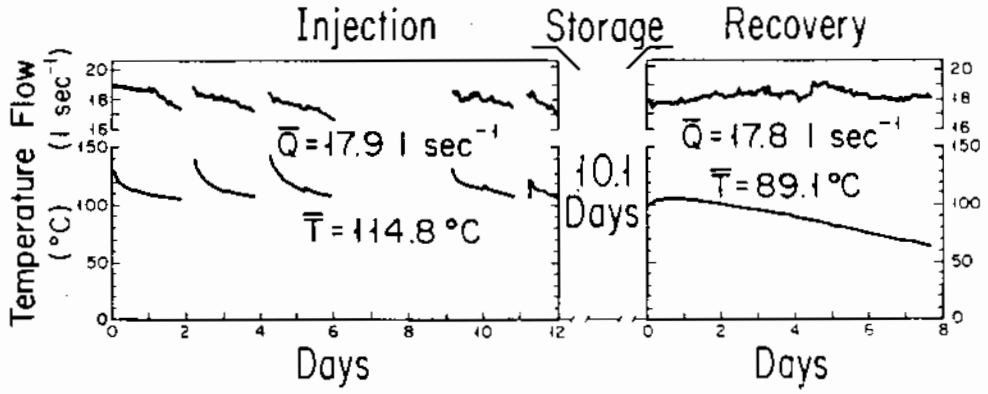

FIGURE 5.8. Flow Rates and Temperatures of Heated Water Injected and Recovered, Plotted Against Time - Cycle 4

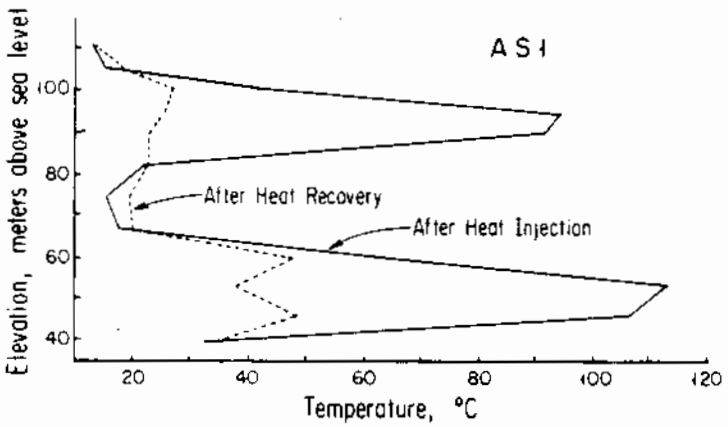

FIGURE 5.9. Temperatures Recorded in Well AS1 After Heat Injection and Recovery Phases - Cycle 4

5.3.5 Discussion

The four short-term test cycles did demonstrate that a significant amount of heat recovery (~60%) is possible even though the containing rock is starting at ambient temperatures. During Cycle 2, with a prolonged storage period (90 days), significantly less heat was recovered (~45%). A likely contributing factor to this lower heat recovery is the multiple nature of the FIG aquifer. The difference in slope between the heat recovery curves of Cycles 1, 3, and 4 and Cycle 2 may reflect the long storage of Cycle 2 (Figure 5.10). The relatively long time (12 hours) to reach the peak temperature may also reflect this complexity in the FIG aquifer.

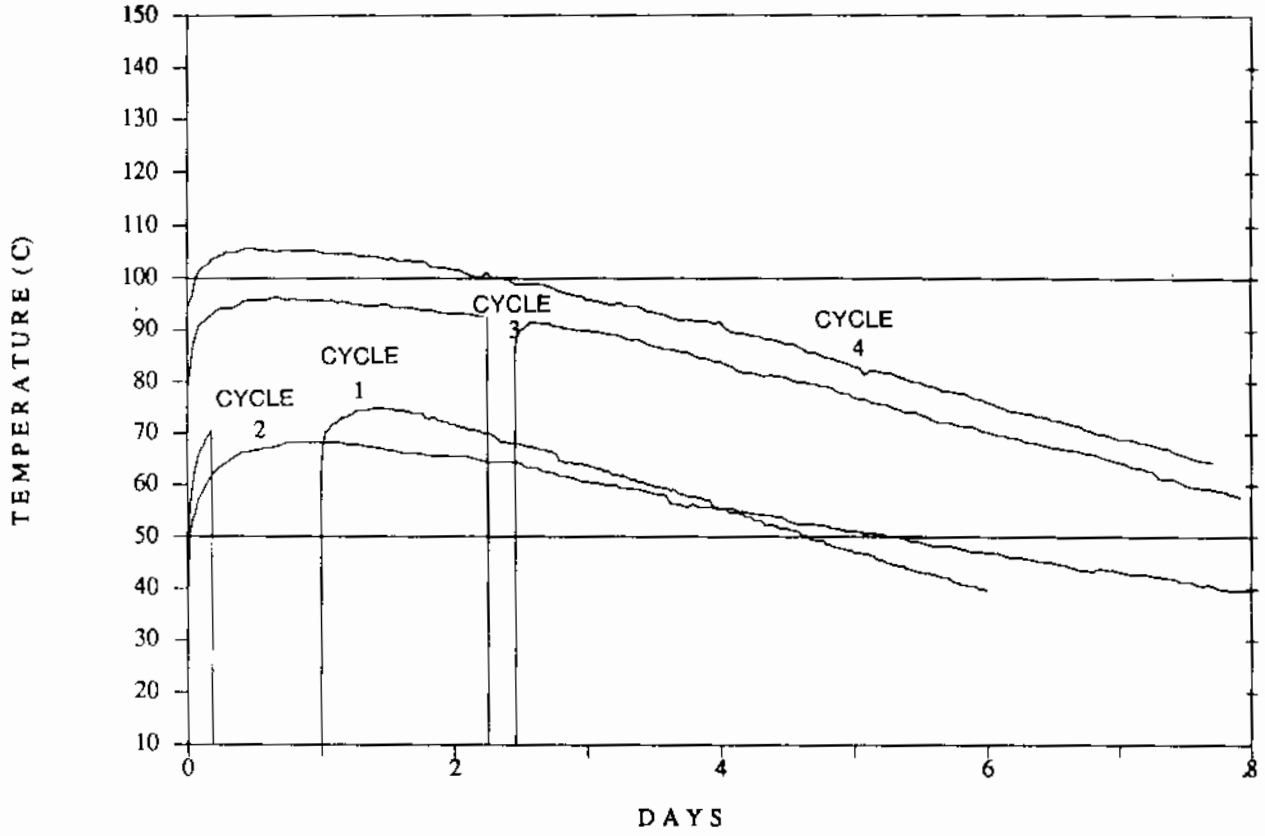

FIGURE 5.10. Recovery Temperatures Versus Time for Short-Term Cycles 1 through 4

6.0 WATER CHEMISTRY

Water chemistry investigations were performed as part of the University of Minnesota ATES project to monitor both water quality and potential system impairment (Holm et al. 1987). The studies were operationally divided into water sampling and analysis, rock dissolution experiments, and chemical equilibrium modeling.

Potential effects of chemical reactions on the feasibility of an ATES project can be grouped into two categories: 1) impairment of system operation and 2) degradation of water quality. System impairment effects can be subdivided into above-ground hardware effects, such as scaling and other damage to piping, valves, and other components and below-ground effects, including well plugging and reduction in aquifer permeability. (Note: it is possible to enhance the permeability of the aquifer as well.) Water quality effects involve increasing the concentrations of dissolved substances to undesirable levels.

The processes most likely to impair the operation of an ATES project include particulate plugging, precipitation from the working fluid, corrosion, biofouling, and particulate mobilization (Allen 1983). The temperature and chemical composition of the injected water and the mineralogy of the aquifer determine the relative impact of the various processes on system performance. For example, Molz et al. (1979) reported that clay swelling caused by injecting water of lower ionic strength than the ambient ground water caused particulate mobilization which seriously reduced the permeability of their test aquifer. The swelling problem was solved by injecting heated water that had been withdrawn from the same aquifer. In this ATES project, precipitation of calcium carbonate resulted in heat exchanger scaling and injection well plugging (Walton and Hoyer 1984). Treating the water to reduce calcium carbonate oversaturation solved the well-plugging problem.

Water quality effects are defined by the water's intended use; i.e., if the aquifer used by an ATES project is also used as a municipal water supply, water quality degradation can be operationally defined as an increase in the concentration of one or more solutes above drinking water standards. As with

ATES system effects, reactions that may affect water quality are functions of injection water chemistry, temperature, and aquifer mineralogy.

Water samples were taken from the ATES system piping during injection and withdrawal of hot water to assess the performance of the water treatment system and to monitor changes in water chemistry during storage. Between ATES cycles, water samples were taken from the observation wells to monitor water quality in the storage aquifer and adjacent aquifers.

The rock dissolution studies were designed to measure the rates of dissolution of aquifer rocks over a range of temperatures. This kinetic information was used to predict dissolution rates under ATES conditions.

Chemical equilibrium computations were used to explain changes in water chemistry during hot water storage. In cases where more than one reaction could produce observed concentration changes, the reaction that was consistent with chemical equilibrium was assumed to be the correct reaction. The kinetic results of the rock dissolution experiments were used to determine the time scale over which chemical equilibrium could be attained. The water analyses were used as input for the computations. Thus, although the various water chemistry studies in the project were operationally independent, they had the common goal of understanding the chemical changes that accompany aquifer thermal energy storage.

6.1 WATER SAMPLING AND ANALYTICAL METHODS

Methods of collecting water samples from the system piping during ATES tests and from monitoring wells between tests are outlined in this section. Field chemical analyses and laboratory analyses are described along with quality assurance measures.

6.1.1 Water Sampling During Cycles

Water sampling locations used during injection or withdrawal of water are shown schematically in Figure 6.1. Water samples were collected from points U (upstream, source); H (heat exchanger effluent); and W (wellhead, injection) during injection. During recovery, samples were collected at point W (wellhead, recovery) only. Sampling points U and W were connected to the

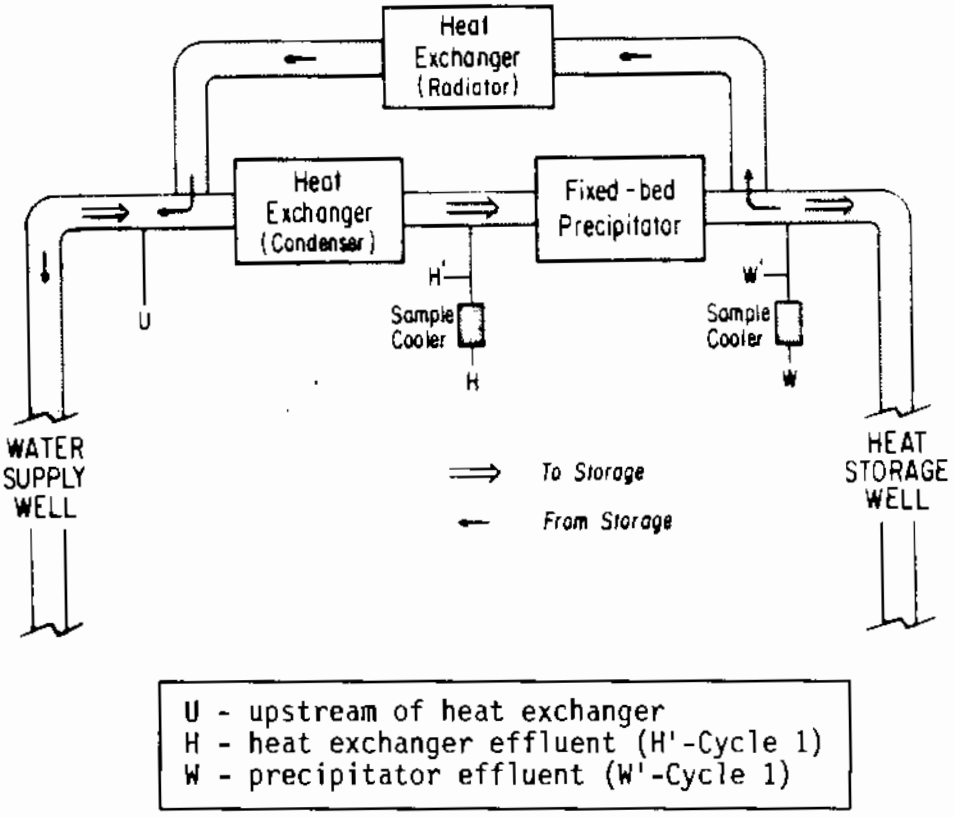

FIGURE 6.1. Location of Water Sampling Points

system piping by approximately 3 m (10 ft) of narrow diameter piping because the points that tapped the system piping were high above the ground and not convenient for sampling.

During ambient temperature pumping tests and the first cycle, the water samples were collected in a stainless steel bottle equipped with a needle valve at either end. The bottle was mounted vertically and filled from the bottom to exclude air and was flushed with several bottle volumes before a sample was obtained. For filtration the sampler was connected to a stainless steel-and-Teflon filter holder. The nominal pore size of the filter membranes was 0.1 μm. A bicycle pump was used to supply pressure to force the water through the filter. During Cycles 2, 3, and 4, the filter holder was connected directly to the sampling points and the system pressure, which was reduced by a needle valve to control flow rate, was used to force water through the filter. At points H and W hot water was cooled to below 100°C, when necessary,

in a sample cooler in which the sample stream flowed through a stainless steel tube that was immersed in flowing tap water. During periods of injection, the outlet valves of sampling points W and U were left open to continuously flush the piping. During recovery, only the valve at point W was left open.

Water samples for metals determinations were filtered into acid-cleaned polypropylene bottles containing concentrated hydrochloric acid (HCl). The final acid concentration was 2% (v/v) to prevent oxidation of ferrous iron (American Public Health Association, American Water Works Association, and Water Pollution Federation 1975). Water samples for alkalinity, total dissolved solids (TDS), dissolved silica, and anions determinations were not acidified. Samples for grease and oil were not filtered but were acidified (0.1% HCl) (American Public Health Association, American Water Works Association, and Water Pollution Federation 1975).

6.1.2 Water Sampling from Monitoring Wells

Several factors contributed to the selection of a method for water sampling in monitoring wells. Static water levels are too far below ground for peristaltic pumps and the monitoring well pipes are too narrow [0.03-m (1.25-in.) diameter] for commercially available submersible pumps. The wells must be flushed to obtain samples representative of the ground water. For certain analyses it is desirable to have a flowing sample. For these reasons cyclic gas pumping, which allows flushing and sampling with the same equipment, was chosen as the water sampling method. Unfortunately, the method proved to be impractical and a bailer, or grab sampler, had to be used.

Two pumps were built and the details of their construction and operation are shown in Figure 6.2. Pump diameter was dictated by the availability of materials and hose connections. The pumps were tested in the laboratory and performed satisfactorily. However, clearance between the pumps and well casings was small, as shown in Figure 6.3. The first field test was performed in well CM1. After pumping less than 1 L of water, the pump failed. While the pump was being retrieved to determine the reason for failure, it got stuck in the well. However, it was freed by lowering a steel rod attached to a cable and striking the top of the stuck pump. A faulty retainer in the lower check valve was found to be responsible for pump failure and both pumps were modified to remedy the situation.

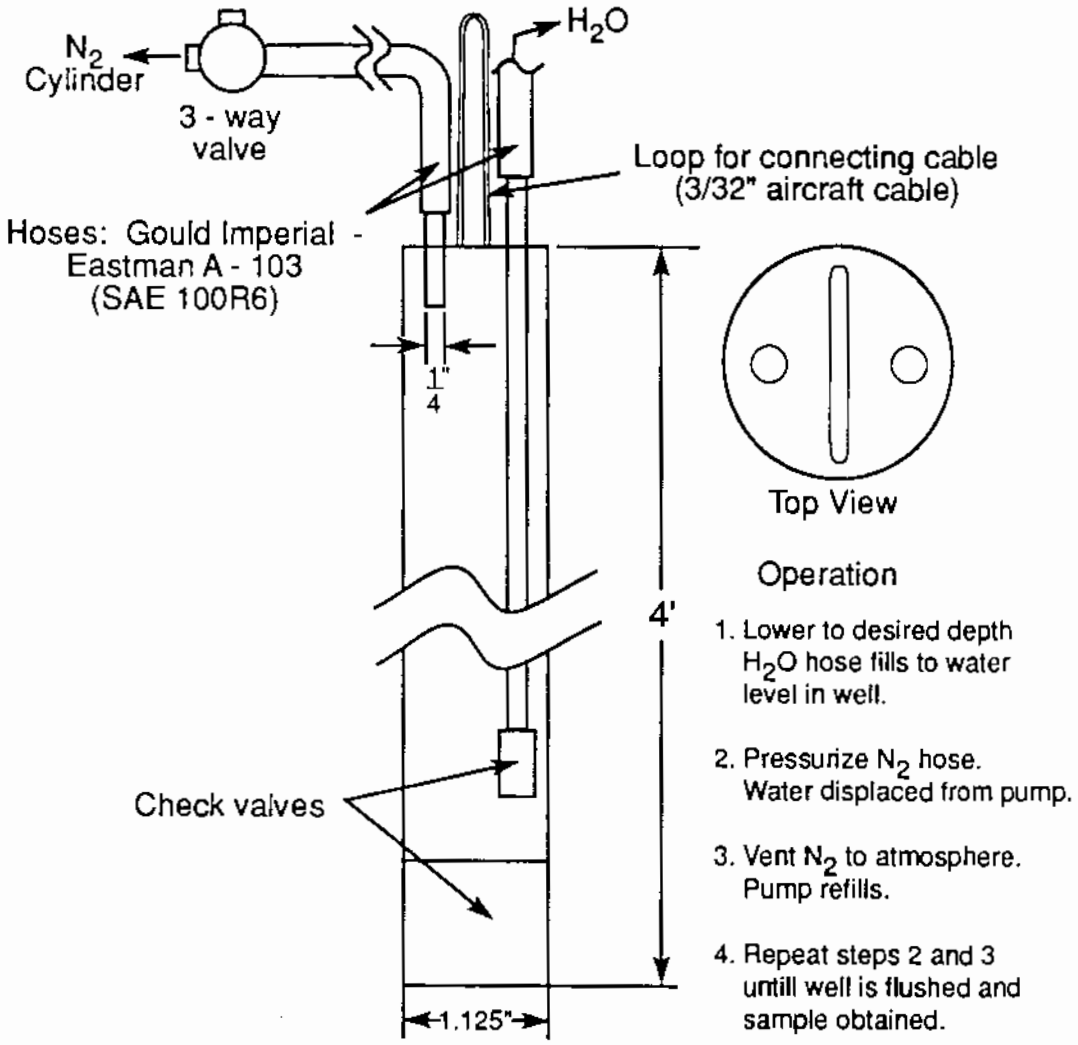

FIGURE 6.2. Gas Cycling Pump Built for Sampling Monitor Wells

Before another field test was run, a dummy pump with dimensions identical to the sampling pumps was lowered to a depth of 213 m (700 ft) in wells CM1IG and CM1UF. The dummy pump, which did not have air and water hoses attached, did not get stuck despite the small clearances. A second field test resulted in a pump getting stuck in well CM1UF and several efforts to free the pump were unsuccessful. Apparently the hoses attached to the pump were responsible for the pump's getting stuck. The gas cycling pump was abandoned in favor of a bailer-type sampler (Figure 6.4).

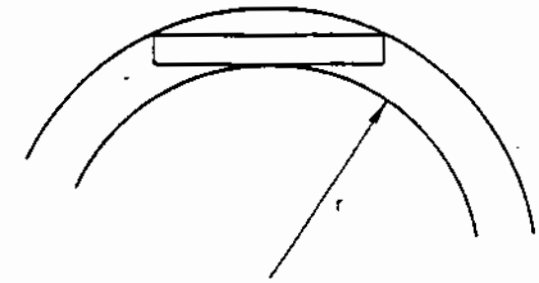

Curved pipe r = radius of curvature
≥920" ≡ 77'

Angled pipe (e.g. at coupling)
θ ≤1.5°

Pump will get stuck if r<920" or θ >1.5°

FIGURE 6.3. Tolerances in Deviation of Well Casings from Linearity

Sampling with a bailer has been shown to be a reliable method for preserving the chemical integrity of well waters (Gibb, Schuller and Griffin 1981), but flushing a deep well using a bailer would be impossible. Nonetheless, there are many reasons for flushing a well before obtaining a water sample. Contact with the atmosphere can result in a gain or loss of CO_2, depending on whether the water is undersaturated or oversaturated. Such gas exchange would cause a change in pH, so that water in the well casing would not be representative of aquifer water. Atmospheric oxygen dissolved in water could oxidize iron and manganese, reducing their solubility (Stumm and Morgan 1981). Dissolved oxygen at the surface need not diffuse to deeper levels to affect water chemistry, because oxide particles may settle from the aerated zone. There may be chemical changes in the aquifer during hot water injection

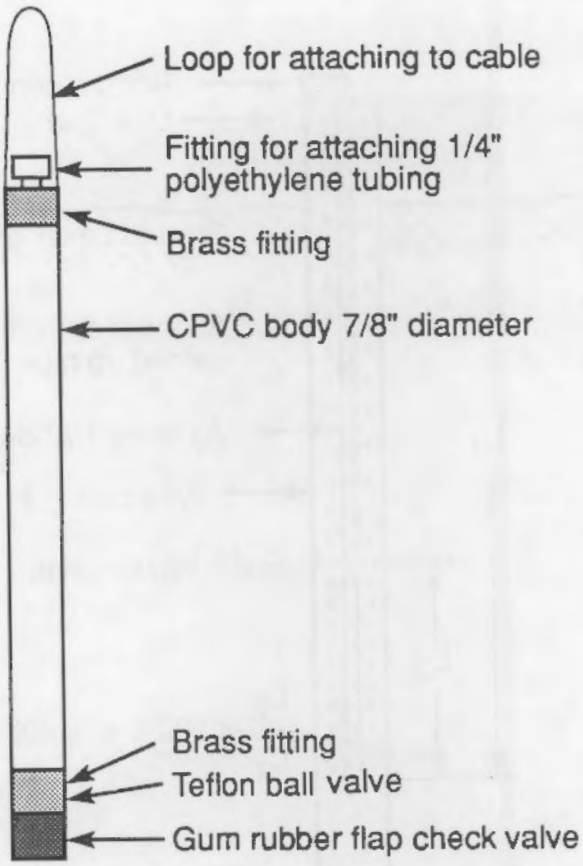

FIGURE 6.4. Grab Sampler for Sampling Water in Deep, Small-Diameter Wells

as the thermal front passes the well; but, unless the casing is flushed, water in the well would not be chemically representative of the aquifer.

Monitoring well flushing was performed by air-lift pumping (Figure 6.5) with a submergence of 30% to 50%, depending on available compressed air pressure and static water level. Pumping rates were between 0.03 and 0.09 L/sec (0.5 and 1.5 gpm), corresponding to average upward flow velocities of 2.4 to 7.2 m/min (7.8 to 23.5 ft/min) below the air hose. The minimum time required to flush the lower portion of a well was calculated by dividing the distance from the end of the air hose to the bottom of the well by the upward water velocity. The wells were flushed for at least twice this minimum time.

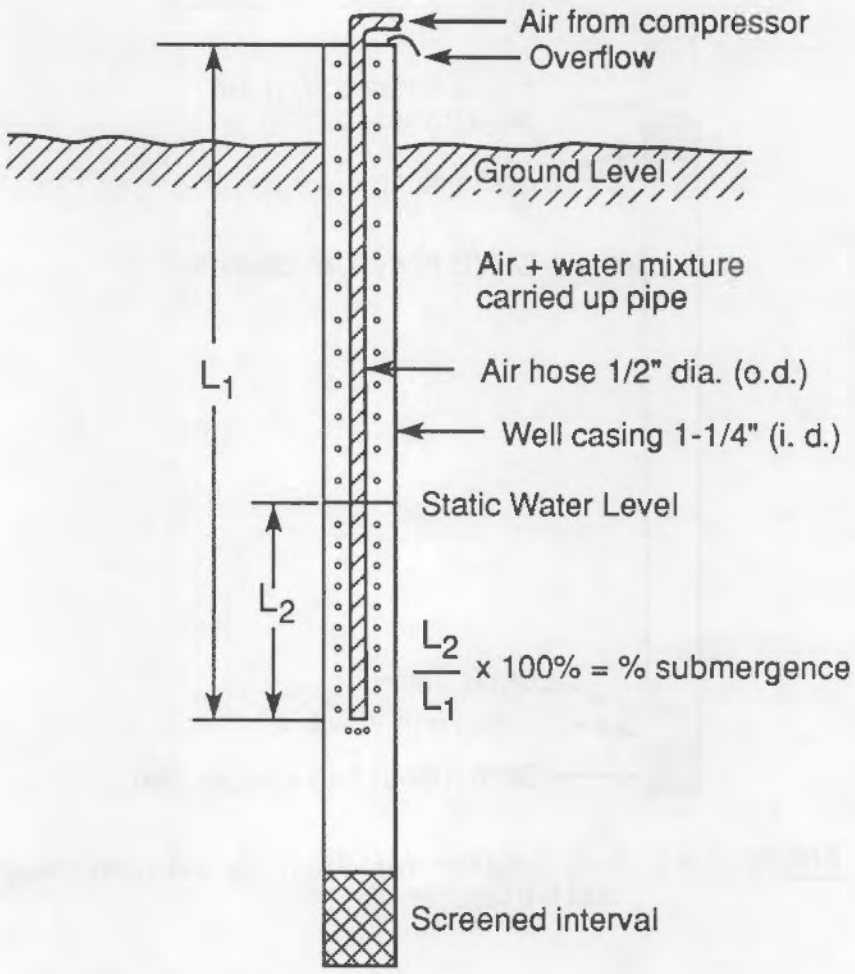

FIGURE 6.5. Air-Lift Pumping

Wells were sampled within 24 hours of flushing, usually within 2 hours. The sampler was lowered at least 61 m (200 ft) below the air hose depth, to avoid O_2 or CO_2 contamination.

An ideal bailer would be open and continuously flushing while being lowered and would be closed while being retrieved, thus retaining a deep water sample. The bailer used to sample the ATES monitoring wells, however, was found to behave nonideally, as indicated by anomalously high dissolved oxygen (DO) concentrations in the first deep well water samples collected. Therefore, modifications of design and operation were necessary to obtain reliable water samples.

The sampler was tested in a stratified eutrophic lake so that the performance of the bailer could be compared with that of a reliable messenger-actuated oceanographic water sampler. Using the oceanographic sampler the hypolimnion of the lake was found to be anoxic. However, duplicate samples obtained from the same depth using the well bailer contained more than 1 mg/L of DO. The Teflon ball in the check valve did not remain seated when the bailer was retrieved as indicated by "tapping" sensations that were transmitted via the cord attached to the sampler. Apparently, water in the sampler was allowed to exchange with ambient water as the sampler was raised or the bailer did not flush completely as it was lowered. A second check valve was installed and the problem of the ball not seating was eliminated. However, DO was still high in the next set of deep well water samples obtained using the modified bailer, apparently because the sampler filled at the water surface and did not completely flush when lowered. Therefore, the sampling technique was modified to increase flushing. The bailer was lowered to within 30 m (100 ft) of the desired sampling depth and raised and lowered 15 m (50 ft) five times. The bailer was then lowered to the sampling depth and again raised and lowered 15 m (50 ft) five times. Samples obtained using this technique and the modified sampler had very low DO concentrations and this was considered to be indicative of adequate performance. The flushing technique was also tested by first obtaining a water sample from well AM2 and determining the specific conductance. The sampler was then filled with 0.00700 M potassium chloride (KCl) (conductance standard), a second water sample was taken from AM2, and the specific conductance measured. Less than 2% of the KCl remained in the sampler as indicated by the conductance measurements.

Before sampling a well, the water sampler was scrubbed with detergent and thoroughly rinsed with distilled water. A new 0.45 μm Millipore filter was mounted in a pressure filter holder. The water sampler was then filled with distilled water and connected to the filter holder. The filter was washed with distilled water to remove any soluble contaminants. The first 30 ml of filtrate (the dead volume of tubing and filter holder) were discarded. Samples for total dissolved solids and alkalinity were filtered first in case any

residual trace metal contamination remained in the filter. (Traces of chemical impurities do not materially affect analyses for TDS and alkalinity.) Typically, the first 200-ml sample was used for immediate analyses, such as pH, and DO, and specific conductance. The next sample was filtered for TDS, anions, and alkalinity. The next sample was filtered and acidified for metals analyses.

6.1.3 On-Site Chemical Analyses

Contact with air can affect pH, dissolved oxygen concentration, specific conductance, and Eh of a water sample. Therefore, these measurements must be performed immediately after a water sample is obtained (American Public Health Association, American Water Works Association, and Water Pollution Federation 1975; Anonymous 1982).

A flow-through cell (Figure 6.6) connected to the system sampling points was used for pH determinations during Cycle 2. The cell was filled from the bottom and was allowed to flush for several cell volumes while the cell temperature stabilized, thus eliminating air contact. After the temperature stabilized, the pH electrode was calibrated. The electrode was then rinsed in the outflow stream from the cell to remove the calibration buffer and immersed in the sample solution. The sample flow was stopped and the pH was recorded. When the injection water temperature was above 100°C, the sample stream was cooled to prevent flashing in the cell.

Cycles 1, 3, and 4 were conducted under colder weather conditions than Cycle 2 and the pH meter could not give stable readings when used outside. For these tests water samples for pH determinations were collected by filling a bottle by means of a tube that extended to the bottom of the bottle. The bottle was allowed to overflow for several bottle volumes. A pH electrode in a rubber stopper was immediately inserted in the mouth of the bottle. The sample bottle was immersed in a water bath and the pH was measured. (The pH electrode had been calibrated in a similar fashion.) The pH of water samples from the monitoring wells was determined by the same procedure used in Cycles 1, 3, and 4 except the sample bottle was filled from the well bailer and only two bottle volumes were used for flushing because of limited sample size.

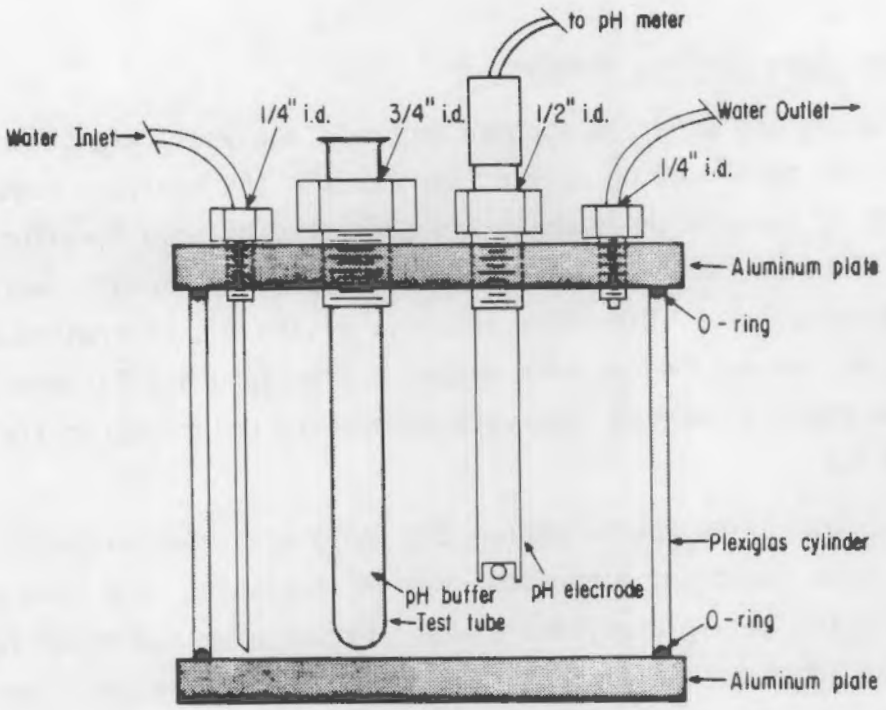

FIGURE 6.6. Flow-Through pH Cell Used During Cycle 2

Water samples for specific conductance determinations were collected similarly to pH samples in Cycles 1, 3, and 4. A test tube was filled from the bottom and several tube volumes were allowed to flush the test tube. The conductivity cell in a stopper was inserted immediately. The test tube was then immersed in a beaker of water at room temperature. The sample resistance was recorded when water temperature and resistance attained steady values. The cell constant of the conductivity cell was determined using a standard KCl solution.

Dissolved oxygen and ammonia were determined colorimetrically using kits with color standards for visual comparison [CHEMetrics[(a)]]. The colorimetric DO method has been found to compare favorably with the standard polarographic DO method (Gilbert, Behymer and Casteneda 1982).

Alkalinity was usually determined within 24 hours of sample collection by potentiometric titration (Anonymous 1982). Gran's method (Stumm and Morgan 1981) was used to locate the end point.

(a) CHEMetrics, Inc., Calverton, Virginia

6.1.4 Laboratory Chemical Analyses

Laboratory analyses (as opposed to field analyses) are those procedures that cannot be performed on site either because the analyses require special instruments or because the samples are preserved by acidification. The anions, chloride, fluoride, sulfate, nitrate, nitrite, and phosphate, were determined by ion chromatography. Dissolved reactive silica was determined colorimetrically by the molybdenum blue method (Strickland and Parsons 1972). Ferrous and total dissolved iron were determined colorimetrically using 1,10 phenanthroline.

Atomic absorption spectrophotometry (AAS) was used for metals determinations. Calcium, magnesium, sodium, potassium, and iron were determined using an air-acetylene flame. For calcium and magnesium, lanthanum (1% w/v) was added to minimize chemical interferences in the flame (Parker 1972). For sodium and potassium, cesium (0.1% w/v) was added as an ionization suppressant (Parker 1972). Iron, manganese, and aluminum were determined by AAS with electrothermal atomization using $Mg(NO_3)_2$ as a matrix modifier (Slavin, Carnrick and Manning 1982). Hardness was determined by titration with standardized EDTA (American Public Health Association, American Water Works Association, and Water Pollution Federation 1975).

6.1.5 Quality Assurance

For quality assurance purposes water samples were assigned to logically related sets. For example, the samples collected during the injection phase of an ATES cycle constituted one set, the samples from the recovery phase made up another set, and the samples taken from the monitoring wells after the test made up a third set. For each set at least one duplicate sample, one spiked sample, and one blank were collected. Poor agreement among duplicates or poor recovery of spikes were grounds for repeating analyses.

The procedures for collecting blanks were designed to duplicate sampling conditions as closely as possible. Blanks for monitoring well sample sets were obtained by filling the well sampler with distilled water and filtering into sample bottles. Blanks for ATES cycle sample sets were obtained using the apparatus shown in Figure 6.7. Pressure was supplied by a bicycle pump.

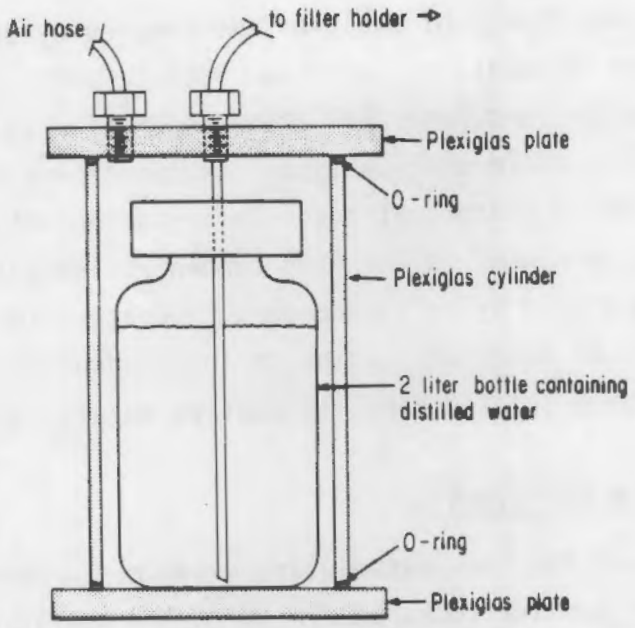

FIGURE 6.7. Device for Obtaining Filtration Blanks

Spiked samples were treated in the same way as non-spiked samples. Acidified samples were spiked with a solution containing calcium, magnesium, sodium, potassium, iron, and manganese. Unacidified samples were spiked with a solution containing sulfate, chloride, fluoride, nitrate, and phosphate. For every set of samples analyzed there was at least one blank and one sample that was spiked in the laboratory in addition to the "field" blank and spiked samples.

The number of laboratory duplicates varied with the procedure, but there was at least one duplicate per set. Colorimetric determinations, alkalinity titrations, and hardness titrations were performed in duplicate. At least two replicates were taken for each flame AAS reading and at least three replicates for each electrothermal AAS reading.

Selected samples were saved and run with subsequent sample sets to make sure that the analyses were consistent from one set to the next. At least one sample of each set was re-run to check for instrumental drift. Standard solutions (Minerals standards 3 and 4 and Trace Metals standards 4, 5, and 6) obtained from the U.S. Environmental Protection Agency were run with each analysis as a check for accuracy.

The internal consistency of analyses was checked by charge balance and conductivity balance calculations (American Public Health Association, American Water Works Association, and Water Pollution Federation 1975). Independent methods were used to confirm some analyses. Hardness was compared to the sum of calcium and magnesium concentrations. The iron concentration determined colorimetrically was compared to the iron concentration determined by AAS. Some samples were analyzed by an independent laboratory (Research Analytical Services, University of Minnesota) using an independent method (inductively coupled plasma emission spectrometry) to confirm metals concentrations.

6.2 ROCK DISSOLUTION EXPERIMENTS

The objectives of the rock dissolution experiments were to measure dissolution rates of aquifer rocks under controlled conditions of temperature and solution composition and to use these kinetic results to predict dissolution rates in the aquifer during hot water storage. Because dissolution rates are proportional to interfacial area (Rimstidt and Barnes 1980; White and Claassen 1979), intrinsic rate constants can be multiplied by estimated aquifer interfacial areas to calculate apparent rate constants under field conditions. This section describes dissolution experiments and surface area measurements using aquifer rocks and interpretation of the results under ATES conditions.

6.2.1 Rock and Solution Characteristics

Three samples of aquifer rock were obtained from cores taken at the site. Table 6.1 presents the characteristics of the core samples. Samples A and B were from the Ironton-Galesville portion of the aquifer where most of the injected hot water is to flow. Thus, chemical changes observed in experiments involving these rocks should be similar to chemical changes in the hot water when it is stored in the aquifer. Rock A was mostly quartz with a small feldspar fraction. Rock B contained quartz and approximately 20% K-feldspar. Sample C was from the Lower Franconia part of the aquifer, having low permeability and was mineralogically complex (Table 6.1). The dissolution experiment involving rock C was designed to study the effects of dissolution of glauconite and dolomite on solution chemistry and also possible dissolution of confining layers.

TABLE 6.1. Components of Rock Samples Used in Dissolution Experiments

Sample, Unit	Core Depth, ft	Porosity, %	Quartz, %	K-Feldspar, %	Dolomite, %	Glauconite, %	Other, %
A[a]	A771.5	21.0	94.7	4.7	-	-	0.6
B[b]	B765.8	21.0	76.9	20.1	-	-	3.0
C[c]	B637.5	14.0	42.9	17.3	13.9	14.7	11.2

(a) Ironton-Galesville
(b) Galesville
(c) Lower Franconia

Preliminary experiments were conducted using synthetic ground water, a carbonate buffer made by bubbling CO_2 gas into a $NaHCO_3$ solution to give an alkalinity of 3 meq/L and a pH of 7.50, and with distilled water. All other experiments were performed using the ground water obtained during a pumping test October 8, 1981, at site A. The ground-water sample had been stored by refrigeration at 10°C in 5 liter polyethylene containers. Table 6.2 presents the natural ground-water chemistry.

TABLE 6.2. Chemical Characterization of Ground Water Used in Rock Dissolution Experiments

Cations	(mM)	Anions	(mM)
Ca	1.57	Alkalinity	4.53
Mg	0.95	SO_4	0.50
K	0.15	F	0.012
Fe	0.005	Cl	0.028
Mn	0.001		
Na	0.27		
pH[a]	7.55		

(a) pH units

6.2.2 Experimental Procedures

High-temperature dissolution experiments were run using a stainless steel, heated, pressure-tight reactor. Fifteen grams of ground rock were added to 500 ml of ground water. Samples of 20 ml were withdrawn through an in-line filter (2 μm nominal pore size) attached to a gas-tight syringe. An initial sample was taken before heating the solution, another as soon as the reactor reached the desired temperature, and further samples were taken periodically throughout the experiment. For each water sample, 5 ml were acidified with HCl for cation analysis, 10 ml were used for anion and dissolved reactive silica analyses, and 5 ml were cooled to 25°C in the syringe for immediate pH and alkalinity measurements. A final sample was taken post-run when the reactor and solution had cooled to 25°C. All samples were completely analyzed within 7 days of the experiment.

The mixture was stirred at a constant speed of 200 rpm under the vapor pressure of the solution (at 150°C, the vapor pressure is 70 psig) in a closed system. The duration of the experiment varied with temperature, from 3 to 9 days. Table 6.3 lists the experiments that were run.

6.2.3 Surface Area Measurements and Dependence of Dissolution Rate on Surface Area

Specific surface areas were measured by BET nitrogen adsorption, nitrogen permeametry, and sieve analysis. The BET apparatus used has a lower detection limit of 0.1 m^2/g of sample, so it is not practical for use on large particles that have a small specific surface area. For this reason, dry sieve analysis and permeametry were used in determining the rock surface area of the coarser fractions. Specific surface area measurements are presented in Table 6.4. A surface area measurement from Rimstidt and Barnes (1980) is included and agrees fairly well with our results. Thus, we feel that our measurements give a good estimate of specific surface area.

The rock fractions used in this study were 2 to 10 μm and 74 to 149 μm, which were ground by mortar and pestle or ring grinder, and the 'coarse' fraction, which was gently ground by hand to separate the individual sand grains. Rock C was ground in the ring grinder only.

TABLE 6.3. Summary of Dissolution Experiments

Sample	Temperature, °C	Solution[a]	Particle diameter, μm	Duration, hours
variable	25	D	74 to 149	432
variable	130	D	74 to 149	24
A	150	D	74 to 149	24[b]
B	150	C	74 to 149	73
A	150	C	74 to 149	51
B	150	C	2 to 10	75
A	125	C	2 to 10	80
B	125	C	2 to 10	79.5
B	150	G	2 to 10	71.5
A	150	G	2 to 10	73
A	110	G	2 to 10	122
A	45	G	2 to 10	218
A	150-85-150	G	2 to 10	208[c]
A	150-step-cool	G	2 to 10	118
C	150	G	2 to 10	93

(a) G = ground water, C = carbonate buffer, D = distilled water
(b) N_2 flushed
(c) recycled

Two basic relationships are followed in dissolution and precipitation kinetics: 1) the rate of material transfer between two phases is directly proportional to the interfacial area (A) between the phases; 2) for a given rate of addition of solute, the rate at which its concentration increases is inversely proportional to the volume of water (V) in the system (Rimstidt and Barnes 1980). The intrinsic reaction rate can thus be calculated by normalizing the apparent rate to A/V. In dissolution experiments using 2 to 10 μm ground rock A, the value of A/V was 21.6 m^2/L, assuming the specific surface area measured by BET. In the aquifer, A/V is 25.7 m^2/L using the geometric mean diameter of sand grains determined by sieve analysis. Grinding the rock allowed use of approximately the same A/V value in experiments

TABLE 6.4. Specific Surface Area Measurements of Samples A, B, and C

Rock Fraction		Sieve Analysis, m^2/gram	Permeametry m^2/gram	BET m^2/gram
coarse:	A	0.0061	0.012 to 0.016	---(a)
	B	0.0075	0.033	---
74 to 149 μm:	A	0.034	---	---
	B	0.039	---	
2 to 10 μm:	A	---	0.15	0.72
	B	---	0.15	1.20
	C	---	---	3.63
25 to 63 μm:(b)		---	---	0.015 to 0.061(b)

(a) No measurement
(b) From Rimstidt and Barnes (1980).

as in the aquifer but with a much smaller ratio of mass of rock to liquid volume than in the aquifer. In other words, if the reactor had been filled with 500 ml of sandstone having 20% porosity, the total liquid volume would have been 100 ml, of which perhaps 50 ml could not have been sampled due to wetting of the sand grains. With finely ground sandstone, 500 ml of water could be added to the reactor with approximately the same value of A/V and virtually all of the water could be sampled for chemical analyses.

The rate law for silica dissolution is given by Equation (6.1)

$$d[Si(OH)_4]/dt = k'(1 - S)$$
$$S = [Si(OH)_4]/K \qquad (6.1)$$

where S is the degree of saturation, K is the equilibrium constant for silica dissolution, and k' is the apparent silica dissolution constant. The intrinsic

dissolution constant and the apparent dissolution constant are related by Equation (6.2)

$$k' = k\ A/V \qquad (6.2)$$

where k is the intrinsic rate constant.

The mass of ground rock withdrawn with each sample was less than would be expected assuming a completely mixed system. (However, we feel that the water samples were representative of the reaction mixture.) That is, in a typical experiment in which 10 samples of 20 ml were withdrawn, the volume of water decreased from 500 ml to 300 ml, a 40% decrease. However, only 1 g of particulate matter was trapped on the filter at the end of the experiment, which was 7% of the original amount. In other words, A/V was not constant. The rate constant was calculated as the slope of the graph of ln(1-S) as a function of At/KV, thus taking the variation in A/V into consideration. Rimstidt and Barnes (1980) found the slope of ln(1-S) versus t and then divided by A/KV to calculate their rate constants.

6.2.4 Experimental Results

6.2.4.1 Silica

Dissolved reactive silica (DRS) concentrations are plotted as a function of time for dissolution experiments using ground water and samples A, B, and C at temperatures of 45°, 110°, and 150°C in Figures 6.8 and 6.9. The initial sharp increase in DRS is probably caused by rapid dissolution of sub-micron size particles that were produced by grinding and that were not separated by sieving (Holdren and Berner 1979). Data from this initial dissolution phase were not used to calculate dissolution rate constants. The rate of increase of DRS after the initial increase tended to increase with temperature, which agrees qualitatively with published results (Rimstidt and Barnes 1980). As can be seen in Figure 6.10, Equation (6.2) adequately fits the experimental data.

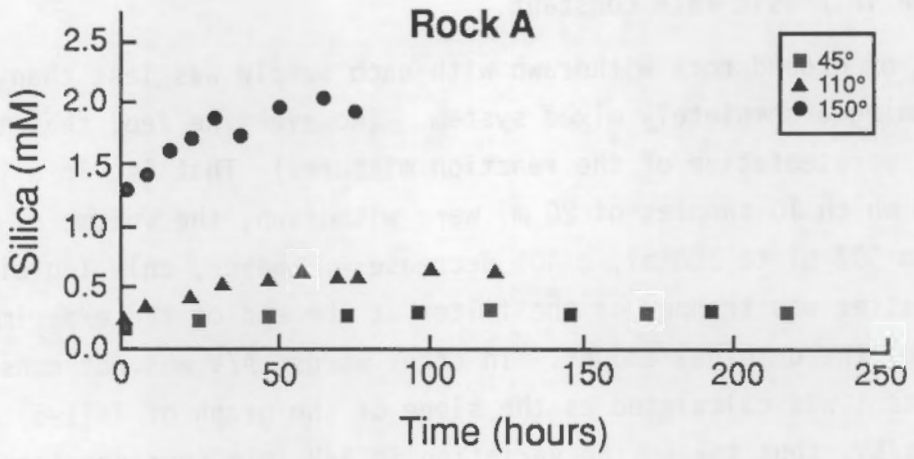

FIGURE 6.8. Dissolved Silica Concentrations in Rock Sample A Dissolution Experiments at 45°, 110°, and 150°C

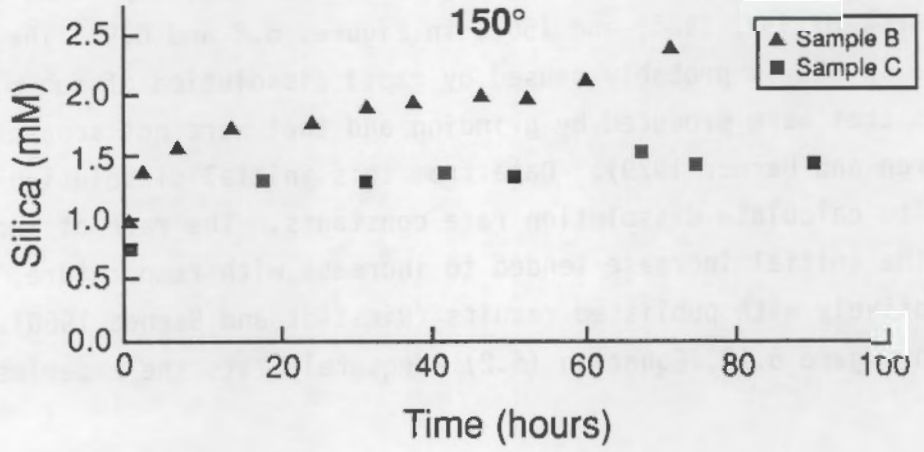

FIGURE 6.9. Dissolved Silica Concentrations in Rock Samples B and C Dissolution Experiments at 150°C

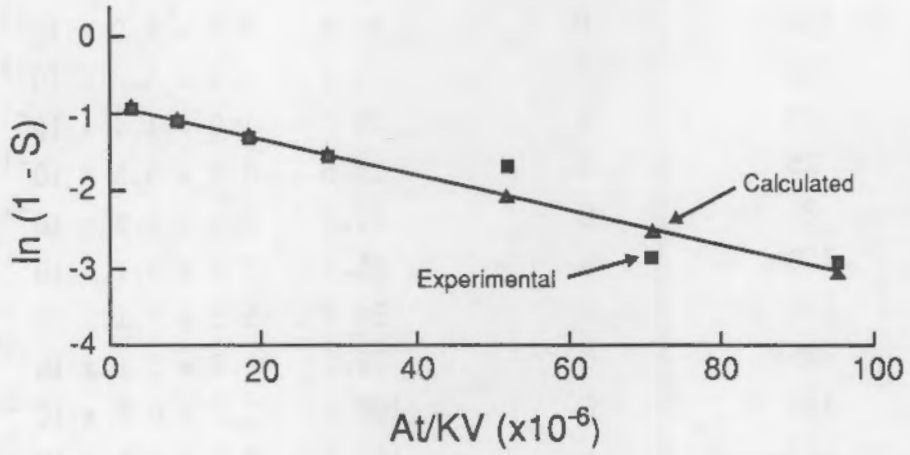

FIGURE 6.10. Transformation of Rock Sample A 150°C Dissolution Experiment Silica Data and Least Squares Linear Regression Fit of Data

In the 45°C and 150°C experiments, dissolved silica concentrations approached the quartz saturation values of 0.21 mM and 2.16 mM, respectively, while in the 110°C experiment the dissolved silica did not come close to 1.07 mM, the quartz saturation concentration. The explanation for this is that at 45°C rapid dissolution of ultra-fine particles brought silica concentration close to quartz saturation while at 150°C the dissolution rate was fast enough to reach quartz saturation. At 110°, there was not sufficient small particle silica to reach saturation and the true dissolution rate was too slow to reach saturation in 5 days.

Dissolution rate constants from the various dissolution experiments are listed in Table 6.5 along with published rate constants for silica dissolution under similar conditions of A/V and temperature. At 150°C, our rate constants agreed with Rimstidt and Barnes within a factor of 2, but at lower temperatures

TABLE 6.5. Rate Constants for Silica Dissolution From Samples of the Franconia-Ironton-Galesville Aquifer

Sample[a]	Temperature, °C	Solution[c]	A/V, m^2/L	k_{+2} mole m^{-2} s^{-1}(d)
A	150	G	21.6	$5.9 \pm 3.2 \times 10^{-10}$
A	150	C	21.6	$4.7 \pm 3.5 \times 10^{-10}$
A	150	D	21.6	$2.3 \pm 1.9 \times 10^{-10}$
A	110	G	21.6	$3.6 \pm 4.0 \times 10^{-11}$
A	45	G	21.6	$1.9 \pm 1.4 \times 10^{-11}$
A	25	D	21.6	$8.9 \pm 4.5 \times 10^{-12}$
A	25	D	21.6	$8.1 \pm 6.0 \times 10^{-12}$
B	150	G	36.0	$5.2 \pm 5.1 \times 10^{-10}$
B	150	C	36.0	$5.5 \pm 7.1 \times 10^{-10}$
B	125	C	36.0	$0.9 \pm 1.1 \times 10^{-10}$
C	150	G	108.9	$1.1 \pm 0.8 \times 10^{-11}$
QS[b]	145		142.0	$2.7 \pm 1.5 \times 10^{-10}$
QS	105		261.0	$7.9 \pm 3.2 \times 10^{-12}$
QS	65		92.0	$1.5 \pm 1.2 \times 10^{-12}$

(a) See Table 6.1
(b) Quartz sand, from Rimstidt and Barnes (1980)
(c) G = ground water, C = carbonate buffer, D = distilled water
(d) Error limits are 95% confidence limits for samples A, B, and C; two standard deviations for sample QS.

our constants were generally an order of magnitude higher than the published constants. It is important to note that all rate constants in Table 6.5 have large coefficients of variation, so the listed constants should be regarded as correct to one significant figure. However, the rate constant for rock C is significantly different from the constants for rocks A and B at the 95% confidence level.

6.2.4.2 Calcium, Magnesium, Alkalinity

Alkalinity, pH, and concentrations of calcium and magnesium are plotted as functions of time in dissolution experiments involving sample A in Figures 6.11 through 6.14. Alkalinity, Ca, and Mg decreased rapidly to a steady value

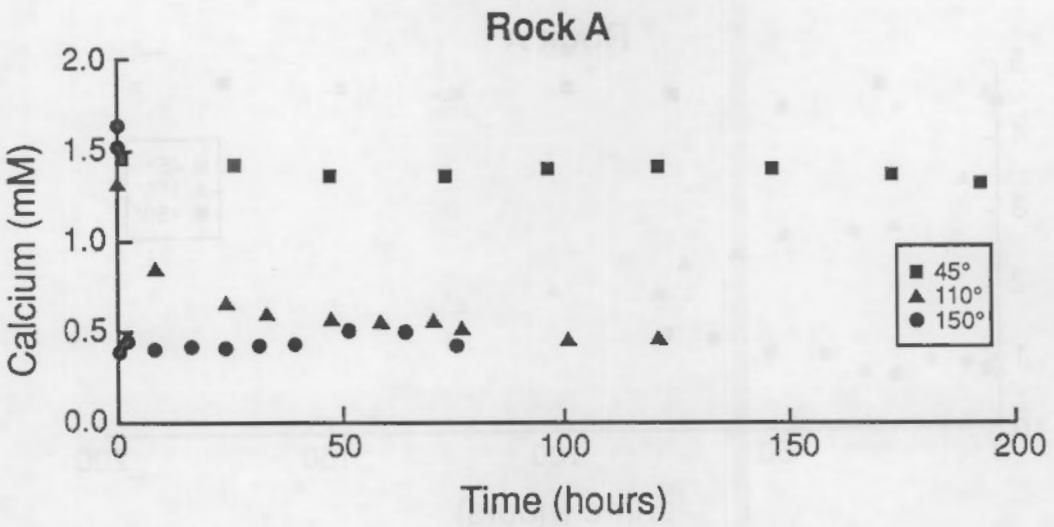

FIGURE 6.11. Calcium Concentrations in Sample Rock A Dissolution Experiments at 45°, 110°, and 150°C

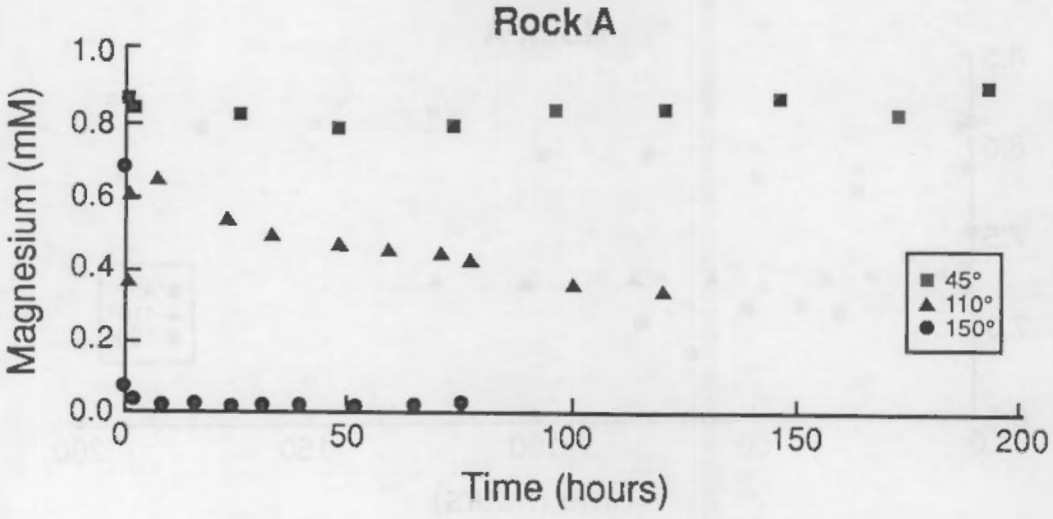

FIGURE 6.12. Magnesium Concentrations in Sample Rock A Dissolution Experiments at 45°, 110°, and 150°C

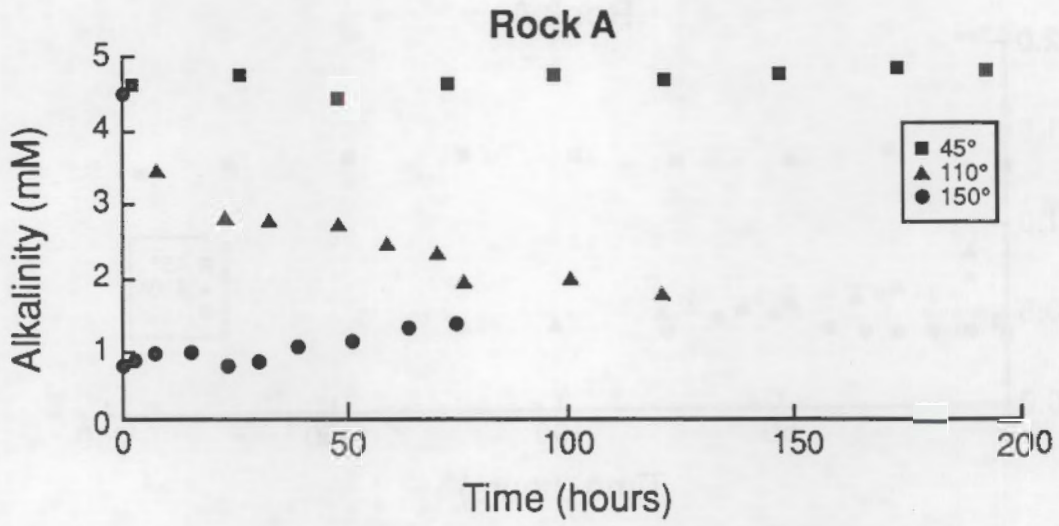

FIGURE 6.13. Alkalinities in Sample Rock A Dissolution Experiments at 45°, 110°, and 150°C

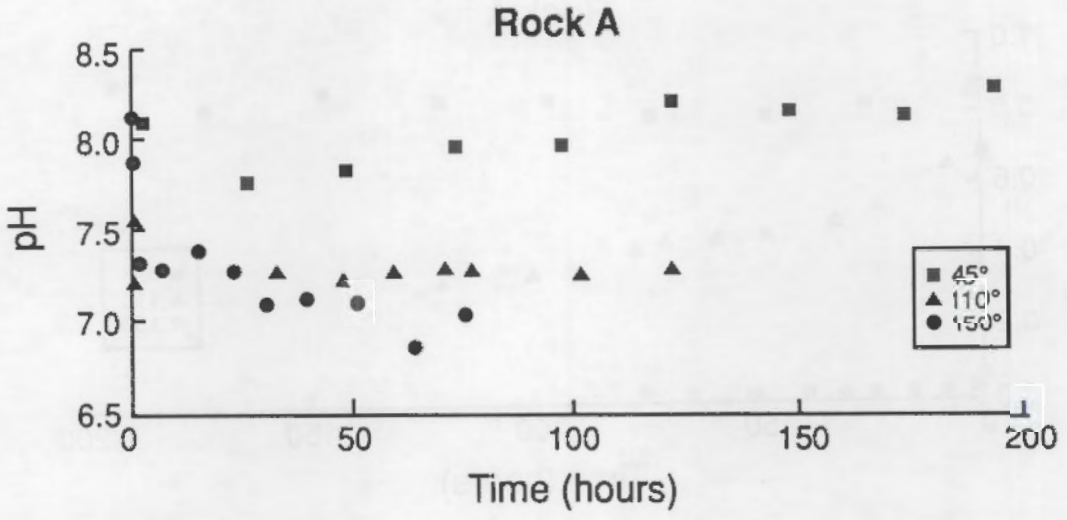

FIGURE 6.14. pH in Sample Rock A Dissolution Experiments at 45°, 110°, and 150°C

in the 150°C experiment, decreased more gradually at 110°C, and did not decrease appreciably at 45°C. Similar changes were observed in pH values. These results suggest that calcium carbonate and a magnesium silicate or aluminosilicate precipitated at 110°C and 150°C and that precipitation was faster at 150° than at 110°C. The lack of change in concentrations at 45°C may have been due to the water being below a critical saturation value (Stumm and Morgan 1981).

Precipitation of calcite and talc, a representative magnesium silicate, is described by Equations (6.3) and (6.4), respectively.

$$Ca^{2+} + 2HCO_3^- = CaCO_3 + H_2CO_3 \quad (6.3)$$

$$3Mg^{2+} + 4Si(OH)_4 + 6HCO_3^- = Mg_3Si_4O_{10}(OH)_2 + 6H_2CO_3 + 4H_2O \quad (6.4)$$

For each reaction, alkalinity is decreased by two equivalents for every mole of Ca^{2+} or Mg^{2+} (two equivalents each). As can be seen in Table 6.6, the changes in calcium, magnesium, and alkalinity are stoichiometrically consistent with precipitation of metal carbonates or silicates in that the molar change in alkalinity is twice the change in calcium plus magnesium.

6.2.4.3 Potassium and Sulfate

Concentrations of potassium and sulfate increased with time in all dissolution experiments. The 150°C experiment using sample B had typical trends in K and SO_4 (Figure 6.15). The K concentration increased by approximately 0.3 mM in the first hour and remained constant for the rest of

TABLE 6.6. Changes in Calcium, Magnesium, and Alkalinity During Rock Sample A 150°C Dissolution Experiment

	Initial Concentration, mM	Final Concentration, mM	Concentration Change, mM	Ratio
Ca	1.64	0.42	1.22	2
Mg	0.68	0.07	0.61	1
Alkalinity	4.53	0.76	3.77	6

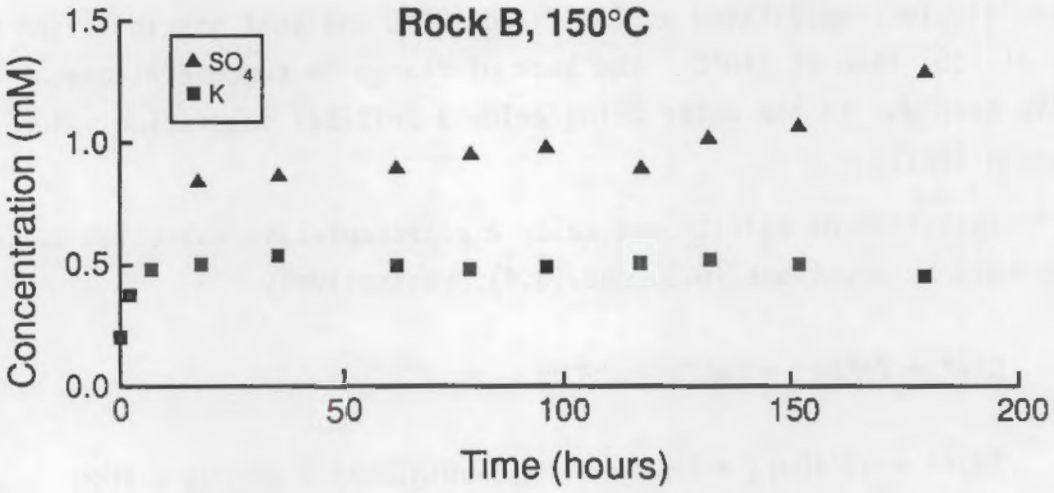

FIGURE 6.15. Potassium (K) and Sulfate (SO_4) in Sample Rock B Dissolution Experiment at 150°C

the experiment. The rapid increase in K may have been caused by dissolution of ultra-fine feldspar particles or by ion exchange. The SO_4 concentrations increased rapidly in the first 10 hours and then more gradually for the remainder of the experiment. The source of SO_4 may have been oxidation of FeS_2 [Equation (6.5)].

$$FeS_2(s) + 8H_2O = Fe^{2+} + 2SO_4^{2-} + 2H^+ + 7H_2(g) \qquad (6.5)$$

Note that the oxidant in Equation (6.5) is H_2O, not O_2, because there was insufficient O_2 in the head space of the reactor to produce the observed SO_4 increase.

6.2.5 Potential Silica Precipitation

Equation (6.1) can be integrated to give Equation (6.6) where S_o is the initial value of S.

$$\ln(1 - S)/(1 - S_o) = -kAt/KV \qquad (6.6)$$

Equation (6.6) can be used to estimate the time required to reach saturation. At equilibrium the value of S is 1.0, in which case the left-hand side of Equation (6.6) is undefined, but if we accept a value of 0.96 as essentially saturated, then hot water stored in the FIG aquifer requires 3.1, 5.6, and 20.9 days to attain quartz saturation at 150°, 110°, and 45°C, respectively. (These are rough estimates due to uncertainties in A/V and k.) When the hot water is withdrawn, it passes through the radiator, where it is cooled to 85°C, and is then reinjected at the supply well, where it is cooled further. We will consider three cases of silica deposition: in the radiator, which may affect radiator performance, in a "shell" around the supply well, which may plug the well, and in the aquifer around the supply well, which may reduce aquifer porosity.

The right-hand side of Equation (6.1) is plotted as a function of temperature in Figure 6.16. The precipitation rate is a maximum at approximately 130°C and decreases as temperature decreases because k decreases faster than S increases. To estimate the amount of silica deposited in the radiator we assume that temperature decreases exponentially from 150° to 85°C over the length of the radiator tubes and solve Equation (6.1). (Radiator specifications from Appendix A.) The change in silica concentration was 1.8×10^{-9} M. (We would have to be able to measure silica concentrations to six significant figures to detect a concentration change this small. Instead, we can measure concentrations to just three significant figures.) The average amount of silica deposited in 8 days would be 2.2×10^{-3} mole/m^2, corresponding to a film thickness of 0.05 μm. A deposit of this thickness would certainly not inhibit heat transfer significantly.

If precipitation is fast enough, the reinjection water may deposit most of its dissolved silica in a shell around the supply well. From Figure 6.16 we see that the deposition rate is a maximum at the well screen because temperature decreases with distance from the well. For 2.16 mM silica and an A/V value of 25.7 m^2/L the precipitation rate is 4.2×10^{-10} mole/Ls. At this rate an interstitial space of 1000 cm^3 accumulates 17 mg of SiO_2 over an 8-day period. Silica can precipitate as an amorphous gel having as little as 1% SiO_2 by weight (Sosman 1965). If the precipitated silica is in the form

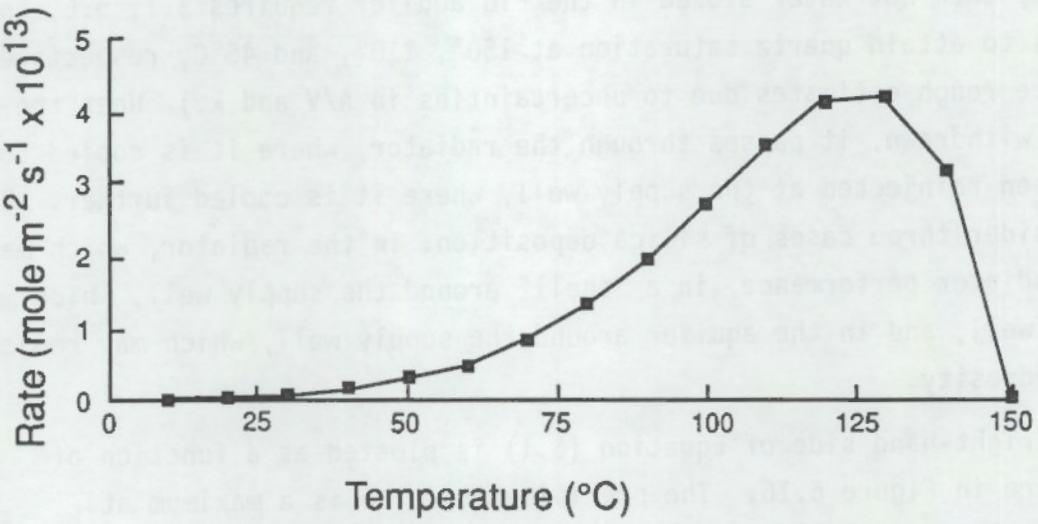

FIGURE 6.16. Silica Precipitation Rate from Water Saturated with Quartz at 150°C

of a 1% gel, the porosity reduction around the supply well is less than 0.1%. Therefore, because of a slow precipitation rate, a silica shell will not form around the supply well.

If the silica does not deposit rapidly near the well, it flows with the reinjection water. The maximum oversaturation would be 2 mM at the edges of the reinjected water mass where the temperature would be close to the ambient temperature of 10° to 12°C. If the silica were to precipitate as a 1% gel, the reduction in porosity would be less than 1%. Thus, silica precipitation in the aquifer should not seriously affect aquifer permeability.

6.3 SHORT-TERM ATES CYCLES

The chemistry of water samples collected during a pumping test, the cold water injection test, and the four short-term ATES cycles is presented in this section. Tables of data are presented in Appendix D. First, data obtained are discussed in chronological order. Next, the performance of the water treatment system is evaluated. Next, mole balance and average concentration

calculations are presented that compare the total amounts of solutes that were injected and recovered during the ATES cycles. Finally, the concentrations of the various solutes are plotted for comparison of the injection and recovery waters of a given cycle and comparison between cycles. Explanations for observed concentration changes between injection and recovery and between cycles are given.

6.3.1 Chemical Data from Short-Term Cycles

The results of chemical analyses of water samples collected during the pumping test in April and the cold water injection test in May 1982 are listed in Table D.1. The major ion concentrations were in the range reported by Ruhl, Wolf and Adolphson (1982) for the Ironton-Galesville aquifer. There was an unexplained problem with measuring Ca by AAS that resulted in very low absorbances for samples, although the standards showed normal absorbances. Therefore, Ca concentrations were calculated by subtracting Mg from hardness. The parentheses around the Ca concentrations indicate that Ca in these samples was not directly measured. Metals were determined in filtered and unfiltered samples for this set of samples. There was very little difference between filtered and unfiltered concentrations, which indicates that the metals were mostly in the dissolved form. Most concentrations were essentially constant throughout these tests and can be considered baseline values. Hardness titrations had an erratic blank that resulted in varying hardness values and, therefore, varying Ca values. The blank problem was corrected and did not interfere in subsequent analyses.

The chemistry of the preliminary hot water injection (May 1982) is listed in Table D.2. On May 15 and May 16 unheated ground water was injected, so the pH electrode was calibrated at 10°C. On May 17 and May 19 the injected water temperature was 85°C. The pH electrode was calibrated at 40°C. (See Section 6.4.3 for an explanation of temperature correction of pH measurements.) Precipitation of $CaCO_3$ in the heat exchanger lowered pH, alkalinity, Ca, and hardness. Iron may have been coprecipitated as siderite, $FeCO_3$, which would explain the reduction in Fe concentrations. Oil and grease, which was not detected in the cold water pumping test (Table D.1) and the cold water phase

of the preliminary injection test, increased to approximately 100 mg/L during the initial hot water injection. We believe this was caused by mobilization of organic matter in the sampling piping rather than the main system piping, because at the injection rate of 18.9 L/sec (300 gpm) almost 7 kg (15 lb) of grease would be injected per hour, an amount that would exceed any possible total amount of lubricant in the system. During this first heated injection, the sampling point was shut off when not sampling. In subsequent tests, water was kept flowing in the sampling piping to flush the pipes and prevent such spurious results and in subsequent tests grease and oil concentrations were below the detection limit of gravimetric grease and oil determinations of 10 mg/L (American Public Health Association, American Water Works Association, and Water Pollution Federation 1975). Instrumental organic carbon measurements confirmed that in samples for which grease and oil was not detected, the organic carbon concentration was much less than 10 mg/L (Table D.5).

Precipitation of $CaCO_3$ had cut the preliminary test short (see discussion, Section 5.2) so water treatment had to be installed for the rest of the tests. Table D.3 lists analyses of water samples collected during the injection phase of Cycle 1. The water treatment consisted of passing the hot water through a bed of crushed limestone to reduce supersaturation with respect to $CaCO_3$ (see Sections 5.2 and 6.3.2). The effects of the water treatment were examined by analyzing water samples taken from various points in the system. Alkalinity, pH, Ca, and hardness were lower in precipitator effluent than in heat exchanger effluent because of $CaCO_3$ precipitation in the precipitator. Similarly, $CaCO_3$ precipitation lowered alkalinity, pH, Ca, and hardness in heat exchanger effluent relative to influent ambient ground water (Table D.1). Iron concentrations in precipitator effluent were consistently higher than in the influent water, which is puzzling because the influent was oversaturated with respect to siderite, $FeCO_3$. All other solutes behaved conservatively on passage through the heat exchanger and precipitator.

The analyses of the recovery water samples from the first cycle are listed in Table D.4. Only two duplicate nonacidified water samples were collected on

12/14/82 in the first few minutes of withdrawal before the pump stopped and the system was shut down for repairs. After the pump was repaired, acidified and non-acidified samples were collected at each sampling time.

The chemical characteristics of water samples collected during the injection and recovery phases of Cycle 2 are listed in Tables D.5 and D.6, respectively. As in Cycle 1, the Fe concentration consistently decreased in the heat exchanger and increased in the precipitator. The analyses of water samples from Cycles 3 and 4 are listed in Tables D.7 through D.10.

Two sets of water samples were submitted to the Research Analytical Laboratory of the University of Minnesota Soil Science Department for analysis by inductively coupled plasma emission spectroscopy (ICP). The first set consisted of seven well-head samples and a filter blank collected during the injection phase of Cycle 2. The second set contained recovery water samples from Cycles 3 and 4. There was good agreement (i.e., within 10%) between ICP and our results for Ca, Mg, Na, K, and Fe. The ICP trace metal results are listed in Tables D.11 and D.12. Concentrations of Al, Mn, Cu, Ni, Cr, and Cd were near or below the detection limit in all samples. There were apparently contamination problems with Pb because the blank had a higher Pb concentration than any of the samples. The format of the ICP report makes low concentrations somewhat ambiguous; e.g., 0.04 could be between 0.035 and 0.044. However, with the exception of Pb, the ICP results at least give order of magnitude estimates of trace metal concentrations.

6.3.2 Water Treatment

The ambient ground water was near saturation with respect to calcite, $CaCO_3$. Therefore, because $CaCO_3$ solubility decreases as temperature increases, $CaCO_3$ precipitated when the water was heated in the preliminary ATES test, plugging the injection well screen and causing premature termination of the test. A fixed-bed precipitator was designed and constructed to reduce the oversaturation of the injection water. The precipitator was packed with crushed limestone to provide nucleation surfaces for $CaCO_3$ precipitation. The form of $CaCO_3$ that precipitated in the ATES system was aragonite, as

determined by x-ray diffraction. The performance of the precipitator can be expressed as the number of transfer units achieved as in Equation (6.7)

$$TU = \ln [(S_{in} - 1)/(S_{out} - 1)] \qquad (6.7)$$

where TU, the number of transfer units, is a dimensionless number and S_{in} and S_{out} are the aragonite saturation indexes of precipitator influent and effluent, respectively (Treybal 1980).

The saturation index computations are described in more detail in Section 6.4.3, Descriptive Chemical Equilibrium Computations. Saturation index and transfer unit calculations for the ATES tests are summarized in Table 6.7. Typically about one transfer unit was achieved. The lowest Ca concentrations occurred just after system maintenance when the heat exchanger was acid-cleaned to remove $CaCO_3$ scale. The rate of $CaCO_3$ deposition was highest at the highest temperatures. The history of precipitator packing, on the other hand, apparently had little effect on Ca removal. For example, in Table D.5 the well-head samples taken at 0945 before the water flow was switched to the fresh precipitator unit and at 1355 just after the switch had the same alkalinities and Ca concentrations.

Mole balance calculations were used to estimate the amounts of $CaCO_3$ removed by the heat exchanger and precipitator. The amount removed by the heat exchanger is given by Equation (6.8)

$$A_H = (Ca_U - Ca_H)V \qquad (6.8)$$

where A_H = amount of $CaCO_3$ precipitated in heat exchanger
Ca_U = calcium concentration in supply water
Ca_H = calcium concentration heat exchanger effluent
V = total injection volume

The results are listed in Table 6.8. In the first three cycles the heat exchanger removed more $CaCO_3$ than the precipitator. [Note: The mole balance method of Equation (6.8) is different from the method described in Section 6.3.3.]

TABLE 6.7. Summary of Fixed-Bed Reactor Performance During Short-Term ATES Cycles

Date	Log SI_{In}	Log SI_{Out}	TU	Date	Log SI_{In}	Log SI_{Out}	TU
(1982)	Cycle 1			(1983)	Cycle 2		
11/16	0.96	0.70	0.71	5/11	0.56	0.21	1.44
11/17	0.82	0.53	0.85	5/12	0.47	0.18	1.33
11/19	0.86	0.53	0.96	5/14	0.45	0.26	0.80
11/24	0.87	0.57	0.86	5/15	0.44	0.21	1.04
12/1	0.84	0.54	0.88	5/16	0.52	0.18	1.50
12/3	0.90	0.57	0.94	5/17	0.36	0.11	1.50
				5/18	0.37	0.27	0.44
				5/19	0.40	0.17	1.15
(1983)	Cycle 3			(1983)	Cycle 4		
9/22	0.37	0.11	1.54	11/10	0.82	0.42	1.26
9/24	0.53	0.29	0.92	11/19	0.68	0.22	1.75
9/27	0.36	0.21	0.73				
9/28	0.36	0.25	0.51				

TABLE 6.8. Calcium Carbonate Removal in the ATES System During Short-Term Cycles

	$CaCO_3$ Removed (10^3 moles)			
	Cycle 1	Cycle 2	Cycle 3	Cycle 4
Heat exchanger	2.2	5.0	3.2	2.6
Precipitator	2.0	2.0	2.6	3.2

6.3.3 Mole Balance and Average Concentration Calculations

Mole balance calculations were used to test whether a given solute (e.g., Ca) participated in a chemical reaction (e.g., $CaCO_3$ dissolution) during hot water storage. If the total amount of a substance injected was the same as the total amount withdrawn, the substance was said to be conservative. If the substance was conservative, it most likely did not react. On the other

hand, if a substance was not conservative, that substance did react and the most probable reaction that can account for the nonconservative behavior can be sought.

The method for calculating the total amount of a substance (e.g., Ca) injected or recovered during a cycle is shown in Figure 6.17. Injection, which was treated differently from recovery because periodic maintenance was required, was subdivided into periods of pumping and maintenance. If three samples were collected during an injection sub-period, the amount of substance injected during that period is given by Equation (6.9)

$$A_i = C_1[(t_1 + t_2)/2 - t_o] + C_2(t_3 - t_1)/2 + C_3[t_f - (t_2 + t_3)/2]Q_i \qquad (6.9)$$

where A_i = amount of substance injected during sub-period i
t_o = time at beginning of sub-period i
t_f = time at end of sub-period i
C_j = concentration of substance in sample j = 1, 2, 3
t_j = time of collection of sample j
Q_i = average flow rate during sub-period i

If two samples were collected during sub-period i, the amount of substance injected is given by Equation (6.10)

$$A_i = r\, C_1[(t_1 + t_2)/2 - t_o] + C_2[t_f - (t_1 + t_2)/2]Q_i \qquad (6.10)$$

The total amount of substance injected during an ATES cycle is given by Equation (6.11), where n is the number of sub-periods.

$$A = A_1 + A_2 + \ldots + A_n \qquad (6.11)$$

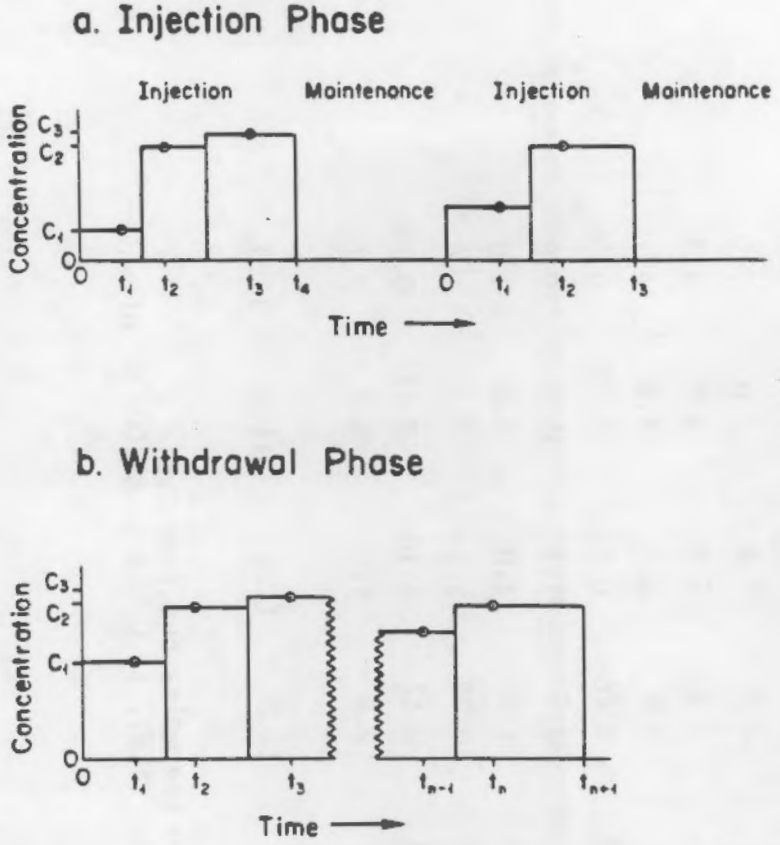

FIGURE 6.17. Methods of Computing Total Amounts of Dissolved Substances Pumped During ATES Cycles

The total amount of substance recovered during a cycle is given by Equation (6.12) where Q is the average flow rate.

$$A = C_1[(t_1 + t_2)/2 - t_o] + C_2(t_3 - t_1)/2 + \ldots + C_i(t_{i+1} - t_{i-1})/2 + \ldots + C_n[t_f - (t_n + t_{n-1})/2]Q \qquad (6.12)$$

The mole balance calculations for the four cycles are summarized in Table 6.9. These results are discussed along with graphs of individual solute concentrations in Section 6.3.4 below.

It is also convenient to compare average solute concentrations in injection and withdrawal waters. A change in average withdrawal water concentration of a given solute from the average injection water concentration indicates non-conservative behavior. Tables 6.10 through 6.13 list the unweighted average concentrations, coefficients of variation, and numbers of

TABLE 6.9. Summary of Mole Balance Calculations for Short-Term Cycles

	Cycle 1		Cycle 2			Cycle 3		Cycle 4	
	in	out	in[(a)]	in	out	in	out	in	out
Ca	6.9	8.8	7.4	10.1	13.5	8.8	10.4	7.7	9.8
Mg	6.1	5.6	6.7	9.0	9.3	8.8	7.6	7.8	7.0
Na	1.9	1.9	2.0	2.8	3.1	2.9	2.9	3.0	3.3
K	1.4	1.9	1.8	2.4	2.6	2.8	3.5	3.5	4.1
Fe	0.03	0.12	0.20	0.26	0.34	0.26	0.21	0.22	0.08
Alk	28.2	32.0	30.5	41.9	47.6	38.6	41.1	35.7	39.8
SO_4	0.41	0.57	0.74	0.95	1.1	1.0	1.0	1.0	1.0
Cl	0.17	0.30	0.35	0.47	0.96	0.70	1.1	1.1	1.4
F	0.11	0.13	0.12	0.17	0.19	0.17	0.18	0.17	0.19
SiO_2	1.0	2.3	1.5	2.1	4.0	2.9	5.9	4.3	7.7
Total flow[(b)]	8.3	8.1	8.1	12.2	12.3	12.2	11.8	11.9	11.9

(a) Values in this column can be directly compared to the moles out from Cycle 1
(b) Total flow units 1000 m^3. Solute units 1000 moles (i.e., in Cycle 1, 83,000 m^3 of water containing 6,900 moles of Ca were injected.)

TABLE 6.10. Average Solute Concentrations in ATES Short-Term Cycle 1

Solute	Concentration Units[a]	Injection			Withdrawal		
		Mean	CV, %[b]	n[c]	Mean	CV, %	n
Ca	mM	0.878	7	9	1.08	9	7
Mg	mM	0.767	4	9	0.694	6	7
Na	mM	0.234	7	9	0.234	4	7
K	mM	0.181	4	9	0.226	7	7
Fe	μM	3.49	49	9	13.4	103	7
Alk	mM	3.59	5	9	3.92	5	7
SO_4	μM	57.0	25	7	69.9	13	7
Cl	μM	21.5	8	7	43.0	51	7
F	μM	13.9	6	7	15.9	9	7
SiO_2	mM	0.125	2	6	0.287	25	7

(a) Concentration units apply only to means
(b) CV is coefficient of variation
(c) n is number of samples

TABLE 6.11. Average Solute Concentrations in ATES Short-Term Cycle 2

Solute	Concentration Units[a]	Injection			Withdrawal		
		Mean	CV, %[b]	n[c]	Mean	CV, %	n
Ca	mM	0.808	14	13	1.10	7	9
Mg	mM	0.735	4	13	0.769	10	9
Na	mM	0.227	7	13	0.254	13	9
K	mM	0.200	5	13	0.207	10	9
Fe	μM	18.9	49	13	26.4	20	9
Alk	mM	3.39	7	13	3.92	5	9
SO_4	μM	76.9	13	13	87.0	6	9
Cl	μM	40.6	30	13	95.9	102	9
F	μM	13.5	5	13	15.7	8	7
SiO_2	mM	0.176	13	13	0.328	26	9

(a) Concentration units apply only to means
(b) CV is coefficient of variation
(c) n is number of samples

TABLE 6.12. Average Solute Concentrations in ATES Short-Term Cycle 3

Solute	Concentration Units[a]	Injection			Withdrawal		
		Mean	CV, %[b]	n[c]	Mean	CV, %	n
Ca	mM	0.705	15	11	0.863	11	8
Mg	mM	0.729	2	11	0.636	1	8
Na	mM	0.243	3	11	0.243	7	8
K	mM	0.235	3	11	0.297	7	8
Fe	μM	22.7	44	8	16.7	48	8
Alk	mM	3.16	6	11	3.42	8	8
SO_4	μM	85.4	8	7	82.3	5	6
Cl	μM	57.3	13	7	91.4	33	6
F	μM	14.1	2	7	14.9	9	6
SiO_2	mM	0.238	7	11	0.517	22	8

(a) Concentration units apply only to means
(b) CV is coefficient of variation
(c) n is number of samples

TABLE 6.13. Average Solute Concentrations in ATES Short-Term Cycle 4

Solute	Concentration Units[a]	Injection			Withdrawal		
		Mean	CV, %[b]	n[c]	Mean	CV, %	n
Ca	mM	0.623	16	11	0.839	15	9
Mg	mM	0.664	5	11	0.595	7	9
Na	mM	0.249	3	10	0.277	4	9
K	mM	0.291	5	10	0.340	9	9
Fe	μM	17.3	71	11	7.18	25	9
Alk	mM	2.96	8	11	3.36	11	9
SO_4	μM	80.7	7	10	83.7	7	7
Cl	μM	93.2	29	9	120.0	20	7
F	μM	14.7	4	10	15.6	11	6
SiO_2	mM	0.359	10	11	0.641	29	8

(a) Concentration units apply only to means
(b) CV is coefficient of variation
(c) n is number of samples.

water samples for injection and withdrawal waters in the four short-term ATES cycles. [The coefficients of variation were calculated by dividing the standard deviations by the means, multiplying by 100%, and rounding off to the nearest integer (Laitinen 1960).] The average concentrations are not as reliable as mole balance calculations for detecting nonconservative behavior because the averages were not weighted with respect to volume.

6.3.4 Behavior of Individual Solutes During Short-Term Cycles

This subsection is arranged by solute (e.g., Ca) rather than chronologically for ease of comparison among cycles. Solute concentrations measured during the four short-term cycles are plotted as functions of cumulative flow rather than time because injections consisted of periods of pumping separated by periods of maintenance, while recovery was continuous. Using cumulative flow as the independent variable, comparisons between injection and recovery are more convenient than if time was the independent variable.

Total flows of water injected and recovered during a cycle are nearly equal. These symmetrical experiments and the negligible crossflow during storage allow the following: if a spike of conservative tracer is injected at volume V and the total injection volume is V_o, the spike will be withdrawn at volume V_o-V (neglecting dispersion). Therefore, it is reasonable to expect that for a conservative substance, the graph of recovery concentrations is the mirror image of the graph of injection concentrations with the axis of reflection being a vertical line at the end of injection and beginning of recovery. Thus, the graphs are used in conjunction with mole balance calculations to check whether or not a solute was involved in a chemical reaction during storage. Solute behavior was judged by the quantitative criterion of mole balance and by the qualitative criterion of appearance of injection and withdrawal graphs.

Calcium concentrations are shown in Figure 6.18. The fluctuations in injection water Ca were discussed in Section 6.3.2. The average injection Ca concentrations decreased from Cycle 1 to Cycle 4 because the average injection temperature increased. Ca concentrations in recovery waters followed the same pattern in all cycles. There was a decrease in Ca from the first sample

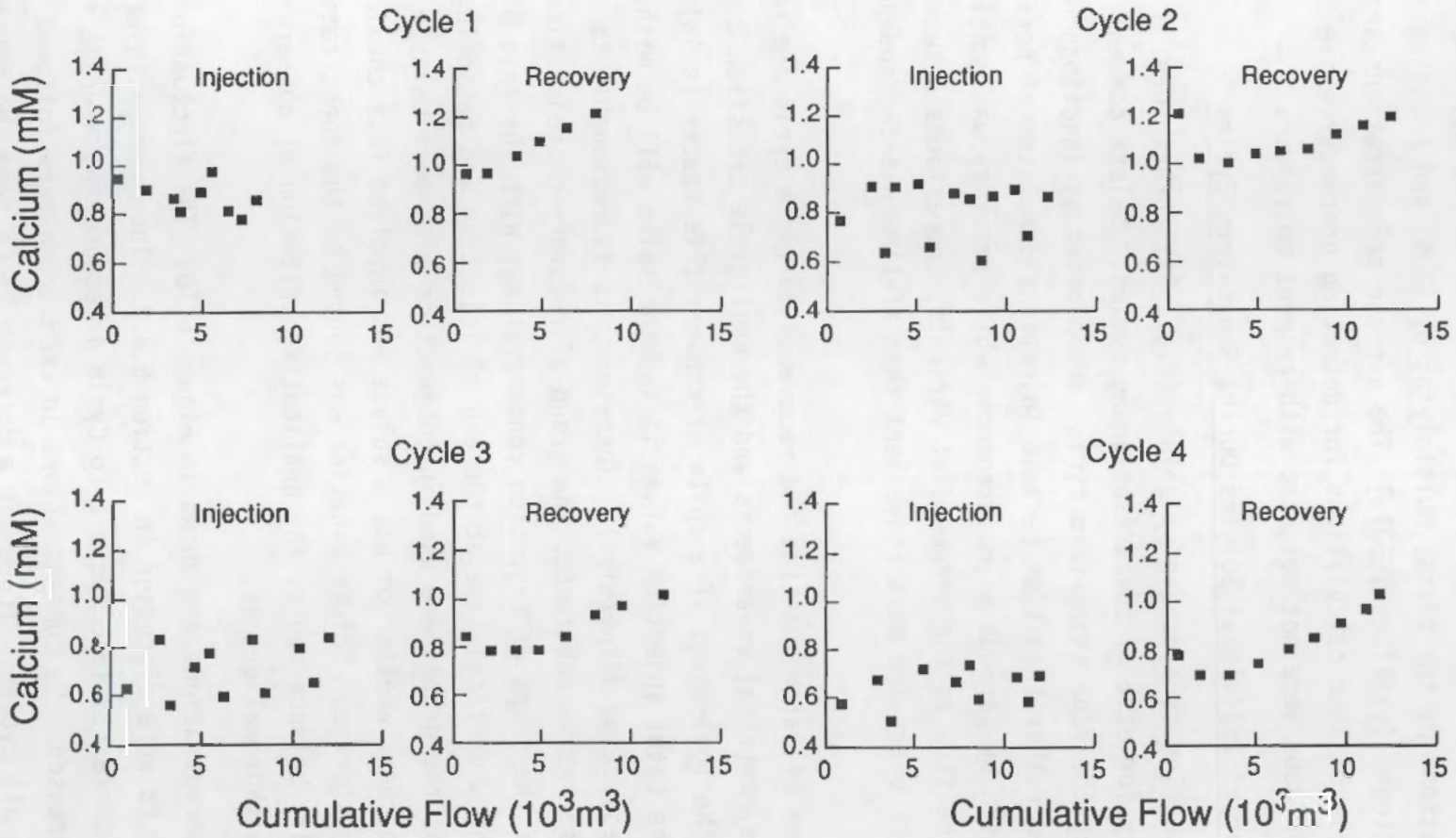

FIGURE 6.18. Calcium Concentrations in Samples of Injected and Recovered Water, Short-Term Cycles

to the second sample followed by a gradual increase in Ca. The minimum in Ca coincided with the maximum in temperature (Figure 6.19). The average recovery Ca concentrations were higher than the average injection concentrations. The average recovery Ca concentrations were highest during Cycle 2, which had the lowest average temperature. Alkalinity concentrations were similar to Ca in every respect (Figure 6.20). Mole balance calculations for Ca and alkalinity support these qualitative observations (Table 6.9).

Alkalinities and Ca concentrations in recovery waters were probably controlled by $CaCO_3$ dissolution during storage. Water that was treated to reduce $CaCO_3$ oversaturation at high temperatures lost heat to the aquifer sandstone and cooled. At the lower temperatures in the aquifer the water became undersaturated and, therefore, dissolved $CaCO_3$. The chemical equilibrium computations support this hypothesis (see Section 6.4).

Dissolved silica concentrations were higher in recovery waters than in injection waters in every cycle (Figure 6.21). The recovery concentrations passed through a maximum that coincided with the temperature maximum. The silica concentrations in recovery waters were highest during the hottest recovery waters of Cycle 4. Dissolution of quartz probably caused the increase in dissolved silica because quartz solubility increases with temperature. Silica concentrations in the four cycles are plotted together in Figure 6.22. Some of the silica precipitated, probably as amorphous silica, while the water was stored at site B between cycles. Silica concentrations increased in the source water because the water temperature increased from cycle to cycle and, therefore, amorphous silica was more soluble.

Magnesium concentrations are shown in Figure 6.23. In Cycle 2, magnesium was conservative with approximately the same number of moles of Mg recovered as injected. The injection concentrations followed a decreasing trend with injection volume, while the withdrawal concentrations (with one outlier excluded) showed a slight increasing trend with recovery volume. In Cycles 1, 3, and 4, on the other hand, the recovery Mg concentrations were lower than the injection concentrations with the exception of one outlier in Cycle 1. The mole balance calculations confirm the Mg decrease in Cycles 1, 3, and 4.

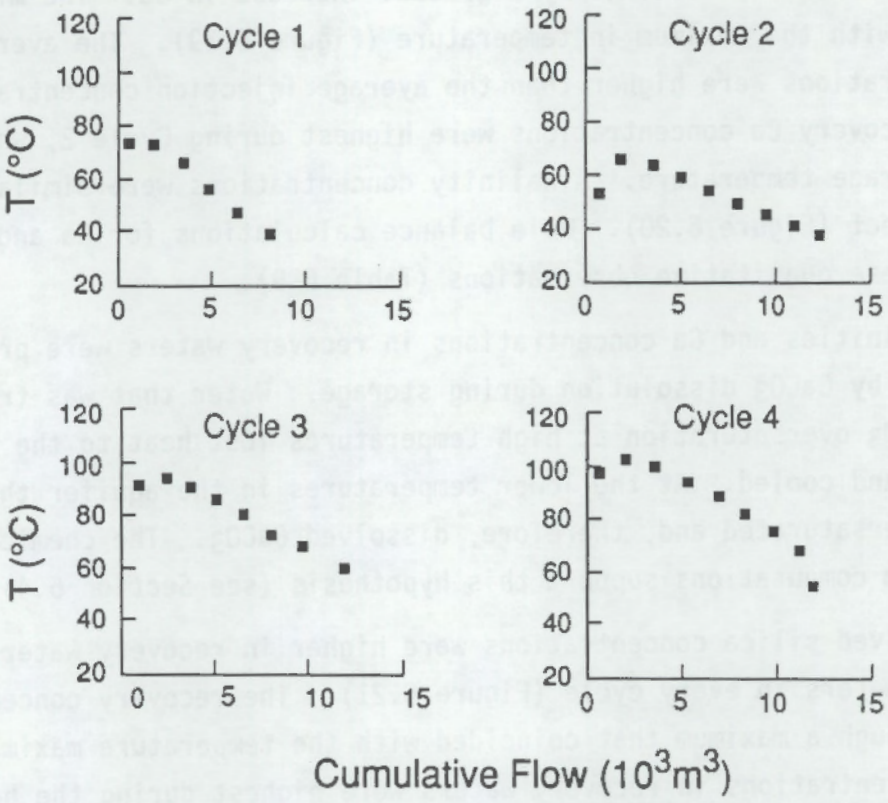

FIGUR E 6.19. Temperatures of Water Sampled During Recovery, Short-Term Cycles

This decrease may have been caused by precipitation of a magnesium silicate, (e.g., talc or sepiolite) or an alumino silicate (e.g., saponite or montmorillonite). The elevated silica concentrations caused by quartz dissolution probably caused the oversaturation with respect to the Mg minerals. Magnesium behaved conservatively during storage between cycles at site B, which explains the decreasing trend in average injection Mg concentrations from Cycle 1 to Cycle 4.

Potassium concentrations were higher in recovery waters than in injection waters in every cycle (Figure 6.24). The maximum K concentration in withdrawal waters coincided with the maximum temperature. Ion exchange or dissolution of potassium feldspar may have been the source of elevated dissolved K.

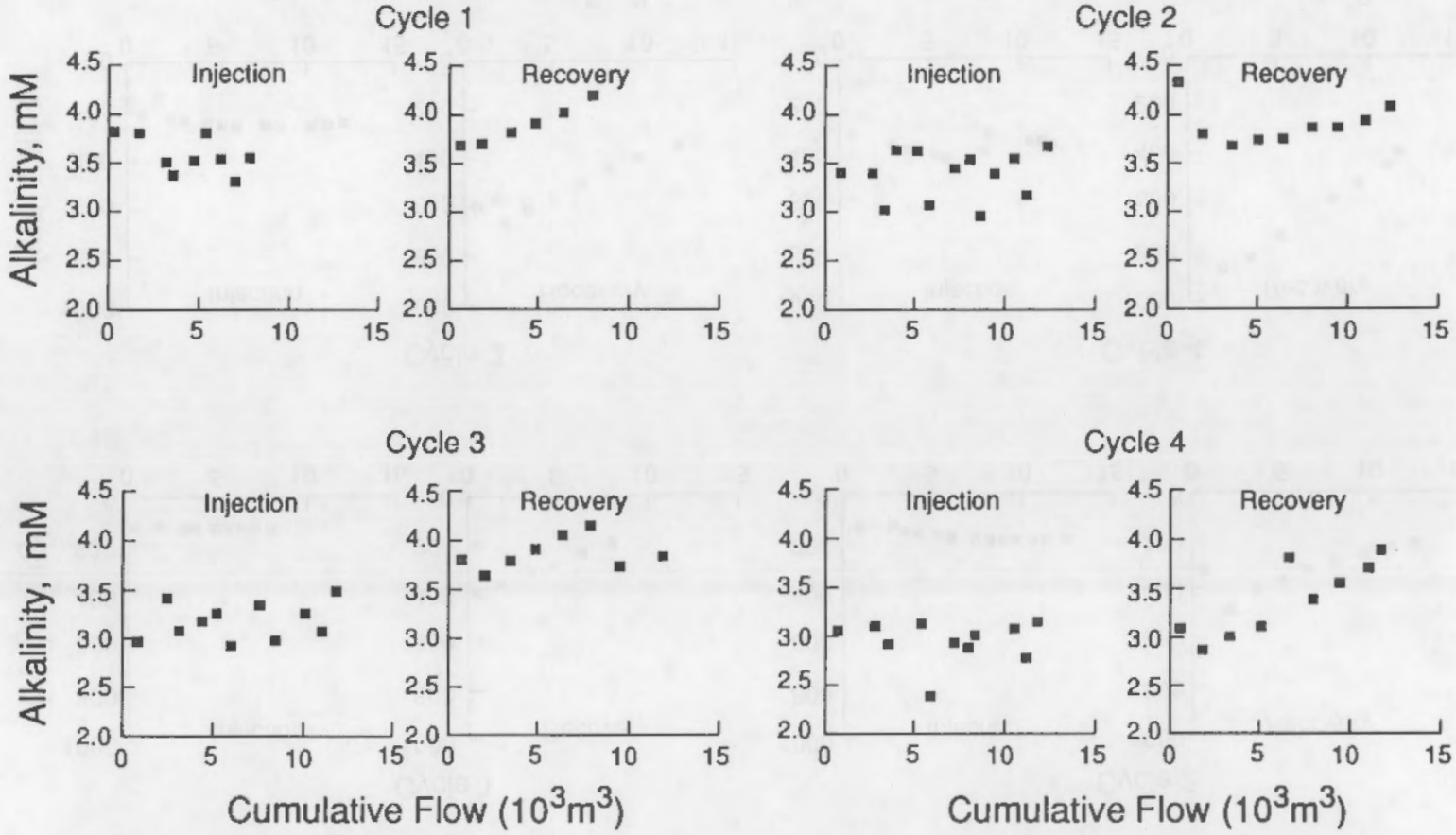

FIGURE 6.20. Alkalinity in Samples of Injected and Recovered Water, Short-Term Cycles

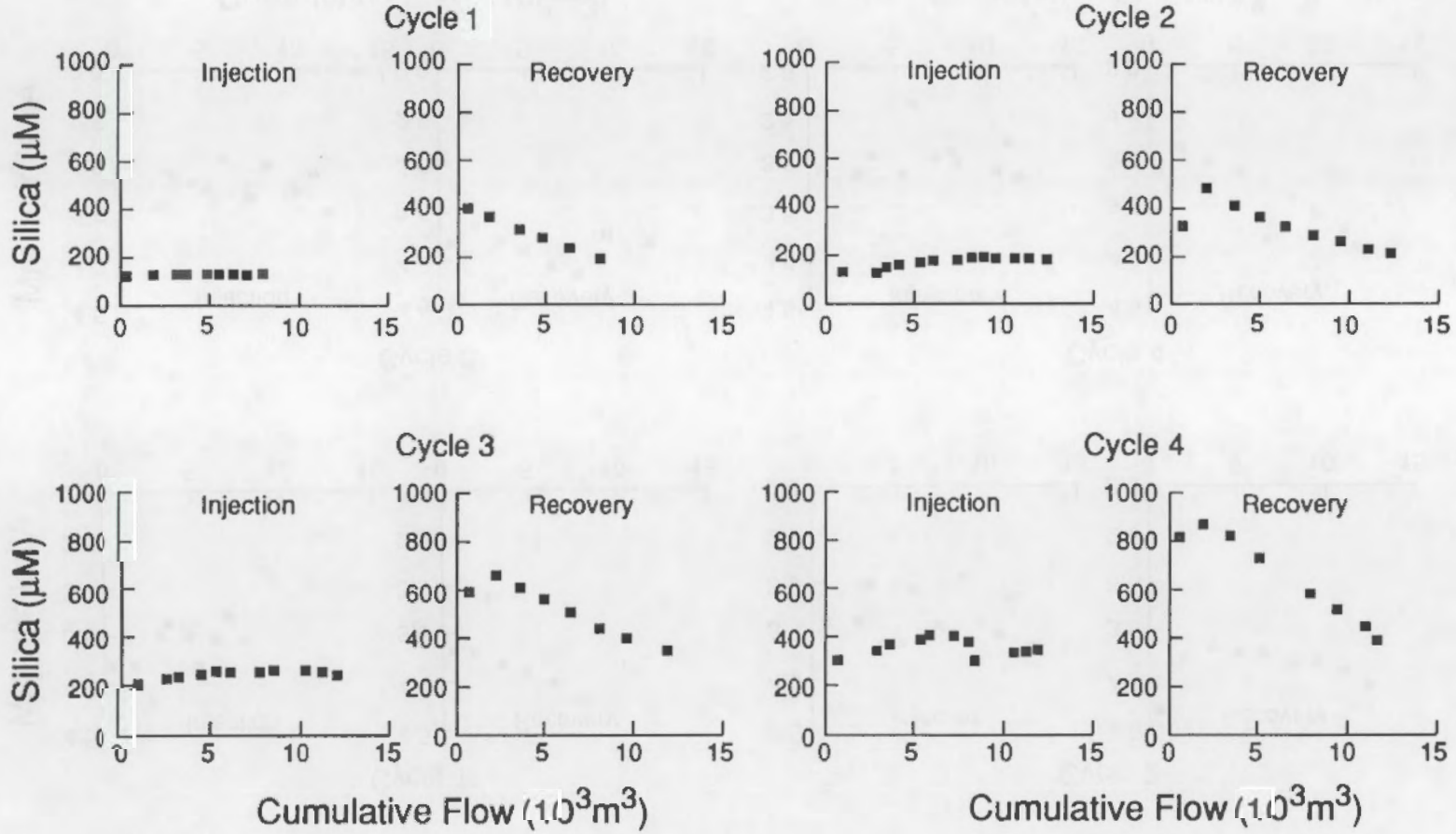

FIGURE 6.21. Silica Concentrations in Samples of Injected and Recovered Water, Short-Term Cycles

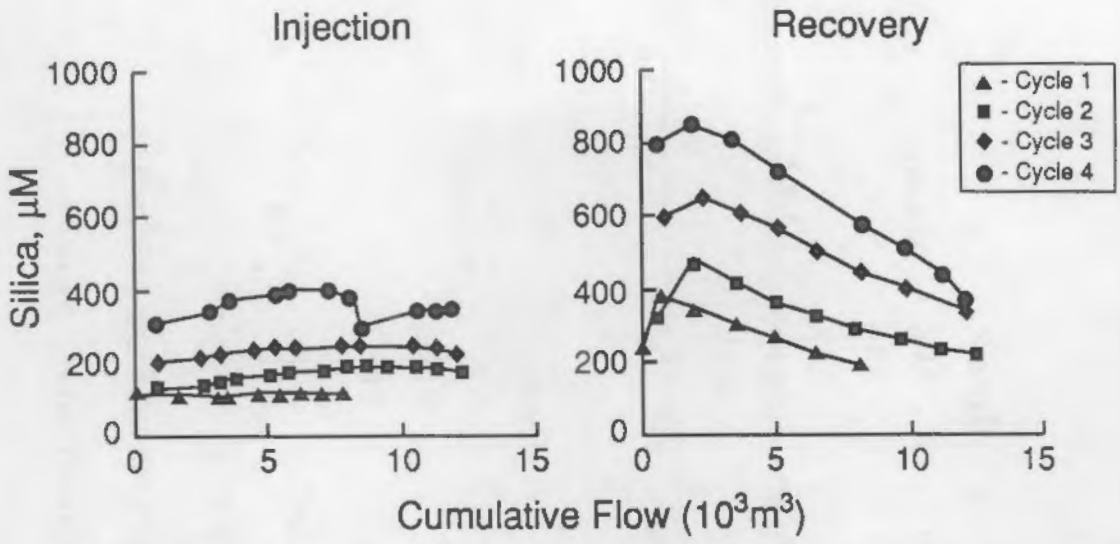

FIGURE 6.22. Comparison of Silica Concentrations in Short-Term Cycles

However, ion exchange is the more likely explanation because feldspar dissolution would have resulted in higher aluminum concentrations than were observed (all Al concentrations were <0.6 µg/L). Potassium appeared to be conservative during storage between cycles at site B because K accumulated in the injection waters from cycle to cycle (Figure 6.25). The mole balance shows that the number of moles of K withdrawn in a given cycle was approximately equal to the number of moles injected in the next cycle. Also, the withdrawal K concentrations decreased from the beginning of withdrawal to the end of withdrawal and the injection K concentrations in the next cycle increased from the beginning of injection to the end of injection. Thus, between cycles during water storage at site B, K satisfied the criteria of conservative behavior.

Sodium (Figure 6.26) was conservative in Cycle 1 with equal amounts injected and withdrawn, an increasing trend in injection concentrations with cumulative volume and a decreasing trend in withdrawal concentrations with cumulative volume. In Cycles 2 and 3 Na satisfied only one of the two criteria for conservative behavior. In Cycle 2 the mirror image criterion was satisfied, but withdrawal Na concentrations were higher than injection

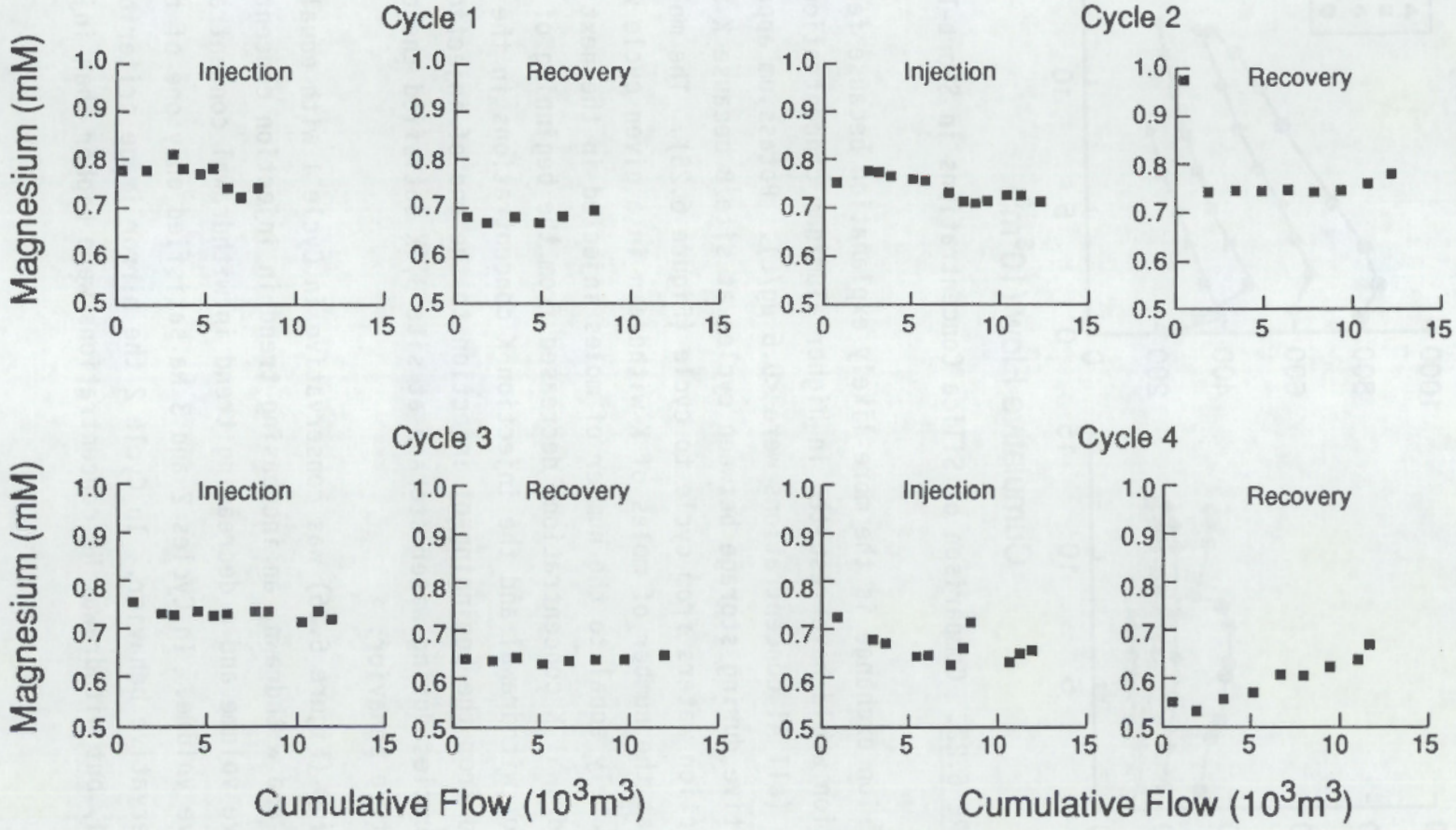

FIGURE 6.23. Magnesium Concentrations in Samples of Injected and Recovered Water, Short-Term Cycles

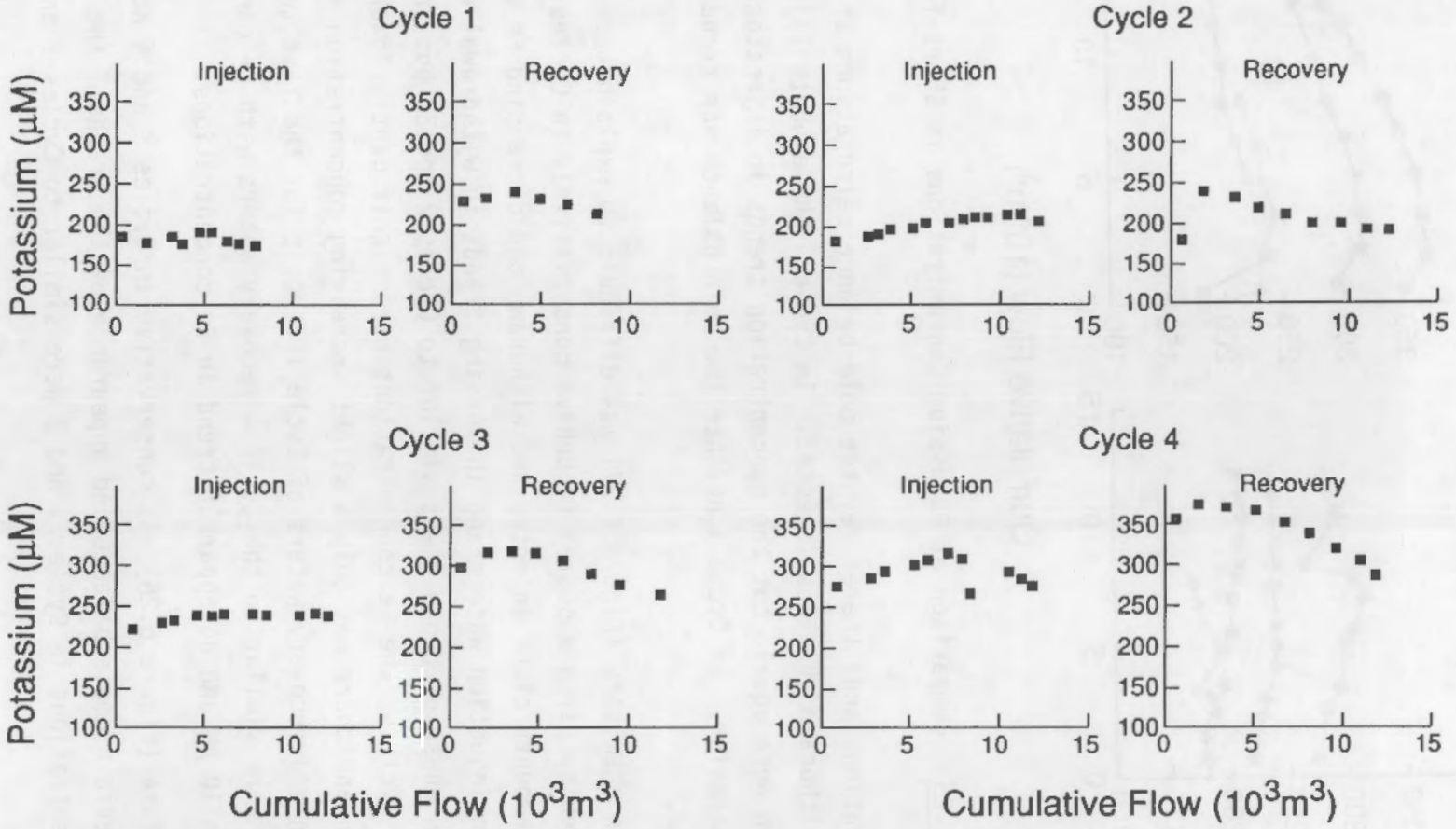

FIGURE 6.24. Potassium Concentrations in Samples of Injected and Recovered Water, Short-Term Cycles

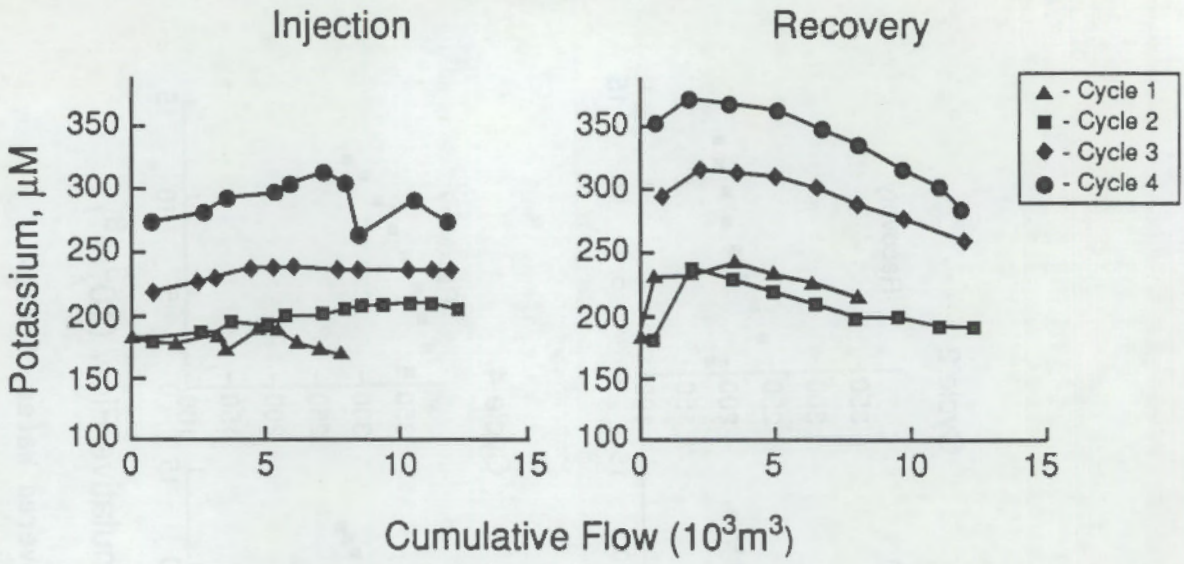

FIGURE 6.25. Comparison of Potassium Concentrations in Short-Term Cycles

concentrations and, therefore, the mole balance calculations showed that more Na was withdrawn than was injected. In Cycle 3 the amounts injected and withdrawn were equal, but the concentration trends in injection and withdrawal were dissimilar. In Cycle 4 neither the mole balance nor trend criteria were satisfied.

Iron chemistry (Figure 6.27) was difficult to explain because of scattered measurements. Iron appeared to behave conservatively in Cycles 2 and 3 with similar amounts of Fe injected and withdrawn and decreasing Fe concentration trends in injection waters and increasing trends in withdrawal waters. The injection phase of Cycle 4 was similar to Cycles 2 and 3, but in the withdrawal phase of Cycle 4, the Fe concentrations were significantly lower than in injection and there was only a slight increasing concentration trend. The injection and recovery waters of Cycle 1 (except for the last two injection samples) were similar to the Cycle 4 recovery waters with Fe concentrations less than 10 µM and no apparent trend in Fe concentrations.

Sulfate (Figure 6.28) was conservative in Cycles 3 and 4 according to the criteria of mole balance and appearance of the graphs. The graphs of SO_4 concentrations in Cycles 1 and 2 were similar to Cycles 3 and 4.

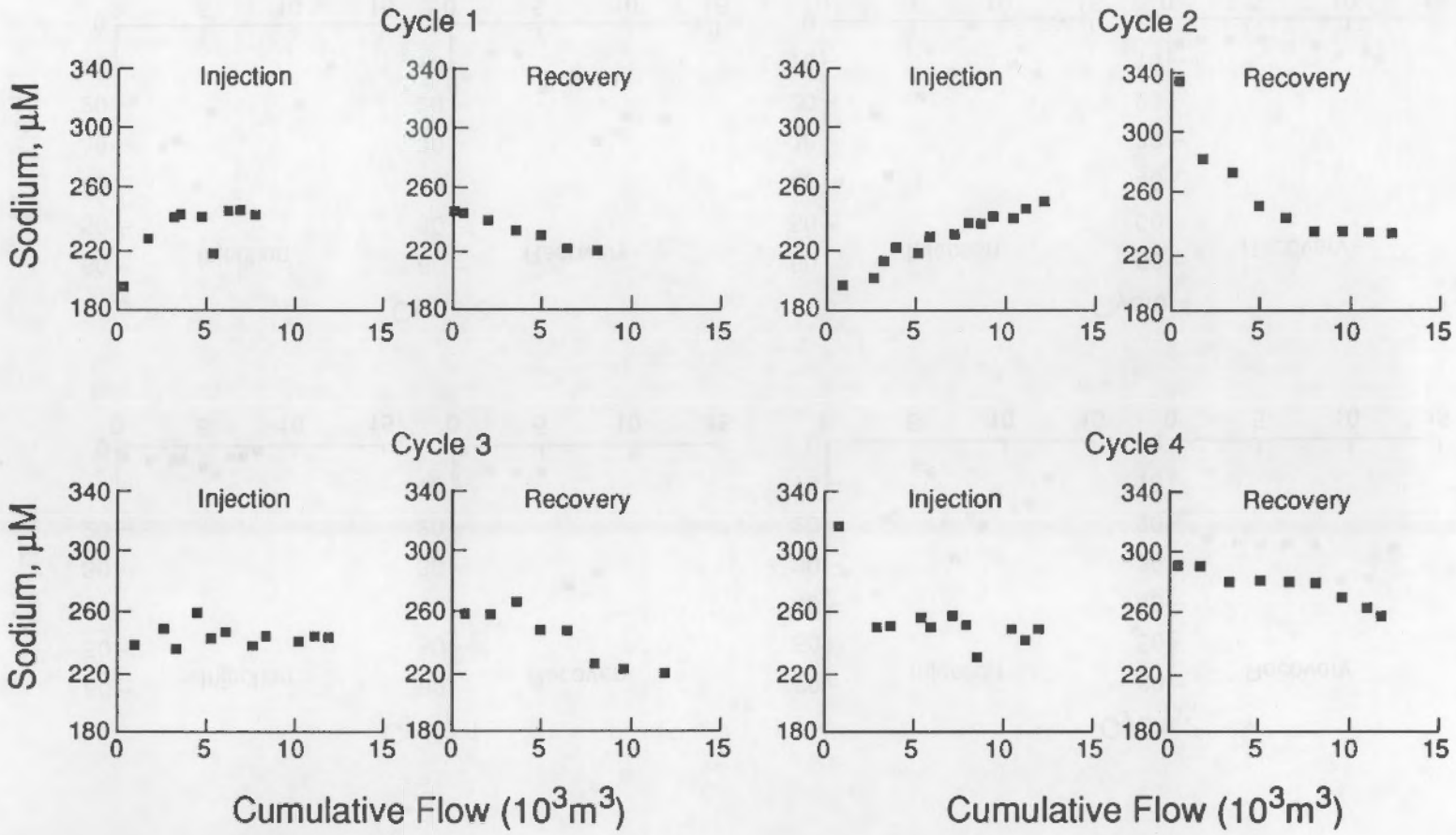

FIGURE 6.26. Sodium Concentrations in Samples of Injected and Recovered Water, Short-Term Cycles

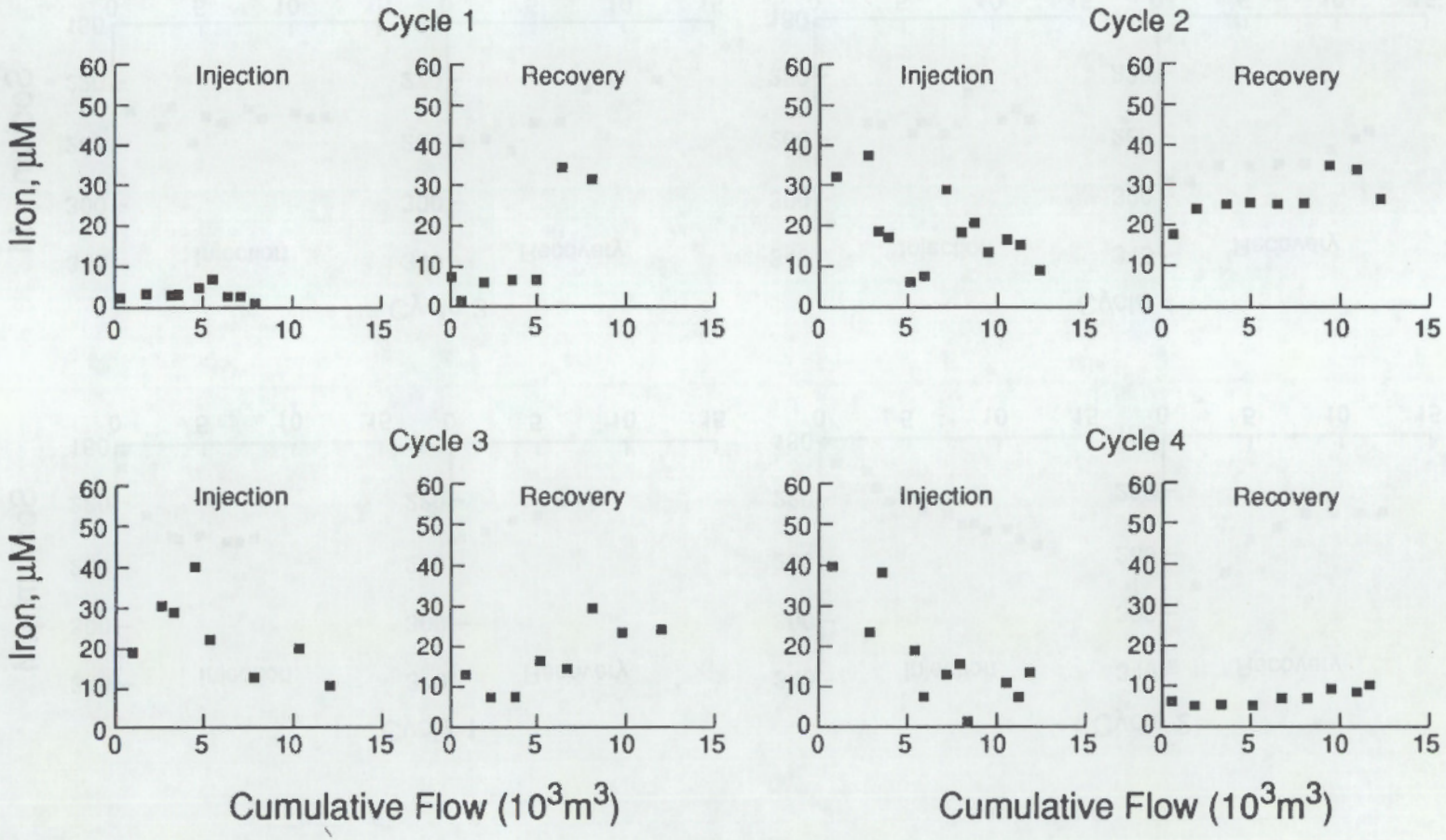

FIGURE 6.27. Iron Concentrations in Samples of Injected and Recovered Water, Short-Term Cycles

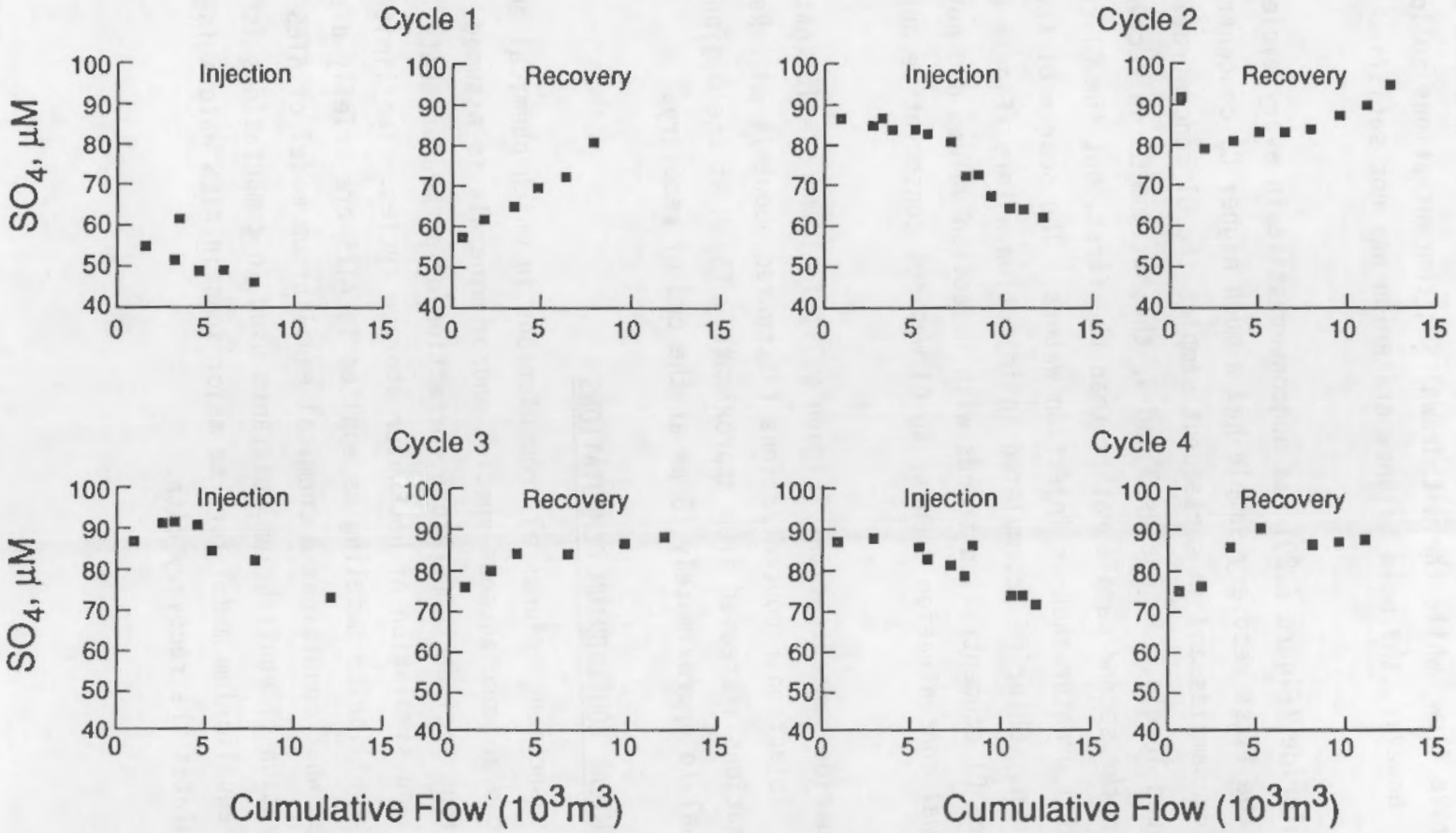

FIGURE 6.28. Sulfate Concentrations in Samples of Injected and Recovered Water, Short-Term Cycles

Concentrations of SO_4 in injection waters tended to decrease with increasing cumulative flow, while the withdrawal SO_4 concentrations followed the opposite trend. However, the mole balance criterion was not satisfied in Cycles 1 and 2.

Chloride (Figure 6.29) was nonconservative in every cycle. In Cycles 1 and 2, the first recovery sample had a much higher Cl concentration than injection samples and in subsequent samples the Cl concentration decreased to background levels. In Cycles 3 and 4, the maximum Cl in recovery waters was found in the second sample rather than the first, but the Cl concentrations were still greater than in injection waters. The source of the elevated Cl is unknown. Chloride accumulated in injection waters (Figure 6.30), but the injection Cl concentration trends with injection volume did not mirror withdrawal concentration trends, so Cl was not conservative during storage at site B.

Fluoride concentrations (Figure 6.31) followed similar patterns in all cycles. Injection F concentrations fluctuated about 14 μM. Recovery concentrations increased from approximately 13 μM at the beginning of withdrawal to approximately 18 μM at the end of recovery.

6.4 CHEMICAL EQUILIBRIUM COMPUTATIONS

This section includes all computations in which chemical equilibrium between two or more aqueous species and/or minerals is assumed. These computations include temperature correction of pH measurements, saturation indices, and simulation of hot water storage cycles. The limitations of chemical equilibrium modeling as applied to ATES are briefly discussed to show under what conditions a chemical equilibrium model of ATES is appropriate. The derivation of equilibrium constants used in computations is described. A chemical equilibrium model for the major ions in ATES waters is presented that simulates the recovery data.

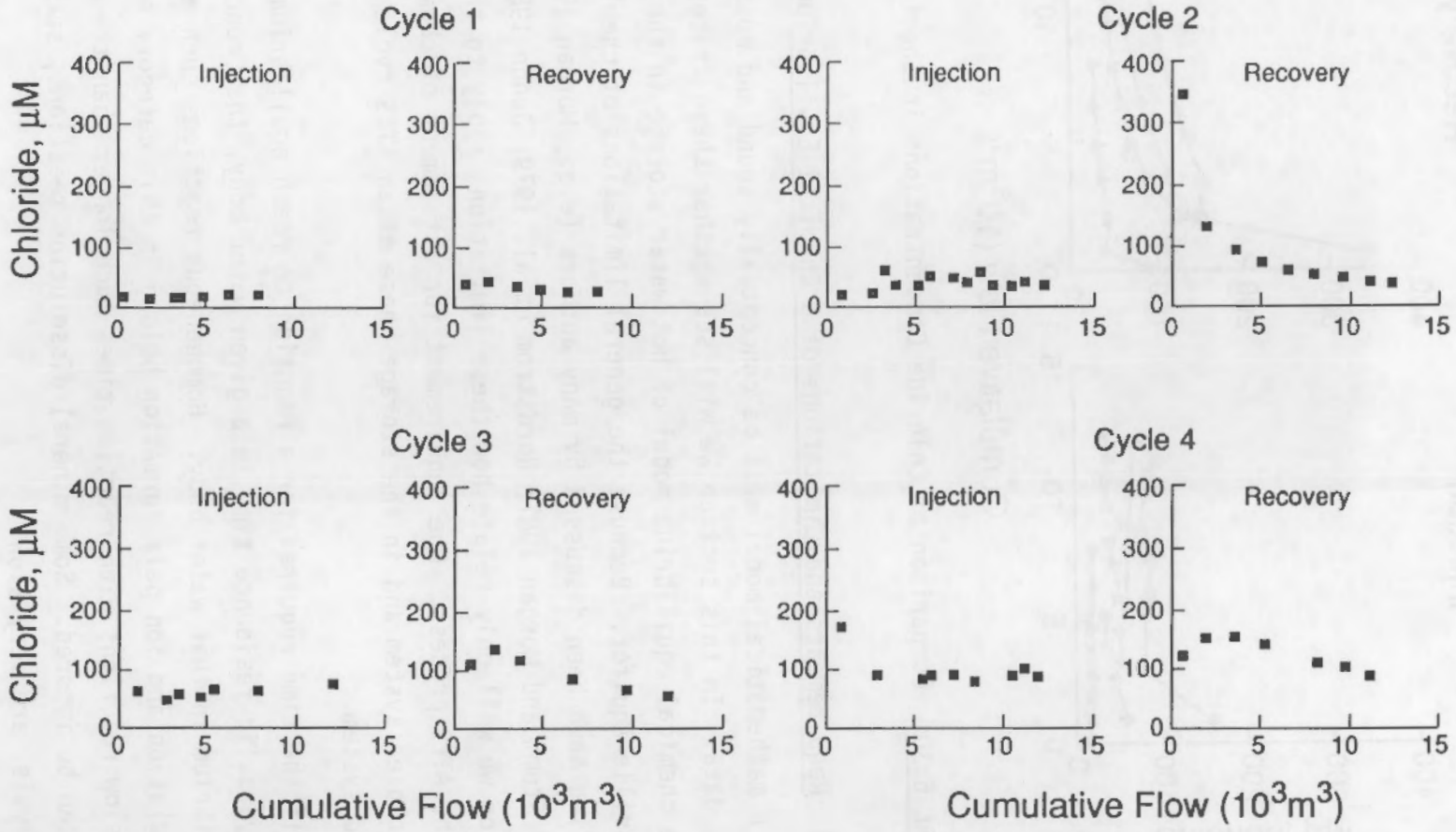

FIGURE 6.29. Chloride Concentrations in Samples of Injected and Recovered Water, Short-Term Cycles

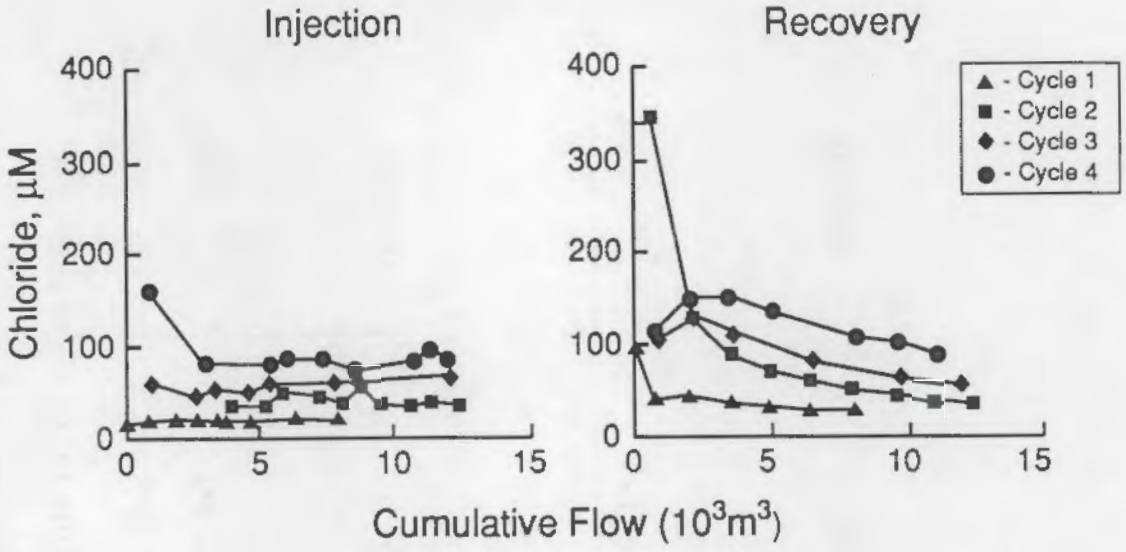

FIGURE 6.30. Comparison of Chloride Concentrations in Short-Term Cycles

6.4.1 Requirements and Limitations of a Chemical Equilibrium Model of ATES

A mathematical model must be conceptually sound and must incorporate valid data. In this section we will see whether these criteria are satisfied for a chemical equilibrium model of hot water storage in the Franconia-Ironton-Galesville aquifer. Because the general limitations of chemical equilibrium modeling have been discussed by many authors (e.g., Morgan 1967; Hoffmann 1981; Stumm and Morgan 1981; Nordstrom et al. 1979; Jenne 1981), in this section we will only relate how these limitations apply to the FIG aquifer and the ATES process. One requirement for attainment of chemical equilibrium is a closed system and in the storage phase of an ATES cycle the aquifer is a closed system.

If the time required for a reaction to reach equilibrium is less than the hydraulic residence time in a given water body, that reaction will reach equilibrium in that water body. Homogeneous reactions such as acid dissociation and ion pair formation belong in this category of fast reactions. Very slow reactions with reaction times much longer than the water storage time can be ignored. Some mineral dissolution reactions, such as feldspar hydrolysis, are very slow.

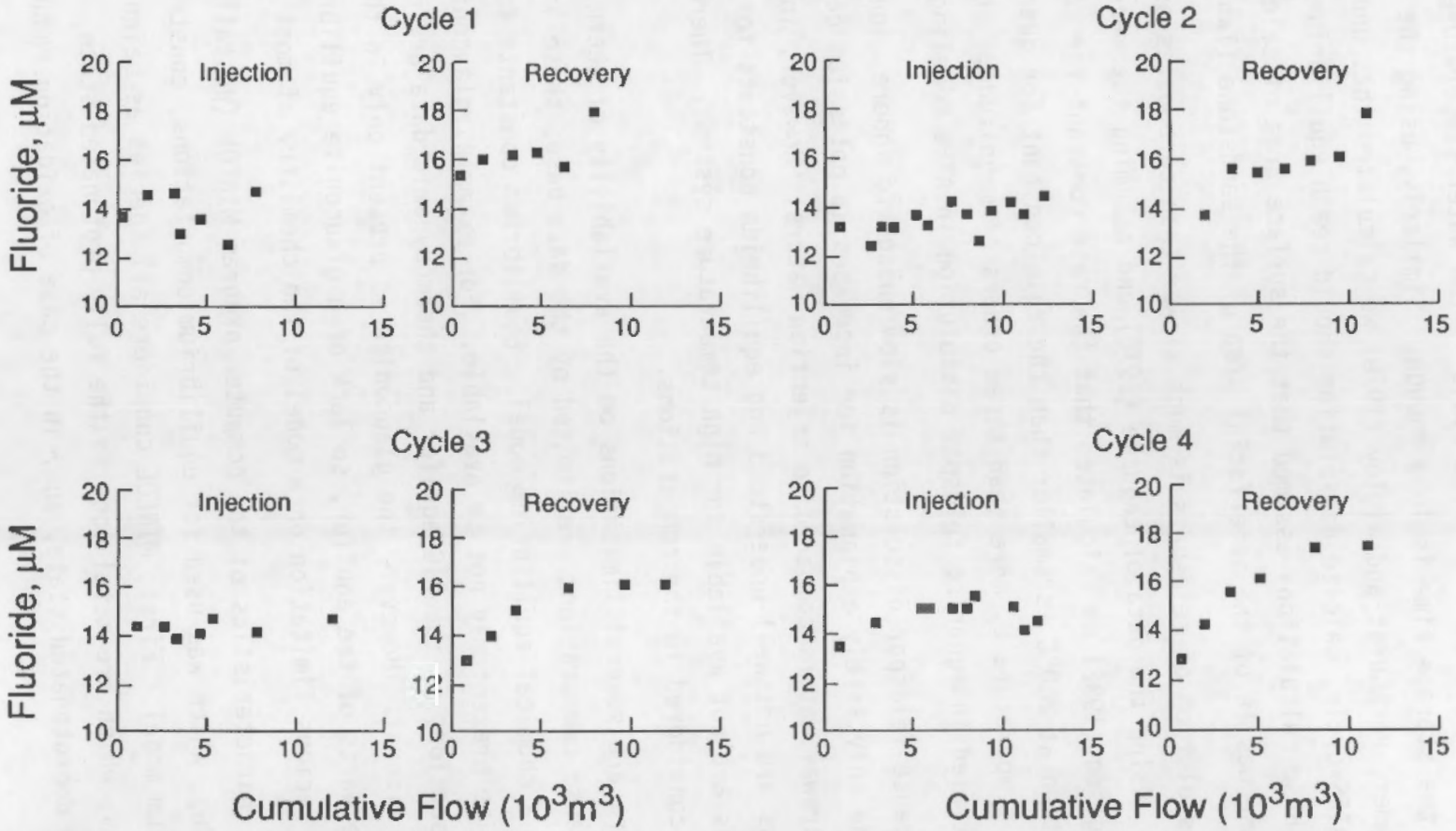

FIGURE 6.31. Fluoride Concentrations in Samples of Injected and Recovered Water, Short-Term Cycles

As was shown in Section 6.2, the dissolution of quartz can be expected to reach equilibrium in an ATES cycle if the water temperature is high enough and/or the storage time is long enough. Similarly, using the rate constants of Plummer, Parkhurst and Wigley (1979) we calculated that under the conditions of an ATES cycle, calcite dissolution should reach equilibrium in less than 1 day. These calculations assumed that the surface area of calcite in FIG sandstone was 1% of the interfacial area of the sandstone (Table 6.4).

Dissolution of feldspars is much slower than carbonates and silica. For example, using the data of Lagache (1976) and assuming the mechanism of Aagaard and Helgeson (1982) we calculated that the rate constant for potassium feldspar dissolution at 200°C is smaller than the rate constant for quartz dissolution at that temperature by more than three orders of magnitude. Therefore, we are justified in ignoring feldspar dissolution in ATES modeling.

Because feldspar dissolution is slow enough to ignore, ion exchange seems to be the only likely explanation for increases in potassium concentrations in withdrawal waters compared to injection waters. However, ion exchange reactions are not well understood and equilibrium constants for ion exchange reactions are not available for high temperature systems. Therefore, potassium was not considered in the computations.

There are several limitations on the availability of thermodynamic data and, because computations are limited by the data base, these limitations apply to a chemical equilibrium model. Equilibrium constants for minerals known to be present may not be available. For example, glauconite is found in some sections of the FIG aquifer and thermodynamic data are not available for this mineral. However, the glauconite is present only in the less permeable parts of the aquifer, so lack of a glauconite equilibrium constant is not a serious limitation on a model of the chemistry of most of the water.

Two characteristics of the computer program MINEQL (Westall, Zachary and Morel 1976), which was used for equilibrium computations, constrain an equilibrium model. First, MINEQL considers all species as being made up of components, which are metal ions in the fully protonated state, ligands in the fully deprotonated state, and, in the case of oxidation-reduction

reactions, electrons. Species must contain four or fewer components. Thus, illite, which is made up of five components, cannot be considered by MINEQL. The second limitation is that the stoichiometric coefficients of MINEQL species are fixed integers. Therefore, phases of variable composition (e.g., allophane) cannot be considered.

The quality of data obviously limits the usefulness of a mathematical model and both the thermodynamic data and water analyses are potential sources of error. The equilibrium constants will be covered in Section 6.4.2. Water analyses for aluminum and pH were less than satisfactory. Good Al data are necessary for computations involving aluminosilicate minerals; however, all aluminum concentrations were below the detection limit of electrothermal atomic absorption. Aluminum concentrations were assumed in computations involving Al. Good pH values are necessary because many equilibria are sensitive to pH. However, pH measurements in injection waters were not as reliable as in recovery waters, as shown in Section 6.4.3.

A final source of uncertainty is the complexity of the ATES system at the University of Minnesota. There are two screened intervals in the wells and the aquifers that these screened intervals provide access to have different transmissivities and thicknesses. As a result, the more permeable Ironton-Galesville aquifer receives more than 70% of the injected hot water and, hence, the water temperatures in the Galesville aquifer are higher than in the Franconia aquifer. When the stored water is recovered, water from the two aquifers mixes, so the chemistry of recovered water is actually intermediate between the two aquifers, although the Galesville water dominates. A further complication is heat exchange between sandstone and water. When water is recovered it is heated as it passes through the sandstone near the well. Hence, the temperature of the withdrawal water may be higher than the water temperature was in the aquifer before withdrawal.

6.4.2 Equilibrium Constants

Equilibrium constants were taken from the series of papers on the chemical equilibrium computer program WATEQ (Truesdell and Jones 1974; Plummer, Jones and Truesdell 1976; Ball, Nordstrom and Jenne 1980). The equilibrium constants

that were expressed as a power series function of temperature were used as listed. For mineral dissolution reactions for which only log K (298°K) and $\Delta H°$ (298°K) were listed, standard thermodynamic methods (e.g., Helgeson 1969) were used to compute equilibrium constants at higher temperatures. Heat capacities for aqueous species were obtained from Helgeson (1969) and heat capacities of minerals were obtained from Helgeson et al. (1978). Nordstrom et al. (1979) states that the van't Hoff approximation, which assumes that the enthalpy change of a reaction ($\Delta H°$) is independent of temperature, is reliable to 100°C. However, for calcite dissolution the van't Hoff approximation diverges from the log K(T) curve by a factor of 5 at 100°C and the divergence increases with temperature (Figure 6.32). In contrast the method described in this report (labeled Thermodynamic Estimate in Figure 6.32) gives a good estimate of log K(T). Therefore, we are confident that our calculated values of log K(T) are reliable.

For complex formation reactions the electrostatic/thermodynamic theory of Helgeson (1967) was used to compute stability constants at elevated temperatures. Helgeson (1967) showed that his theory worked well for several

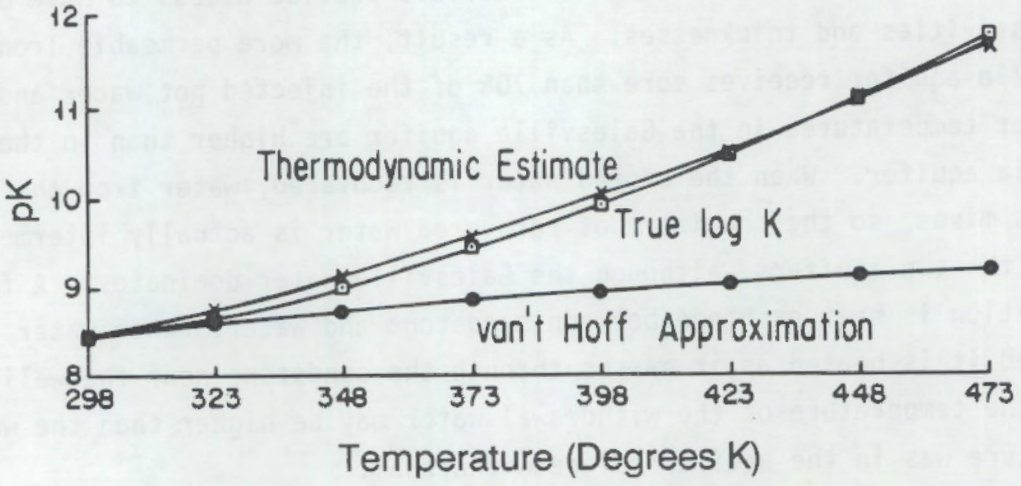

FIGURE 6.32. Comparison of van't Hoff and Thermodynamic Estimate of Calcite Dissolution Equilibrium Constants at Elevated Temperatures with True Log K

ion pair and acid dissociation reactions. A further test is provided by the data of Siebert and Hostetler (1977a,b) for the dissociation of the ion pairs $MgHCO_3^+$ and $MgCO_3(aq)$. The equilibrium constants determined by Siebert and Hostetler are listed in Table 6.14 along with equilibrium constants predicted by the Helgeson (1967) theory. The Helgeson method works very well for $MgCO_3$ and also for $MgHCO_3^+$ at all temperatures except for 90°C where the computed stability constant differs from the actual constant by more than the experimental error.

The equilibrium constants were fit by least squares regression to Equation (6.13), where K_j is the equilibrium constant for reaction i; a_j, b_j, and c_j are constants characteristic of reaction i; and T is the absolute temperature. Equation (6.13) is a common form for expressing temperature-dependent equilibrium constants.

$$\log K(T_j) = a_j + b_j T + c_j T^{-1} + d_j \log T + e_j/T^2 \qquad (6.13)$$

It is more convenient than storing tables of log K(T) and interpolating for each computation or recomputing log K(T) using heat capacities of reactants

TABLE 6.14. Comparison of a Theoretical Method for Computing Stability Constants of Elevated Temperatures with Experimental Data

T, °K	log K(a)	$MtHCO_3^+$ S(b)	log K_H(c)	log K	$MgCO_3^0$ S	log K_H
283	1.051	0.018	1.023	2.890	0.019	2.910
298	1.066	0.012	1.066	2.984	0.028	2.984
313	1.108	0.059	1.111	3.070	0.021	3.060
328	1.160	0.011	1.159	3.180	0.026	3.150
343	1.230	0.017	1.209	3.280	0.042	3.240
363	1.337	0.007	1.281	3.410	0.067	3.380

(a) K = Experimentally determined stability constant (Siebert and Hostetler, 1977a,b)
(b) S = Standard deviation of log K
(c) K_H = Stability constant computed according to Helgeson (1967)

and products. The standard deviation of the regression [Equation (6.14)] was less than 0.03 for all reactions, so Equation (6.14) is a reliable storage method.

$$s_i = 1/(n - 1) \; [\log K(T_j) - a_i - b_i T_j - c_i T^{j-1} - d_i \log T - e_i/T^2]^2 \; 1/2 \quad (6.14)$$

The data for computing equilibrium constants are listed in Table 6.15, which lists species identification numbers and the coefficients of Equation (6.13). The dielectric constant of water was computed according to Bradley and Pitzer (1979). The Davies approximation was used for ionic strength corrections (Stumm and Morgan 1981).

6.4.3 Descriptive Chemical Equilibrium Computations

Chemical equilibrium computations are divided into the categories "mass transfer", which involves equilibria between the aqueous phase and solid phases (i.e., precipitation and dissolution), and "descriptive", which involves only the aqueous phase. From a practical standpoint the descriptive computations are relatively simple (a programmable calculator was used), while the more general mass transfer computations required a computer. Also, because only homogeneous equilibria are considered in computing free-ion concentrations, the kinetic criterion for chemical equilibrium is surely satisfied.

Correction of pH measurements for temperature was necessary because in most of the ATES cycles the pH of flowing water was measured at a temperature that was lower than the temperature of the actual process stream. When the flow-through pH cell was used, the sample stream cooled while flowing through the piping connecting the cell to the ATES piping. In other cases, the water had to be cooled to below 100°C to prevent flashing to steam. Temperature correction of pH values was performed in two steps. First, the speciation of Ca, Mg, H, and CO_3 were computed from the sample pH, alkalinity, and Ca and Mg concentrations and the temperature at which the pH was measured. For these computations the pH was fixed and the mole balance for CO_3^{2-} was given by Equation (6.15), where square brackets indicate molar concentrations.

$$\text{Alkalinity} = [HCO_3^-] + 2[CO_3^{2-}] + [CaHCO_3^+] + [MgHCO_3^+] \quad (6.15)$$

TABLE 6.15. Data for Calculating Equilibrium Constants

ID No.	Species	a	b	c	d	e
Complexes						
1000	CaCO3 (aq)	-1228.7320	-0.299444	35512.75	485.818	
1010	CaHCO3 +	1317.0000	0.345470	-39916.80	-517.708	563713.9
1020	CaSO4 (aq)	-5.7651	0.014942	1082.50		
1350	CaOH +	-0.3907	-0.002383	-3430.60		
1360	MgCO3 (aq)	0.9910	0.006670	0.00		
1370	MgHCO3 +	-12.5270	0.036590	3883.70		
1380	MgSO4 (aq)	-7.6864	0.021617	1047.00		
1390	MgF +	-6.7383	0.019305	839.70		
1740	MgOH +	1.2906	-0.003821	-3551.80		
1960	KSO4 -	-1.5505	0.006919	100.09		
2000	NaCO3 -	-9.8954	0.028560	796.38		
2010	NaSO4 -	-1.9387	0.005596	297.40		
2070	FeSO4 +	-8.3477	0.024037	1000.40		
2670	FeOH 2+	15.8610	-0.010806	-4473.80		
2680	Fe(OH)2 +	-9.4614	-0.025321	-1224.10		
2700	Fe(OH)3 (aq)	-20.2210	0.037609	-3715.00		
2710	Fe(OH)4 -	-10.4050	0.027835	-211.80		
2720	FeSO4 (aq)	-4.1668	0.012008	805.00		
10030	AlSO4 +	-5.8646	0.016866	115.32		
10040	Al(SO4)2 -	-8.9246	0.025682	1850.30		
10050	AlF 2+	-9.4752	0.027440	2478.80		
10060	AlF2 +	-17.9000	0.051563	4520.70		
10070	AlF3 (aq)	-23.2990	0.067116	5973.10		
10080	AlF4 -	-26.3000	0.075859	6808.50		
10340	AlOH 2+	-5.1230	0.014060	-1209.00		
10350	Al(OH)4 -	-12.5200	0.034370	-5928.00		
12530	HCO3 -	107.8871	0.032528	-5151.79	-38.926	563713.9
12540	H2CO3 (aq)	464.1965	0.093448	-26986.16	-165.760	2248628.9
12550	HSO4 -	-5.2880	0.018287	539.06		
12580	HS -	11.2130	-0.011685	1183.80		
12590	H2S (aq)	4.4812	-0.032161	7431.00		
12710	SiO(OH)3 -	-33.1100	0.049581	8949.20		
12720	Si(OH)4 (aq)	-39.4780	0.065927	12355.00		
13595	OH -	3.2086	-0.012776	-3991.80		
Oxidation-Reduction Reactions						
15000	Fe3+ +e = Fe2+	-7.2508	0.020886	4193.80		
15040	SO42- + 8H+ + 8e = S2- + 4H2O	-12.2190	-0.005526	10022.00		

TABLE 6.15. Continued

ID No.	Species	a	b	c	d	e
Minerals						
20000	calcite	171.9070	0.077993	-2893.30	-71.595	
20001	aragonite	171.9770	0.077993	-2903.30	-71.595	
20010	gypsum	-4.9230	0.021138	992.38		
20020	fluorite	-6.8551	0.024910	2523.50		
20140	magnesite	-8.8534	0.033395	1980.40		
20200	brucite	3.0720	-0.004187	-5505.60		
20310	amorph. Fe(OH)	4.0763	0.008002	-3354.40		
20320	siderite	-3.2478	0.029764	1512.10		
20330	mackinawite	8.7613	0.002028	2835.20		
20370	rhodochrosite	-7.8080	0.033540	2452.00		
21160	kaolinite	-59.4480	0.124120	17790.00		
21180	amorph. Al(OH)	-2.0872	0.001420	-1969.80		
21181	crypt. gibbsit	15.0900	-0.009476	6406.00		
21182	gibbsite	15.0800	-0.949040	-6024.00		
21440	quartz	-41.3590	0.067955	13915.00		
21441	amorph. SiO2	-39.8110	0.066716	13195.00		
21450	pyrite	32.6190	0.023370	6145.80		
21460	magnetite	26.1720	0.013780	-7083.20		
30000	dolomite	-21.3820	0.070545	5106.90		
30010	microcline	-172.4300	0.284960	45108.00		
30020	sepiolite	-110.1100	0.189470	30591.00		
30030	chlorite	-49.8840	0.143700	-375.00		
30040	talc	-149.1900	0.254930	41128.00		
30050	muscovite	-133.9100	0.266160	30905.00		
30060	chrysotile	-14.7500	0.034740	4600.00		
30090	enstatite	-34.2770	0.062697	7706.60		
30100	diopside	-73.4980	0.128700	17443.00		
30110	Ca-montmorill.	-664.4400	1.371400	207530.00		
30111	Mg-montmorill.	-665.5200	1.374000	207530.00		
30120	forsterite	-28.0510	0.058813	855.00		
30130	fayalite	-27.4840	0.061539	4039.10		
30140	alunite	25.5730	0.021526	-9070.50		
Gas						
25000	CO2 gas	355.8105	0.073597	-20069.57	-125.308	1579263.9

The total concentrations of H^+ and CO_3^{2-} were computed according to Equations (6.16) and (6.17), respectively, where $[H_2CO_3^*]$ is the sum of $H_2CO_3(aq)$ and $CO_2(aq)$ (Stumm and Morgan 1981).

$$H_T = [H^+] + [HCO_3^-] + 2[H_2CO_3^*] + [CaHCO_3^+] + [MgHCO_3^+] \quad (6.16)$$

$$C_T = [CO_3^{2-}] + [HCO_3^-] + [H_2CO_3^*] + [CaHCO_3^+] + [MgHCO_3^+] \quad (6.17)$$

Preliminary computations showed that complexes of Ca^{2+} and Mg^{2+} with SO_4^{2-}, F^-, and OH^- made up very small fractions of total Ca and Mg (i.e., less than 1%), so these species were not included in pH temperature corrections.

In the second step of temperature correction the equilibrium composition of the solution was computed at the true sample temperature with the mole balance on H^+ and CO_3^{2-} given by Equations (6.16) and (6.17), respectively. H_T and C_T were also used as input for mass transfer computations.

Because the pH temperature correction also yielded free, or uncombined, concentrations of Ca^{2+}, Mg^{2+}, and CO_3^{2-}, the saturation indices of several minerals could be computed simultaneously. As an example, Equation (6.18) defines the saturation index of aragonite, where K' is the solubility product of aragonite corrected for ionic strength.

$$S = [Ca^{2+}][CO_3^{2-}]/K' \quad (6.18)$$

The values of H_T and C_T were very sensitive to measured pH values. Therefore, saturation indices and mass transfer computations were also sensitive to pH. Equations (6.19) and (6.20), which were derived using a standard error propagation formula (Laitinen 1960), show the dependence of relative errors in H_T and C_T on pH. The symbol Δ signifies error in the quantity X and [Alk] stands for alkalinity.

$$\Delta H_T/H_T = \Delta[Alk]/[Alk] + f(pH,T)\ pH \quad (6.19)$$

$$\Delta C_T/C_T = \Delta[Alk]/[Alk] + g(pH,T)\ pH \qquad (6.20)$$

The values of the function f(pH,T) ranged from 1.00 to 1.33 and the function g(pH,T) ranged from 0.64 to 0.93 in ATES cycles. H_T values in the injection and withdrawal phases of Cycle 2 are shown in Figure 6.33, which was typical of the cycles. With the exclusion of one outlier the withdrawal H_T values had a much smaller standard deviation than the injection values. The scatter in injection values was probably caused by difficulties in measuring pH at the higher temperatures of injection and the pH temperature correction. There was no evidence for chemical reactions that could have changed H_T.

Saturation index computations are also useful in testing for equilibrium between a water and a mineral. Saturation indexes for several minerals in ATES withdrawal waters are shown in Figures 6.34 through 6.39 in which the abscissae are cumulative volumes as in Figures 6.18 through 6.31. The quartz saturation indexes of recovery waters are shown in Figure 6.34. The recovery

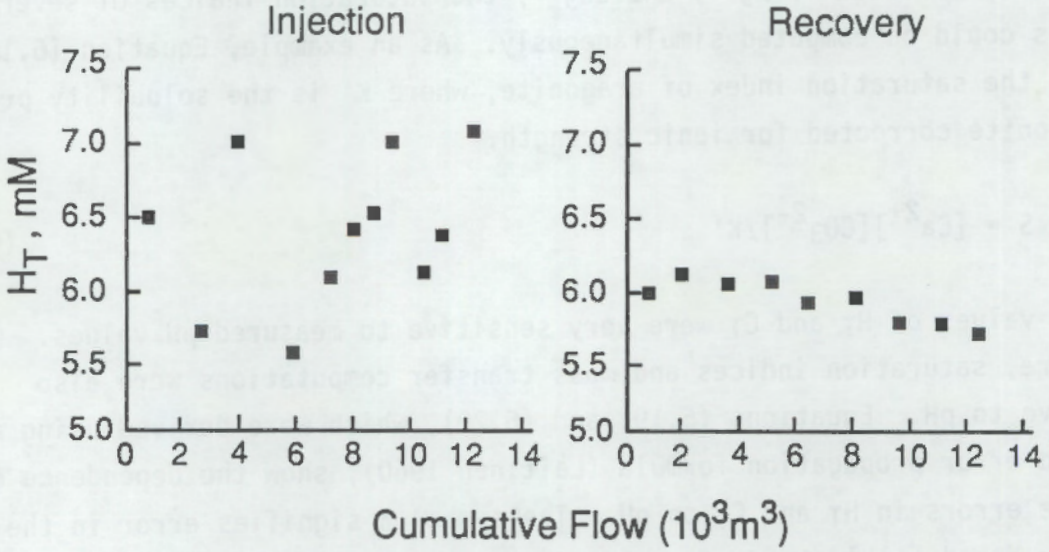

FIGURE 6.33. Total Hydrogen Ion Concentrations in Injected and Recovered Water, Short-Term Cycle 2

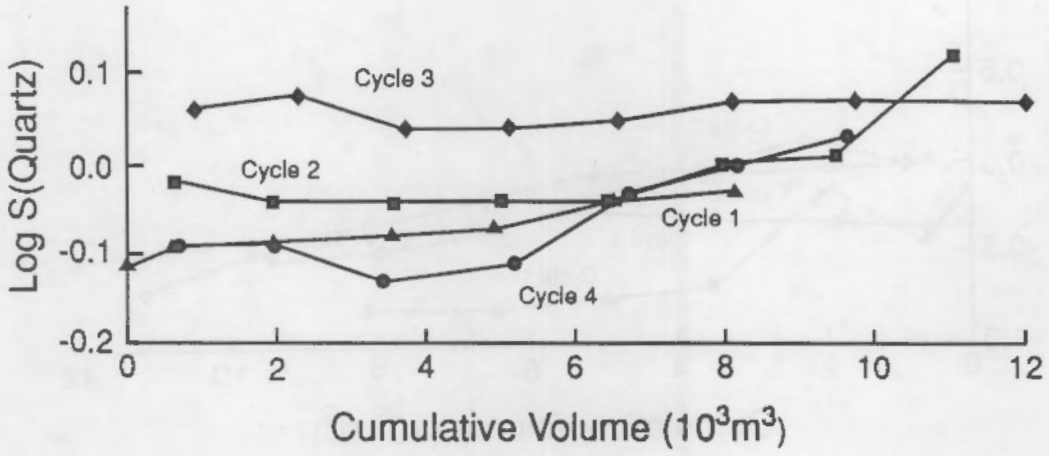

FIGURE 6.34. Quartz Saturation Indexes of Water Recovered During Short-Term Cycles

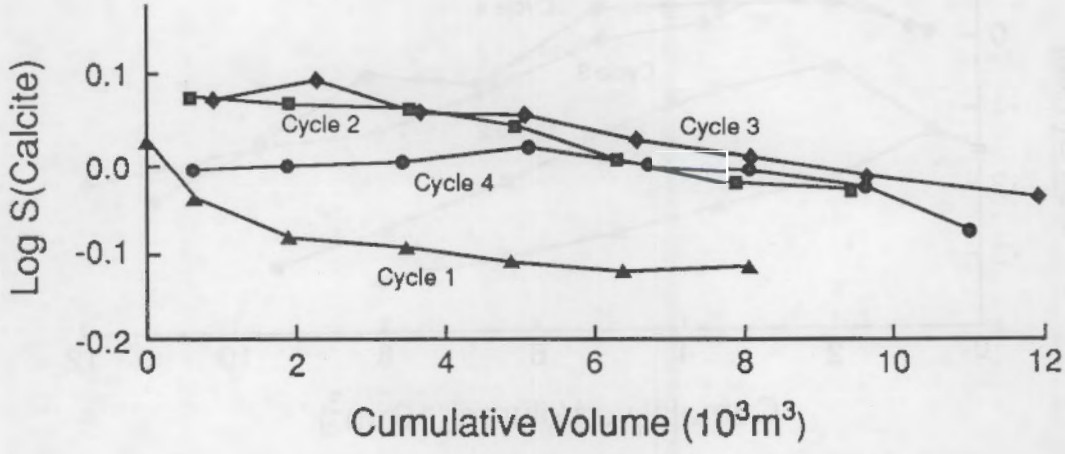

FIGURE 6.35. Calcite Saturation Indexes of Water Recovered During Short-Term Cycles

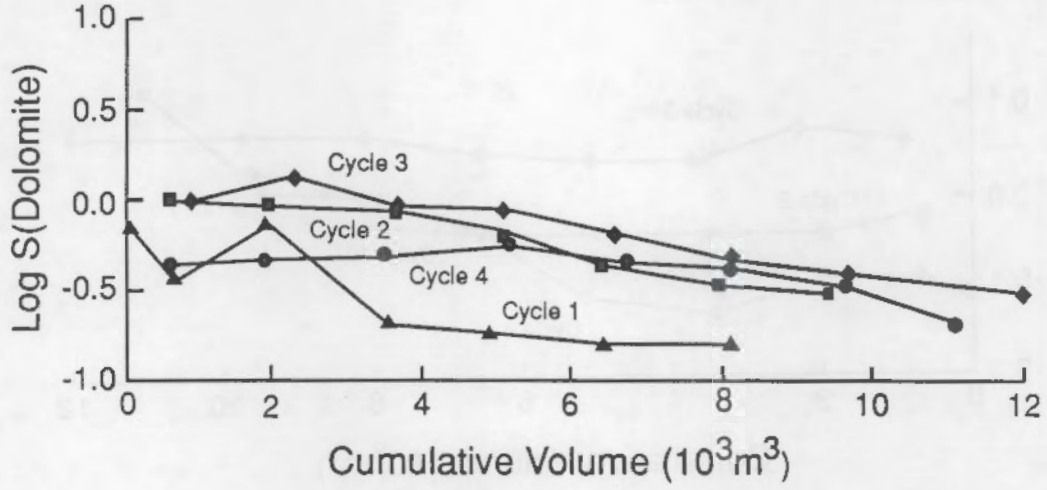

FIGURE 6.36. Dolomite Saturation Indexes of Water Recovered During Short-Term Cycles

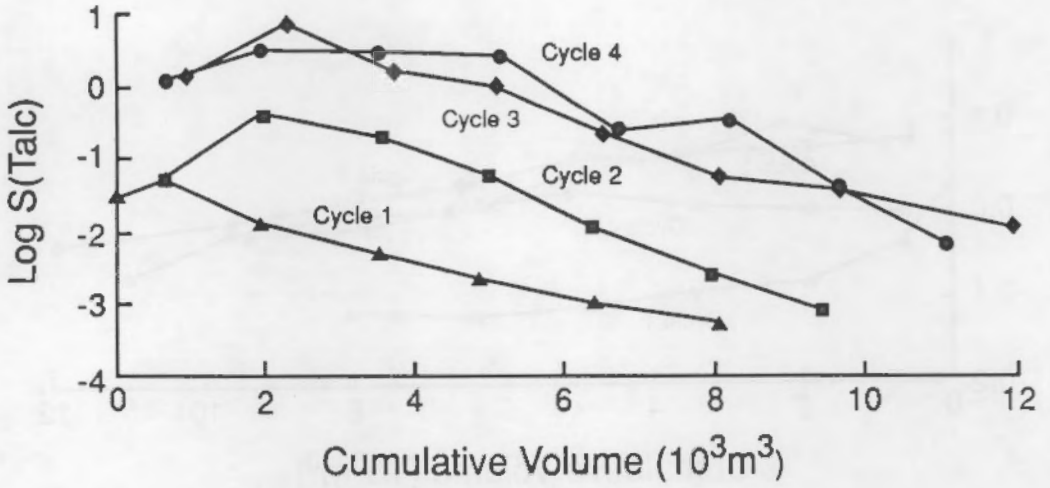

FIGURE 6.37. Talc Saturation Indexes of Water Recovered During Short-Term Cycles

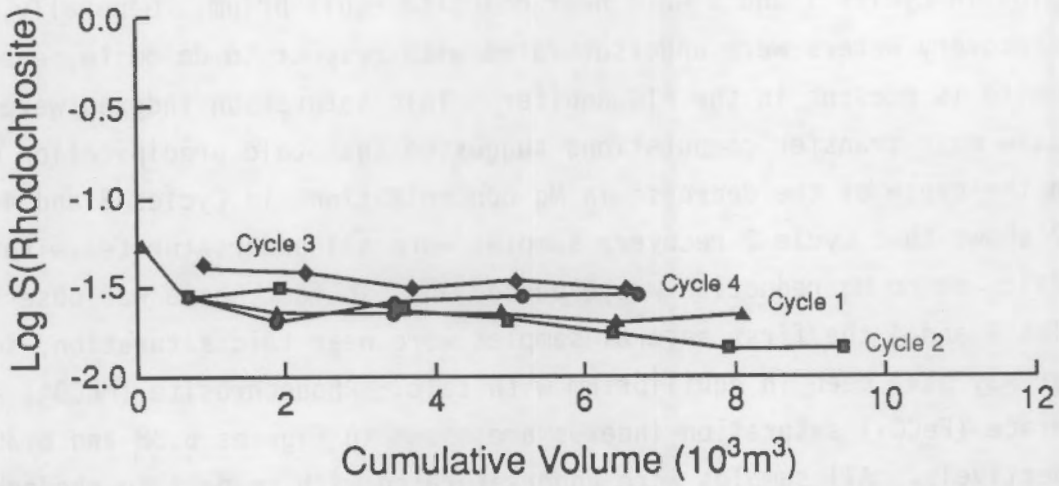

FIGURE 6.38. Rhodochrosite Saturation Indexes of Water Recovered During Short-Term Cycles

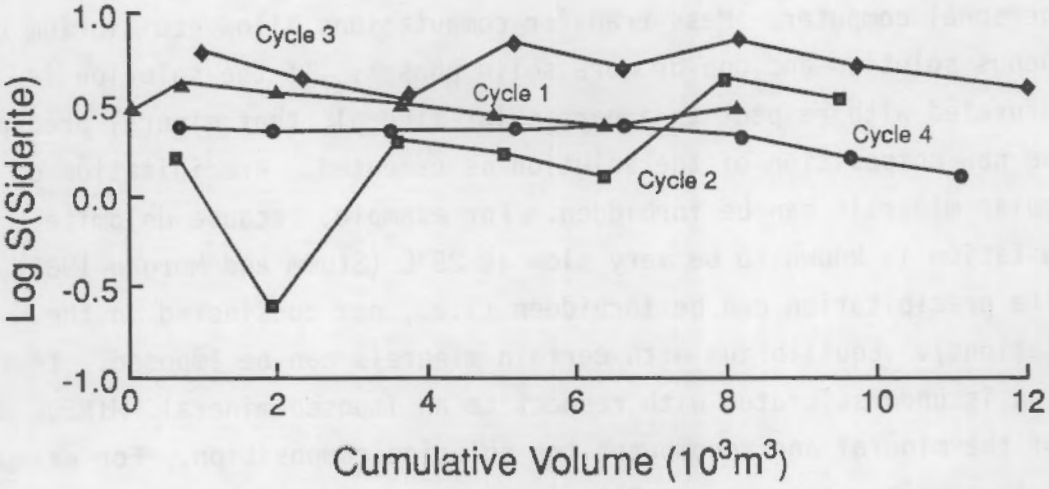

FIGURE 6.39. Siderite Saturation Indexes of Water Recovered During Short-Term Cycles

waters appeared to be near quartz saturation in all cycles. Calcite saturation indexes are shown in Figure 6.35. The recovery waters were near equilibrium with calcite. Figure 6.36 shows dolomite saturation indexes. Early recovery samples in Cycles 1 and 3 were near dolomite equilibrium. Generally, however, the recovery waters were undersaturated with respect to dolomite, even though dolomite is present in the FIG aquifer. Talc saturation indexes were computed because mass transfer computations suggested that talc precipitation may have been the cause of the decrease in Mg concentrations in Cycles 3 and 4. Figure 6.37 shows that Cycle 2 recovery samples were all undersaturated with respect to talc, so no Mg reduction was expected and, in fact, none was observed. In Cycles 3 and 4 the first several samples were near talc saturation, so the water may have been in equilibrium with talc. Rhodochrosite ($MnCO_3$) and siderite ($FeCO_3$) saturation indexes are shown in Figures 6.38 and 6.39, respectively. All samples were undersaturated with respect to rhodochrosite and, with the exception of one sample in Cycle 1, all samples were oversaturated with respect to siderite.

6.4.4 Mass Transfer Computations

Mass transfer equilibrium computations were performed using MINEQL (Westall, Zachary and Morel 1976), which was rewritten in UCSD Pascal to run on a personal computer. Mass transfer computations allow equilibrium between an aqueous solution and one or more solid phases. If the solution is oversaturated with respect to a particular mineral, that mineral precipitates and the new composition of the solution is computed. Precipitation of particular minerals can be forbidden. For example, because dolomite precipitation is known to be very slow at 25°C (Stumm and Morgan 1981), dolomite precipitation can be forbidden (i.e., not considered in the computations). Equilibrium with certain minerals can be imposed. If the solution is undersaturated with respect to an imposed mineral, MINEQL dissolves some of the mineral and recomputes the solution composition. For example, quartz is a major component in FIG sandstone, so equilibrium with quartz can be imposed in a computation. In a chemical equilibrium model this imposition can be justified if the water temperature is high enough and the storage time long enough to attain equilibrium with quartz. Mass transfer computations

were used to model two of the dissolution experiments described earlier and three of the ATES short-term cycles.

The method used to determine temperature and input component concentrations for mass transfer computations and abscissae of computed results is shown in Figure 6.40. Symmetrical flow was assumed, i.e., the first water injected was the last withdrawn. Thus, if injection water sample j was collected when the cumulative injection volume was V_j and the total volume of water injected was V_o, the same water mass would have been recovered at cumulative volume V_o-V_j. The temperature used to compute equilibrium constants was the temperature of recovery water at volume V_o-V_j. The component concentrations used in the computation were taken from analyses of sample j. The computed concentrations were plotted at volume V_o-V_j for comparison with observed concentrations.

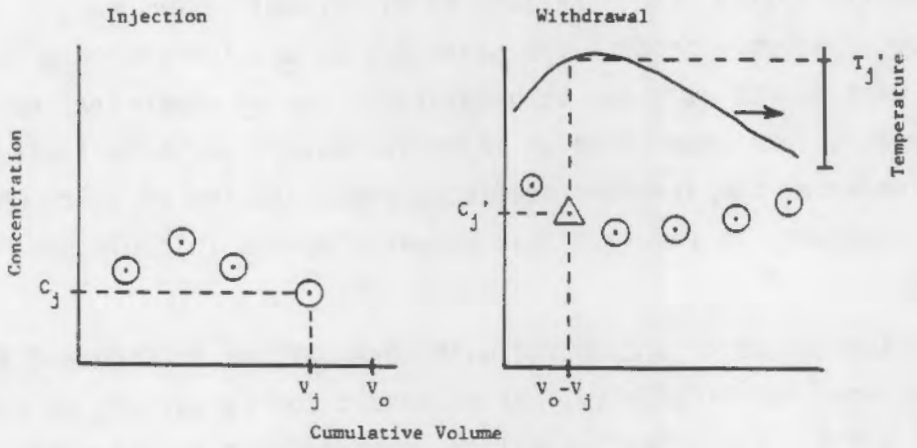

FIGURE 6.40. Method of Assigning Temperatures and Abscissae in Chemical Equilibrium Modeling of the Short-Term ATES Cycles

The chemical equilibrium model of Cycle 2 is compared with observed concentrations in Figure 6.41. The model sandstone contained quartz and calcite, i.e., these minerals were imposed in the computations. Agreement between theory and observation was good for Ca, pH, and alkalinity. The model concentrations were similar to measured concentrations and the trends in concentration change also agreed well. For dissolved silica the patterns of concentration changes in the model computations and observations were similar, but the recovery waters appeared to be oversaturated. The water probably reached equilibrium with quartz at high temperatures after injection. After 3 months of storage, the water cooled somewhat and became oversaturated with respect to quartz dissolution, but not with respect to amorphous silica precipitation. The model did not precipitate Mg and no decrease in Mg was observed.

The model of Cycle 3 is compared with observations in Figure 6.42. As for Cycle 2, predicted Ca and alkalinity concentrations agreed very well with measured values. Silica concentrations in withdrawal waters were undersaturated, probably because the storage time was too short to reach equilibrium with quartz at these temperatures. The Mg concentrations in withdrawal waters were lower than in injection waters and essentially constant. The first five model computations predicted precipitation of talc, which reduced Mg. However, in the last five computed points talc did not precipitate.

The model of Cycle 4 is compared with observations in Figure 6.43. Agreement was good for alkalinity, but agreement for Ca was not as good as for Cycles 2 and 3. For dissolved silica, computations agreed with observations very well. Talc precipitated in all computations, resulting in decreased Mg concentration. As in Cycle 3, the computed reduction in Mg in the first few samples was greater than the observed reduction. Computed pH values agreed with observed values fairly well.

In summary, even though no adjustable fitting parameters were used to optimize agreement between model computations and experimental data, chemical equilibrium computing was reasonably successful at simulating the major ion chemistry of hot-water storage. However, true verification of the model is

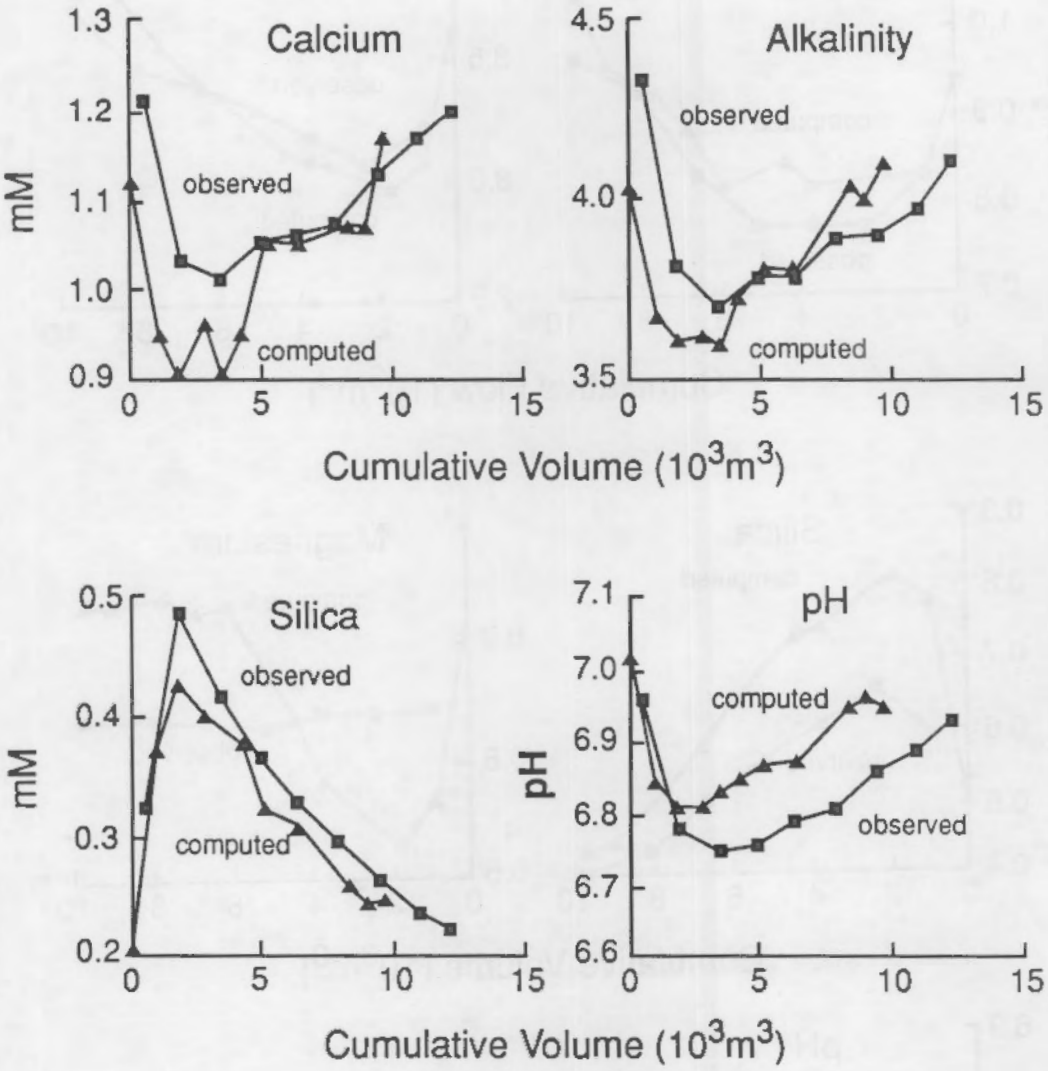

FIGURE 6.41. Comparison of Chemical Equilibrium Model and Observed Concentrations, Short-Term Cycle 2

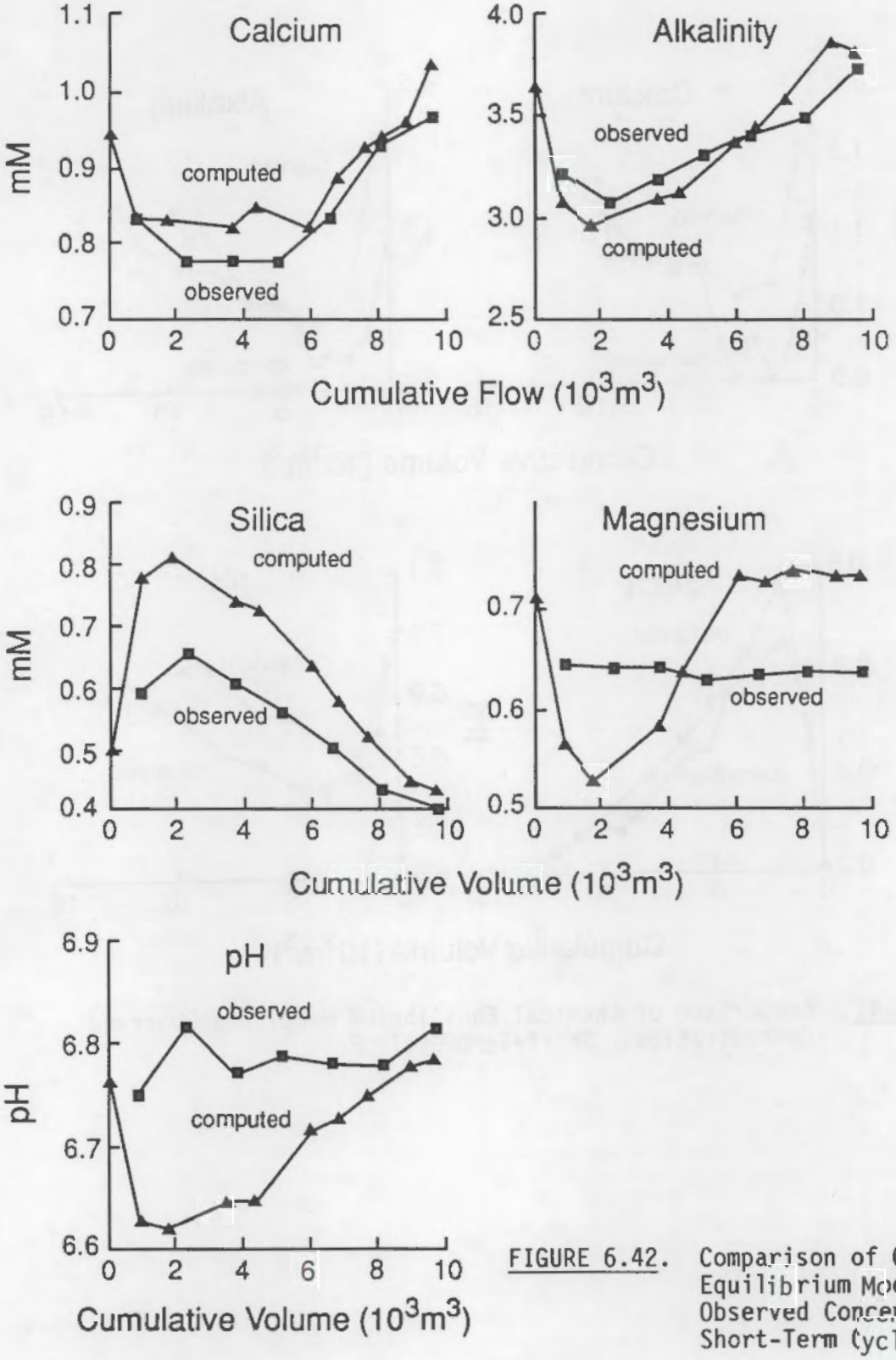

FIGURE 6.42. Comparison of Chemical Equilibrium Model and Observed Concentrations, Short-Term Cycle 3

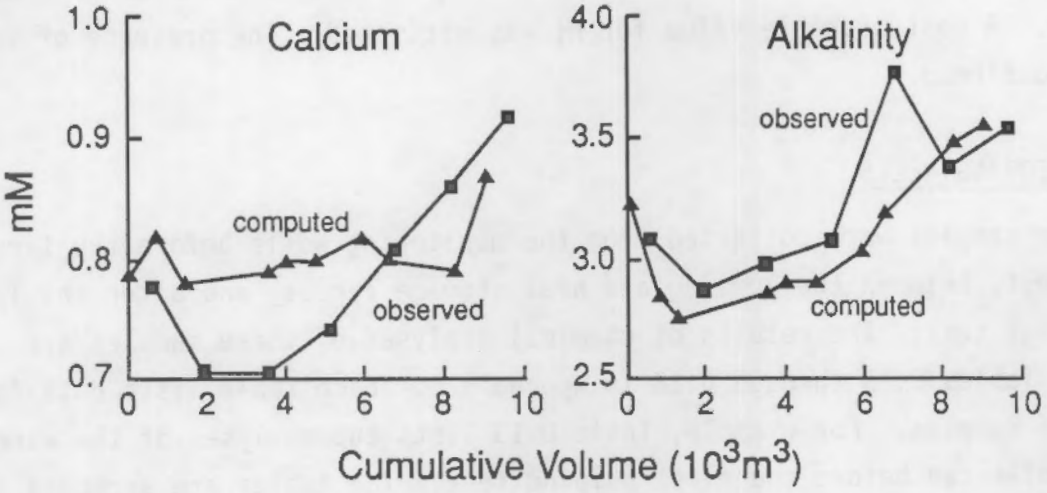

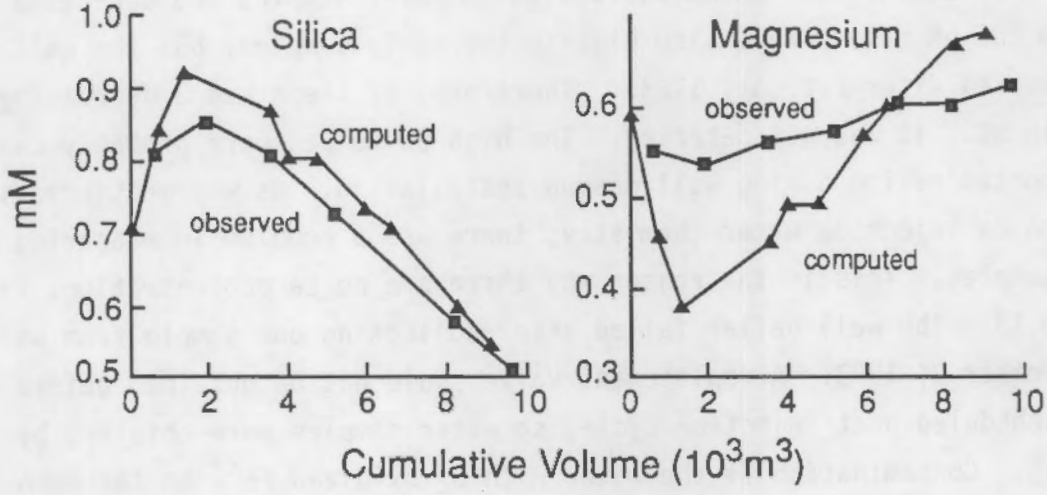

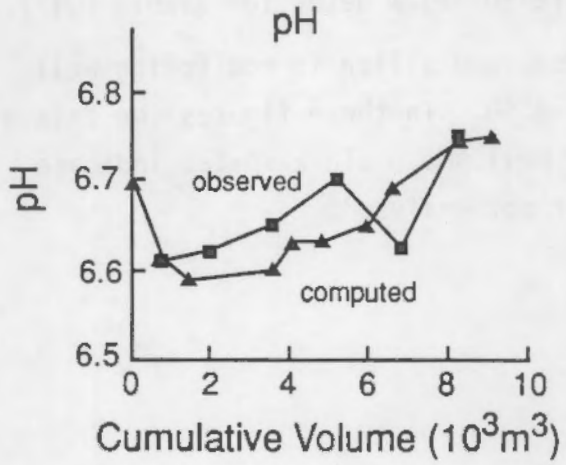

FIGURE 6.43. Comparison of Chemical Equilibrium Model and Observed Concentrations, Short-Term Cycle 4

precluded for the present time by some of the limitations discussed earlier. The actual temperatures in the Franconia and Ironton-Galesville aquifers were not known. A most probable value for H_T was estimated. The presence of talc must be confirmed.

6.5 MONITORING WELLS

Water samples were collected from the monitoring wells before the first pumping test, between the pumping and heat storage cycles, and after the last heat storage test. The results of chemical analyses of these samples are listed in Tables D.13 through D.18 in Appendix D. Each table lists data for one set of samples. For example, Table D.13 lists the analyses of the water samples collected before the first pumping test. The tables are arranged in chronological order of sample sets. The pH values of the AS1 samples, both Jordan and Mt. Simon, were anomalously high in early samples and decreased with time. The BC1 pH values were also high in the early samples, but the well was not sampled after February 1983. Therefore, if there was a decreasing pH trend in BC1, it was not detected. The high pH values were probably caused by grout contamination during well casing installation. As was mentioned in the section on injection water chemistry, there was a problem in measuring Ca in early samples. This is the reason why there are no Ca concentrations listed in Table D.13. The well bailer failed after collecting one sample from well AM2 on November 2, 1983. A replacement valve could not be obtained before the next scheduled heat injection cycle, so water samples were obtained by air lifting. Contamination of the water with O_2 oxidized Fe^{2+} to the much more insoluble Fe^{3+} and reduced soluble Fe to below detection (Table D.17).

The concentration of major ions, iron, and silica in monitoring well waters are shown in Figures 6.44 through 6.50. In these figures the data are grouped by well, e.g. Figure 6.44 is for well AM2. Blank spaces indicate that samples were either not collected or not analyzed.

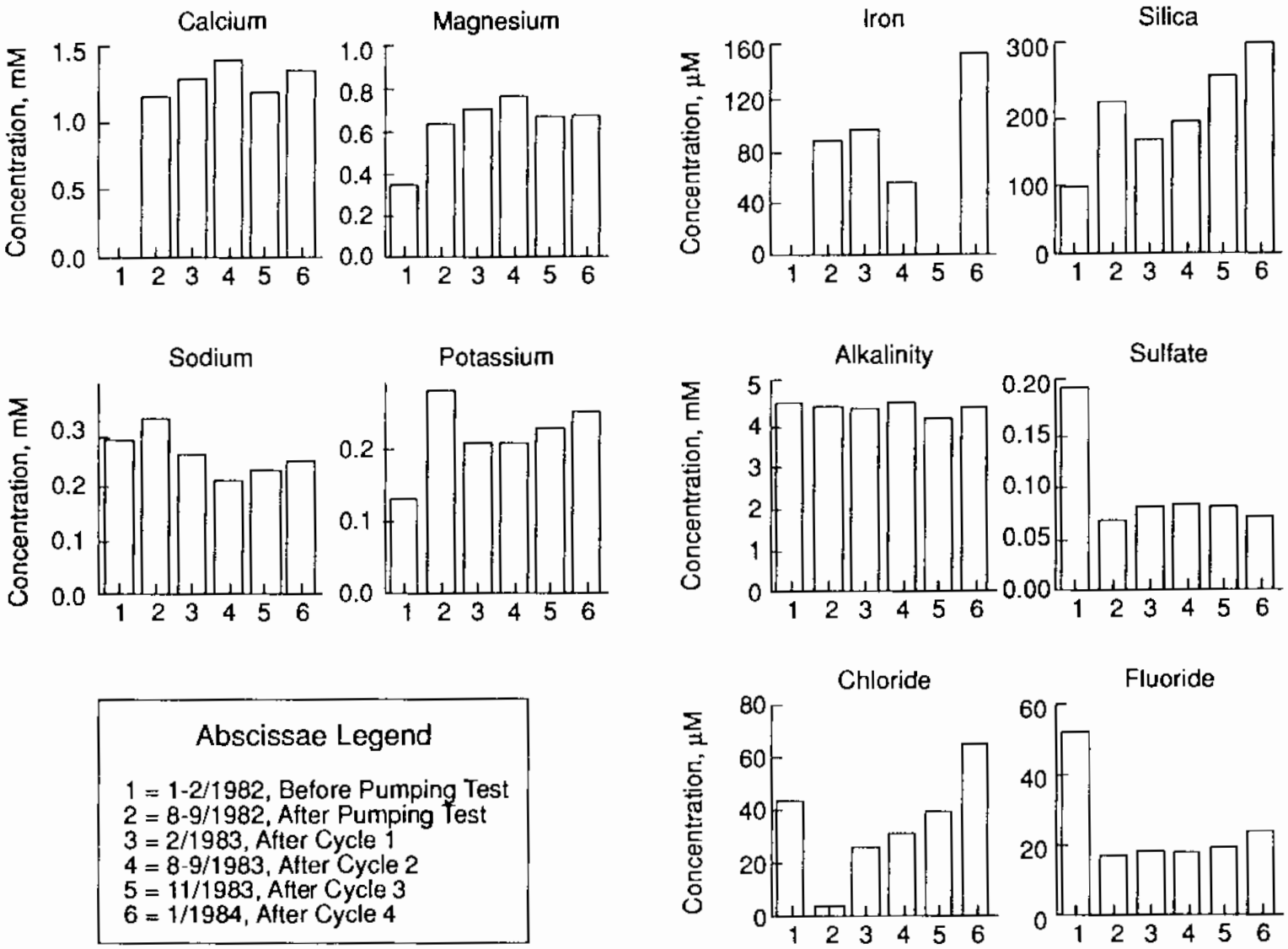

FIGURE 6.44. Chemistry of Water Samples from Well AM2

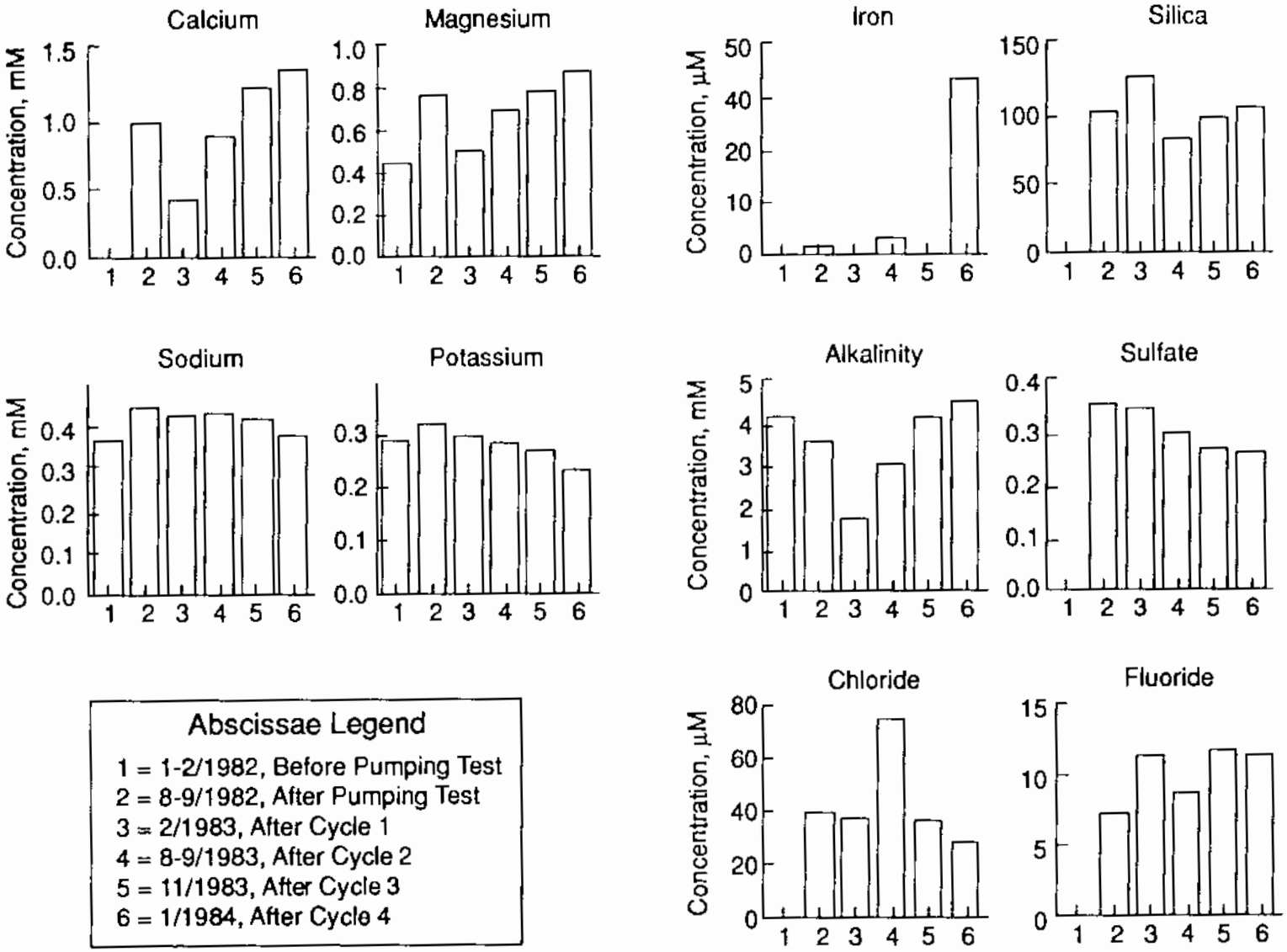

FIGURE 6.45. Chemistry of Water Samples from Well AS1-Jordon

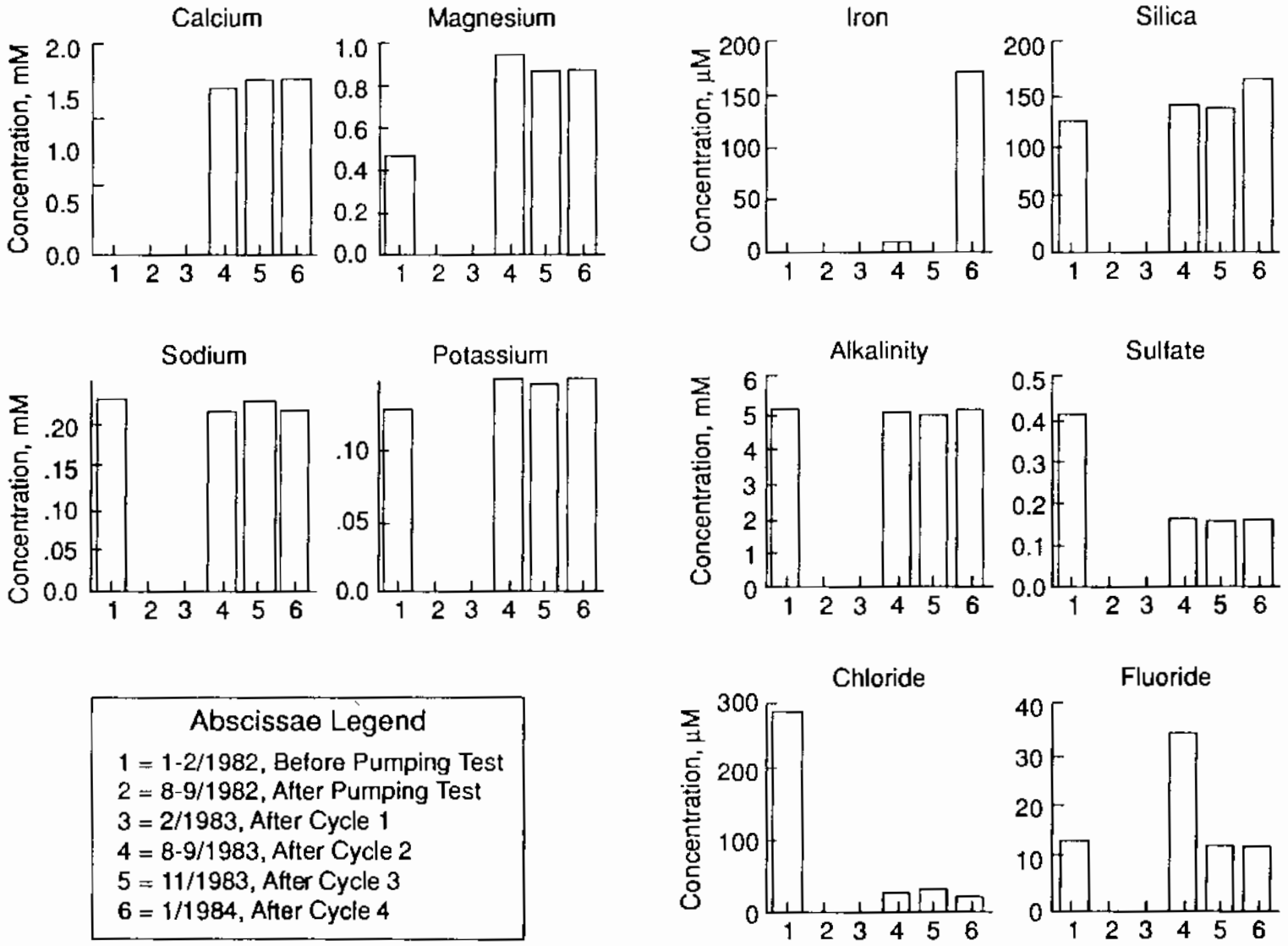

FIGURE 6.46. Chemistry of Water Samples from Well AM1-St. Lawrence

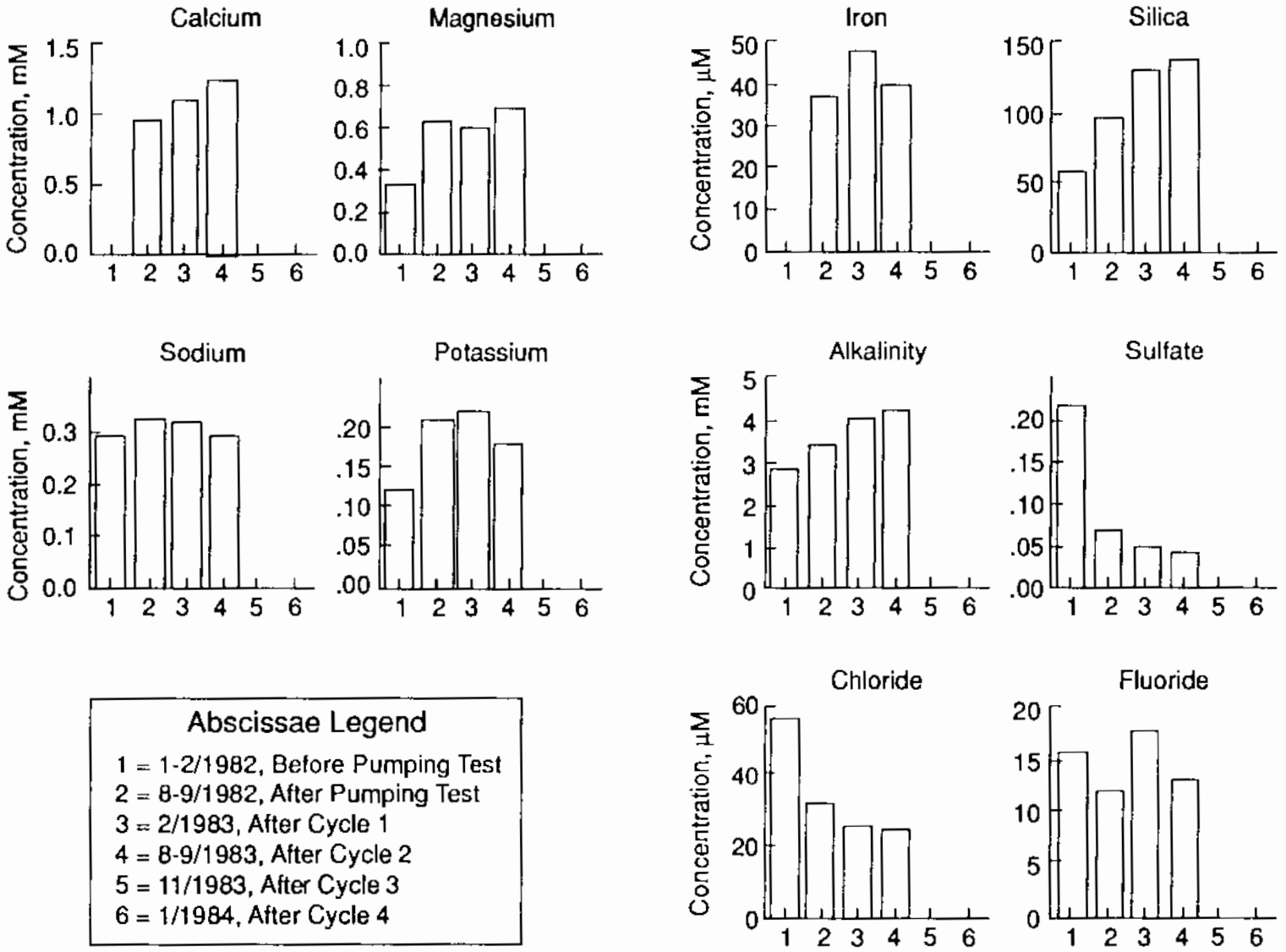

FIGURE 6.47. Chemistry of Water Samples from Well CM1

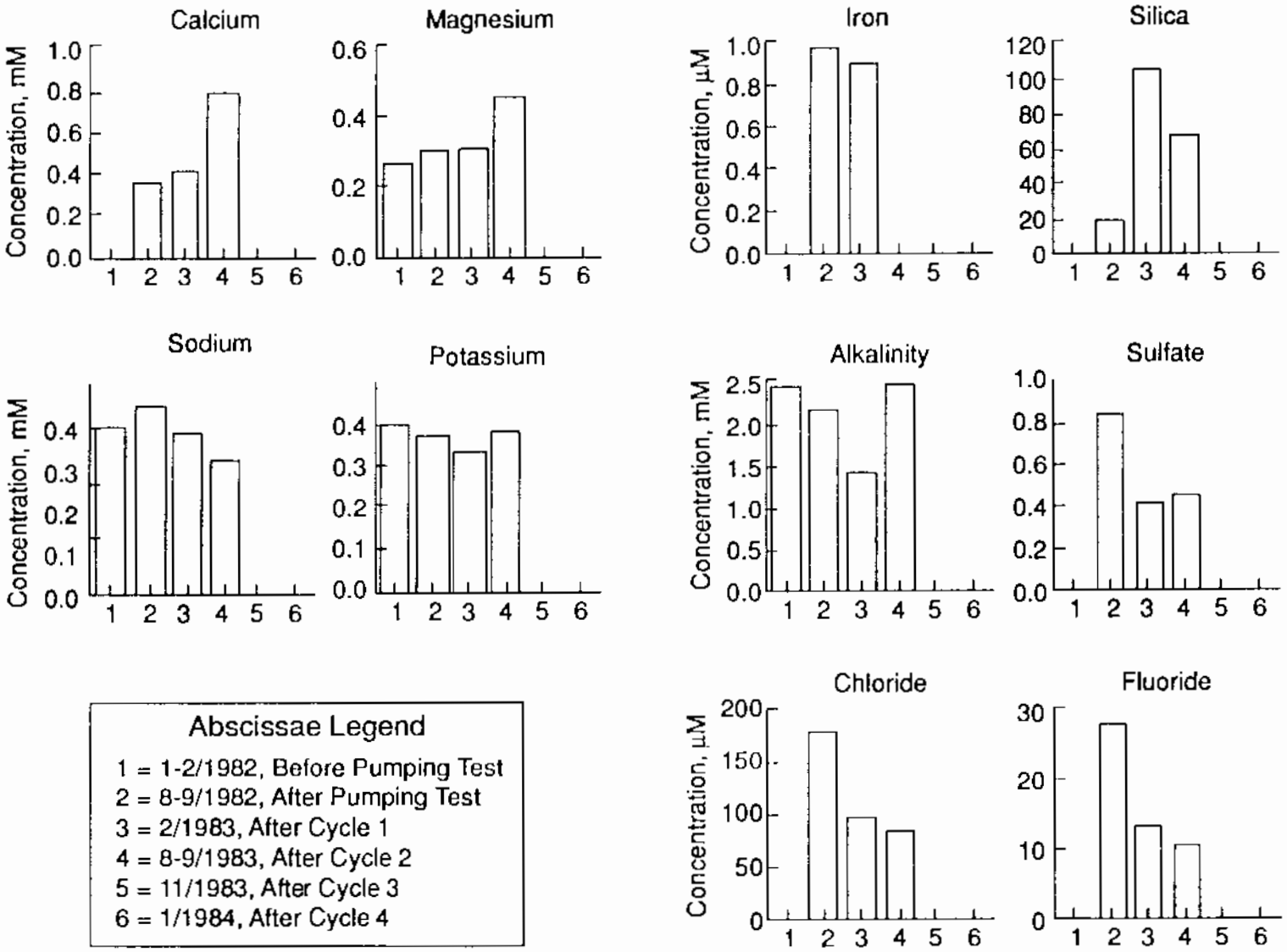

FIGURE 6.48. Chemistry of Water Samples from Well AS1-Mt. Simon

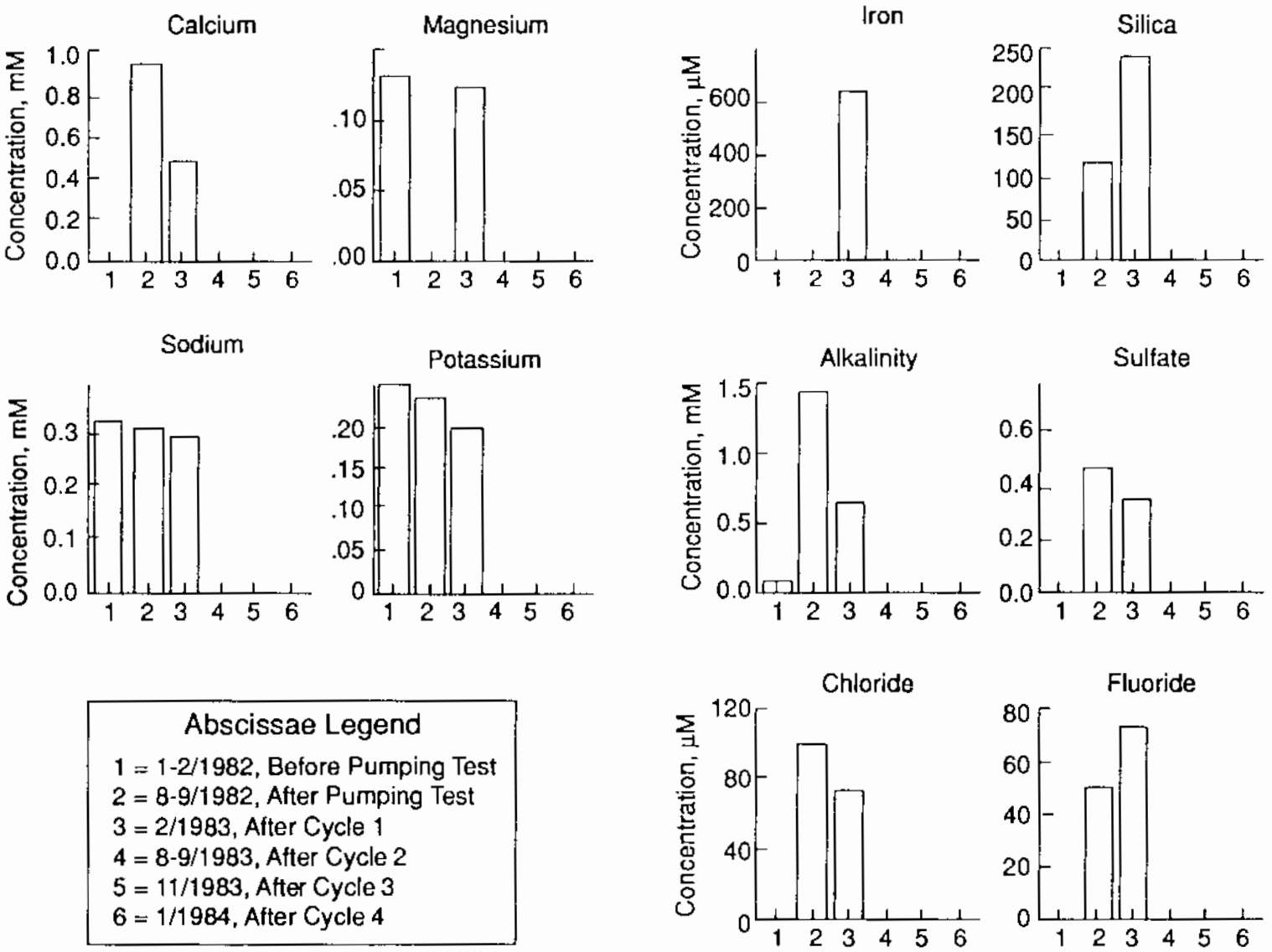

FIGURE 6.49. Chemistry of Water Samples from Well BC1

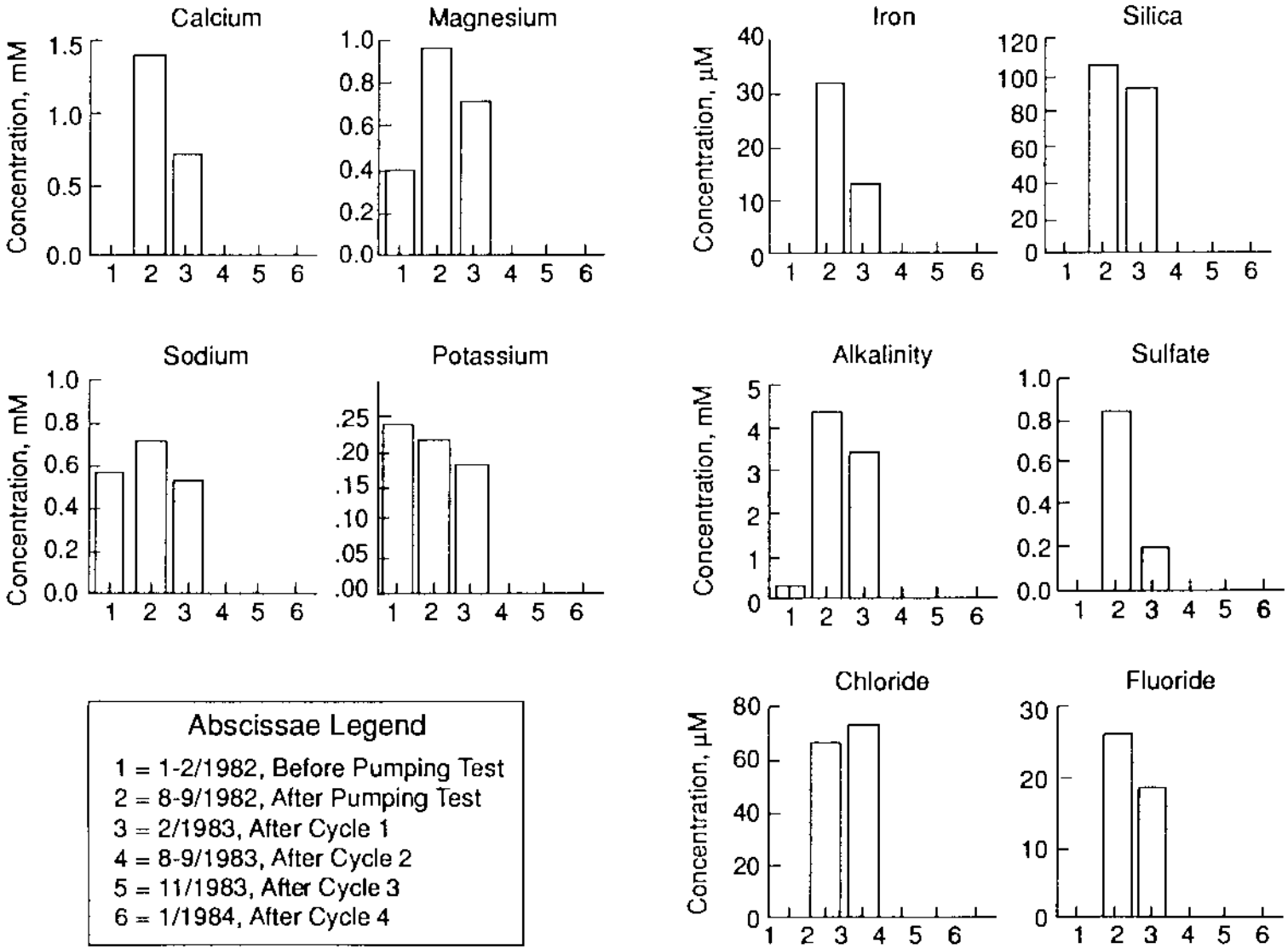

FIGURE 6.50. Chemistry of Water Samples from Well BS1

6.6 SUMMARY

Rock dissolution experiments, water sampling and analysis, and chemical equilibrium modeling of the ground-water chemistry at the University of Minnesota ATES field test facility was an integral part of the work preceding and during the ATES short-term cycles.

A series of laboratory experiments was conducted to measure dissolution rates of aquifer rocks under controlled conditions in a pressure vessel and to apply the rates obtained to calculate rate constants under field conditions. Core samples, ground water from the FIG aquifer, and synthetic ground water were used for the experiments. Rate constants obtained agreed, in general, with Rimstidt and Barnes (1980) results at 150°C. The results also suggested that precipitation of calcium carbonate scale would be the only significant problem during the heat-storage cycles at the FTF; a suggestion that proved to be correct.

Samples of the source, heated, injected, and recovered ground water during the cycles and from the monitoring wells before and after each of the cycles were collected and analyzed. Ambient ground water is near saturation with respect to calcium carbonate. Water chemistry of the FIG ground water in the immediate vicinity of the FTF was changed by the ATES short-term cycles. Most changes that took place were as expected based on equilibrium modeling results of heating water of FIG ground water composition and upon storage in the FIG aquifer.

Equilibrium modeling results for the ionic concentrations in recovery water, using an extended version of MINEQL, was successful in modeling trends for many components, even with the many limitations of both the model and the input data. Temperatures used for equilibrium and modeling calculations were those of the recovered water. These temperatures were a limitation because they were "composite" temperatures. The actual temperatures at the two screened intervals in the storage well were not available.

Calcium carbonate precipitation from the heated ground water was the critical water chemistry problem. Prevention of calcium carbonate scale

accumulation in the storage well was accomplished by installing a precipitator (fixed-bed reactor) in the system piping (see Sections 2.3.2 and 5.2). Calcium carbonate precipitated in the condenser and the precipitator reducing the degree of $CaCO_3$ supersaturation of the injected water to a level that proved to be satisfactory. The condenser and the precipitator each removed approximately the same amount of calcium carbonate from the heated ground water. Calcium carbonate scale did not accumulate in the storage well during the cycles.

Recovered water had a higher total dissolved solid content than the source or the stored water. Calculated saturation indexes for the recovered water indicated that levels were close to saturation for those species calculated for all temperatures. For example, dissolved silica was highest in the hottest water recovered and lowest in the coolest water recovered. Calcium and magnesium were lowest in the hottest water and highest in the coolest water recovered, an expected result, because the calcium and magnesium bicarbonate saturation level is higher at low temperatures. Recovered amounts of calcium, magnesium, sodium, potassium, iron, sulfate, chloride, and dissolved silica were all greater than the amounts introduced during injection. The suggested causes are dissolution of quartz and calcite, ion exchange with feldspars and/or clay minerals, and mixing during the hot water storage. Equilibrium modeling and mass balance calculations support this; however, the apparent absence of calcite in the rock does not support the dissolving of calcite during storage. Ion-exchange of hydrogen for potassium from feldspar and/or clay minerals may be the reason potassium increased during recovery. Mass balances, average solute concentrations and trends modeled, and experimental results are compared. Definitive conclusions are difficult to reach because of the many limitations both of the model and of the field observations. Additional laboratory and field work are required for more definitive conclusions.

Results of monitoring well sampling suggest that:

1. Monitoring wells must be thoroughly flushed following completion to obtain representative samples.

2. Future monitoring wells should be of a larger diameter pipe than the 1-1/4-in. pipes in the monitoring wells installed at the ATES FTF.

3. Following sufficient flushing, consistent and representative samples may be obtained by air-lift flushing (and sampling) and bailer sampling.

4. Trends from the monitoring wells were not clear following the short-term cycles (in part because of insufficient flushing of the wells prior to initial sampling).

7.0 BACTERIOLOGICAL ANALYSES OF WATERS

Bacteriological analysis was conducted on water collected from ATES project wells. The water samples were analyzed for both coliform organisms and total aerobic bacteria in accordance with the Membrane Filtration Technique described in American Public Health Association, American Water Works Association, and Water Pollution Federation (1975).

The coliform determination is used to indicate potential pollution of ground water by animal fecal matter. Coliform counts of 1.0 or more colony-forming units (cfu) per 100 milliliters of water (>1.0 cfu/100 ml) indicate potential pollution. Obviously, higher counts are more indicative than low counts. Counts less than 1.0 cfu/100 ml indicate that the water is not polluted.

The determination of total aerobic bacteria was done to examine the bacteriological profile of the water. This determination cannot be used as an indicator for either pollution or water quality. For instance, very high quality water (i.e., activated carbon-treated deionized distilled water) can support extremely high concentrations (10^6 to 10^7 cfu/ml) of aerobic bacteria. However, the total aerobic bacteria content of well water should be extremely low relative to surface water.

Analysis for coliform organisms showed that the water from all wells sampled was free of these organisms except during the initial flushing stage of wells A and B (Table 7.1). During the initial flushing of wells A and B and the piping system connecting these wells, a low number of coliform were detected (well A - 4 cfu/100 ml, well B - 3 cfu/100 ml). The low number of coliform detected initially and none on subsequent analysis strongly suggest that the coliform isolated were from originally contaminated pipes, pump, etc., used in the system and not from the water sources. In fact, this is so common that it is mandatory to decontaminate potable well water systems (e.g., casing, pumps, pipes) with a chlorine disinfectant solution prior to placing them in operation. The system of wells in the ATES project was extensively flushed but was not decontaminated with a chlorine disinfectant solution.

TABLE 7.1. Coliform Analyses of Water from Various Sources at the Aquifer Thermal Energy Storage Project 1981-1983

Source of Sample	Date	Colony-Forming Units/100 ml
Before test cycles		
Well A	12/09/81	4
Well B	12/09/81	3
Well AM1	02/05/82	<1
Well AS1 (Jordan)	02/08/82	<1
	02/08/82	<1
Well AS1 (Mt. Simon)	02/17/82	<1
Well CM1 (Galesville)	03/11/82	<1
Well A	05/04/82	<1
Well B	05/04/82	<1
Well A	05/17/82	<1
Well B	05/17/82	<1
Well A	09/22/82	<1
Well B	09/22/82	<1
Ouring test cycles		
Well B	11/08/82[a]	<1
	11/16/82[a]	<1
	11/19/82[a]	<1
	11/23/82[a]	<1
Well A	12/16/82	<1
	12/18/82	<1
	12/22/82	<1
Well B	05/04/83[a]	<1
	05/09/83[a]	<1
	05/11/83[a]	<1
	05/12/83[a]	<1
	09/21/83[a]	<1
	11/08/83[a]	<1
	11/18/83[a]	<1

(a) Samples of both unheated and heated water were collected. Results for each were the same.

Total aerobic bacteria content in the various samples was determined at incubation temperatures of 7° and 35°C to determine if the organisms were psychrophilic or mesophilic [i.e., organisms able to multiply at low (7°C) or middle (35°C) temperatures, respectively] (Table 7.2). The vast majority (about 90%) of the organisms isolated were psychrophiles. In addition, they were also found to be gram-negative rods.

The initial source of these organisms, which is unknown, may have been contaminated construction materials. However, once established, many gram-negative bacteria will proliferate in the well water because the water environment is their natural habitat. Such bacteria are very common in well waters. Note that during the hot water injection run (11/8 to 11/23/82) (Tables 7.2 and 7.3) the bacteria content of the cold water from well B was relatively stable at 10^3 cfu/ml even after an extensive volume of water had been pumped through the system.

Results from the four cycles of heated-water injection and withdrawal (Cycles 1 through 4) are tabulated in Table 7.3. Note that in Cycle 4 aerobic bacteria were not recovered in the unheated water sample (11/18/83). The most likely reason for this is that the water from well B was still fairly hot (48°C) during the fourth cycle.

In addition, a sample of the high-calcium limestone particles used in the reactor was collected on 11/8/82 in a sterile container and then analyzed for coliform and total aerobic bacteria. This was done by adding sterile buffer distilled water to the known weight of the rocks and then sampling the water that was added after the mixture (water and rock) had been shaken for 10 minutes. The results showed coliforms at <1 cfu/50 grams of rock, and total count at 100 cfu/50 grams of rock.

TABLE 7.2. Total Aerobic Bacteria Analyses of Water from Various Sources at the Aquifer Thermal Energy Storage Project

Source of Sample	Date	Colony-Forming Units/ml 7°C		35°C
Before test cycles				
Well A	12/09/82	$>3.0 \times 10^2$		1.2×10^1
Well B	12/09/82	$>3.0 \times 10^2$		7.0×10^0
Well AM1	02/05/82	$>3.0 \times 10^2$		9.0×10^1
Well AS1 (Jordan)[a]	02/08/82	3[a]		<1
Well AS1 (Mt. Simon)	02/17/82	1.0×10^2		7.0×10^0
Well CM1 (Galesville)	03/11/82	1.2×10^3		2.5×10^2
Well A	05/04/82	2.6×10^2		3.4×10^1
Well B	05/04/82	2.1×10^2		3.3×10^1
Well A	05/17/82	2.8×10^2		2.8×10^1
Well B	05/17/82	2.0×10^2		1.1×10^1
During test cycles				
Well B	11/08/82	3.4×10^3	U[b]	-
	11/08/82	<1	H[c]	
	11/16/82	2.3×10^3	U	-
	11/16/82	<1	H	
	11/19/82	2.7×10^3	U	-
	11/19/82	<1	H	
	11/23/82	2.5×10^3	U	-
	11/23/82	<1	H	
Well A[d]	12/16/82	<1		<1
	12/18/82	<1		6
	12/22/82	<1		7
Well B	05/04/83	4.1×10^4	U	
	05/11/83	8.2×10^4	U	
	05/11/83	<1	H	
	05/12/83	4.9×10^3	U	
	05/12/83	<1	H	
	09/21/83	4.3×10^4	U	
	09/21/83	<1	H	
	11/18/83	<1	U	
	11/18/83	<1	H	
Well A[d]	12/16/82	<1		<1
	12/18/82	<1		6
	12/22/82	<1		7
	06/17/83	<1		<1
	10/12/83	<1		<1
	12/02/83	<1		<1

(a) Alkalinity was very high; pH = 11; result not meaningful
(b) Unheated water before heater
(c) Heated water after reactors
(d) Heated water being returned to Well B

TABLE 7.3. Results of Bacteriological Analysis of FIG Water Collected During Short-Term ATES Cycles

Date	Type	Unheated	Heated, 195 to 200°F
Cycle 1, Injection			
11/08/82	Coliform	<1 cfu/100 ml	<1 cfu/100 ml
	Total count	3.4×10^3 cfu/ml	<1 cfu/ml
11/16/82	Coliform	<1 cfu/100 ml	<1 cfu/100 ml
	Total count	2.3×10^3 cfu/ml	<1 cfu/ml
11/19/82	Coliform	<1 cfu/100 ml	<1 cfu/100 ml
	Total count	2.7×10^3 cfu/ml	<1 cfu/ml
11/23/82	Coliform	<1 cfu/100 ml	<1 cfu/100 ml
	Total count	2.5×10^3 cfu/ml	<1 cfu/ml
Cycle 1, Recovery			
12/16/82	Coliform	<1 cfu/100 ml	<1 cfu/100 ml
	Total count	<1 cfu/ml	-
12/18/82	Coliform	<1 cfu/100 ml	<1 cfu/100 ml
	Total count	6 cfu/ml	12 cfu/ml
12/22/82	Coliform	<1 cfu/100 ml	<1 cfu/100 ml
	Total count	7 cfu/ml	19 cfu/ml
Cycle 2, Injection			
05/04/83	Coliform	<1 cfu/100 ml	<1 cfu/100 ml
	Total count	4.0×10^4 cfu/ml	<1 cfu/ml
05/09/83	Coliform	<1 cfu/100 ml	<1 cfu/100 ml
	(Sample lost)		
05/11/83	Coliform	<1 cfu/100 ml	<1 cfu/100 ml
	Total count	8.2×10^4 cfu/ml	<1 cfu/ml
05/12/83	Coliform	<1 cfu/100 ml	<1 cfu/100 ml
	Total count	4.9×10^3 cfu/ml	<1 cfu/ml
Cycle 2, Recovery			
06/17/83	Coliform	<1 cfu/100 ml	<1 cfu/100 ml
	Total count	<1 cfu/ml	<1 cfu/ml
Cycle 3, Injection			
09/21/83	Coliform	<1 cfu/100 ml	<1 cfu/100 ml
	Total count	4.3×10^4 cfu/ml	<1 cfu/ml
Cycle 3, Recovery			
10/12/83	Coliform	<1 cfu/100 ml	<1 cfu/100 ml
	Total count	<1 cfu/ml	<1 cfu/ml
Cycle 4, Injection			
11/18/83	Coliform	<1 cfu/100 ml	<1 cfu/100 ml
	Total count	<1 cfu/ml	<1 cfu/ml
Cycle 4, Recovery			
12/2/83	Coliform	<1 cfu/100 ml	<1 cfu/100 ml
	Total count	<1 cfu/ml	<1 cfu/ml

8.0 ENVIRONMENTAL AND INSTITUTIONAL CONSIDERATIONS

As originally planned, the goal of phase I, after completion of aquifer tests and the short-term cycles, was to develop the design for a 20-MW ATES system to be tied into the University of Minnesota Physical Plant heating/cooling system. This goal was abandoned when it became apparent that the 5-MW ATES system as built could not be used at the higher flow rate of 1200 gpm (instead of the 300 gpm) necessary for the larger system. Other factors also weighed against the implementation of a full-scale system to tie into the existing high-pressure or a possible low-pressure steam distribution system on the campus. However, because of the prospect of significant insight to be gained by carrying the program forward, the University continued at the less ambitious scope of a high-temperature field test of the ATES concept in a deep, confined aquifer.

The State of Minnesota has a specific regulation that prohibits the reinjection of waters in aquifers of the state. The purpose of this ordinance is to protect ground water from pollution. The first major obstacle to the project was obtaining a permit that would allow the operation of the injection/recovery wells for the ATES experiments. Agencies involved in the oversight and protection of ground water are the Minnesota Department of Natural Resources (DNR), the Minnesota Pollution Control Agency (MPCA), and the Minnesota Department of Health (MDH). The DNR oversees the water use and withdrawals by a permit and reporting system. The MPCA oversees the discharges and construction within aquifers. The MDH oversees the construction of water wells in the state by reviewing plans for wells, licensing well drillers, and maintaining a reporting system.

Permits from DNR, MPCA, and MDH were required for the ATES project to proceed. The DNR and MDH staffs can take action on permit requests. The MPCA staff can recommend approval or disapproval of a permit or variance request to the MPCA Board, a citizen's board with final authorization responsibilities.

In the course of seeking a variance, several individuals and groups objected to the ATES project, perceiving it to be a serious threat to the environment. Specific charges included that the project would be likely to induce earthquakes because of high injection pressures, and that the project activities would pollute the ground water of the FIG aquifer. These specific charges were made even though: 1) the fluid injection pressures would be much lower than those necessary to induce effects on the rock; 2) the only change in the water imposed by the experiments is temperature; 3) the effects are highly restricted to the immediate vicinity of the site; and 4) the water cycled during ATES experiments is from an aquifer that is not used by others in the vicinity of the site.

A public hearing, a legal action, was required before the proposal could be acted upon by the MPCA Board. In July 1980 the MPCA Board approved the issuance of a permit to conduct the short-term cycles. The initial permit, and an accompanying permit from MDH, was for five (5) short-term cycles, each with no more than eight (8) days of injection and withdrawal (recovery), and an eight (8) to thirty (30) day storage period, subject to experimental plan. The language of the permit issued specifically set a limit of 300°F for the temperature of the injected water and a limit of 300 gpm for the rate of injection. Included in the permit was a specific prohibition of the addition of "water-treatment chemicals". The expiration date of this permit was December 31, 1981.

Delays caused by problems with drilling monitoring wells and the pumping/injection wells, and problems with pressure transducer failures, required an extension to the permits. This extension was granted with an expiration date of December 31, 1982. In 1982 the ATES experiment began; however, as recounted in Section 5, significant problems with the storage well due to failure of lineshaft bearings and carbonate precipitation caused a 4-month delay. Following the rehabilitation of the storage well and the development of the precipitators to reduce calcium carbonate supersaturation in the injected water, the first short-term ATES test cycle was conducted in November and December, 1982.

A request for another extension to the already extended permit was sought from MPCA and MDH. An expiration date of December 31, 1984 was requested (in case further mechanical system delays were encountered) to allow the completion of a total of four planned short-term cycles. In April 1983 the MPCA Board granted an extension with the December 1984 expiration date. No other conditions of the permit were changed.

Monitoring and reporting requirements of the permit were adhered to. All periodic progress reports were sent to MPCA, MDH, and DNR for their review at the time they were submitted to PNL. All data obtained are accessible to appropriate agency personnel upon request at any time. Following Cycle 2, a meeting with representatives of the agencies was held to review the status of the project and the results obtained. Following the conclusion of Cycle 4, another meeting was held with agency representatives to discuss overall project results, the scope of this report, and probable time schedule. The initial version of this report was submitted to the state agencies and PNL in February 1984. A revised draft was submitted in June 1988.

During the course of the project, there have been frequent contacts with agency staff personnel. The staffs have demonstrated a clear commitment to their responsibility to protect the resources of the state and to deal with complex issues in a professional manner. Concerns raised about the project were addressed in a professional manner.

Objections to the project raised by individuals caused significant delay, but the airing of them may have served a useful purpose by establishing clearly exactly what the project's scope and limits are and providing a degree of publicity because of the public permitting process.

9.0 CONCLUSIONS

Aquifer thermal energy storage (ATES) in a deep, confined aquifer is a technically feasible method of storing surplus energy available as sensible heat on a cyclical basis for use at a later time.

Results from short-term cycles using the Franconia-Ironton-Galesville aquifer at the St. Paul Field Test Facility (FTF) reveal that storage of superheated water in a confined aquifer can be done successfully. More than 50% of the energy stored was recovered in the experiments where the storage period was approximately of the same duration as the injection period.

Adequate characterization of the aquifer system must be available to design the well field, anticipate potential problems, plan an appropriate monitoring system, and model energy and mass-flow in any proposed system.

Good regional hydrogeologic information on an aquifer provides a preliminary basis for determining the feasibility of an ATES system. Site-specific studies and test results are necessary to provide the final design constraints imposed by the aquifer. Standard water analyses combined with temperature constraints provide the basis for anticipating chemical problems.

Specific findings and conclusions from the short-term test program include:

1. The FIG aquifer at the ATES site is made up of five hydrologic zones and is areally anisotropic.
2. Isolation of the FIG from overlying and underlying aquifers is satisfactory.
3. Water quality is high, and remains high after testing. Water quality aspects include both dissolved and suspended materials. Monitoring of both is important.
4. Chemical equilibrium of the water-rock system is approached even during short-term storage.

5. Particulates are relatively abundant during construction and initial hydraulic testing and tend to disappear as the system settles into normal operation. The reappearance of particulates may signal some problem or anomaly, as for example, metal particles indicating abnormal wear in pump bearings.

6. Water temperature, and hence the quality of energy recovered declines as length of storage increases.

7. Water treatment to reduce the calcium carbonate precipitation is absolutely essential where the ground water is nearly saturated with respect to calcite. Precipitation systems, such as the one devised for this test program, to reduce supersaturation after heating will protect the wells and aquifer, but will not protect the mechanical systems used to heat the water. Water treatment prior to heating or a "self-cleaning" heat exchanger is required for an efficient operating system.

8. Wells must be designed properly for both water injection and withdrawal and for reliable performance through the full range of water temperature and flow anticipated in the system.

9. Injection systems must be designed so that at all points in the system water pressure exceeds the pressure at which gas bubbles can form.

10. Radial-flow modeling based on preliminary hydraulic test results and test well logging can provide a reasonable approximation of system behavior if the degree of anisotropy of the aquifer system is small.

11. Three-dimensional modeling can provide a very close approximation to system behavior in all cases, but at significantly higher cost.

12. Monitoring wells must be surveyed for deviation to determine where observations are in fact taking place in order to compare observed parameters with actual thermal fronts. Deviation in position of 0.1 m can affect thermal front arrival data by a significant period of time.

13. No obvious environmental effects resulting from hot water injection, storage and withdrawal have been detected at the surface. However, the rock within a few meters of both pumping wells is assumed to have been affected to some degree by mineral dissolution and precipitation in response to changes in water temperature. The effect on the aquifer could not be observed directly, but on the basis of experimental investigations of water chemistry and water-rock interactions, it should be very slight. There has been no change in the hydraulic characteristics of the rock sufficient to cause an appreciable change in well efficiency during the test program.

14. The regional hydraulic gradient at the ATES site is very low; therefore, migration of water from the site must be slow. The water has been shown to reach chemical equilibrium with the rock quickly as it returns to normal ambient temperature. Therefore, any water that migrates from the ATES site is expected to become quickly indistinguishable from resident ground water.

Major physical and systems problems encountered during the course of the project include:

1. Well drilling and well construction encountered the normal problems associated with drilling in weak, friable sandstone and jointed, broken dolomite. These problems caused delays of 5 months.

2. Reliable pressure transducers to withstand the specified range of pressure and temperature in the downhole environment could not be found, contrary to the claims of suppliers. After repeated failures, and failure to meet delivery schedules, manual measurements were considered the reliable alternative for water level measurements in monitoring wells. This problem caused delays of more than 12 months and cost a considerable amount.

3. Failures also were encountered in trying to install strings of thermocouples in open holes while piezometers were being installed. Installation inside small diameter pipe casings proved effective and allowed removal or replacement of the thermocouple strings.

4. Rapid clogging in the aquifer occurred when air bubbles were allowed to form in the descending water column in the injection well. Adequate backpressure is needed at all times in the injection well.

5. Synthetic rubber lineshaft bearings quickly failed when the water approached the specified injection temperature, although the bearings were rated for appreciably higher temperature. Bronze and bronze-graphite bearings were used successfully as replacements.

6. Precipitation of calcium carbonate when normal ground water was heated and became supersaturated with calcium carbonate was the biggest problem, and a recurrent theme in this report. Precipitation occurred in the heat exchanger and at all points downstream in the injection system. Interposing a precipitator between the heat exchanger and the injection well adequately protected the well and the aquifer, but did nothing to control precipitation in the heat exchanger, necessitating frequent interruptions in the injection phase of each test cycle to clean the heat exchanger and recharge the precipitator. Control of water chemistry by effective water treatment before heating is essential to a practical ATES system.

Environmental protection regulations have a direct impact upon ATES systems. ATES systems must be operated in compliance with existing environmental protection regulations dealing with ground water. Several state agencies are charged with various aspects of the protection and use of ground water in Minnesota. Because ATES is a new concept, and entails pumping, heating, and reinjecting appreciable quantities of ground water, the project underwent close scrutiny by the state agencies. A permit for the proposed use was required from the Department of Natural Resources, and because state law specifically forbids unauthorized reinjection of ground water into subsurface aquifers, a variance was required from the Minnesota Pollution Control Agency and the Minnesota Department of Health. Compliance with state regulations for the construction of water wells was also monitored by the Minnesota Department of Health. The variance and permits were granted with strict requirements

for monitoring and reporting all aspects of the project, and with the stipulation that no chemical additives be used for treatment of the water.

The zealous scrutinizing of this innovative project by the responsible state agencies was expected and appropriate. Excellent communication and rapport was established and has continued with the agencies. Opposition to the project came from several organizations and individuals on the grounds that the project posed an unacceptable threat to ground water resources and the environment. The opposition led to formal hearings on the variance application, which entailed a significant delay.

ATES is a non-consumptive and environmentally benign use of a limited volume of ground water to capture energy that is now being wasted. ATES in effect substitutes non-polluting and renewable or wasted energy for energy from nuclear or fossil fuels. It is hoped that as the development of ATES continues and its benefits and environmentally benign character are demonstrated, public understanding will grow and ATES will be seen, as it is seen in many advanced countries in the world, as a potentially significant contribution to energy conservation and reduction in pollution from fossil and nuclear fuels.

Economic feasibility was not a part of this study. Much of the cost incurred in developmental programs is not directly comparable to costs in a developed system under routine operation. Moreover the test program has dealt only with the heat input and output side of the economic equation in a series of short-term test cycles. It has not dealt at all with the heat delivery and use side under full seasonal operating constraints. Nevertheless this test program is a major step in visualizing the design, construction, and operation of a full seasonal ATES system and suggests some comments on economic and social questions and the additional work needed to answer them.

1. Cost of energy input: Our results indicate that at least 50% but probably not much more than 60% of the heat input in an ATES system can be recovered at useful temperatures for heating. This means that ATES systems, except for certain peak load situations, can be justified only

where an essentially "free" source of thermal energy that would otherwise be wasted can be captured. Solar energy, rejected heat from power and industrial plants, and trash burning plants are potential sources. The cost of energy from these sources is related to the marginal capital and operating cost of the systems needed to capture it. Since the heat is "free," the relatively low efficiency of an ATES system is not important, once the investment has been made.

2. Operating cost: ATES systems can and should be largely automated. The main operating costs are monitoring, maintenance, and energy for pumping. Pumping cost is very small in relation to the amount of energy stored in an ATES system. Monitoring and maintenance should be comparable to these costs in other large automated heating systems.

3. Capital cost: The major cost item in an ATES system is the construction of at least two large capacity pumping wells. Depending on the depth to the aquifer and the character of the geology, the wells are likely to cost $100,000 to $500,000 each. The other large items are the heat exchanger, piping, and the water treatment system. Heat exchangers, piping, and water piping treatment costs are easily established by standard engineering practice.

4. Depreciation: As yet there is very little basis for estimating the operating life of an ATES system. The primary concern is the life of the wells. There was no appreciable loss of well efficiency during the short-term test program. Ordinary, properly constructed high capacity water wells last for decades without need for overhaul, but the added effects of seasonal heating cycles on long-term well life is not known. Long-term test data are needed before useful projections can be made.

10.0 REFERENCES

Aagaard, P., and H.C. Helgeson, 1982, Thermodynamic and kinetic constraints on reaction rates among minerals and aqueous solutions. I. Theoretical considerations: American Journal of Science, 282(3):237-285.

Allen, R.D., 1983, Relationship of regional water quality to aquifer thermal energy storage. PNL-4929, Pacific Northwest Laboratory, Richland, Washington.

American Public Health Association, American Water Works Association, and Water Pollution Federation, 1975, Standard methods for the examination of water and wastewater, 14th ed.

Anonymous, 1982, Handbook for sampling and sample preservation of water and wastewater: U.S. Environmental Protection Agency, EPA-60D/4-82-D29.

Austin, G.S., 1969, Paleozoic lithostratigraphic nomenclature for southeastern Minnesota. Minnesota Geological Survey Information Circular 6, 11 p.

Ball, J.W., D.K. Nordstrom, and E.A. Jenne, 1980, Additional and revised thermochemical data and computer code for WATEQ2 -- A computerized chemical model for trace and major element speciation and mineral equilibria of natural waters: U.S. Geological Survey Water Resources Investigations, WRI 78-116.

Bradley, D.J., and K.S. Pitzer, 1979, Thermodynamics of electrolytes, 12, Dielectric properties of water and Debye-Huckel parameters to 350°C and 1 kbar: Journal of Physical Chemistry, 83:1599-1603.

Bredehoeft, J.O., and I.S. Papadopolus, 1965, Rates of vertical ground-water movement estimated from the earth's thermal profile: Water Resources Research, 1(2):325-328.

Freeze, A., and Cherry, J., 1979, Groundwater. Prentice Hall, New York, p. 604.

Frolov, N.M., 1976, Gidrogeotermiya [Hydrogeothermy]. Moscow, Nedra, 280 p.

Gibb, J.P., R.M. Schuller, and R.A. Griffin, 1981, Procedures for the collection of representative water quality data from monitoring wells: Cooperative Groundwater Report 7, Illinois State Water Survey, 61 p.

Gilbert, T.W., T.D. Behymer, and H.B. Casteneda, 1982, Determination of dissolved oxygen in natural and waste waters: American Laboratory, 14:119.

Gussein-Zade, M.A., 1961, Nekotorye voprosy ucheta pronitsaemosti krovli i podoshvy plasta [Some problems in consideration of permeability of the top and bottom of a layer] Trudy MNI im Gubkina, Vyp. 33, Moscow, Gostoptehizadat, 1961.

Helgeson, H.C, 1967, Thermodynamics of complex dissociation in aqueous solution at elevated temperatures: Journal of Physical Chemistry, 10:3121-3136.

Helgeson, H.C, 1969, Thermodynamics of hydrothermal systems at elevated temperatures and pressures: American Journal of Science, 267:729-804.

Helgeson, H.C., J.M. Delany, H.W. Nesbitt, and D.K. Bird, 1978, Summary and critique of the thermodynamic properties of rock-forming minerals: American Journal of Science, 278-A:1-229.

Hoffmann, M.R, 1981, Thermodynamic, kinetic, and extrathermodynamic considerations in the development of equilibrium models for aquatic systems: Environmental Science and Technology, 15:345-353.

Holdren, G.C., and R.A. Berner, 1979, Mechanism of feldspar weathering. I. Experimental studies: Geochimica et Cosmochimica Acta, 43:1161-1171.

Holm, T.R., S.J. Eisenreich, H.L. Rosenberg, and N.P. Holm, 1987. Groundwater geochemistry of short-term aquifer thermal energy storage test cycles: Water Resources Research, v. 23.

Horn, M.A., 1983, Ground-water-use trends in the Twin Cities Metropolitan area, Minnesota, 1880-1980: U.S. Geological Survey Water Resources Investigations 83-4033, 37 p.

Jenne, E.A, 1981, Geochemical modeling: A review. PNL-3574, Pacific Northwest Laboratory, Richland, Washington.

Kanivetsky, R., and M. Walton, 1979, Hydrogeologic map of Minnesota, bedrock hydrogeology -- a discussion to accompany State Map Series S-2: Minnesota Geological Survey, 11 p.

Kovalevsky, V.S., 1968, Metodicheskoe rukovodstvo po izutseniyu regima podzemnykh vod v raionakh vodozaborov [Methodical manual to study groundwater regime in areas of groundwater development]: Moscow, VSEGINGEO, Ministry of Geology, USSR, 197 p.

Lagache, M, 1976, New data on the kinetics of the dissolution of alkali feldspars at 200°C in CO_2 charged water: Geochimica et Cosmochimica Acta, 40:157-162.

Laitinen, H.A., 1960, Chemical Analysis. McGraw-Hill, New York, 611 p.

Madsen, E.L., and R.F. Norvitch, 1979, Hydraulic properties and tunneling constraints, plate 7 of Norvitch, R. F., and M. Walton, eds., Geologic and hydrologic aspects of tunneling in the Twin Cities area, Minnesota: U.S. Geological Survey Miscellaneous Investigations Series I-1157.

Miller, R.T., 1984, Anisotropy in the Ironton and Galesville Sandstones near a thermal-energy-storage well, St. Paul, Minnesota: Ground Water, v. 22, p. 532-537.

Miller, R.T., 1985, Preliminary modeling of an aquifer thermal-energy storage system: in Subitzky, S. ed., Selected Papers in the Hydrologic Sciences, U.S. Geological Survey Water-Supply Paper 2270, p. 1-19.

Miller, R.T., 1989, Cyclic injection, storage, and withdrawal of heated water in a sandstone aquifer at St. Paul, Minnesota: Field observations, preliminary model analysis, and aquifer thermal efficiency: U.S. Geological Survey Open-File Report 89-261, 100 p.

Miller, R.T., and C.I. Voss, 1986, Finite-difference grid for a doublet well in an anisotropic aquifer: Ground Water, v. 24, p. 490-496.

Molz, F.J., A.D. Parr, P.F. Andersen, and V.D. Lucido, 1979, Thermal energy storage in the confined aquifer: Experimental results: Water Resources Research, 15(6):1509-1514.

Morgan, J.J., 1967, Applications and limitations of thermodynamics in water systems: in ACS Advances in Chemistry Series 67, Wastumm (ed.), Equilibrium concepts in natural water systems. American Chemical Society, Washington, D.C., p. 1-29.

Mossler, J.H., 1972, Paleozoic structure and stratigraphy of the Twin Cities region: in Sims, P.K. and Morey, G.B., eds., Geology of Minnesota: A centennial volume: Minnesota Geological Survey, St. Paul, p. 485-497.

Mossler, J.H., 1983, Paleozoic lithostratigraphy of southeastern Minnesota: Minnesota Geological Survey Miscellaneous Map Series M-51, 8 plates.

Neuman, S.P. and P.A. Witherspoon, 1972, Field determination of the hydraulic properties of leaky multiple aquifer systems: Water Resources Research, 8(5):1284-1298.

Nordstrom, D.K., L.N. Plummer, T.M.L. Wigley, T.J. Wolery, J.W. Ball, E.A. Jenne, R.L. Bassett, D.A. Crerar, T.M. Florence, B. Fritz, M. Hoffmann, G.R. Holdren, Jr., G.M. Lafon, S.V. Mattigod, R.E. McDuff, F. Morel, M.M. Reddy, G. Sposito, and J. Thrailkill, 1979, A comparison of computerized chemical models for equilibrium calculations in aqueous systems: in ACS Symposium Series 93, E.A. Jenne (ed.), Chemical modeling in aqueous systems. American Chemical Society, Washington, D.C., p. 857-894.

Norvitch, R.F., T.G. Ross, and A. Brietkrietz, 1973, Water resources outlook for the Minneapolis-St. Paul metropolitan area, Minnesota: Metropolitan Council of the Twin Cities Area, 219 p.

Odom, I.E., 1975, Feldspar-grain size relations in Cambrian arenites, Upper Mississippi Valley: Journal of Sedimentary Petrology, v. 45, p. 636-650.

Odom, I.E., 1976, Microstructure, mineralogy, and chemistry of Cambrian glauconite pellets and glauconite, central U.S.A.: Clays and Clay Minerals, v. 24, p. 232-238.

Parker, C.R, 1972, Water analysis by atomic absorption spectroscopy. Varian Techtron, Ltd., Springvale, Australia, 78 p.

Plougina, T.A., 1979, Opredelenie skorosti peretekaniya po gidrokhi-micheskim danym [Determination of vertical leakage from hydrochemical data]: Methods for evaluation of ground-water resources, NAUKA Moscow, p. 213-216.

Plummer, L.N., B.F. Jones, and A.H. Truesdell, 1976, WATEQF - A FORTRAN IV version of WATEQ, a computer program for calculating chemical equilibria of natural waters: U.S. Geological Survey Water Resources Investigations WRI 76-13.

Plummer, L.N., D.L. Parkhurst, and T.M.L. Wigley, 1979, Critical review of the kinetics of calcite dissolution and precipitation: in ACS Symposium Series 93, E.A. Jenne (ed.), Chemical modeling in aqueous systems. American Chemical Society, Washington, D.C., p. 537-576.

Rimstidt, J.D., and H.L. Barnes, 1980, The kinetics of silica-water reactions: Geochimica et Cosmochimica Acta, 44:1683-1699.

Ruhl, J.F., R.J. Wolf, and D.G. Adolphson, 1982, Hydrogeologic and water-quality characteristics of the Ironton-Galesville aquifer, southeast Minnesota: U.S. Geological Survey Water Resources Investigations WRI 82-4080.

Sibley, O.F., 1982, The origin of common dolomite fabrics: clues from the Pliocene: Journal of Sedimentary Petrology, v. 52, p. 1087-1100.

Siebert, R.M., and P.B. Hostetler, 1977a, The stability of the magnesium bicarbonate ion pair from 1D° to 90°C: American Journal of Science 277(6):697-715.

Siebert, R.M., and P.B. Hostetler, 1977b, The stability of the magnesium carbonate ion pair from 10° to 90°C: American Journal of Science, 277(6):716-734.

Slavin, W., G.R. Carnrick, and D.C. Manning, 1982, Magnesium nitrate as a matrix modifier in the stabilized temperature platform furnace: Analytical Chemistry, 54:621-624.

Sosman, R.B, 1965, The phases of silica. Rutgers University Press, New Brunswick, New Jersey.

Steinhilber, W.L., and H.L. Young, 1979, Plan of study for Northern Midwest Regional aquifer system analysis: U.S. Geological Survey Water Resources Investigations 79-44, 20 p.

Strickland, J.D.H., and T.R. Parsons, 1972, A practical handbook of seawater analysis: Fisheries Research Board of Canada Bulletin 167, 2nd ed., 31D p.

Stumm, W., and J.J. Morgan, 1981, Aquatic chemistry, 2nd ed. Wiley-Interscience, New York, 780 p.

Treybal, R.E., 1980, Mass transfer operations. McGraw-Hill, New York, 784 p.

Truesdell, A.H., and B.F. Jones, 1974, WATEQ, a computer program for calculating chemical equilibria of natural waters: Journal of Research, U.S. Geological Survey, 2:233-248.

Walton, M., 1981, The Aquifer Thermal Energy Storage (ATES) program, University of Minnesota: in Proceedings of International Conference on Seasonal Thermal Energy Storage, Oct. 19-21, 1981, Seattle, Washington, p. 133-140.

Walton, M., and M.C. Hoyer, 1984, University of Minnesota Aquifer Thermal Energy Storage field test facility: Seasonal Thermal Energy Storage Newsletter, 6(2):2-4, Earth Science Laboratory, Lawrence Berkeley Laboratory, Berkeley, California.

Weast, R.C., and M.J. Astle, 1979, Handbook of chemistry and physics. CRC Press, Inc.

Westall, J.C., J.L. Zachary, and F.M.M. Morel, 1976, MINEQL: A computer program for the calculation of chemical equilibrium composition of aqueous systems. Technical Note 18, Department of Civil Engineering, R.M. Parsons Water Quality Laboratory, M.I.T., Cambridge, Massachusetts, 91 p.

White, A.F., and H.C. Claassen, 1979, Dissolution kinetics of silicate rocks - application to solute modeling: in ACS Symposium Series 93, E.A. Jenne (ed.), Chemical modeling in aqueous systems. American Chemical Society, Washington, D.C., p. 446-473.

Zenger, D.H., J.B. Dunham, and R.L. Ethington, 1980, Concepts and models of dolomitization. Society of Economic Paleontologists and Mineralogists Special Publication 28, 320 p.

APPENDIX A

ATES SYSTEM
ENGINEERING DESIGN AND CONSTRUCTION

APPENDIX A

ATES SYSTEM
ENGINEERING DESIGN AND CONSTRUCTION

A.1 SYSTEM CONCEPT

Aquifer thermal energy storage (ATES) refers to the storage of thermal energy in an aquifer. In its simplest form the ATES Project is composed of a pair of water wells (well doublet) drilled into an aquifer, piped to a series of heat exchangers and a source of heat (either waste or process).

During operation of an ATES system using a well doublet, the ground water is withdrawn from one well, heated in a heat exchanger, and then returned to the same aquifer through the second well some distance away. The distance between the wells prevents any aquifer interfacing of the withdrawal and injection waters, which are at significantly different temperatures. The thermal energy is stored in the aquifer until needed. During recovery, hot water from the second well is circulated through a heat exchanger to recapture the stored energy and then returned to the aquifer through the first well. The thermal energy thus recovered can be used for space or process heating.

The ATES system at the University of Minnesota is a 1/4-scale feasibility study designed to evaluate high-temperature heat storage and recovery in the Franconia-Ironton-Galesville aquifers below the University's St. Paul campus. The heat source used for the study is 150 psig steam from the University heating plant. An air-cooled radiator is used to simulate a heat user and extract stored heat from the water. The well doublet has a spacing of 854 ft.

A.2 SYSTEM COMPONENTS AND OPERATION

The ATES system uses well pumps and a booster pump to move the aquifer water from one well through the system and back down the other well.

Aquifer water (AW) is heated by steam using two heat exchangers. One is a steam-to-water heat exchanger and is called the condenser; the other is

water-to-water and is called the subcooler. The term condenser and subcooler refer to what happens to the heating steam as it passes through them to heat the AW. An air-to-water heat exchanger called a radiator is used to cool the AW.

Aquifer water, after it is heated, is circulated through vessels called fixed bed precipitators, which remove part of the calcium hardness.

The heating operation involves pumping AW from well B through the subcooler, the condenser, and the precipitator, then reinjecting it back into the aquifer through well A.

As AW flows through the condenser, it is heated to final temperature by 150 psig steam that is introduced through a control valve. As steam gives off heat in the condenser it condenses. The condensate flows from the condenser to the subcooler where it gives off more heat to incoming AW.

For heat extraction or cooling of AW, water is pumped from well A through the radiator and back into the aquifer through well B.

A booster pump is available to be used in pumping the AW in either the heating or heat extraction mode if required. At this writing, the well pumps have sufficient discharge heat and the booster pump is not required.

Steam to the condenser is regulated by a control valve, which is controlled by the temperature of the AW leaving the condenser.

Figures A.1 and A.2 show flows during the heating mode and the heat extraction mode.

A.3 DESIGN CONSIDERATIONS

The University of Minnesota, St. Paul campus was selected as the site for the ATES field experiment. Core borings were taken to define the aquifer in that area. The Franconia-Ironton-Galesville aquifer exhibits suitable traits (e.g., thermal insulation, flow capacity) and was not being used in the Twin Cities as a significant source for water. The University's utility tunnels provided easy access and routing for the interconnecting piping, electrical, instruments, power, and source of heat.

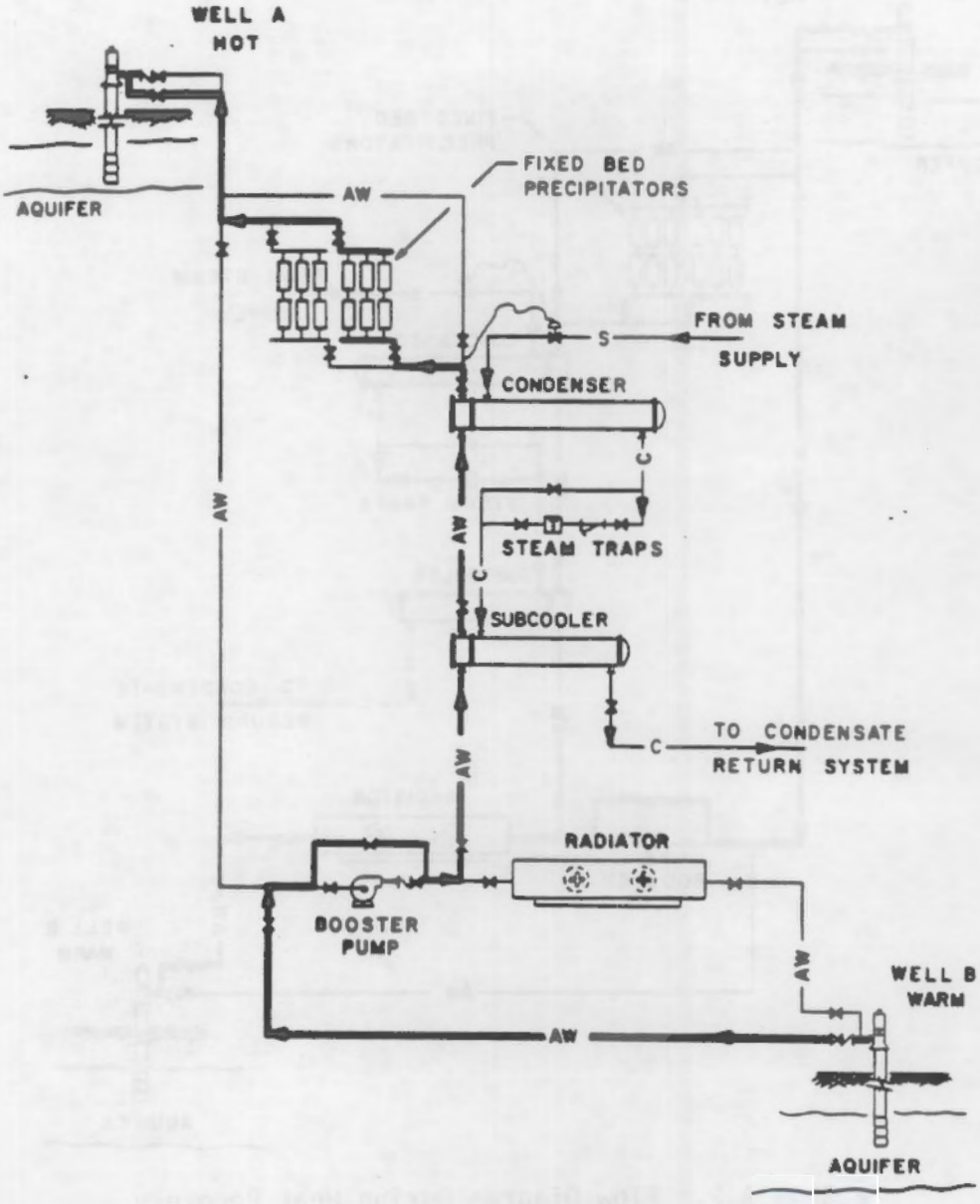

FIGURE A.1. Flow Diagram During Heat Injection

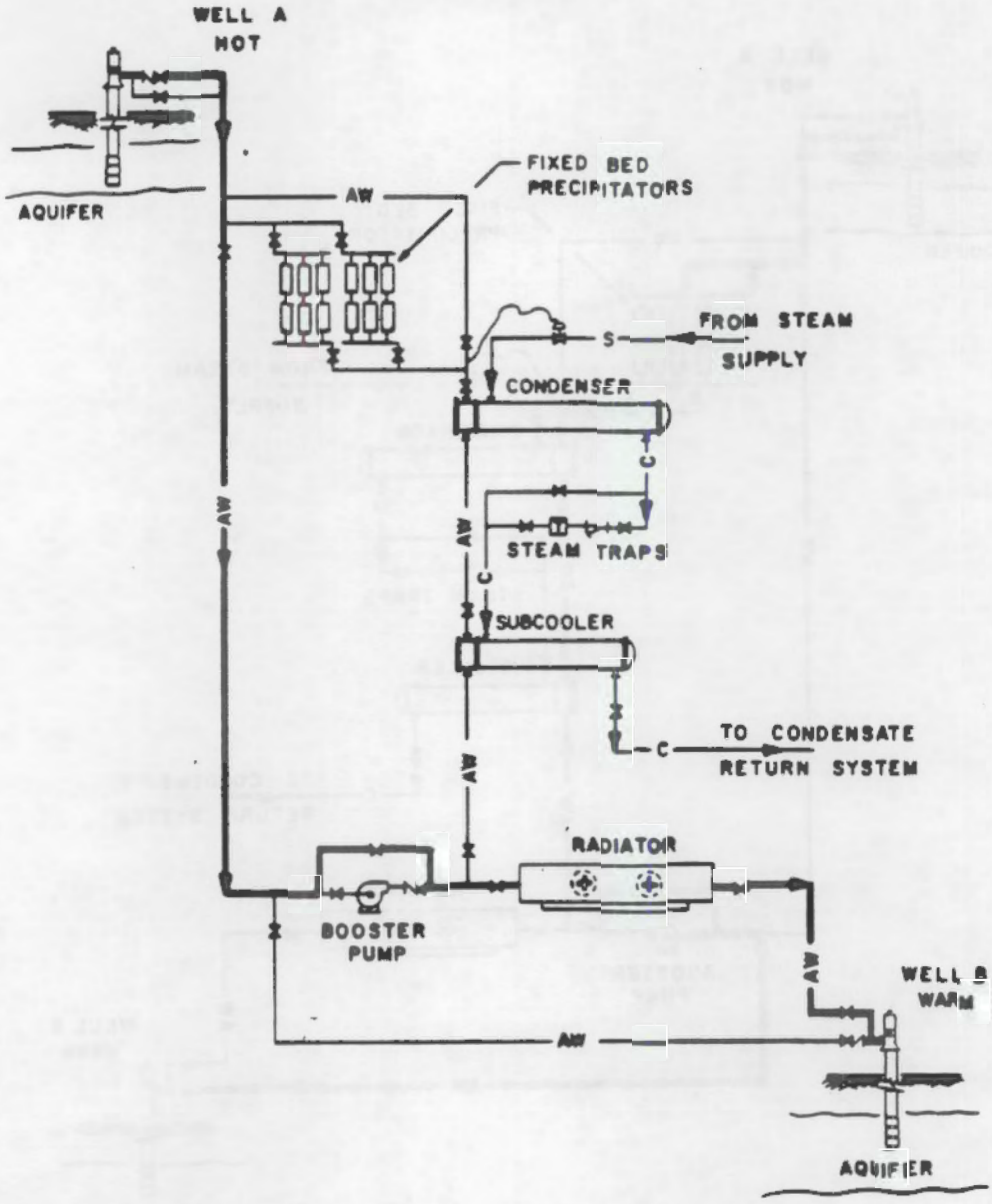

FIGURE A.2. Flow Diagram During Heat Recovery

Various permits were applied for from the Minnesota Pollution Control Agency (MPCA); the Department of Natural Resources (DNR); the Health Department; and Federal, State and Local Agencies with respect to public health and environmental impacts. After the various permits were obtained, actual system design could proceed.

The University of Minnesota, St. Paul campus ATES system was designed as an outdoor installation for operation during non-freezing weather. It was necessary to provide for draining of all piping and system components for layup during the winter. An enclosure such as a sheet metal building would have extended the operating season.

A.3.1 Well Pumps

The well pumps are multiple stage vertical turbine type shaft driven with the motor at the surface. Submersible pumps were considered, but the anticipated temperature of 305°F was too hot for a submerged motor. It was intended to reinject hot water in the well casing, but this was changed so that well injection was done back through the pump discharge line. The change was made to eliminate well plugging due to air entrainment.

The vertical turbine pump was ideally suited for this installation. The motor and electrical equipment are at ambient temperatures outdoors and the pump bowls are submerged in the aquifer. The pumps are designed for the 300°F water to be pumped. They have 25 stages and are rated for 300 gpm at 661 ft dynamic head. Motors are 75 hp and operate at 1760 rpm.

A.3.2 Heat Exchangers

Aquifer water is heated in two stages by heat exchangers (subcooler and condenser) connected in series. The AW and the heating steam flow counter to each other through the heat exchangers. Water passes through the subcooler, then the condenser. Heating is by 150 psig steam, which provides final heating of the AW in the condenser. Condensate from the condenser flows through float and thermostatic traps into the subcooler where it gives off more heat to the incoming AW. The AW flows from the subcooler to the condenser where it is heated to final temperature by the 150 psig steam.

The heat exchanger train is designed for a water flow of 300 gpm heated by 150 psig steam throttled through a temperature control valve. With 53°F inlet AW design, AW outlet is 212° with a condensate discharge of 160°. At 176°F inlet, AW design outlet is 305°F with a condensate discharge of 195°F.

The heat exchanger has carbon steel shells and carbon steel tubes. Fouling factor is 0.001. Tube thickness is 0.065 in. The shells have removable heads for tube cleaning. They are ASME Code constructed and stamped 200 psig for the condenser shell and 150 psig for the subcooler shell. Both exchanger designs are 200 psig and 300°F in the tubes and 400°F in the shell. Heat exchanger shells have 3/4 "xl" relief valves, thermostatic vents, and vacuum breakers. Both heat exchangers are single pass on the shell side and two pass on the tube side. They have straight tubes for ease of cleaning.

The heat exchangers are arranged so that condensate flows by gravity and pressure through float and thermostatic traps from the condenser to the subcooler. Steam and condensate connections are flanged.

The AW temperature is controlled by a self-operated control valve in the steam inlet line. The valve is controlled by a filled temperature bulb in the hot AW line leaving the condenser.

A.3.3 Radiator

A fan-cooled water-to-air heat exchanger or radiator is used to simulate a heat user by cooling water withdrawn from the aquifer. The radiator is designed to cool 300 gpm of water from 300°F to 170°F. It was specified to have a rating of 20 x 10^6 Btu/hr at 80° ambient with a fouling factor of 0.001. Maximum tube side pressure drop is 8 psig. The tubes have extended aluminum surfaces with no more than 12 fins per inch. Tubes were specified to be at least 1 in. in diameter with 0.065-in. thick walls. Design pressure is 200 psig. The unit is straight tube with clean out provision in the headers.

The radiator has two 15-hp two-speed fans with adjustable blades. Motors are fan cooled and totally enclosed. Fan blades are manually adjustable. The fans have adjustable temperature controllers that sense water temperature. They also have vibration shut offs. Air flow may also be controlled by louvers, which are manually operated.

A.3.4 Fixed-Bed Precipitators

During initial heating cycle operation of the ATES system, the heat exchangers (particularly the condenser) scaled badly and the well screen plugged. This was the result of heating the aquifer water, which reduced the calcium carbonate solubility.

The University designed a fixed-bed precipitator, which is a set of vessels filled with limestone fill material. The hot aquifer water flows through the vessels, and calcium salts precipitate onto the limestone. The precipitator is regenerated by removing and replacing the fill material.

The University experimented with dolomitic limestone, sand, and calcite. The calcite material in the form of crushed 98% calcium carbonate limestone was found to be superior. Tests for optimum flow rates and residence time determined the size and number of the precipitator vessels.

The final arrangement uses vessels 14-in. in diameter and 6-ft long. Two of these vessels are connected in series to form a set. Three sets make a bank designed for 300 gpm flow.

Two banks of precipitators are installed so that one bank can be in operation while the other bank is out of service for a change of fill material. Material is changed after pressure drop reaches a certain level. Material replacement is the only form of regeneration.

The precipitators are only effective after the water is heated so they must be downstream of the heat exchangers (condenser and subcooler). Initially the main benefit will be protection of the well screens.

It is anticipated that reduction of calcium hardness will also have future benefit to the heat exchangers as the water is pumped back and forth and achieves a lower concentration of calcium salts.

A.3.5 Booster Pump

Aquifer water is pumped through the system and back into the aquifer by the well pumps. A booster pump can be used to increase the pressure of the AW through the system. The booster pump intake is supplied by the well pump

discharge. In normal operation, the booster pump is by-passed. The pump is a single-stage end suction designed for 300 gpm at a head of 200 ft. It has a 25-hp motor.

A.3.6 Instrumentation and Control

Steam and AW flows are measured using orifice plate meters with differential pressure cells, square root extraction, and totalizers or integrators. Output is displaced on a strip chart recorder.

The system is designed to control heated AW at a set value between 212°F and 305°F and to control cooled aquifer water between 160°F and 260°F. Heated water temperature is controlled by a steam inlet valve at the condenser.

Cooled AW is controlled by temperature sensors which actuate step controllers on the two-speed radiator fan motors. The sensors are in the water leaving the radiator.

Aquifer water flow is controlled by a manual flow-control valve or by a self-contained, self-operated inline Griswald flow control valve.

A 20 point strip chart recorder with three chart ranges is used to record flows, pressure drops, and temperatures. Ten points are being used: steam flow to the condenser; AW flow; condenser subcooler and radiator pressure drop; condenser inlet temperature; subcooler inlet and outlet temperatures; and Well A and B inlet/outlet temperatures. The recorder is located in a trailer. It has alarm contacts for: AW flows, AW heated water temperature, and AW cooled water temperature. A horn and lights annunciate the alarm points.

A.3.7 Design Discussion

Field operation proved the overall design integrity of the system. Nevertheless, as is always the case, a few things would be done differently with the benefit of hindsight.

A line to the storm sewer to allow flushing and testing of the wells, piping, and system operation, was found to be absolutely necessary, and the University added it to the system.

The testing season was longer than anticipated and had to be terminated because the system was not designed for cold weather operation. A sheet metal enclosure or an inflatable enclosure could have extended the time available for testing.

The booster pump is not required in this case, but determining well drawdown and subsequent well discharge pressures is not exact enough to warrant leaving it out on initial design.

Larger traps in the condensate line between the condenser and subcooler would aid cold start-up when condensate flows are greater than steady-state design.

Instrumentation lines into the well casing were connected through explosion-proof fittings to provide for possible pressurization when 300°F water is introduced and flashes to steam.

The magnitude of the precipitation of calcium carbonate when the water was heated was greatly underestimated. A precipitation system was added and was crucial to making the tests possible. Replacing the high-purity limestone in the precipitators allowed system operations and protected the heat-storage well. Acid cleaning of the condenser tubes was also essential, and caused tubes to be etched out. The condenser tubes were replaced twice. The carbon steel tubes in the original plans were completely replaced with stainless steel tubes before the second cycle. These tubes developed pinhole leaks rapidly, and were replaced with carbon-steel tubes again. Thorough flushing is required after acid cleaning of the condenser tubes.

The open-shaft turbine pump design with EPDM bearings failed during operation at 185°F and above. This failure occurred even though these materials are rated to 300+°F for operation. Failure occurred as a result of the bearings swelling and seizing the shaft. A modified enclosed tube assembly with bronze and graphite-alloy bearings operated satisfactorily.

A.4 SYSTEMS HARDWARE

Table A.1 lists system valves and their positions during system operation. Figure A.3 is a schematic of the mechanical system. Table A.2 lists specifications of the valves, gauges, piping, and controls.

TABLE A.1. Valves on the ATES System and Valve Positions During Operation

VALVE NUMBER	SIZE and SERVICE	TYPE	MFG. and FIGURE #	VALVE POSITION HEAT STORAGE	VALVE POSITION HEAT RECOVERY
1	6-AW	E	D-118	O	C
2	6-AW	E	D-118	C	O
3	6-AW	E	D-118	O	C
4	6-AW	E	D-118	C	O
5	6-AW	E	D-118	O	C
6	6-AW	E	D-118	O	C
7	6-AW	E	D-118	O	O
8	6-AW	G	CR-33XU	O	O
9	6-AW	E	D-118	C	C
10	6-AW	FCV	G-3478	SO	SO
11	6-AW	E	D-118	C	C
12	6-AW	E	D-118	O	O
13	6-AW	E	D-118	C	C
14	6-AW	SC	GR-6300	SO	SO
15	6-AW	E	D-118	C	C
16	6-AW	E	D-118	O	C
17	6-AW	E	D-118	C	O
18	6-AW	E	D-118	O	C
19	6-AW	E	D-118	O	C
20	6-H	G	CR-33XU	C	C
21	6-H	GV	CR-151XU	O	C
22	6-H	TCV	S-ET14	SO	SO
23	6-H	GV	CR-151XU	O	C
24	1-H	GV	P-1503N	NC	NC
25	-	TV	A-TV	SO	SO
26	-	S	C-	SO	SO
27	2-C	GV	P-2375	O	C
28	2-C	GV	P-2375	O	C
29	2-C	GV	P-2375	O	C
30	2-C	GV	P-2375	O	C
31	2-C	GV	P-2375	O	C
32	2-C	GV	P-2375	O	C
33	2-C	G	GR-3130	C	C
34	1-C	GV	P-2375	NC	NC
35	-	S	C-	SO	SO
36	-	FV	A-FV	SO	SO
37	2-C	GV	GR-3270	O	C
37A	2-AW	GV	GR-3270	NC	NC
37B	2-C	GV	GR-3270	NC	NC
38	2-C	PRV	F-95H	SO	SO
39	2-C	GV	GR-3130	C	C
40	2-C	GV	GR-3270	O	C
41	-	S	C-	SO	SO
42	-	FV	A-FV	SO	SO
43	6-AW	E	D-118	C	O
44	6-AW	E	D-118	O	C
45	6-AW	E	D-118	C	O
46	6-H	GV	GR-6200	O	C
47	2-C	GV	GR-3270	O	C
48	6-AW	SCOWL	CR-383	SO	SO
49	6-AW	SCOWL	CR-383	SO	SO
50	3/4-AW	GV	P-2375	NC	NC
51	3/4-AW	GV	P-2375	NC	NC
52	3/4-AW	GV	P-2375	NC	NC

TABLE A.1. (continued)

VALVE NUMBER	SIZE and SERVICE	TYPE	MFG. and FIGURE #	VALVE POSITION HEAT STORAGE	VALVE POSITION HEAT RECOVERY
53	3/4-AW	GV	P-2375	NO	NO
54	3/4-AW	GV	P-2375	NO	NO
55	3/4-AW	GV	P-2375	NC	NC
56	3/4-AW	GV	P-2375	NC	NC
57	3/4-AW	GV	P-2375	NC	NC
58	3/4-AW	GV	P-2375, P-116	NO	NO
59	3/4-AW	GC	P-2375, P-116	NO	NO
60	3/4-AW	GC	P-2375	NC	NC
61	6-AW	E	D-118	C	C
62	6-AW	E	D-118	C	C
63				C	O

NOTE:

Size and Service
- # Refers to pipe diameter (in.)
- AW - Aquifer Water line
- C - Condensate line
- H - Steam line

Valve Type.
- E - Eccentric
- FCV - Flow Control Valve
- FV - Float Vent
- G - Globe
- GC - Gate and check valve used as vacuum breaker.
- GV - Gate Valve
- PRV - Pressure Reducing Valve
- S - Safety Relief Valve
- SC - Swing Check
- SCOWL - Swing check outside weight and lever
- TCV - Temperature Control Valve
- TV - Thermostatic Vent

Valve Manufacturer (MFG.)
- A - Armstrong
- C - Consolidated
- CR - Crane
- D - DeZurick
- F - Fisher
- G - Griswald
- GR - Grinnell
- P - Powell
- S - Spencer

Valve Positions.
- O - Open
- C - Closed
- NO - Normally open
- NC - Normally Closed
- SO - Self Operated

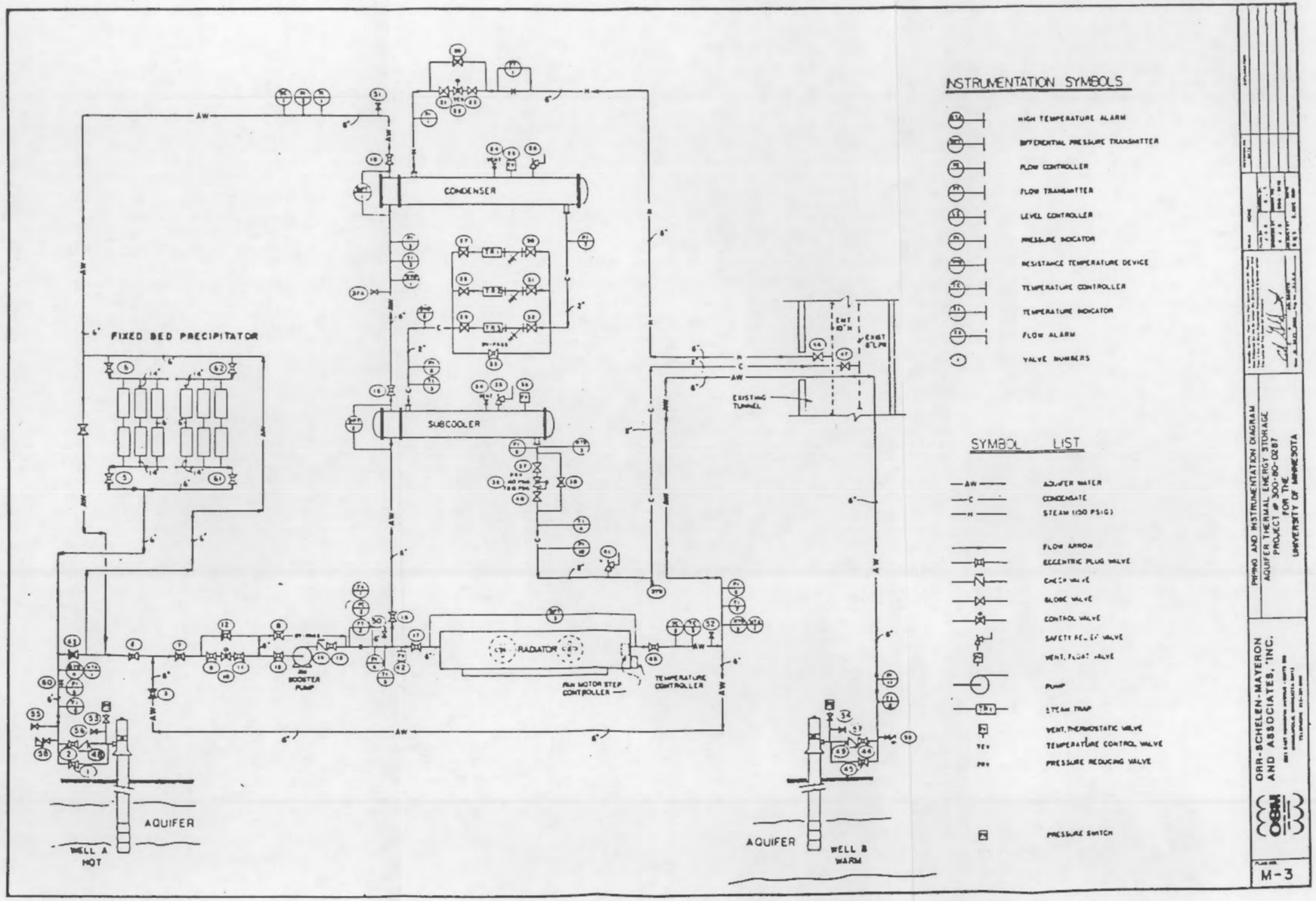

FIGURE A.3. Schematic of the Mechanical Systems, ATES Field Test Facility University of Minnesota

TABLE A.2. System Equipment

WELL PUMPS A AND B

Pumps

Manufacturer: Peabody Floway Pumps, Inc.
Type: vertical turbine, 8JKM, 25 stages, 6 x 16-1/2 in., 1-1/4 in. line shaft, 6 in. column
Fluid: water, temperature from 50°F to 310°F, specific gravity 1 to 0.915
Capacity: 300 gpm at 661 ft TDH., 1760 rpm
Pump bowl: CL 30 C.I.E.
Impeller: enclosed, SAE 40 BRZ
Bearings (bowl): cast iron
Bearings (line shaft): EPDM(a)
Pipe column: Schedule 40 steel
Pipe column lengths: pump A - 530 ft
pump B - 505 ft
Line shaft: C-1045
Bowl shaft: 416 stainless steel
Shaft packing: JCASB #811

(a) Replaced following failure. Revised design includes:
Bearings (line shaft): bronze, bronze-graphite(a); bronze-1
Line shaft: enclosed, 416 stainless steel
Pipe column lengths: pump A - 505 ft
pump B - 505 ft

Motors

Manufacturer: Westinghouse
Type: VHS, non-reverse ratchet
Performance: 75 hp at 1760 rpm
Electrical characteristics: pump A - 200/3/60
pump B - 460/3/60
Frame no.: 360 TP
Enclosure: WP-1
Pumps supplied by: New Mech
1608 Como Avenue West
St. Paul, MN 55108

Well pump A - serial no. 81-2064
Well pump B - serial no. 81-2063

TABLE A.2. (continued)

BOOSTER PUMP

Manufacturer: Weinman Pump, LFE Corp.
Type: horizontal single stage, end suction centrifugal pump 2-1/2 KB
Fluid: water, temperature from 50°F to 310°F, specific gravity 1 to 0.915
Capacity: 300 gpm at 200 ft TDH, 3500 rpm
Casting: cast iron, vertically split
Shaft: C-1045
Impeller: bronze, enclosed, dynamically balanced
Radial bearing: ball, grease lubricated
Thrust bearing: ball, grease lubricated
Casing gasket: asbestos
Gland: bronze, bronze nuts and studs
Shaft sleeve: bronze, renewable
Discharge position: 1
Motor: ODP, 25 hp at 3600 rpm, 200/3/60, 256T frame
Pump and motor mounted on common base. Motor coupled to pump.
Pump supplied by: New Mech
1608 Como Avenue West
St. Paul, MN 55108

FIXED BED PRECIPITATORS

The fixed bed precipitators were designed and fabricated by the University of Minnesota. The precipitators are arranged in two banks. Each bank of precipitators is designed for the rated flow of 300 gpm.

A bank consists of three sets of precipitator vessels operated in parallel. Each set is two vessels in series.

A bank has a total of six vessels arranged in three parallel flow streams. The vessels are each 14 in. in diameter by 6 ft long.

Precipitator fill material is 98% calcium carbonate crushed limestone. The bed material is replaced based on pressure drop (see Section 2).

TABLE A.2. (continued)

CONDENSER

Manufacturer: Whitlock Manfacturing Co.
Size: B-C-208
Type: MHTP-2-S-STL
Surface/unit: 368 FF
Total: 1 shell/unit
Surface/shell: 362 FF

Performance Data	Shell Side	Tube
Fluid circulated	150 psig steam	water
Total entering	17,830 lb/hr	300 gpm
Liquid		300 gpm
Steam	17,830 lb/hr	
Steam condensed	17,830 lb/hr	
Specific gravity		0.9403
Viscosity	0.0181 CP	0.2327 CP
Specific heat		1.02 Btu/lb
Latent heat vapors	857.2 Btu/lb	
Temperature in	365.8°F	198°F
Temperature out	365.8°F	305°F
Operating pressure		
Number of passes	1	2
Velocity		4.3 ft/sec
Pressure drop	1.4 psig	1.8 psig
Fouling		0.001
Thermal conductivity		0.3944
Heat exchanged - Btu/hr	15,280,000 MTD (corrected)	105°F
Transfer rate - service	402 clean	778
Design pressure	200 psig	200 psig
Test pressure	300 psig	300 psig
Design temperature	400°F	300°F

Tubes: carbon steel no. 74 (note: retubed twice, first - stainless tubes; second - carbon steel) O.D. 1.00 in., wall thickness 0.065 in., length 228 in.
Shell: carbon steel, O.D. 14 in.
Shell cover: floating
Channel: carbon steel
Channel cover: carbon steel
Tube sheet: carbon steel stationary; carbon steel floating
Baffles: carbon steel
Tube supports: carbon steel
Gaskets: comp. asbestos; Viton o-rings
Connections: shell - in 6 in., out 4 in. - 300 lb RF ANSI
channel - in 4 in., out 4 in. - 150 lb RF ANSI
Corrosion allowance: shell 1/16 in., tube 1/16 in.
Code requirement: TEMA C
Unit design, construction, and stamped, in accordance with ASME Boiler and Pressure Vessel Code, Section VIII, Unfired Pressure Vessels.

TABLE A.2. (continued)

SUBCOOLER

Manufacturer: Whitlock Manufacturing Co.
Size: 10-C-174
Type: MHTP-2-S-STL
Surface/unit: 167
Total: 1 shell/unit
Surface/shell: 166 FF

Performance Data	Shell Side	Tube
Fluid circulated	condensate	water
Total entering	18,740 lb/hr	300 gpm
Liquid	18,740 lb/hr	300 gpm
Steam		
Steam condensed		
Specific gravity	0.9273	0.9675
Viscosity	0.2036 CP	0.331 CP
Specific heat	1.02 Btu/lb	1 Btu/lb
Latent heat vapors		
Temperature in	365.8°F	176°F
Temperature out	195°F	198.5°F
Operating pressure		
Number of passes	1	2
Velocity	3 ft/sec	7.3 ft/sec
Pressure drop	5 psig	4.4 psig
Fouling		0.001
Thermal conductivity	0.3949	0.3898
Heat exchanged - Btu/hr	3,278,000 MTD (corrected)	53.1°F
Transfer rate - service	372 clean	651
Design pressure	150 psig	200 psig
Test pressure	225 psig	300 psig
Design temperature	400°F	300°F

Tubes: carbon steel no. 44, O.D. 1.00 in., wall thickness 0.065 in., length 174 in.
Shell: carbon steel, O.D. 10.75 in.
Shell cover: floating
Channel: carbon steel
Channel cover: carbon steel
Tube sheet: carbon steel stationary; carbon steel floating
Baffles: carbon steel
Tube supports: carbon steel
Gaskets: comp. asbestos; Viton o-rings
Connections: shell - in 4 in., out 4 in. - 300 lb RF ANSI
channel - in 4 in., out 4 in. - 300 lb RF ANSI
Corrosion allowance: shell 1/16 in., tube 1/16 in.
Code requirement: TEMA C
Unit design, construction, and stamped, in accordance with ASME Boiler and Pressure Vessel Code, Section VIII, Unfired Pressure Vessels.

TABLE A.2. (continued)

RADIATOR

Manufacturer: VOSS
Service: water cooler
Model: 9W-34L-29F
Type: forced
External surface: 28,348 ft^2
Heat exchanger: 20,000,000 Btu/hr
Effective MTD: 106.7°F
External surface transfer rate: 6.50 Btu/hr ft^2 °F
Shutters to cover tube area. Manual positioners
Dry weight: 18,700 lb

Tube Side

Fluid: water
Flow: 300 gpm
Temperature: in 300°F, out 150°F
Viscosity: 0.25 CP
Allowable pressure drop: 8.0 psig
Design pressure drop: 7.85 psig

Air Side

Air quantity: 893,346 lb/hr
Air quantity/fan: 104,840 ACFM
Pressure drop: 0.416 in. water
Temperature in: 80°F
Temperature out: 171.8°F

Design Parameters

Design pressure: 200 psig
Test pressure: per code
Design temperature: 400°F

Section Construction

Size: 135-8-34ST10-3
No. Bay: 1
1 section
Material: carbon steel

Header Construction

Type: box
Material: carbon steel
No. passes: 4
No. layers: 3
Corrosion allowance: 1/16 in.
ASME "U" stamped

TABLE A.2. (continued)

RADIATOR (contd)

Tube Construction

Material: carbon steel
O.D.: 1 in.
Wall thickness: 0.065 in.
No./section: 135
Length: 34 ft
Fin: aluminum, O.D. 2.5 in., 11 per in., 0.018 in. wall thickness

Fan (2)

Type: propeller, two total, 9 ft diameter, four blades, 12.7 hp at 424 rpm, aluminum construction

Motor (2)

two speed, 1800/900 rpm, TEFC, 15 hp, 220/3/60

PIPING

Steam "H" Line Designation (piping material)

Pipe: 2 in. and under - Schedule 80, carbon steel, ASTM A-53 or A-106
2-1/2 in. and larger - Schedule 40, carbon steel, ASTM A-53 or A-106
Fitting: 2 in. and under - Schedule 80, 3000 lb, socket-welded
2-1/2 in. and larger - Schedule 40, 150 lb, butt-welding type, LR elbows
Flanges: 150 lb ANSI, 1/16 in. raised face
Gasket: 1/16 in. Chesterton asbestos flat ring ANSI 150 lb design
Bolts: stud type THRD, entire length ASTM A-193-B7 or A-193-2H
Nuts: hex nuts, semi-finish ASTM A-194-2H

Aquifer Water "AW" Line Designation (piping material)

Pipe: 2 in. and under - Schedule 80, carbon steel, ASTM A-53 or A-106
2-1/2 in. and larger - Schedule 40, carbon steel, ASTM A-53 or A-106
Fitting: 2 in. and under - Schedule 80, 3000 lb, socket-welded
2-1/2 in. and larger - Schedule 40, 150 lb, butt-welding type, LR elbows
Flanges: 150 lb flat face
Gasket: soft copper corrugated metallic, ANSI 150 lb design
Bolts: stud type THRD, entire length ASTM A-193-B7 or A-193-2H
Nuts: hex nuts, semi-finish ASTM A-194-2H

TABLE A.2. (continued)

PIPING (contd)

Condensate "C" Line Designation (piping material)

Pipe: 1/2 in. and larger - Schedule 80, carbon steel, ASTM A-53
Fittings: screwed fittings, 300 lb malleable iron

VALVES AND CONNECTIONS

Gate Valves

P-2375: Powell, 200 lb, threaded ends, bronzed body, stainless steel rings, rising stem, union bonnet.

P-1503N: Powell, 150 lb, flanged ends, bolted flanged yoke - bonnet, outside screw, rising stem, cast steel construction, satellite faced seat rings.

CR-33XU: Crane, 300 lb, flanged ends, OS & Y bolted bonnet, carbon steel body and bonnet, seat and trim - 13% chromium ANSI type 410 stainless steel to cobalt base alloy. Hard facing.

GR-3130: Grinnell, 300 lb, threaded ends, bronze body, rising stem, union bonnet, stainless steel seat rings.

Globe Valves

CR-151XU: Crane, 300 lb, flanged ends, OS & Y bolted bonnet, carbon steel body and bonnet, seat and trim - 13% chromium ANSI type 410 stainless steel to cobalt base alloy. Hard facing.

GR-3270: Grinnell, 300 lb, threaded ends, union bonnet, bronze body and bonnet, plug and seat ring S-42000 stainless steel hardened.

GR-6200: Grinnell, 125 lb, flanged ends, IBBM, rising stem.

Checks

CR-333: Crane, 125 lb, flanged ends, IBBM, bolted cap, swing outside lever and weight.

GR-6300: Grinnell, 125 lb, flanged ends, IBBM swing check.

P-116: Powell, 200 lb, threaded ends, bronze construction, horizontal lift check, union cap.

TABLE A.2. (continued)

VALVES AND CONNECTIONS (contd)

PRV (Pressure Reducing Valves)

F-95H: Fisher, Model 95H self-contained pressure reducing valve, threaded ends, cast iron body, stainless steel diaphragm, service - water at 220°F maximum, 150 psig, reduced to 15 psig.

This valve reduces condensate from the subcooler to 15 psig before discharging to the plant return system.

Plug Valves

D-118: DeZurick, series 100, eccentric plug, Figure 118, flanged ends, cast iron body and plug, Viton plug face, Buna packing nickel seats. 0600, Figure 118, F, 6, RS48, ANG.

Flow Control Valve (FCV)

G-3478: Griswald Model #3478, 300 lb, flanged ends, ductile iron body, 500 psi/40D°F rating, ANSI type 300 series passivated stainless steel internal parts, 8 to 128 psig pressure drop range, set flow rate 300 gpm.

Temperature Control Valve (TCV)

This valve controls temperature of heated water leaving the heat exchangers. A temperature sensing bulb is located in the aquifer water discharge from the condenser. The bulb is connected by capillary to a valve that controls steam to the condenser. Description of this valve is as follows:

S-ET14: Spence, temperature regulator, single seat of hardened stainless steel, packless construction, actuated by a metal diaphragm, self-operated by capillary and bulb, iron body, 250 lb flanged ends. Service to regulate steam at 150 psig saturated to maintain temperature setpoint.
Thermostat style: 700 with range 150 to 300°F
Bulb material: bronze
Flexible tubing length: 15 ft
Capillary tubing material: copper
Thermostatic well no. 728, bronze

TABLE A.2. (continued)

VALVES AND CONNECTIONS contd

Vent, Thermostatic Valve (TV)

A-TV: Armstrong Machine Works, Model TTF-1, stainless steel body, threaded ends, straight through flow, beryllium - copper encased in stainless steel thermostatic element, valve and seats of stainless steel.

Service: water, 150 psig, 220°F
Differential pressure: approximately 140 psig.

Vent, Float Valve (FV)

A-FV: Armstrong Machine Works, Automatic Air Vent Model 1AV, cast iron body and cap, compressed asbestos gasket, stainless steel float and leverage, bottom inlet, 250 psi at 450°F rating.

Steam Traps (TR-1, -2 and -3) (removes condensate from the condenser)

2 in.: Armstrong Machine Works, float and thermostat Model 175-J8, cast iron construction, stainless steel with heat-treated chrome steel valve and seat float mechanism, stainless steel and brass with beryllium copper bellow air vent encased in stainless steel.

Service: condensate, 150 psig, 400°F

Strainers

2 in.: Armstrong Machine Works, "Y" pattern, 150 lb cast iron body, screwed ends, stainless steel screen with 0.045-in. perforations, stainless steel clad asbestos gasket.

Service: water, 150 psig, 400°F.

Flexible Connections

Flexible connections - Flexonics, 150 lb plate flanged ends of carbon steel, hose and braid of stainless steel, style 401M, 16-in. overall length, 305°F, 200 psig operation, 1/2 in. lateral movement.

INSULATION

Steam and Water Piping

Johns Manville "Micro Lok 650", 3-in. thick fiberglass insulation, type AP for indoor service, type ML aluminum cover (0.01 in. wall thickness) for outdoor service.

TABLE A.2. (continued)

INSULATION (contd)

Heat Exchangers

Johns Manville "Micro Lok 650", 4-in. thick fiberglass insulation, type ML aluminum cover (0.01 in. wall thickness).

Condensate Piping

Johns Manville "Micro Lok 650", 2-in. thick fiberglass insulation, type AP for indoor service, type ML aluminum cover (0.01 in. wall thickness) for outdoor service.

Fittings, Valve Bodies and Flanges

4 in. and smaller - insulate with mineral fiber cement to thickness of adjacent pipe insulation.

5 in. and larger - insulate with pre-molded fittings. All fittings located outdoors - aluminum cover (0.01 in. wall thickness).

Protection Sleeves

Elcen Figure 218 at all pipe supports.

GAUGES, SENSORS, RECORDERS

Temperature Gauges

Manufactured by Tel-Tru Manufacturing Co., Model BC-550R, 5-in. diameter head, bottom outlet connection, dial type, rigid stem, bi-metallic helix coil actuated, rustproof, dustproof and hermetically sealed case. 316 stainless steel separable socket.

Temperature Gauge Number	Range, °F	Fluid	Location
TI-1	100 to 400	Aquifer water	Condenser outlet
TI-2	100 to 400	Aquifer water	Condenser inlet
TI-3	30 to 240	Condensate	Subcooler inlet
TI-4	30 to 240	Condensate	Subcooler outlet
TI-5	100 to 400	Aquifer water	Booster pump discharge
TI-6	100 to 400	Aquifer water	Well A inlet-outlet
TI-7	30 to 240	Aquifer water	Well B inlet-outlet (at Site A)
TI-8	30 to 240	Aquifer water	Well B inlet-outlet

TABLE A.2. (continued)

GAUGES, RECORDERS, SENSORS

Pressure Gauges

U.S. Gauge Division "Solfront" Model 1901T, cast aluminum, back flanged case and snap-lock, bayonet ring, black finish, stainless steel pressure relieving back, borden tube and connection - phas. bronze, brass. Lever handle cocks for isolation. Steam lines have coil syphons.

Pressure Gauge Number	Range, psig	Fluid	Location
PI-1	0 to 300	Steam	Condenser inlet
PI-2	0 to 300	Aquifer water	Condenser outlet
PI-3	0 to 300	Aquifer water	Condenser inlet
PI-4	0 to 300	Aquifer water	Booster pump discharge
PI-5	0 to 300	Aquifer water	Well A inlet-outlet
PI-6	0 to 300	Aquifer water	Well B inlet-outlet (at Site A)
PI-7	0 to 300	Condensate	Condenser outlet
PI-8	0 to 300	Condensate	Subcooler inlet
PI-9	0 to 300	Condensate	Subcooler outlet
PI-10	0 to 60	Condensate	PRV outlet
PI-11	0 to 300	Aquifer water	Well B inlet-outlet

Resistance Thermal Devices (RTD)

Rosemount Model 78F, three-wire design, platinum resistance type, 100 ohms ±0.1 ohms at 0°C, element housed in 316 stainless steel sheath, 316 stainless steel protective well for insertion into lines.

RTD Number	Range, °F	Fluid	Location
RTD-1	0 to 400	Aquifer water	Condenser inlet
RTD-2	0 to 400	Condensate	Subcooler inlet
RTD-3	0 to 400	Condensate	Subcooler outlet
RTD-4	0 to 400	Aquifer water	Well A inlet-outlet
RTD-5	0 to 300	Aquifer water	Well B inlet-outlet (at Site A)

Flow Measuring Devices

Flow Transmitter

Rosemount Model 1151, two wire, 4 to 20 ma output with integral equalizing and square root extractor, forced balance, plug-in circuit board, explosion proof, accuracy ±0.25% calibrated span, ±0.25% of upper range, three-way valve manifold with blow down.

Flow Transmitter	Range	Fluid	Location
FT-1	0 to 40,000 lb/hr	Steam	Condenser inlet
FT-2	0 to 400 gpm	Aquifer water	Booster pump discharge

TABLE A.2. (continued)

GAUGES, SENSORS, RECORDER (contd)

Flow Measuring Devices (contd)

Flow Element

304 stainless steel concentric, paddle type orifice plates, installed in 6-in. diameter Schedule 40 steel pipe, 300 lb weld neck orifice flanges with flange taps.

Plate	Average Flow	Fluid	AP Range	Bore
FT-1	23,000 lb/hr	Steam	150 in. H_2O	4.074 in.
FT-2	280 gpm	Aquifer water	50 in. H_2O	3.889 in.

Recorders

Leeds and Northrup - Speedomax 250 series multipoint strip chart recorder, split chart - one side receiving 100 ohm platinum RTD range of 4 to 40 to 350°F, inputs three-wire directly to recorder, five RTDs; second side - two ranges, 0 to 30 ft and 0 to 400 gpm, input 4 to 20 ma using a 10 ohm precision dropping resistor. Recorder has three chart speeds: 1, 6, 12 in. per hour; all scales direct read; adjustable print rate from 1 sec. to 180 sec. per point; full-scale response less than 1 sec.; six digit non reset totalizer for steam and aquifer water flow.

Point	Fluid	Range	Location
FT-1	Steam	0 to 40,000 lb/hr	Condenser inlet
FT-2	Aquifer water	0 to 400 gpm	Booster pump discharge
DPT-1	Aquifer water	0 to 30 ft	Condenser
OPT-2	Aquifer water	0 to 30 ft	Subcooler
OPT-3	Aquifer water	0 to 30 ft	Radiator
RTD-1	Aquifer water	0 to 400°F	Condenser inlet
RTD-2	Condensate	0 to 400°F	Subcooler inlet
RTD-3	Condensate	0 to 400°F	Subcooler outlet
RTD-4	Aquifer water	0 to 400°F	Well A inlet-outlet
RTD-5	Aquifer water	0 to 400°F	Well B inlet-outlet (at Site A)

ALARMS

Alarms with horn are part of strip chart recorder, alarms have acknowledge and test pushbuttoms with indicator lamp.

Point	Fluid	Range Setpoint	Flow Location
FA-1	Aquifer water	0 to 300 gpm	FT-2
HTA-1	Aquifer water	300 to 350°F	RTD-4
HTA-2	Aquifer water	180 to 212°F	RTO-5

APPENDIX B

NATURAL ENVIRONMENTS: SITE DESCRIPTION

APPENDIX B

NATURAL ENVIRONMENTS: SITE DESCRIPTION

The biological communities that encompass and surround the two ATES facility sites are typically urban. The fenced-off area at site B and the area around the piping and heat exchangers at site A is barren of plant and animal life, while the adjacent grounds are landscaped. Vegetation consists of well kept coniferous and deciduous trees. Animal life is limited to a few grey squirrels, cottontail rabbits, thirteen-lined ground squirrels, and various songbirds.

B.1 FIELD SITE A

Site A, located on the northwest corner of the intersection of Gortner and Fitch Avenues, covers an area approximately 200 ft by 115 ft. A cyclone fence surrounds this area with a driveway entrance from the east side, from Gortner Avenue. Within the confines of the fence, the majority of the ground is covered with crushed rock, gravel, or sand. Grass lawn is limited to the southeast quarter of the site. Scattered weeds make up the limited ground vegetation on the remaining three-quarters of this site. The most common of these include smartweek (Polygonem sp.), lamb's quarters (Chenopodium album) and foxtail (Alopecurus sp.). The only other significant plant on the site itself is a single mature silver maple tree (Acer saccharinum) located in the southeast corner.

Surrounding the site proper, but within 50 ft of the fence, the grounds are neatly landscaped. This is especially true for the east and north sides of the site. On the east side, between the fence and Gortner Avenue, the lawn is well kept and scattered with mature hackberry (Celtis occidentalis) trees. To the north, one row of arbor vitae (Thuja sp.) and three rows of gooseberries (Ribes sp.) border approximately two-thirds of the fence. A number of hackberry trees and one mature basswood (Tilia americana) tree can also be found. The grass lawn is quite lush. To the west of the fence, however, the

lawn is spotty and scalped in spots. Dandelions (Taraxacum officinale) predominate. Seven hackberry trees can also be found here. Between the fence and Fitch Avenue, south side, there exists a sparse lawn infested with quackgrass (Agropyron repens). There is but one tree on this side, a Kentucky coffeetree (Gymnocladus diocia). See Figure B.1 for illustration of site A.

B.2 FIELD SITE B

Site B, at the northwest corner of Gortner and Commonwealth Avenues, occupies a much smaller area than site A. The portion of this site that is actually fenced-off is approximately 40 ft by 50 ft. A crushed rock driveway accesses the site from Commonwealth, the north end of which is widened to accommodate two wells. The fenced area contains an electric power panel, pump B, and some steel piping. No plants or animals (other than insects) are found at this location.

Neighboring site B is the Veterinary Science building to the northwest; well maintained lawn to the north, east, and west; and a perimeter of young coniferous and deciduous trees bordering Gortner and Commonwealth Avenues. These trees are planted, well spaced, in single rows and include Colorado blue spruce (Picea purgens), sugar maple (Acer saccarum), silver maple (Acer saccharinum), and hackberry (Celtis occidentalis). See Figure B.2 for details.

B.3 ATES CONSTRUCTION AND OPERATION IMPACTS

The construction and operation impacts to the biological communities at the ATES sites are minimal. The construction phase brought a significant amount of traffic to the site disrupting the landscaped surface that had been there. The piping, trailer well heads, and the fences are visible from the greatest distances. The characters of the sites were changed from what had been open and park-like. Sod was removed and a limited amount of tree removal occurred. (It should be noted that all the trees on and around field sites A and B were either long ago or recently planted there by the University, and in many cases are not native species.) Crushed rock, gravel, and sand replaced

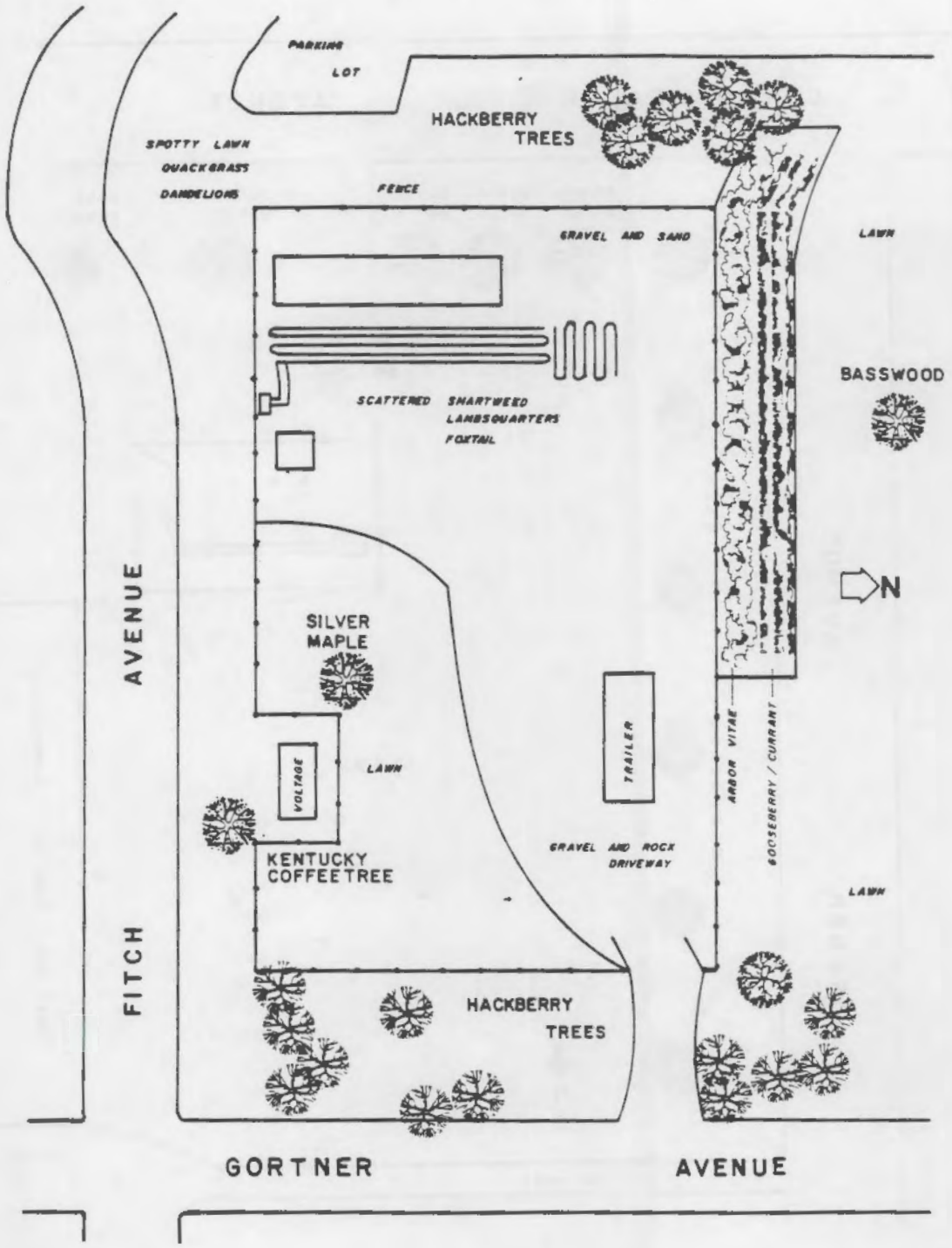

NOT TO SCALE

FIGURE B.1. Field Site A, Biological Description

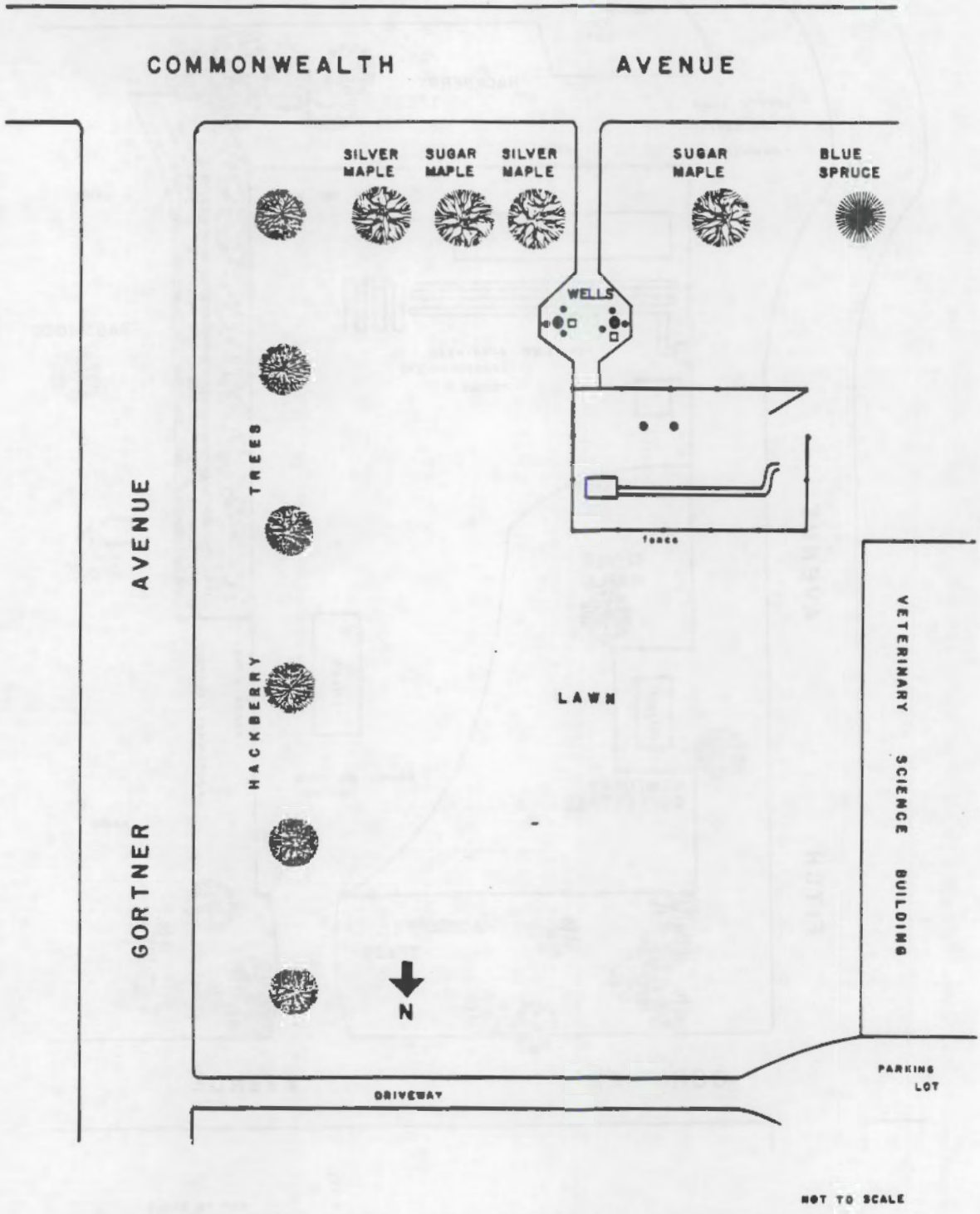

FIGURE B.2. Field Site B, Biological Description

most of the existing lawn and a mobile trailer office, wells, piping, and mechanical equipment filled some of the previous open space. Outside the fences, at each of the sites, the landscape remains and will remain essentially unaffected by the project. In addition, the value of either site for potential wildlife habitat was unchanged due to construction and/or operation of the ATES system, as the suitability of habitat was extremely limited before construction.

APPENDIX C

LITHOLOGIC AND DOWNHOLE GEOPHYSICAL DATA

APPENDIX C

LITHOLOGIC AND DOWNHOLE GEOPHYSICAL DATA

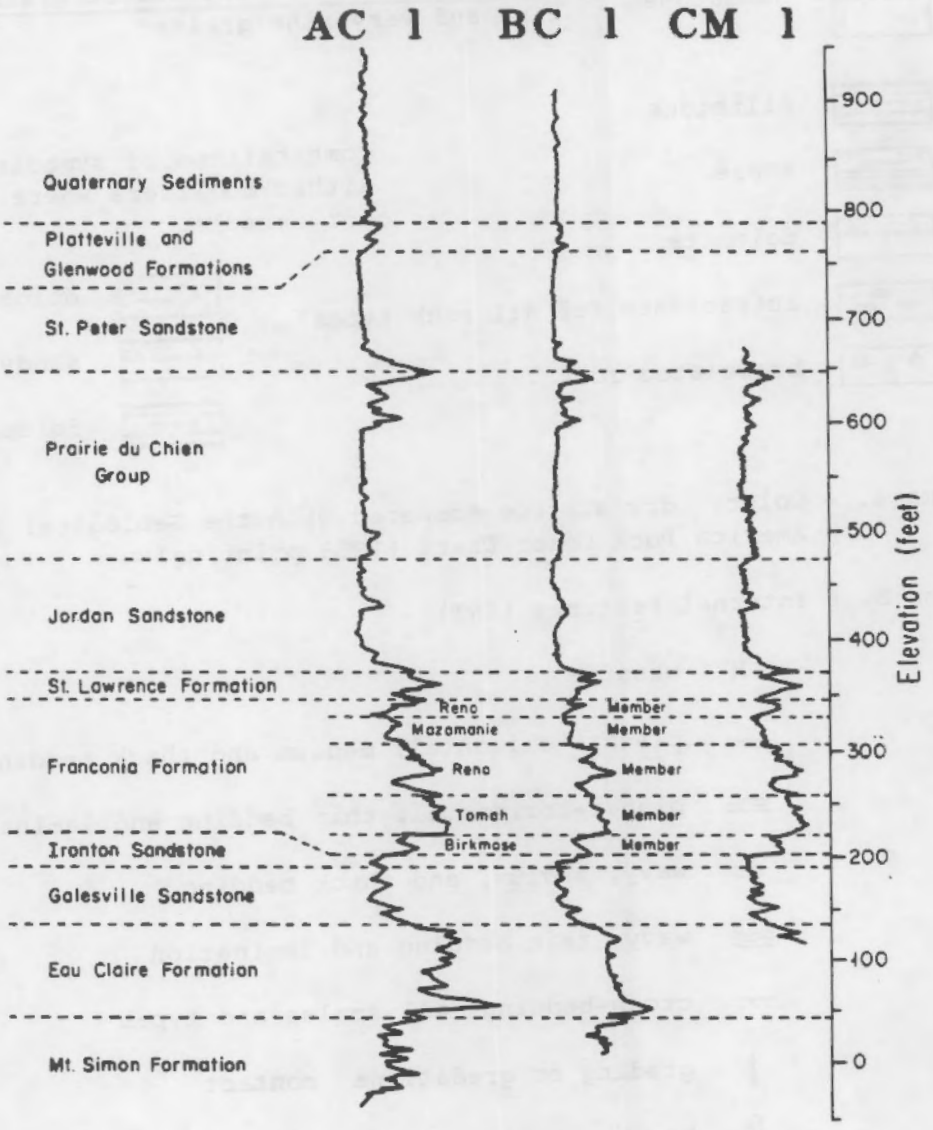

FIGURE C.1. Natural Gamma Logs of ATES Drill Cores

The key to the symbols used in preparing the log in this appendix is as follows:

Column 1. - Vertical scale in feet.

Column 2. - Formations and members. Informal members are shown in quotation marks.

Column 3. - Rock type (RT)

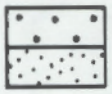

sandstone — medium, coarse, and very coarse grained / fine and very fine grained

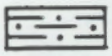

siltstone

shale

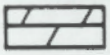

dolomite

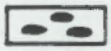

intraclasts (of all rock types)

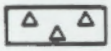

brecciated rock

Combinations of symbols are used as lithic modifiers where appropriate, for example:

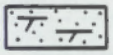

dolomitic sandstone

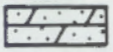

sandy dolomite

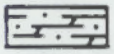

dolomitic siltstone

Column 4. - Color: dry surface compared with the Geological Society of America Rock Color Chart (1963 printing)

Column 5. - Internal Features (INT)

M massive

planar-horizontal; medium and thick bedding

planar-horizontal; thin bedding and lamination

wavy, medium, and thick bedding

wavy, thin bedding and lamination

cross-bedding, all scales and types

grading or gradational contact

burrow mottled (bioturbated)

FIGURE C.2. Lithologic Log of Core AC1

fossiliferous

g glauconitic

⊙ oolitic

o vuggy

(g) rare
g moderately abundant
g very abundant

Column 6. - Grain size range (GS)

f fine

m medium

c coarse

v very

x crystalline

example: f is fine grained
fx is finely crystalline
f-m is fine to medium grained
( ) parentheses indicate minor constituent

Column 7. - Sample number (NO) - taken for thin section and x-ray analyses. Location of sample is shown by ◀ on rock type (RT) column.

Column 8. - Graph of composition and grain size (for St. Lawrence, Franconia, Ironton, Galesville, and part of Eau Claire)

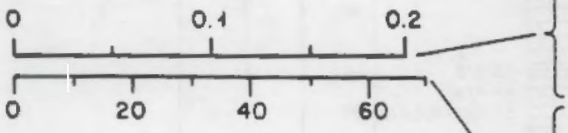

Size in mm of approximately 80% of grains (from Table 3.1)
o—o grain size range
○→ size larger than 0.2 mm

Composition in percent (from Table 3.1)
q---q quartz
f——f K-feldspar (grains and overgrowths)
g·····g glauconite
d--d dolomite
c clayey matrix

FIGURE C.2. Lithologic Log of Core AC1 (continued)

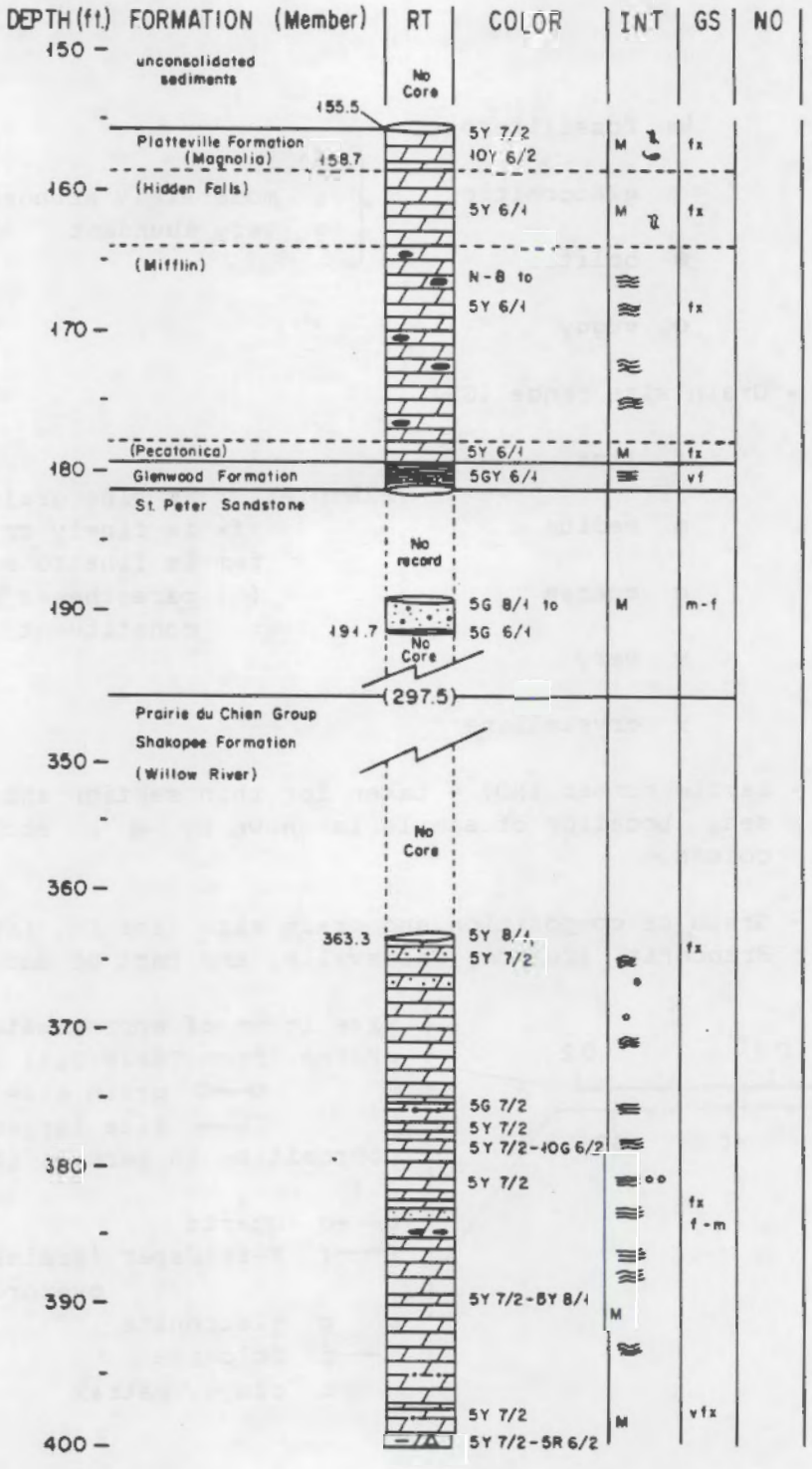

FIGURE C.2. Lithologic Log of Core AC1 (continued)

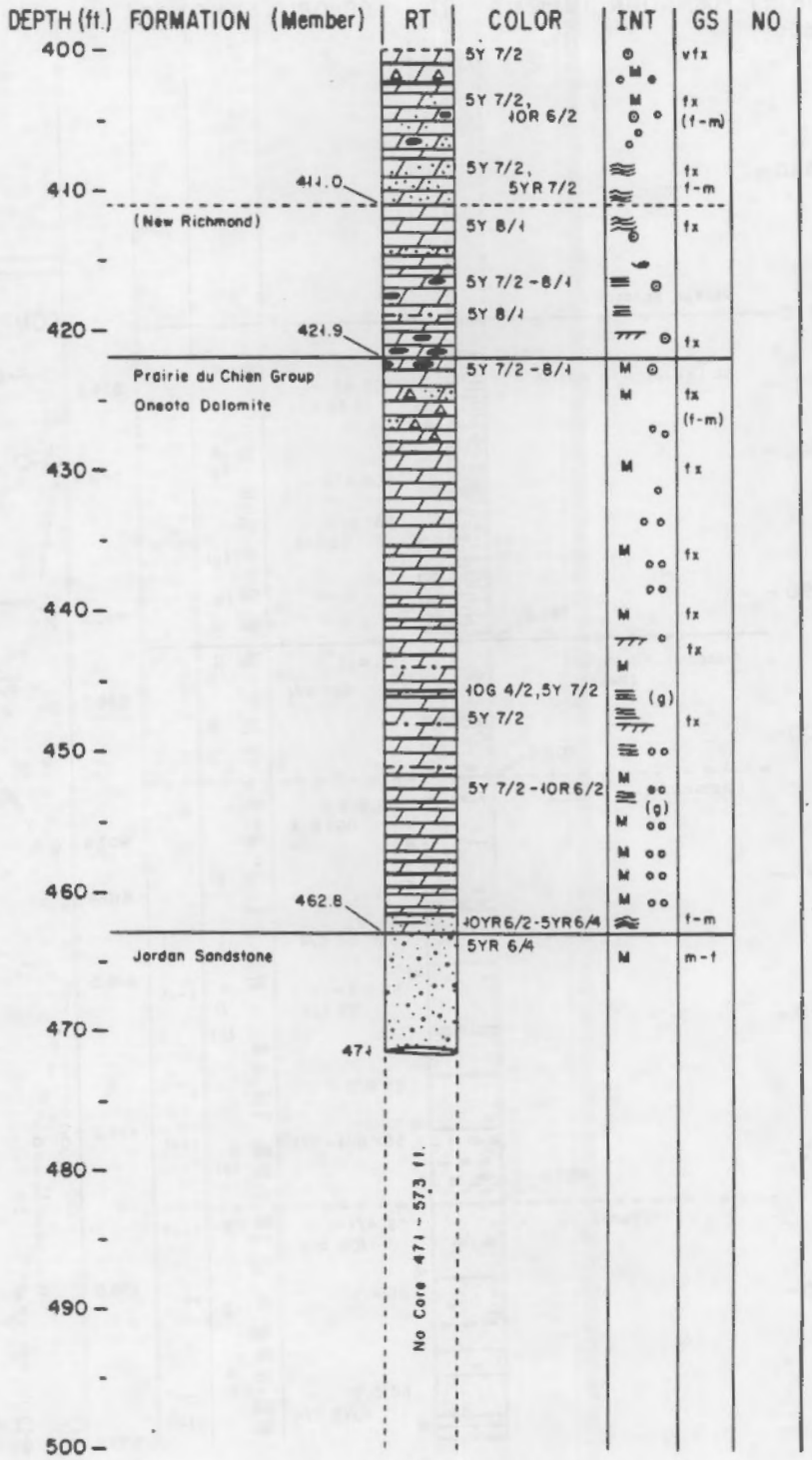

FIGURE C.2. Lithologic Log of Core AC1 (continued)

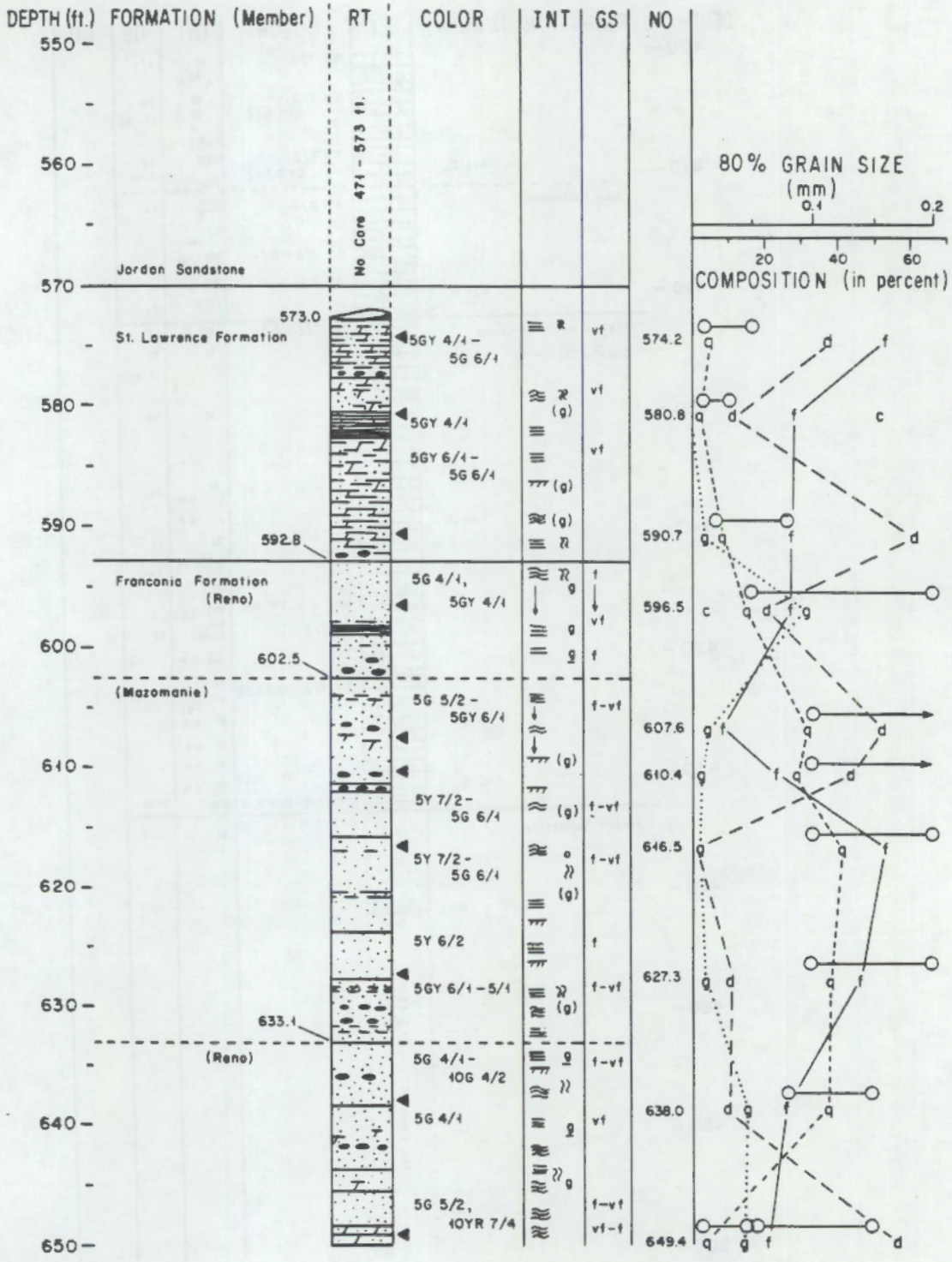

FIGURE C.2. Lithologic Log of Core AC1 (continued)

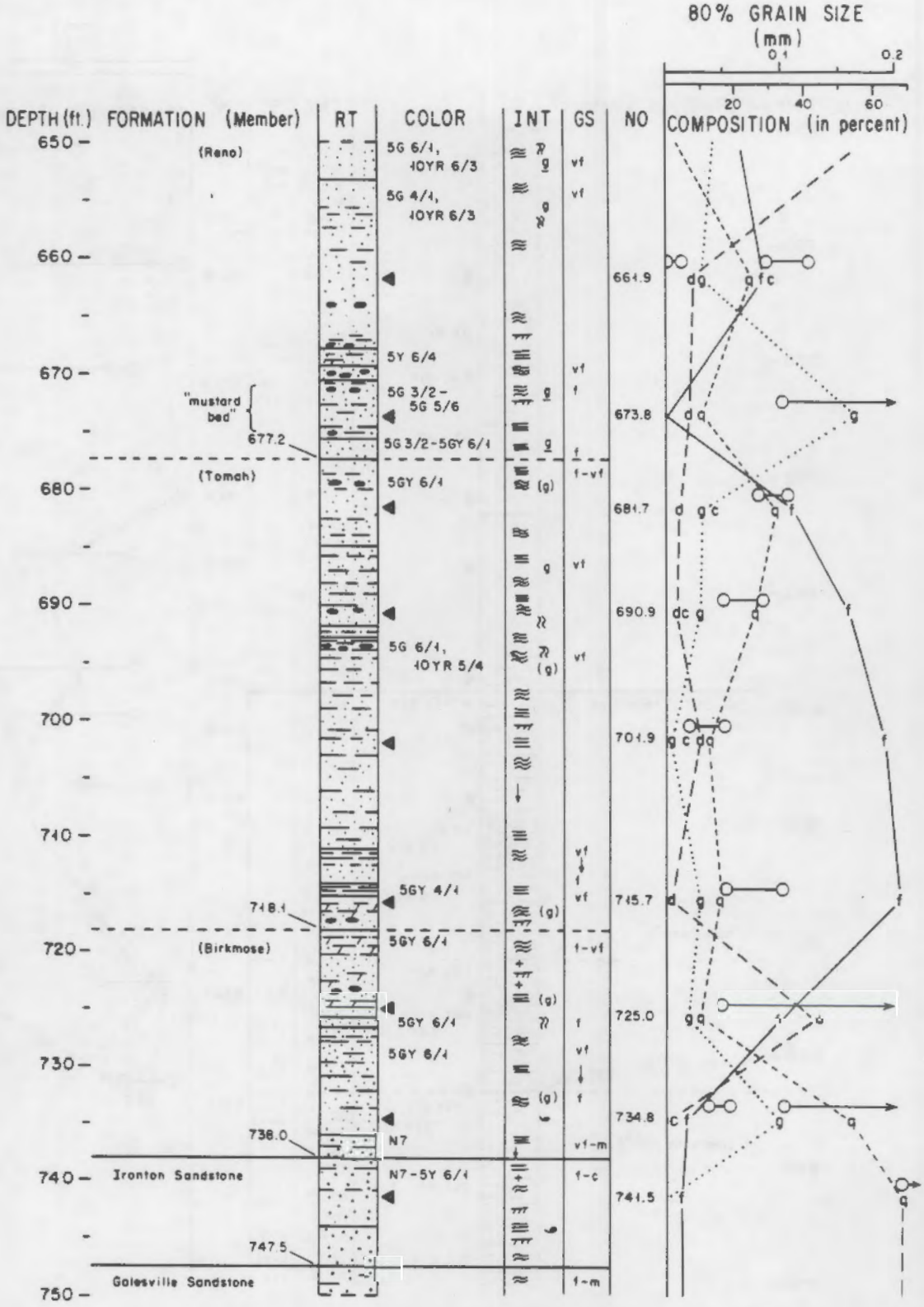

FIGURE C.2. Lithologic Log of Core AC1 (continued)

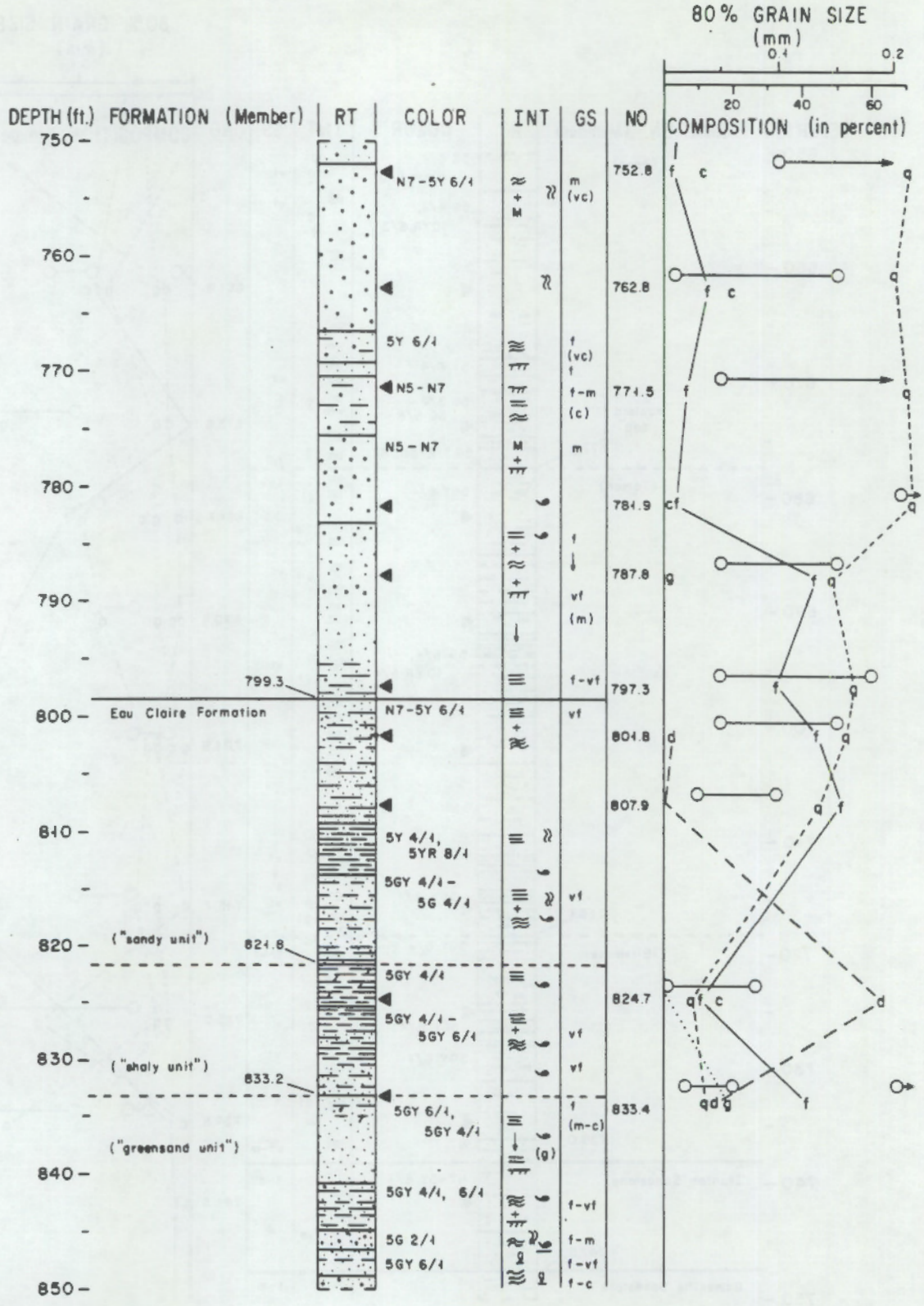

FIGURE C.2. Lithologic Log of Core AC1 (continued)

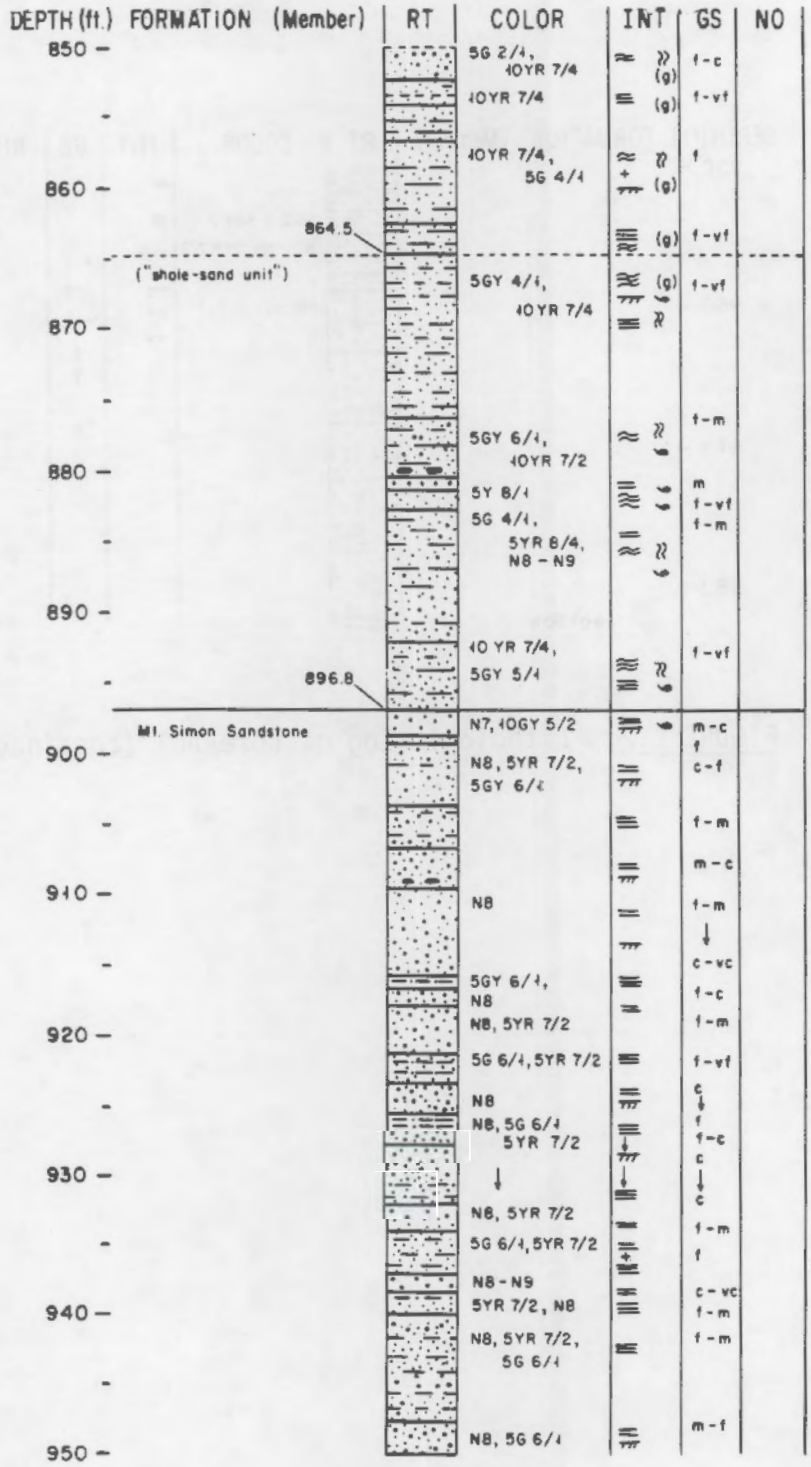

FIGURE C.2. Lithologic Log of Core AC1 (continued)

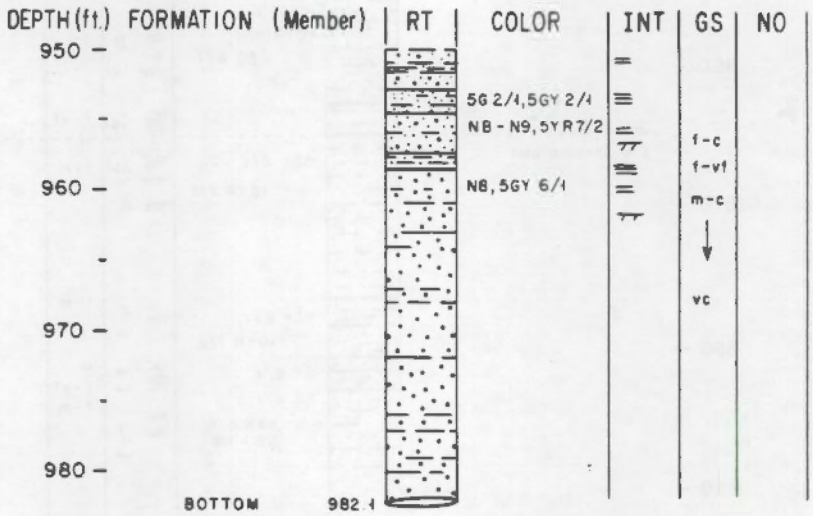

FIGURE C.2. Lithologic Log of Core AC1 (continued)

APPENDIX D

CHEMICAL ANALYSES OF GROUND WATER SAMPLES COLLECTED AT THE ATES FIELD TEST FACILITY

APPENDIX D

CHEMICAL ANALYSES OF GROUND WATER SAMPLES COLLECTED AT THE ATES FIELD TEST FACILITY

Many tables of water analyses are included in Appendix D. Ionic changes have been omitted on all tables, e.g. sulfate is symbolized by SO_4 rather than SO_4^{2-}. Samples taken during the preliminary pumping are in Table D.1. Samples collected during the initial heated-water injection attempt are in Table D.2. Tables D.3 through D.6 and D.8 through D.11 present the analyses of samples taken during the short-term cycles. Tables D.7 and D.12 present trace metal concentrations in samples analysed by ICP. Monitoring well sample analyses are presented in Tables D.13 to D.18.

On the tables, uM stands for micromoles per liter; mM stands for millimoles per liter; mg/L stands for milligrams per liter; and umho cm^{-1} stands for micromoles per centimeter. ND is not detected. Dashes indicate that no analysis was made on that sample.

TABLE D.1. Chemical Analyses of Water Samples Collected During Pumping Test and Cold Water Injection (April-May 1982)

Date (1982)	4/27	4/29	4/30	5/2	5/3	5/4	5/5
pH	7.44	7.55	7.56	7.46	7.45	7.43	7.46
Eh (mv)	-	-	-	-	-	+111	+128
SC (umho cm^{-1})	331	319	328	372	352	341	343
DO (mg/L)	-	-	-	-	0.2	0.5	0.35
NH_3 (mg/L)	-	ND	ND	-	ND	ND	ND
Alkalinity (mM)	4.90	4.90	4.86	4.87	4.88	4.89	4.93
SO_4 (uM)	96.4	129.	-	100.	-	94.5	83.9
Cl (uM)	21.8	27.4	-	26.2	-	25.4	24.8
F (uM)	13.7	13.7	-	13.7	-	13.7	13.7
NO_3 (uM)	ND	ND	-	ND	-	ND	ND
Ca (mM)	1.58	1.69	-	1.19	-	1.56	-
Mg (mM)	0.83(F,U)	0.87(F,U)	-	0.87	-	0.88(F) 0.90(U)	0.89(F) 0.93(U)
Na (mM)	0.24(F,U)	0.25(F,U)	-	0.24	-	0.26	0.27(F,U)
K (mM)	0.13(F,U)	0.13(U) 0.14(F)	-	0.69	-	0.7(F,U)	0.69(F) 0.70(U)
Fe (uM)	12.8(U) 10.5(F)	14.3(U)	-	25.6	-	18.8(F,U)	17.7(F) 23.3(U)
SiO_2 (uM)	-	123	-	122	-	-	122
Hardness (mM)	2.41	2.56	-	2.06	-	2.44	-
TDS (mg/L)	-	233.8	-	246.1	-	-	236.9
O&G (mg/L)	-	-	-	-	-	ND	-

Legend: (U) = unfiltered, (F) = filtered, SC = specific conductance, DO = dissolved oxygen, TDS = total dissolved solids, O&G = oil and grease, uM = micromoles per liter, mM = millimoles per liter, mg/L = milligrams per liter, umho cm^{-1} = micromoles per centimeter, ND = not detected, - indicates no analysis was made on that sample.

TABLE D.1. (continued)

Date (1982)	5/6	5/7	5/8	5/9
pH	7.47	7.48	7.49	7.47
Eh (mv)	+106	-	+108	+118
SC (umho cm^{-1})	320	330	349	345
DO (mg/L)	0.35	0.5	0.6	-
NH_3 (mg/L)	ND	ND	ND	ND
Alkalinity (mM)	4.81	4.84	4.63	4.61
SO_4 (uM)	-	-	62.4	-
Cl (uM)	-	-	26.0	-
F (uM)	-	-	14.2	-
NO_3 (uM)	-	-	ND	-
Ca (mM)	-	-	1.51	1.69
Mg (mM)	-	-	0.84(F) 0.80(U)	0.69
Na (mM)	-	-	0.30(F,U)	-
K (mM)	-	-	0.71(F,U)	0.69(F) 0.70(U)
Fe (uM)	-	-	ND	17.3(F) 23.3(U)
SiO_2 (uM)	-	-	122	-
Hardness (mM)	-	-	2.35	2.38
TDS (mg/L)	-	-	239.4	-
O&G (mg/L)	-	-	-	-

Legend: (U) = unfiltered, (F) = filtered, SC = specific conductance, DO = dissolved oxygen, TDS = total dissolved solids, O&G = oil and grease, uM = micromoles per liter, mM = millimoles per liter, mg/L = milligrams per liter, umho cm^{-1} = micromoles per centimeter, ND = not detected, - indicates no analysis was made on that sample.

TABLE D.2. Chemical Analyses of Water Samples Collected During Initial Heated Water Injection Test

Date (1982)	5/15	5/16	5/17	5/18	5/19
pH	7.46	7.45	7.25[a]	7.29[a]	7.32[a]
Eh (mv)	+108	+107	-	-	-
SC (umho cm^{-1})	352	338	515[a]	517[a]	519[a]
DO (mg/L)	0.6	0.1	0.3	0.2	0.2
NH_3 (mg/L)	ND	ND	ND	ND	ND
Alkalinity (mM)	4.63	4.53	4.24	4.34	-
SO_4 (uM)	52.8	-	48.8	48.4	47.6
Cl (uM)	37.8	-	20.6	19.5	25.2
F (uM)	11.9	-	11.6	11.7	11.7
NO_3 (uM)	1.3	-	ND	ND	ND
Ca (mM)	1.37	1.35	1.22	1.20	1.20
Mg (mM)	0.81	0.80	0.77	0.76	0.75
Na (mM)	0.21	-	0.18	-	0.22
K (mM)	0.014	0.014	0.014	0.014	0.014
Mn (uM)	ND	ND	ND	ND	ND
Fe (uM)	15.5	15.5	0.77	0.77	0.77
SiO_2 (uM)	104	105	104	106	106
Hardness (mM)	2.11	2.11	1.98	1.96	1.96
TDS (mg/L)	216.2	225.1	174.2	213.0	219.0
O&G (mg/L)	ND	ND	97.6	96.0	100.3

(a) measured at 40°C

Legend: SC = specific conductance, DO = dissolved oxygen, TDS = total dissolved solids, O&G = oil and grease, uM = micromoles per liter, mM = millimoles per liter, mg/L = milligrams per liter, umho cm^{-1} = micromoles per centimeter, ND = not detected, - indicates no analysis was made on that sample.

TABLE 0.3. Chemical Analyses of Water Samples Collected During Injection - Cycle 1

Date (1982)	11/16	11/16	11/17	11/17	11/17[b]	11/19	11/19	11/19	11/23	11/23[b]
Sample Point[a]	H	W	H	W	W	W	H	W	W	W
Time	1600	1645	1100	0930	0930	0850	0940	2045	1600	1600
pH	7.17	6.99	7.19	7.02	-	7.00	7.18	7.00	7.05	-
SC[c] (umho cm^{-1})	-	-	-	362	-	359	-	-	357	-
DO (mg/L)	-	-	-	0.1	-	0.05	-	0.2	0.1	-
NH_3 (mg/L)	-	-	-	0.1	-	0.1	-	0.1	0.1	-
Alkalinity (mM)	4.15	3.83	4.29	3.82	3.87	3.50	3.98	3.50	3.40	3.40
SO_4 (uM)	87.0	87.0	55.1	55.1	55.1	51.7	-	-	61.7	61.7
Cl (uM)	23.1	20.0	21.7	20.9	20.9	21.4	-	-	20.6	21.7
F (uM)	15.3	13.7	15.8	14.7	14.7	14.7	-	-	13.1	12.6
NO_3 (uM)	ND	ND	ND	ND	ND	ND	-	-	1.13	0.83
Ca (mM)	1.06	0.95	1.11	0.91	0.91	0.87	1.12	0.87	0.82	0.81
Mg (mM)	0.78	0.78	0.78	0.78	0.83	0.81	0.78	0.78	0.78	0.72
Na (mM)	0.19	0.20	0.24	0.23	0.22	0.24	0.25	0.24	0.24	0.24
K (mM)	0.18	0.18	-	0.18	0.18	0.18	-	0.20	0.18	0.19
Fe (uM)	5.6	2.4	1.9	3.1	2.1	3.1	0.13	1.9	3.7	4.9
Mn (uM)	0.30	0.25	0.18	0.20	0.21	0.20	0.16	0.19	0.16	0.15
Fe(II)[d] (uM)	1.88	2.27	0.37	3.60	2.82	2.43	0.30	1.50	3.85	5.24
Fe Total (uM)	-	2.21	1.81	2.93	2.04	1.57	0.32	1.21	3.99	5.27
SiO_2 (uM)	-	123	-	-	-	124	-	-	123	124
Hardness (mM)	1.82	1.70	1.86	1.64	1.64	1.58	1.80	-	1.52	1.52
Vol.[e] Ca (mM)	1.12	0.96	1.19	0.94	0.94	0.90	1.17	-	-	-
TDS (mg/L)	164.3	-	-	190.1	-	182.2	-	165.3	169.4	85.6

(a) H = heat exchanger effluent, W = reactor effluent--injection water, U = heat exchanger influent--source water.
(b) Duplicate samples.
(c) Specific conductance. Samples were cooled to 25°C ±2°C before measurement of SC. Temperature was measured to nearest 0.1°C and recorded along with SC.
(d) Col. Colorimetric, 1,10 phenanthroline.
(e) Vol. Volumetric, EDTA titration.
Legend: DO = dissolved oxygen, TDS = total dissolved solids, uM = micromoles per liter, mM = millimoles per liter, mg/L = milligrams per liter, umho cm^{-1} = micromoles per centimeter, ND = not detected, - indicates no analysis was made on that sample.

TABLE D.3. (continued)

Date (1982)	11/24	11/24	11/24	11/30	11/30	12/1	12/1	12/2	12/3	12/3
Sample point[a]	U	H	W	H	W	H	W	W	H	W
Time	0920	1120	1015	1700	1730	1015	0930	2130	1100	0930
pH	-	7.21	7.05	-	7.00	7.16	7.01	7.00	7.20	7.02
SC[c] (umho cm^{-1})	-	-	361	-	395	-	354	348	-	360
OO (mg/L)	-	-	0.1	-	0.05	-	0.05	-	-	0.05
NH_3 (mg/L)	-	-	0.1	-	0.1	-	0.1	-	-	0.1
Alkalinity (mM)	4.51	4.02	3.52	4.17	3.81	3.96	3.55	3.32	4.04	3.56
SO_4 (uM)	48.83	-	48.83	-	-	47.58	48.83	-	-	46.20
Cl (uM)	21.15	-	21.15	-	-	22.84	25.10	-	-	21.00
F (uM)	14.73	-	13.68	-	-	15.78	12.62	-	-	14.73
NO_3 (uM)	NO	-	2.86	-	-	NO	NO	-	-	ND
Ca (mM)	1.39	1.12	0.90	1.19	0.98	1.10	0.82	0.79	1.13	0.86
Mg (mM)	0.74	0.70	0.77	0.79	0.78	0.75	0.74	0.72	0.73	0.74
Na (mM)	0.27	-	0.24	-	0.22	0.24	0.23	0.24	-	0.24
K (mM)	0.20	-	0.19	-	0.19	-	0.17	0.093	-	0.17
Fe (uM)	15.5	0.98	5.1	5.3	7.1	0.69	3.0	2.8	0.38	1.1
Mn (uM)	0.31	0.18	0.31	0.27	0.16	0.20	0.22	0.15	0.18	0.21
Fe(II)[d] (uM)	13.99	0.39	2.10	0.05	6.40	0.05	1.58	0.88	0.02	1.06
Fe Total (uM)	14.19	0.48	2.63	0.17	6.87	0.25	1.84	1.23	0.11	1.19
SiO_2 (uM)	124	-	127	-	-	127	127	-	-	126
Hardness (mM)	2.09	1.88	1.60	1.96	1.74	1.82	1.60	1.53	1.89	1.64
Vol.[e] Ca (mM)	1.41	1.22	0.97	1.19	-	1.22	0.88	0.84	1.14	1.01
TDS (mg/L)	235	-	177	-	196	185	-	176	-	177

(a) H = heat exchanger effluent, W = reactor effluent--injection water, U = heat exchanger influent--source water.
(b) Duplicate samples.
(c) Specific conductance. Samples were cooled to 25°C ±2°C before measurement of SC. Temperature was measured to nearest 0.1°C and recorded along with SC.
(d) Col. Colorimetric, 1,10 phenanthroline.
(e) Vol. Volumetric, EDTA titration.
Legend: OO = dissolved oxygen, TDS = total dissolved solids, uM = micromoles per liter, mM = millimoles per liter, mg/L = milligrams per liter, umho cm^{-1} = micromoles per centimeter, ND = not detected, - indicates no analysis was made on that sample.

TABLE 0.4. Chemical Analyses of Water Samples Collected During Heat Recovery - Cycle 1

Date (1982)	12/14	12/14[a]	12/16	12/16[a]	12/17	12/18	12/19	12/20	12/20(b)	12/21	12/22
Time	1450		1650		1945	1120	1205	0930		0935	1055
pH	-	-	7.06	-	6.95	6.93	6.95	6.98	-	7.02	7.07
SC (umho cm^{-1})	-	-	415	-	368	388	362	404	-	406	407
DO (mg/L)	-	-	-	-	0.1	-	-	-	-	0.1	-
NH_3 (mg/L)	-	-	-	-	-	-	-	-	-	0.1	-
Alkalinity (mM)	4.03	4.01	4.13	-	3.68	3.70	3.82	3.91	3.89	4.01	4.19
SO_4 (uM)	73.9	75.1	79.5	78.3	57.6	62.3	65.1	70.1	70.1	73.24	81.4
Cl (uM)	96.7	97.0	90.5	90.2	42.7	44.9	35.3	32.7	31.3	28.2	26.5
F (uM)	12.1	12.1	13.2	12.6	15.5	16.1	16.3	16.3	16.3	15.8	17.9
NO_3 (uM)	1.62	1.62	ND	ND	ND	ND	ND	ND	ND	ND	ND
Ca (mM)	-	-	1.15	1.12	0.96	0.96	1.03	1.09	1.12	1.14	1.21
Mg (mM)	-	-	0.79	0.78	0.68	0.67	0.68	0.67	0.67	0.68	0.69
Na (mM)	-	-	0.25	0.25	0.25	0.24	0.23	0.23	0.23	0.22	0.22
K (mM)	-	-	0.20	0.20	0.23	0.24	0.24	0.24	0.24	0.23	0.22
Fe (uM)	-	-	6.9	7.2	0.68	6.3	6.6	6.9	7.8	34.9	31.6
Mn (uM)	-	-	0.33	0.26	0.26	0.21	0.20	0.21	0.21	0.20	0.22
Fe(II) (uM)	-	-	4.44	7.00	0.32	5.18	5.96	6.93	8.23	31.22	26.00
Fe Total (uM)	-	-	6.36	7.52	0.48	5.29	5.96	6.93	8.25	31.45	26.45
SiO_2 (uM)	251	251	251	-	391	357	310	276	274	229	194
Hardness (mM)	-	-	1.92	1.93	1.64	1.63	1.70	1.76	1.77	1.86	1.94
TDS (mg/L)	-	213	-	-	206	209	210	207	209	213	221

(a) Duplicate samples.

Legend: SC = specific conductance, DO = dissolved oxygen, TDS = total dissolved solids, uM = micromoles per liter, mM = millimoles per liter, mg/L = milligrams per liter, umho cm^{-1} = micromoles per centimeter, ND = not detected, - indicates no analysis was made on that sample.

TABLE D.5. Chemical Analyses of Water Samples Collected During Injection - Cycle 2

Date (1983)	5/9	5/10	5/10	5/11	5/11	5/11	5/12	5/12	5/12	5/12	5/12
Sample Point[a]	W	U	W	W	H	U	W	W	H	U	W
Time	2005	0950	1035	1730	1850	1930	0945	0945	1115	1200	1355
pH	6.67	7.15	6.78	6.63	6.61	-	6.68	-	6.81	7.11	-
pH T (°C)	80	20	78	90	70	-	85	-	88	23	-
SC (umho cm^{-1})	361	10	357	321	380	454	274	-	419	438	364
SC T (°C)	23.6	20.2	22.3	25.0	25.5	25.2	24.2	-	24.0	23.4	23.7
Alkalinity (mM)	3.42	4.73	3.41	3.04	3.66	4.78	3.65	3.63	4.10	4.66	3.63
SO_4 (uM)	87.3	-	85.7	87.3	-	-	84.8	84.8	-	-	84.8
Cl (uM)	21.4	-	23.4	61.2	-	-	37.5	36.4	-	-	36.7
F (uM)	13.2	-	12.4	13.2	-	-	13.2	13.2	-	-	13.7
NO_3 (uM)	ND	-	ND	ND	-	-	ND	ND	-	-	ND
Ca (mM)	0.772	1.505	0.900	0.634	0.931	1.463	0.906	0.911	1.167	1.428	0.911
Mg (mM)	0.754	0.767	0.775	0.771	0.779	0.771	0.763	0.766	0.760	0.752	0.756
Na (mM)	0.198	0.202	0.202	0.212	0.209	0.215	0.220	0.218	0.225	0.220	0.217
K (mM)	0.181	0.185	0.186	0.189	0.189	0.191	0.195	0.194	0.194	0.195	0.194
Mn (uM)	0.57	-	0.64	0.53	-	-	0.54	0.57	-	-	0.31
Fe(II) (uM)	31.5	50.9	37.2	18.9	7.6	37.0	17.5	21.4	9.1	55.4	6.5
Fe Total (uM)	32.1	50.4	37.9	18.9	7.6	36.4	17.4	21.9	9.0	54.5	6.6
SiO_2 (uM)	131	-	137	154	-	-	165	167	-	-	169
Hardness (mM)	1.55	2.25	1.69	1.40	-	2.23	1.65	1.67	-	-	1.66
TDS (mg/L)	170	224	177	147	-	-	194	191	-	-	-
O&G (mg/L)	-	-	-	ND	-	-	-	-	-	-	-

(a) H = heat exchanger effluent, W = reactor effluent--injection water, U = heat exchanger influent--source water.

Legend: SC = specific conductance, TDS = total dissolved solids, O&G = oil and grease, uM = micromoles per liter, mM = millimoles per liter, mg/L = milligrams per liter, umho cm^{-1} = micromoles per centimeter, ND = not detected, - indicates no analysis was made on that sample.

TABLE D.5. (continued)

Date (1983)	5/13	5/13	5/13	5/14	5/14	5/14	5/15	5/15	5/16
Sample Point[a]	W	H	U	W	H	U	W	H	W
Time	1820	2000	1945	1225	1154	1115	1100	1200	1830
pH	6.81	6.65	7.10	6.79	6.84	7.03	6.74	6.79	6.62
pH T (°C)	95	87	23	89	88	23	85	80	92
SC (umho cm^{-1})	316	362	425	340	361	366	358	396	275
SC T (°C)	24.0	24.2	22.0	20.0	19.4	18.5	24.0	24.6	19.7
Alkalinity (mM)	3.09	3.54	4.46	3.46	3.98	4.46	3.56	4.02	2.98
SO_4 (uM)	83.57	-	-	81.38	-	-	72.93	-	72.93
Cl (uM)	51.32	-	-	47.09	-	-	38.78	-	60.63
F (uM)	13.15	-	-	14.20	-	-	13.68	-	12.62
NO_3 (uM)	0.0	-	-	0.0	-	-	0.0	-	0.0
Ca (mM)	0.660	0.888	1.362	0.880	1.099	1.339	0.859	1.099	0.608
Mg (mM)	0.752	0.740	0.740	0.725	0.725	0.721	0.709	0.705	0.706
Na (mM)	0.227	0.228	0.232	0.230	0.233	0.231	0.235	0.236	0.236
K (mM)	0.201	0.201	0.205	0.201	0.207	0.207	0.207	0.209	0.209
Mn (uM)	0.50	-	-	0.64	-	-	0.58	-	0.63
Fe(II) (uM)	7.7	-	-	28.9	5.9	-	27.7	6.6	20.6
Fe Total (uM)	7.9	-	-	29.1	6.7	-	18.7	6.8	196.4
SiO_2 (uM)	182	-	-	189	-	-	197	-	-
Hardness (mM)	1.40	-	-	1.60	-	-	1.57	-	1.31
TDS (mg/L)	-	-	-	201	-	-	201	-	178
O&G (mg/L)	-	-	-	ND	-	-	-	-	-

(a) H = heat exchanger effluent, W = reactor effluent--injection water, U = heat exchanger influent--source water.

Legend: SC = specific conductance, TDS = total dissolved solids, O&G = oil and grease, uM = micromoles per liter, mM = millimoles per liter, mg/L = milligrams per liter, umho cm^{-1} = micromoles per centimeter, ND = not detected, - indicates no analysis was made on that sample.

TABLE D.5. (continued)

Date (1983)	5/16	5/16	5/17	5/17	5/18	5/18	5/18	5/18	5/19	5/19	5/19
Sample Point[a]	H	U	W	H	W	U	H	W	U	H	W
Time	1920	1945	1200	1300	0745	2100	2120	2045	1140	1120	1100
pH	6.82	7.01	6.64	6.74	6.80	-	6.73	6.71	-	6.79	6.68
pH T (°C)	93	24	87	84	86	-	94	94	-	83	85
SC (umho cm^{-1})	318	386	402	444	330	-	354	298	427	414	358
SC T (°C)	20.8	21.1	25.0	27.2	22.7	-	26.0	23.5	24.9	26.6	24.5
Alkalinity (mM)	3.32	4.41	3.42	3.89	3.58	4.39	3.48	3.20	4.36	3.91	3.68
SO_4 (uM)	-	-	67.97	-	64.79	-	-	64.79	62.01	62.01	62.01
Cl (uM)	-	-	37.06	-	36.94	-	-	38.92	35.53	35.53	36.52
F (uM)	-	-	13.76	-	14.20	-	-	13.68	13.62	13.89	14.41
NO_3 (uM)	-	-	NO	-	NO	-	-	NO	ND	NO	NO
Ca (mM)	0.775	1.302	0.874	1.078	0.900	1.297	0.848	0.707	1.308	1.083	0.869
Mg (mM)	0.705	0.709	0.709	0.705	0.717	0.698	0.698	0.717	0.709	0.705	0.705
Na (mM)	0.236	0.236	0.241	0.240	0.240	0.244	0.241	0.245	0.246	0.257	0.249
K (mM)	0.211	0.209	0.208	0.211	0.210	0.208	0.208	0.210	0.207	0.206	0.205
Mn (uM)	-	-	0.45	-	0.52	-	-	0.38	0.48	0.40	0.49
Fe(II) (uM)	1.4	39.2	13.8	6.6	16.3	-	4.7	15.0	25.9	3.7	9.6
Fe Total (uM)	2.0	39.7	14.0	7.0	7.0	-	5.0	15.8	26.2	3.9	9.6
SiO_2 (uM)	-	-	192	-	192	-	-	192	-	-	188
Hardness (mM)	-	-	1.59	-	1.59	-	-	1.38	1.99	1.77	1.58
TDS (mg/L)	-	-	212.5	-	208.2	-	-	181.3	-	-	202.9
O&G (mg/L)	-	-	0.55	-	-	-	-	-	-	ND	-

(a) H = heat exchanger effluent, W = reactor effluent--injection water, U = heat exchanger influent--source water.

Legend: SC = specific conductance, TDS = total dissolved solids, O&G = oil and grease, uM = micromoles per liter, mM = millimoles per liter, mg/L = milligrams per liter, umho cm^{-1} = micromoles per centimeter, ND = not detected, - indicates no analysis was made on that sample.

TABLE D.6. Chemical Analyses of Water Samples Collected During Heat Recovery - Cycle 2

Date (1983)	8/18	8/19	8/20	8/20	8/21	8/22	8/23	8/23[a]
Time	1844	1001	1202	1204	1256	0844	0839	0842
Temp. (°C)[b]	54.4	67.5	65.4	-	60.2	55.5	51.1	-
pH	6.96	6.78	6.75	-	6.76	6.79	6.81	-
pH T (°C)	52	63	62	-	57	54	50	-
SC (umho cm^{-1})	476	399	380	-	393	399	396	-
SC T (°C)	26.1	24.0	23.5	-	24.6	23.8	22.6	-
Alkalinity (mM)	4.34	3.82	3.70	3.78	3.78	3.78	3.89	3.84
SO_4 (uM)	93.3	79.8	81.8	81.8	83.9	83.9	84.9	86.0
Cl (uM)	346.0	128.0	89.5	87.5	70.8	60.2	50.2	51.5
F (uM)	-[c]	13.7	15.6	15.9	15.4	15.6	15.9	15.9
NO_3(uM)	ND	ND	ND	ND	ND	NO	ND	ND
Ca (mM)	1.21	1.03	1.01	1.01	1.05	1.06	1.07	1.08
Mg (mM)	0.969	0.733	0.738	0.738	0.738	0.758	0.730	0.738
Na (mM)	0.332	0.277	0.265	0.277	0.248	0.243	0.234	0.234
K (mM)	0.218	0.286	0.276	0.272	0.262	0.253	0.246	0.246
Mn (uM)	0.65	0.44	0.39	0.38	0.42	0.45	0.42	-
Fe(II) (uM)	16.9	23.4	25.4	25.1	24.2	25.4	25.2	25.7
Fe Total (uM)	17.1	23.7	25.4	25.3	25.5	25.3	25.3	25.5
SiO_2 (uM)	323	488	417	418	368	330	299	300
Hardness (mM)	2.15	1.74	1.72	1.72	1.74	1.77	1.81	1.79
TDS (mg/L)	254.0	231.0	231.0	216.0	228.0	210.0	215.0	222.0

(a) Duplicate sample.
(b) Temperature of water withdrawn from well.
(c) Fluoride interference.
Legend: SC = specific conductance, TDS = total dissolved solids, uM = micromoles per liter, mM = millimoles per liter, mg/L = milligrams per liter, umho cm^{-1} = micromoles per centimeter, NO = not detected, - indicates no analysis was made on that sample.

TABLE D.6. (continued)

Date (1983)	8/24	8/24[a]	8/25	8/26
Time	0901	0905	0906	0900
Temp. (°C)[b]	46.9	-	43.0	39.4
pH	6.86	-	6.89	6.93
pH T (°C)	47	-	41	39
SC (umho cm^{-1})	401	-	403	424
SC T (°C)	24.2	-	24.0	23.8
Alkalinity (mM)	3.90	-	3.97	4.01
SO_4 (uM)	88.0	-	91.1	96.2
Cl (uM)	43.8	-	39.9	35.4
F (uM)	16.1	-	17.8	-
NO_3 (uM)	ND	-	ND	ND
Ca (mM)	1.13	1.15	1.17	1.20
Mg (mM)	0.738	0.757	0.753	0.769
Na (mM)	0.229	0.234	0.231	0.227
K (mM)	0.240	0.242	0.235	0.227
Mn (uM)	0.47	0.46	0.45	0.44
Fe(II) (uM)	34.6	-	33.5	26.6
Fe Total (uM)	34.9	36.8	33.9	26.9
SiO_2 (uM)	267	-	239	223
Hardness (mM)	1.86	1.84	1.89	1.96
TDS (mg/L)	206.0	-	213.0	216.0

(a) Duplicate sample.
(b) Temperature of water withdrawn from well.
(c) Fluoride interference.
Legend: SC = specific conductance, TDS = total dissolved solids, uM = micromoles per liter, mM = millimoles per liter, mg/L = milligrams per liter, umho cm^{-1} = micromoles per centimeter, ND = not detected, - indicates no analysis was made on that sample.

TABLE D.7. Trace Metals Concentration in Cycle 2 Injection Water Samples Analyzed by ICP

Element[a] (mg/L)	Blank[b]	1983 5/9	5/11	5/13	5/13[c]	5/15	5/17	5/19
Al	ND[d]	ND	0.09	0.14	ND	0.07	0.14	ND
Mn	ND	0.02	0.02	0.01	0.01	0.02	0.01	0.01
Zn	0.05	0.07	0.06	0.05	0.05	0.04	0.05	0.04
Cu	ND	ND	ND	0.01	ND	ND	ND	ND
Pb	0.31	0.25	0.09	0.21	ND	0.12	0.27	0.15
Ni	0.05	ND	0.05	ND	ND	ND	ND	ND
Cr	0.02	ND	0.01	0.01	0.01	ND	0.02	ND
Cd	ND	ND	0.01	0.01	ND	0.01	0.01	0.01

(a) Results should be considered to be qualitative. See text.
(b) Blank is filter blank, other samples are well head samples.
(c) Duplicate.
(d) Not detected. Detection limits are (mg/L): Al 0.07, Cu 0.01, Pb 0.08, Ni 0.05, Cr 0.01, Cd 0.01.

TABLE 0.8. Chemical Analyses of Water Samples Collected During Injection - Cycle 3

Date (1983)	9/21	9/22	9/22	9/22	9/23	9/23[b]	9/24	9/24	9/24	9/25
Sample Point[a]	W	U	H	W	W	W	U	H	W	W
Time	1600	0900			2041	2041				1100
Temp. (°C)	111.1	37.8	100.0	100.0	119.3	-	-	-	102.9	102.7
pH	6.62	7.04	6.57	6.51	6.84	-	-	6.78	6.76	6.87
pH T (°C)	81	36	75	79	92	-	-	78	86	92
SC (umho cm^{-1})	324	461	440	375	288	-	-	-	315	345
SC T (°C)	24.8	24.8	27.2	27.5	22.1	-	-	-	23.2	24.1
Alkalinity (mM)	2.98	4.30	3.56	3.41	3.06	3.12	4.17	3.71	3.18	3.24
SO_4 (uM)	86.4	-	-	91.2	91.2	91.2	90.1	90.1	90.1	84.0
Cl (uM)	59.8	-	-	45.8	53.4	54.8	50.3	49.9	50.6	64.2
F (uM)	14.2	-	-	14.2	13.7	14.2	15.8	14.4	13.9	14.5
NO_3 (uM)	NO	-	-	-	-	-	ND	ND	ND	ND
Ca (mM)	0.626	-	1.23	0.824	0.546	0.546	1.20	0.945	0.711	0.968
Mg (mM)	0.757	-	0.728	0.731	0.728	0.731	0.728	0.737	0.737	0.724
Na (mM)	0.239	-	-	0.249	0.237	0.242	0.247	0.247	0.259	0.241
K (mM)	0.220	-	-	0.228	0.231	0.231	0.232	0.232	0.239	0.239
Mn (uM)	0.76	-	-	0.51	0.35	-	-	-	-	0.36
Fe(II) (uM)	18.3	-	-	29.9	28.0	27.6	81.6	4.75	40.0	21.5
Fe Total (uM)	18.6	-	-	30.3	28.5	28.5	81.2	5.11	40.1	21.6
SiO_2 (uM)	199	-	-	220	232	231	233	244	240	250
Hardness (mM)	1.43	-	-	1.58	1.28	1.30	1.98	1.69	1.48	1.48
TDS (mg/L)	158.0	-	-	190.2	163.0	-	-	-	6.0	180.0
O&G (mg/L)	-	-	-	-	-	-	-	-	-	-

(a) W = well head--injection water, H = heat exchanger effluent, U = upstream from heat exchanger--source water.

(b) Duplicate sample.

Legend: SC = specific conductance, TDS = total dissolved solids, O&G = oil and grease, uM = micromoles per liter, mM = millimoles per liter, mg/L = milligrams per liter, umho cm^{-1} = micromoles per centimeter, ND = not detected, - indicates no analysis was made on that sample.

TABLE D.8. (continued)

Oate (1983)	9/26	9/26	9/26	9/27	9/27	9/27	9/27	9/28
Sample Point[a]	U	H	W	W	U	H	W	H
Time	1830	1900	1930	1230	1320	1400	1430	-
Temp. (°C)	-	-	125.1	-	-	-	-	-
pH	-	6.26	6.12	-	-	6.64	6.61	6.54
pH T (°C)	-	80	68	-	-	79	87	83
SC (umho cm^{-1})	-	-	321	-	-	-	367	-
SC T (°C)	-	-	26.0	-	-	-	24.8	-
Alkalinity (mM)	4.23	3.19	2.92	3.38	4.10	3.59	3.30	3.20
SO_4 (uM)	-	-	-	82.9	81.9	81.9	81.9	-
Cl (uM)	-	-	-	58.6	66.5	88.4	59.9	-
F (uM)	-	-	-	14.4	15.8	14.8	13.9	-
NO_3 (uM)	-	-	-	NO	ND	NO	ND	-
Ca (mM)	-	0.740	0.584	0.749	1.18	0.924	0.829	0.725
Mg (mM)	-	0.720	0.728	0.728	0.728	0.728	0.737	0.709
Na (mM)	-	-	0.247	0.239	0.249	0.244	0.237	-
K (mM)	-	-	0.239	0.235	0.235	0.229	0.237	-
Mm (uM)	-	-	-	0.56	0.60	0.38	-	-
Fe(II) (uM)	-	-	-	28.0	52.3	16.7	6.9	-
Fe Total (uM)	-	-	-	28.3	54.6	17.4	12.1	-
SiO_2 (uM)	-	-	243	-	251	254	253	-
Hardness (mM)	-	-	-	1.50	1.95	1.62	1.54	-
TDS (mg/L)	-	-	156.0	165.0	-	-	-	-
O&G (mg/L)	-	-	ND	-	-	-	-	-

(a) W = well head--injection water, H = heat exchanger effluent, U = upstream from heat exchanger--source water.
(b) Duplicate sample.
Legend: SC = specific conductance, TDS = total dissolved solids, O&G = oil and grease, uM = micromoles per liter, mM = millimoles per liter, mg/L = milligrams per liter, umho cm^{-1} = micromoles per centimeter, NO = not detected, - indicates no analysis was made on that sample.

TABLE D.8. (continued)

Date	9/28	9/29	9/29	9/29[b]	9/30	10/1
Sample Point[a]	W	H	W	W	W	W
Time	-	-	1211	1208	1120	1000
Temp. (°C)	-	-	-	-	-	-
pH	6.48	-	6.88	-	6.76	6.83
pH T (°C)	73	-	88	-	82	80
SC (umho cm^{-1})	327		368	-	329	347
SC T (°C)	26.0		25.9	-	24.3	23.5
Alkalinity (mM)	2.95	3.74	3.25	3.57	3.04	3.44
SO_4 (uM)	-	-	-	77.8	-	72.7
Cl (uM)	-	-	-	68.2	-	67.2
F (uM)	-	-	-	13.6	-	14.4
NO_3 (uM)	-	-	-	ND	-	ND
Ca (mM)	0.603	1.06	0.787	0.787	0.645	0.834
Mg (mM)	0.728	0.728	0.709	0.720	0.728	0.709
Na (mM)	0.242	-	0.239	0.239	0.242	0.242
K (mM)	0.237	-	0.237	0.237	0.237	0.237
Mm (uM)	-	-	0.41	-	-	0.23
Fe(II) (uM)	-	-	19.9	-	-	10.5
Fe Total (uM)	-	-	19.9	-	-	10.5
SiO_2(uM)	251	-	254	-	246	230
Hardness (mM)	-	-	1.50	-	-	1.57
TDS (mg/L)	163.0	-	178.0	-	160.0	185.0
O&G (mg/L)	-	-	-	-	-	ND

(a) W = well head--injection water, H = heat exchanger effluent, U = upstream from heat exchanger--source water.
(b) Ouplicate sample.
Legend: SC = specific conductance, TOS = total dissolved solids, O&G = oil and grease, uM = micromoles per liter, mM = millimoles per liter, mg/L = milligrams per liter, umho cm^{-1} = micromoles per centimeter, NO = not detected, - indicates no analysis was made on that sample.

TABLE D.9. Chemical Analyses of Water Samples Collected During Heat Recovery - Cycle 3

Date (1983)	10/11	10/12	10/13	10/13	10/14	10/15	10/16	10/16	10/17	10/18
Time	1430	0900	1000	Dup.	1000	1030	1400	Dup.	0900	1200
Temp. (°C)	93.5	96.1	92.6	-	88.6	82.5	74.3	-	69.9	62.3
pH	6.73	6.78	6.75	6.80	6.80	6.77	6.78	-	6.82	6.85
pH T (°C)	90	90	90	90	90	82	72	-	70	63
SC (umho cm^{-1})	311	299	311	326	326	319	361	-	387	343
SC T (°C)	22.3	22.4	22.1	22.8	22.8	22.0	23.3	-	25.0	22.1
Alkalinity (mM)	3.23	3.08	3.20	3.09	3.31	3.40	3.49	3.48	3.76	3.88
SO_4 (uM)	75.2	79.3	83.3	83.3	-	83.3	-	-	85.4	87.4
Cl (uM)	107	131	113	110	-	80.0	-	-	62.8	54.5
F (uM)	12.9	13.9	14.9	14.9	-	15.9	-	-	15.9	15.9
NO_3 (uM)	ND	ND	ND	ND	-	ND	ND	-	ND	ND
Ca (mM)	0.834	0.778	0.778	0.778	0.778	0.834	0.929	0.929	0.966	1.01
Mg (mM)	0.642	0.637	0.640	0.620	0.627	0.632	0.635	0.635	0.635	0.642
Na (mM)	0.258	0.258	0.266	0.252	0.247	0.247	0.225	0.223	0.223	0.220
K (mM)	0.295	0.317	0.315	0.315	0.313	0.305	0.290	0.288	0.278	0.261
Mn (uM)	0.29	0.22	0.22	0.22	-	0.30	-	-	0.34	-
Fe(II) (uM)	13.0	7.23	7.01	7.01	16.0	14.2	29.1	-	22.9	23.9
Fe Total (uM)	13.3	7.31	7.10	7.31	-	14.2	-	-	22.9	24.0
SiO_2 (uM)	594	662	611	610	567	508	440	-	405	345
Hardness (mM)	1.51	-	-	1.46	-	1.53	-	-	1.66	-
TDS (mg/L)	208.2	216.6	207.9	206.6	-	199.7	211.0	-	215.1	212.1

Legend: SC = specific conductance, TDS = total dissolved solids, uM = micromoles per liter, mM = millimoles per liter, mg/L = milligrams per liter, umho cm^{-1} = micromoles per centimeter, ND = not detected, - indicates no analysis was made on that sample.

TABLE D.10. Chemical Analyses of Water Samples Collected During Injection - Cycle 4

Date (1983)	11/7	11/8	11/8	11/9	11/9	11/10	11/10	11/10	11/11	11/12
Sample Point(a)	W	W	W	W	W	U	H	W	W	W
Time	1753	0949	0955	1305	2001	1331	1459	1444	1830	
Temp. (°C)	115.0	112.8	-	-	122.8	-	111.6	111.6	135.5	116.7
pH	6.73	6.96	-	-	6.74	-	7.08	6.79	6.67	6.72
pH T (°C)	92	91	-	-	92	-	92	92	92	91
SC (umho cm^{-1})	307	266	-	-	249	-	361	329	276	323
SC T (°C)	23.9	21.0	-	-	20.9	-	27.0	25.0	25.0	25.0
Alkalinity (mM)	3.12	3.18	3.12	2.94	2.92	3.93	3.43	3.13	2.40	2.92
SO_4 (uM)	86.3	87.4	88.5	87.3	-	85.2	84.1	85.2	82.7	81.6
Cl (uM)	163.	82.1	82.1	76.0	-	78.6	79.7	79.7	87.1	87.1
F (uM)	13.5	14.5	14.5	15.7	-	15.3	15.3	15.0	15.0	15.0
NO_3 (uM)	ND	ND	ND	ND	-	ND	ND	ND	ND	ND
Ca (mM)	0.573	0.673	0.673	0.642	0.504	1.09	D.864	0.716	0.420	0.663
Mg (mM)	0.723	0.680	0.680	0.653	0.673	0.670	0.673	0.643	0.647	0.627
Na (mM)	0.315	0.250	0.250	0.261	0.250	0.250	0.248	0.255	0.250	0.257
K (mM)	0.275	0.282	0.279	0.302	0.294	0.303	0.299	0.299	0.305	0.313
Mn (uM)	0.706	0.38	0.38	0.36	-	1.31	0.31	0.16	0.06	0.13
Fe(II) (uM)	39.6	22.9	29.4	21.4	37.8	17.9	15.0	19.0	6.86	12.8
Fe Total (uM)	39.9	23.5	30.4	21.0	38.3	17.9	16.1	19.2	7.51	12.9
SiO_2 (uM)	302	349	347	383	373	373	383	388	405	405
Hardness (mM)	1.38	1.40	1.42	1.35	1.23	1.81	1.57	1.40	1.10	1.33
TDS (mg/L)	185.9	194.0	190.5	-	174.4	-	-	188.4	-	190.8
O&G (mg/L)	-	-	-	-	-	-	-	-	ND	-

(a) W = well head--injection water, H = heat exchanger effluent, U = upstream from heat exchanger--source water.

Legend: SC = specific conductance, TDS = total dissolved solids, O&G = oil and grease, uM = micromoles per liter, mM = millimoles per liter, mg/L = milligrams per liter, umho cm^{-1} = micromoles per centimeter, ND = not detected, - indicates no analysis was made on that sample.

TABLE D.10. (continued)

Date (1983)	11/12	11/12	11/13	11/16	11/17	11/18	11/19	11/19	11/19
Sample Point[a]	U	H	W	W	W	W	W	U	H
Time				1800	1200	1800	1130		
Temp. (°C)	-	-	104.7	118.6	115.6	25.0	107.3	-	-
pH	-	6.94	6.79	6.69	6.60	6.72	6.68	-	6.99
pH T (°C)	-	91	92	91	91	92	94	-	94
SC (umho cm^{-1})	-	355	295	248	322	251	311	-	-
SC T (°C)	-	27.0	21.6	20.9	24.3	20.9	23.0	-	-
Alkalinity (mM)	3.87	3.30	2.88	2.99	3.07	2.77	3.16	4.08	3.58
SO_4 (uM)	-	-	78.2	86.1	73.9	74.0	71.7	70.5	71.7
Cl (uM)	-	-	430	74.7	82.2	99.0	83.5	80.1	83.8
F (uM)	-	-	15.0	15.5	15.0	14.1	14.5	15.4	14.8
NO_3 (uM)	-	-	0.0	0.0	0.0	0.0	0.0	0.0	0.0
Ca (mM)	-	-	0.732	0.594	0.689	0.594	0.695	1.13	0.916
Mg (mM)	-	-	0.663	0.710	0.633	0.647	0.655	0.660	0.664
Na (mM)	-	-	0.252	0.232	0.250	0.243	0.250	0.252	0.241
K (mM)	-	-	0.304	0.263	0.292	0.282	0.273	0.274	0.273
Mn (uM)	-	-	0.36	0.32	0.22	0.18	0.31	-	-
Fe(II) (uM)	-	-	11.1	1.57	10.3	6.63	13.6	-	-
Fe Total (uM)	-	-	15.7	2.04	10.7	7.14	13.5	17.9	11.9
SiO_2 (uM)	-	-	383	300	345	349	351	348	356
Hardness (mM)	-	-	1.38	1.30	1.33	-	1.38	1.85	1.64
TDS (mg/L)	-	-	-	174	206	171	179	-	-
O&G (mg/L)	-	-	-	-	ND	-	-	-	-

(a) W = well head--injection water, H = heat exchanger effluent, U = upstream from heat exchanger--source water.

Legend: SC = specific conductance, TDS = total dissolved solids, O&G = oil and grease, uM = micromoles per liter, mM = millimoles per liter, mg/L = milligrams per liter, umho cm^{-1} = micromoles per centimeter, ND = not detected, - indicates no analysis was made on that sample.

TABLE D.11. Chemical Analyses of Water Samples Collected During Heat Recovery - Cycle 4

Date (1983)	11/29	11/30	12/1	12/1	12/2	12/3	12/4	12/5	12/6	12/6	12/7
Time	1730	0900	1001	1002	1030	1430	1200	1130	0947	0948	0910
Temp. (°C)	98.4	103.5	100.4	-	95.4	89.9		76.5	69.8	69.8	55.4
pH	6.59	6.58	6.63	-	6.73	6.63	6.76	-	6.80	-	6.85
pH T (°C)	90	92	92	-	94	85	75	-	67	-	60
SC (umho cm^{-1})	228	295	249	-	263	259	316	310	288	-	335
SC T (°C)	18.0	23.2	19.6	-	20.1	19.9	21.7	20.3	19.7	-	21.1
Alkalinity (mM)	3.09	2.87	2.99	2.91	3.08	3.78	3.38	3.54	3.68	3.75	3.86
SO_4 (uM)	74.9	75.9	85.3	85.3	89.5	-	86.4	86.8	87.4	89.5	-
Cl (uM)	115	146	150	147	135	-	108	102	85.1	84.4	-
F (uM)	12.9	14.3	15.6	16.6	16.1	-	17.3	-	17.4	18.2	-
NO_3 (uM)	ND	ND	ND	ND	ND	-	ND	ND	ND	ND	-
Ca (mM)	0.781	0.705	0.705	0.705	0.744	0.809	0.861	0.922	0.983	0.983	1.04
Mg (mM)	0.554	0.536	0.560	0.560	0.572	0.603	0.603	0.624	0.636	0.636	0.670
Na (mM)	0.290	0.290	0.280	0.278	0.280	0.280	0.280	0.271	0.263	0.266	0.258
K (mM)	0.356	0.374	0.371	0.371	0.365	0.351	0.338	0.317	0.303	0.302	0.284
Mn (uM)	0.26	0.19	0.23	0.20	-	0.27	-	0.33	0.38	0.39	-
Fe(II) (uM)	1.15	0.43	0.43	-	0.33	0.54	0.22	0.33	0.22	0.17	10.3
Fe Total (uM)	6.55	5.16	5.37	-	5.50	7.36	6.96	8.91	8.41	-	10.4
SiO_2 (uM)	810	859	811	803	721	633	581	511	439	439	387
Hardness (mM)	1.37	1.23	-	1.28	-	1.43	-	1.55	1.66	1.66	-
TDS (mg/L)	209	216	202	-	229	214	210	224	217	-	226

Legend: SC = specific conductance, TOS = total dissolved solids, uM = micromoles per liter, mM = millimoles per liter, mg/L = milligrams per liter, umho cm^{-1} = micromoles per centimeter, ND = not detected, - indicates no analysis was made on that sample.

TABLE D.12. Trace Metals Concentration in Withdrawal Water Samples Taken During Cycle 2 and Cycle 4, Analyzed by ICP

Element (mg/L)	1983					
	8/20	8/25[a]	8/25[a]	12/1	12/6[a]	12/6[a]
Al	ND[b]	ND	ND	ND	ND	ND
Fe	1.34	1.84	1.80	0.29	0.50	0.48
Mn	0.02	0.03	0.03	0.01	0.02	0.02
Zn	ND	ND	ND	ND	ND	ND
Cu	ND	ND	ND	ND	ND	ND
Pb	ND	ND	ND	ND	ND	ND
Ni	ND	ND	ND	ND	ND	ND
Cr	ND	ND	ND	ND	ND	ND
Cd	ND	ND	ND	ND	ND	ND

(a) Duplicate determinations.
(b) Not detected. Detection limits are (mg/L): Zn 0.01, Cu 0.01, Pb 0.11, Ni 0.03, Cr 0.01, Cd 0.01, Al 0.05

TABLE D.13. Chemical Analyses of Water Collected From Monitoring Wells Before First Pumping Test

Well[a]	AS1(J)	AS1(J)	AS1(MS)	AS1(MS)	AM1(SL)	AM2(IG)	AM2(IG)	BS1(J)	BC1(MS)	CM1(IG)
Date (1982)	1/20	2/18	1/21	2/17	2/1	2/4	3/12	2/22	2/23	3/11
pH	9.05	8.55	10.93	8.77	7.69	7.83	7.78	8.13	9.82	8.09
SC (umho cm^{-1})	235	313	222	-	351	321	-	-	-	-
Alkalinity (mM)	2.11	4.06	0.85	2.33	5.38	4.78	4.17	0.16	0.09	2.90
SO_4 (uM)	511	517	568	701	419	174	-	807	14	-
Cl (uM)	92	12	279	122	293	8	-	93	32	-
F (uM)	9	18	20	20	14	19	-	20	20	-
Mg (mM)	0.34	0.44	0.14	0.34	0.47	0.43	0.36	0.40	0.13	0.33
Na (mM)	0.38	0.36	0.48	0.39	0.23	0.24	0.29	0.58	0.33	0.29
K (mM)	0.33	0.29	0.36	0.31	0.13	0.17	0.13	0.24	-	0.12
SiO_2 (uM)	110	57	76	122	131	101	62	60	51	37
TDS (mg/L)	-	218	145	251	197	155	-	263	81	-

(a) J = Jordan, MS = Mt. Simon, SL = St. Lawrence, IG = Ironton-Galesville

Legend: SC = specific conductance, TDS = total dissolved solids, uM = micromoles per liter, mM = millimoles per liter, mg/L = milligrams per liter, umho cm^{-1} = micromoles per centimeter, - indicates no analysis was made on that sample.

TABLE D.14. Chemical Analyses of Water Samples Collected From Monitoring Wells After First Pumping Test

Well[a]	AM2(IG)	AS1(J)	AS1(J)	CM1(IG)	BC1(MS)	BS1(J)	AS1(MS)
Date (1982)	8/30	8/31	8/31	9/2	9/3	9/3	9/1
pH	7.27	8.50	-	8.14	11.42	8.14	8.42
SC (umho cm^{-1})	0.305	0.283	-	D.214	0.269	0.321	0.182
DO (mg/L)	0.2	ND	-	0.2	-	0.05	0.05
Alkalinity (mM)	4.35	3.60	3.56	3.41	1.45	4.41	2.15
SO_4 (uM)	65.1	358	358	69.5	480	842	842
Cl (uM)	2.82	22.8	23.12	-	-	-	62.0
F (uM)	16.8	7.89	5.79	12.1	42.6	14.7	22.1
NO_3 (uM)	147.8	ND	ND	ND	ND	ND	10.7
Ca (mM)	1.16	0.957	0.986	0.957	0.929	1.29	0.357
Mg (mM)	D.640	0.773	0.751	0.629	ND	0.972	0.396
Na (mM)	0.246	0.330	0.312	0.240	0.236	0.538	0.331
K (mM)	0.289	0.319	0.304	0.201	0.235	0.216	0.373
Fe(II) (uM)	85.2	1.43	1.52	36.80	-	30.45	0.98
Fe Total (uM)	89.3	0.36	2.05	36.9	-	2.0	0.45
SiO_2 (uM)	222	99.2	99.2	97.1	117	106	19.9
Hardness (mM)	1.96	1.76	1.83	1.71	0.96	2.36	0.83
TDS (mg/L)	236	228	224	201	160	316	167

(a) J = Jordan, MS = Mt. Simon, SL = St. Lawrence, IG = Ironton-Galesville

Legend: SC = specific conductance, DO = dissolved oxygen, TDS = total dissolved solids, uM = micromoles per liter, mM = millimoles per liter, mg/L = milligrams per liter, umho cm^{-1} = micromoles per centimeter, ND = not detected, - indicates no analysis was made on that sample.

TABLE D.15. Chemical Analyses of Water Samples Collected From Montoring Wells After Cycle 1

Well[a]	AM2(IG)	AS1(J)	AS1(MS)	CM1(IG)	BC1(MS)	BS1(J)	AM2(IG)	AM2(IG)
Date (1983)	2/15	2/16	2/16	2/18	2/19	2/19	2/22	2/22
Time	1530	1200	1500	1400	1300	1000	1140	1255
pH	7.32	9.06	8.64	7.46	9.58	8.04	7.28	-
SC (umho cm^{-1})[b]	401	259	248	372	156	356	415	-
Alkalinity (mM)	4.29	1.75	1.43	4.03	0.65	3.46	4.16	4.52
SO_4 (uM)	78.6	352	423	49.8	367	194	78.6	79.5
Cl (uM)	25.9	36.9	97.0	26.2	73.9	73.9	24.8	24.8
F (uM)	18.3	11.5	13.2	17.8	17.1	18.5	18.31	-
NO_3 (uM)	ND	ND	11.4	ND	ND	ND	ND	ND
Ca (mM)	1.27	0.400	0.400	1.01	0.480	0.85	1.25	1.27
Mg (mM)	0.711	0.501	0.405	0.605	0.122	0.722	0.696	0.706
Na (mM	0.260	0.420	0.380	0.314	0.298	0.526	0.214	0.238
K (mM)	0.213	0.300	0.339	0.211	0.199	0.183	0.220	0.220
Fe(II) (uM)	90.6	-	-	43.2	-	1.7	54.9	64.2
Fe Total (uM)	96.4	0.47	0.90	46.9	0.64	14.0	61.2	66.1
SiO_2 (uM)	163	124	104	132	244	93.0	166	175
Hardness (mM)	2.14	0.95	0.82	1.83	0.62	1.72	2.10	2.14
TDS (mg/L)	216	165	152	211	122	224	247	-

(a) J = Jordan, MS = Mt. Simon, SL = St. Lawrence, IG = Ironton-Galesville
(b) At room temperature.
Legend: SC = specific conductance, TDS = total dissolved solids, uM = micromoles per liter, mM = millimoles per liter, mg/L = milligrams per liter, umho cm^{-1} = micromoles per centimeter, ND = not detected, - indicates no analysis was made on that sample.

TABLE D.16. Chemical Analyses of Water Samples Collected From Monitoring Wells After Cycle 2

Well[a]	AM2(IG)	AM2(IG)	AS1(MS)	AS1(J)	CM1(IG)	AM1(SL)
Date (1983)	8/31	8/31	9/1	9/1	9/2	9/3
pH	7.18	-	8.23	8.39	7.52	7.78
SC	375	-	304	319	365	464
Temp. (°C)	21.0	-	22.3	22.0	22.0	23.0
DO (mg/L)	0.6	-	0.2	0.1	1.0	0.1
Alkalinity (mM)	4.45	4.46	2.46	3.04	4.15	5.17
SO_4 (uM)	81.1	79.6	454	304	43.5	171
Cl (uM)	31.2	30.2	87.1	74.6	25.6	29.0
F (uM)	17.9	20.4	10.5	8.8	13.2	34.7
NO_3 (uM)	ND	ND	12.7	ND	1.07	ND
Ca (mM)	1.41	1.41	0.77	0.86	1.24	1.58
Mg (mM)	0.77	0.77	0.60	0.69	0.70	0.95
Na (mM)	0.21	0.21	0.32	0.43	0.29	0.21
K (mM)	0.21	0.21	0.38	0.28	0.17	0.15
Fe (uM)	55.2	51.2	ND	3.36	39.7	10.6
Mn (uM)	1.30	1.30	0.72	0.53	0.46	0.65
SiO_2 (uM)	190	189	67.1	80.1	140	140
Hardness (mM)	2.18	2.15	1.31	1.54	1.92	2.45
TDS (mg/L)	255	248	217	206	241	316

(a) J = Jordan, MS = Mt. Simon, SL = St. Lawrence, IG = Ironton-Galesville

Legend: SC = specific conductance, DO = dissolved oxygen, TDS = total dissolved solids, uM = micromoles per liter, mM = millimoles per liter, mg/L = milligrams per liter, umho cm^{-1} = micromoles per centimeter, ND = not detected, - indicates no analysis was made on that sample.

TABLE D.17. Chemical Analyses of Water Samples Collected From Monitoring Wells After Cycle 3

Well[a]	AM2(IG)[b]	AM2(IG)	AM1(SL)	AS1(J)
Date (1983)	11/2	11/2	11/3	11/3
pH	-	7.25	8.22	8.28
Alkalinity (mM)	4.41	4.08	5.19	4.17
SO_4 (uM)	75.5	77.7	164	274
Cl (uM)	44.3	39.5	31.2	35.7
F (uM)	21.8	19.0	12.5	11.9
NO_3 (uM)	ND	ND	ND	ND
Ca (mM)	-	1.18	1.64	1.20
Mg (mM)	-	0.693	0.877	0.787
Na (mM)	-	0.228	0.228	0.410
K (mM)	-	0.234	0.147	0.266
Fe(uM)	-	ND	ND	ND
SiO_2 (uM)	216	256	136	94.9
Hardness (mM)	-	1.90	2.52	1.99
TDS (mg/L)	-	-	-	-

(a) J = Jordan, MS = Mt. Simon, SL = St. Lawrence, IG = Ironton-Galesville
(b) This sample was collected using a bailer; all others on this table collected by air-lifting.
Legend: TDS = total dissolved solids, uM = micromoles per liter, mM = millimoles per liter, mg/L = milligrams per liter, ND = not detected, - indicates no analysis was made on that sample.

TABLE D.18. Chemical Analyses of Water Samples Collected From Monitoring Wells After Cycle 4

Well[a]	AM1(SL)	AM2(IG)	AM2(IG)	AS1(J)
Date (1984)	1/17	1/18	1/18	1/19
pH	7.58	7.44	-	7.74
T (°C)	16.8	18.3	-	19.8
SC (umho cm^{-1})	342	311	-	383
DO (mg/L)	0.05	0.1	-	0.1
Alkalinity (mM)	5.21	4.31	-	4.57
SO_4 (uM)	171	68.7	62.6	267
Cl (uM)	24.4	64.6	63.2	28.6
F (uM)	12.2	23.7	21.7	11.6
NO_3 (uM)	ND	ND	ND	ND
Ca (mM)	1.65	1.33	-	1.34
Mg (mM)	0.877	0.681	-	0.866
Na (mM)	0.216	0.247	-	0.375
K (mM)	0.151	0.256	-	D.228
Fe(II) (uM)	-	162	-	41.7
Fe Total (uM)	171	154	-	40.9
SiO_2 (uM)	163	299	287	102
Hardness (mM)	2.56	2.04	-	2.21
TDS (mg/L)	325	278	283	294

(a) J = Jordan, MS = Mt. Simon, SL = St. Lawrence, IG = Ironton-Galesville

Legend: SC = specific conductance, DO = dissolved oxygen, TDS = total dissolved solids, uM = micromoles per liter, mM = millimoles per liter, mg/L = milligrams per liter, umho cm^{-1} = micromoles per centimeter, ND = not detected, - indicates no analysis was made on that sample.

DISTRIBUTION

No. of Copies

OFFSITE

U.S. Department of Energy
Attn: R. Eaton
Office of Energy Storage & Dist.
Forrestal Bldg, CE-142 5E-036
Washington, DC 20585

U.S. Department of Energy
Attn: K. Klunder
Office of Energy Storage & Dist.
Forrestal Bldg, CE-142 5E-036
Washington, DC 20585

U.S. Department of Energy
Attn: E. Reimers
Office of Energy Storage & Dist.
Forrestal Bldg, CE-142 5E-036
Washington, DC 20585

12 DOE/Office of Scientific and Technical Information

Argonne National Laboratory
Attn: A. Gorski
Building 362
9700 S. Cass Avenue
Argonne, IL 60439

Auburn University
Attn: F. J. Molz
School of Engineering
Auburn, AL 36830

Walter Hauz
4520 Via Vistosa
Santa Barbara, CA 93110

Illinois State Water Survey
Attn: T. R. Holm
2204 Griffith Drive
Champaign, IL 61820

No. of Copies

Herbert Jaehne
3290 Warrenville Center Rd
#211
Cleveland, OH 44122

Lawrence Berkeley Laboratory
Attn: C-F. Tsang
University of California
Bldg. 90, Room 1012-H
1 Cyclotron Road
Berkeley, CA 94720

Charles F. Meyer
1141 Cima Linda Lane
Santa Barbara, CA 93108

Minnesota Geological Survey
Attn: P. C. Grew
2642 University Avenue
St. Paul, MN 55114

New York State Energy
Research & Development
Agency
Attn: G. Walmet
2 Rockefeller Plaza
Albany, NY 12223

Oak Ridge National Laboratory
Attn: J. Tomlinson
Building 9204-1, MS 8045
Y-12 Plant, Box 2009
Oak Ridge, TN 37831-8045

Office of Congressman
Sid Morrison
1330 Longworth Bldg.
Washington, DC 20515

Office of Congressman
Tom Bevil
2302 Rayburn Bldg.
Washington, DC 20515

No. of
Copies

Oregon State University
Attn: S. W. Childs
Dept. of Soil Science
Corvallis, OR 97331

Resource Efficiency, Inc.
Attn: M. Spurr
340 Daly Street
St. Paul, MN 55102

Sandia National Laboratories
Technical Library
Division 3141
Albuquerque, NM 87185

Southern Company Services, Inc.
Attn: K. Vakhshoorzadeh
PO Box 2625
Birmingham, AL 35202

The California State University
Attn: Mr. Edward Knipe, P.E.
Chief of Energy and Utilities
Programs
Seal Beach, CA 90740-7502

University of Alabama
Attn: E. Brett
School of Mines and Energy
Development
Box 870164
Tuscaloosa, AL 35487-0164

University of Alabama
Attn: C. Midkiff
School of Mines and Energy
Development
Box 870164
Tuscaloosa, AL 35487-0164

University of Massachusetts
at Amherst
Attn: D. Breger
Oept. of Mechanical Eng.
Eng. Laboratory Bldg.
Amherst, MA 01003

No. of
Copies

University of Massachusetts
at Amherst
Attn: J. E. Sunderland
Dept. of Mechanical Eng.
Eng. Laboratory Bldg.
Amherst, MA 01003

University of Minnesota
Attn: S. Markham
Physical Plant Operations
615 15th Avenue S.E.
Minneapolis, MN 55455

University of Minnesota
Attn: P. Blackshear
Dept. of Mechanical Eng.
111 Church Street S.E.
Minneapolis, MN 55455

20 University of Minnesota
Attn: M. Hoyer
Underground Space Center
Dept. of Civil and Mineral Eng.
790 Civil and Mineral Eng. Bldg.
Minneapolis, MN 55455

University of Minnesota
Attn: R. L. Jackson
Physical Planning-Civil Eng.
615 15th Avenue S.E.
Minneapolis, MN 55455

University of Minnesota
Attn: R. L. Sterling
Underground Space Center
Dept. of Civil and Mineral Eng.
790 Civil and Mineral Eng. Bldg.
Minneapolis, MN 55455

University of Minnesota
Attn: M. Walton
Underground Space Center
Dept. of Civil and Mineral Eng.
790 Civil and Mineral Eng. Bldg.
Minneapolis, MN 55455

No. of
Copies

US Army Corps of Engineers
Attn: C. W. Sohn
Construction Engineering
Research Laboratory
PO Box 4005
Champaign, IL 61820-1305

US Department of Interior
Attn: Natural Resources
Library
Serials Branch (G/E)
Washington, DC 20240

US Geological Survey - WRD
Attn: G. Stoner
702 Post Office Building
St. Paul, MN 55101

US Geological Survey
Attn: B. Nemickas
Water Resources Div.
5 Aerial Way
Syosset, NY 11791

Wehran Engineering
Attn: R. Miller
666 E. Main St.
PO Box 2006
Middletown, NY 10940

Wilke and Associates
Attn: D. Wilke
38 Roosevelt Avenue
Glen Head, NY 11545

FOREIGN

Bengt Hidemark Gosta Danielson
Arkitekter SAR
Attn: A. Boysen
Jarntorget 78
S-11 29 Stockholm
Sweden

No. of
Copies

Commission of European
Communities
Attn: P. Zegers
DG XII, E3
200 Weststraat
Brussels, Belgium

DFVLR
Attn: M. Becker
Bereich Projekttragerschaften
Linder Hohe
5DOD Koeln 90
Germany

Helsinki University of
Technology
Attn: P. Lund
Otakaari 3
SF-D2150 Espoo
Finland

I.E.N.E.R.
EPF-Ecublens
Attn: B. Saugy
1015 Lausanne
Switzerland

IF Technology
Attn: A. Snijders
Frombregstraat 1
6814 RE Arnhem
The Netherlands

Institut Fisica Universite
Attn: F. Reale
P. le Tecchio
80125 Napoli
Italy

Institut fur Kernenergetik
und Energiesystems
Attn: M. Groll
Universitat Stuttgart
Pfaffenwaldring 31
Postfach 801140
7000 Stuttgart 80
Germany

No. of
Copies

Institut fur Thermodynamik and
Waermetechnik
Attn: U. Gross
Universitat Stuttgart
Pfaffenwaldring 6
7000 Stuttgart 80
Germany

KFA Julich
Projektleitung Energieforschung
Attn: F. J. Friedrich
PO Box 1913
D-5170 Julich
Germany

KFA Julich, PLE
Attn: V. Lottner
PO Box 1913
D-5170 Julich
Germany

KM Kjessler & Mannerstrale AB
Attn: S. Lundin
PO Box 7124
S-171 07 Solna
Sweden

Laboratory for Energetics
Attn: B. Qvale
Technical University of Denmark
DTH Building 403
DK-2800 Lyngby
Denmark

B. Matthey
Consulting-Engineers Ltd.
CH-2205 Montezillon-Neuchatel
Switzerland

Ministry of Trade and Industry
Energy Department
Attn: Pirjo-Liisa Vainio
Acting Head of R&D Division
Pohjoinen Makasiininkatu 6
00130 Helsinki
Finland

No. of
Copies

NOVEM
Attn: G. J. van Mourik
PO Box 8242
Leidseveer 35
3503 RE Utrecht
The Netherlands

Public Works Canada
Attn: E. L. Morofsky
C456 Sir Charles Tupper Bldg.
Riverside Dr. and Heron Rd.
Ottawa, Ontario
K1A OM2 Canada

Riso National Laboratory
Attn: P. L. Christensen
DK-4000 Roskilde
Denmark

Strata Engineering
Attn: C. Mirza
170 The Donway West
Don Mills, Ontario M3C 2G3
Canada

Swedish Council for Building
Research
Attn: W. Raldow
St. Goransgatan 66
S-11233 Stockholm
Sweden

Swedish Council for Building
Research
Attn: B. T. Sellberg
Sankt Goransgatan 66
S-11233 Stockholm
Sweden

Universitat Stuttgart
Attn: R. Giebe
Pfaffenwaldring 6
7000 Stuttgart 80
Germany

No. of
Copies

ONSITE

DOE Richland Operations Office

R. B. Goranson, A5-90

27 Pacific Northwest Laboratory

M. K. Drost , K5-21
E. A. Jenne, K3-61
L. D. Kannberg, K5-02 (15)
B. L. Mohler, K5-02
J. R. Raymond, K6-77
L. W. Vail, K6-77
G. L. Work, K7-02
Publishing Coordination
Technical Report Files (5)